

**Changing ventilation of the Mediterranean Sea
studies with a suite of novel halogenated
transient tracers**

Dissertation

zur Erlangung des Doktorgrades
der Mathematisch-Naturwissenschaftlichen Fakultät
der Christian-Albrechts-Universität zu Kiel

vorgelegt von

Pingyang Li

Kiel, 2020

**Changing ventilation of the Mediterranean Sea
studies with a suite of novel halogenated
transient tracers**

Dissertation

zur Erlangung des Doktorgrades
der Mathematisch-Naturwissenschaftlichen Fakultät
der Christian-Albrechts-Universität zu Kiel

vorgelegt von

Pingyang Li

Kiel, 2020

Erster Gutachter: Prof. Dr. Arne Körtzinger
Zweiter Gutachter: PD. Dr. Christa Marandino
Tag der mündlichen Prüfung: 23.06.2020
Zum Druck genehmigt: 23.06.2020

gez. Prof. Dr. Frank Kempken, Dekan

Eidesstattliche Erklärung

Hiermit erkläre ich, Pingyang Li, dass ich diese Doktorarbeit, abgesehen durch die Beratung meiner Betreuerin, selbstständig verfasst, sowie alle wörtlichen und inhaltlichen Zitate als solche gekennzeichnet habe.

Die Arbeit wurde unter Einhaltung der Regeln guter wissenschaftlicher Praxis der Deutschen Forschungsgemeinschaft verfasst.

Sie hat weder ganz, noch in Teilen, einer anderen Stelle im Rahmen eines Prüfungsverfahrens vorgelegen, ist nicht veröffentlicht und auch nicht zur Veröffentlichung eingereicht.

Kiel, April 2020

gez. Pingyang Li

Acknowledgments

First and foremost, I would like to thank Dr. Toste Tanhua for supervising my thesis, for sharing his scientific views on our studies and feedback throughout my thesis. Special thanks go to Prof. Dr. Arne Körtzinger to be a member of my ISOS committee and for his instructions and financial supports at conferences and expensive standard gas. A huge ‘Thank you!’ goes to Boie Bogner and Tim Steffens, who offered me great help to develop the instrument. I also highly appreciate the assistance of Dr. Birgit Quack, who always supports and encourages me whenever I ask for help.

Hereby I also would like to acknowledge scientists from the other institutes. I am really grateful to the AGAGE group, including Prof. Dr. Ray F. Weiss, Dr. Jens Mühle, Dr. Peter Salameh from SIO, Prof. Dr. Paul J. Fraser from CSIRO, Prof. Dr. David E. Oram from UEA, Dr. Martin Vollmer from Empa and Dr. Bo Yao from MOC, CMA. They supported me a lot on the instrument maintenance, including repairing and development of hardware and updating of software. They, combined with Dr. Stephen A. Montzka and Dr. Benjamin R. Miller from the NOAA, provided data in reconstructing the atmospheric histories of potential transient tracers. I also acknowledge the scientists and staff behind these scientists, such as those in various stations. Besides, I also acknowledge Prof. Dr. Minggang Cai, Dr. Peng Huang, and Weimin Wang for their help in sampling in the Western Pacific Ocean.

The members of the Chemical Oceanography Department at GEOMAR have immensely contributed to making my time as a Ph.D. student easier. They lent me the devices and provided the tremendous help in the laboratory. Special thanks go to Dr. Dennis Booge, who is always open for questions and help. Also, thank Tim Steffens for helping me take samples in the Baltic Sea, cooperated with Dennis, Melf Paulsen and Li Zhou. In addition, I am grateful to Martina Schütt for supporting my work in the laboratory and Frank Malien for supporting my sampling in the Boknis Eck. I acknowledge Dr. Tim Stöven for his instructions on some MATLAB scripts. Besides, I am also grateful to Dr. Johannes Karstensen from the Physical Oceanography Department for his introduction to the OMP model, although the model has not been used.

Here I would like to show my appreciation to my friends at GEOMAR including Mingshuang Sun, Xiao Ma, Li Zhou, Dr. Qixing Ji, Dr. Yaping Lin, Dr. Yue Jia, Dr. Xupeng Chi, Dr. Xinyu Li and Kechen Zhu; and some other friends including Dr. Yingying Wang, Dr. Jiawen Wu, Dr. Bo Chen, Chaogui Lei, and Qianqian Mao and so on. They make me not alone and make my life easier and enjoyable in Kiel.

Last but not least, I am particularly grateful to Dr. Yanjun Ren and my dear family, for their loving support, unlimited encouragement and irrevocable belief in me.

Manuscript contributions

This dissertation is based on the following manuscripts:

1. **Manuscript I:** Pingyang Li and Toste Tanhua: Recent changes in deep ventilation of the Mediterranean Sea; evidence from long-term transient tracer observations, *Frontiers in Marine Science*, in review, 2020.

Author contributions: PL performed the data processing, contributed figures and tables and wrote the paper. TT conducted the sampling from cruises ESAW2, CRELEV2016, TALPro2016 and MSM72 and supported the writing process.

2. **Manuscript II:** Pingyang Li, Jens Mühle, Stephen A. Montzka, David E. Oram, Benjamin R. Miller, Ray F. Weiss, Paul J. Fraser, and Toste Tanhua: Atmospheric histories, growth rates and solubilities in seawater and other natural waters of the potential transient tracers HCFC-22, HCFC-141b, HCFC-142b, HFC-134a, HFC-125, HFC-23, PFC-14 and PFC-116, *Ocean Science*, 15, 33–60, <https://doi.org/10.5194/os-15-33-2019>, 2019.

Author contributions: The work was carried out by PL as a Ph.D. candidate under the supervision of TT. JM, SAM, DEO, BRM, RW and PJF provided the atmospheric mole fraction data. PL collected the solubility data. PL analyzed and interpreted all the data based on discussion with TT. All authors worked on the paper.

3. **Manuscript III:** Pingyang Li and Toste Tanhua: Medusa-Aqua system: simultaneous measurement and evaluation of novel potential halogenated transient tracers HCFCs, HFCs and PFCs in the ocean, *Ocean Science Discussion*, <https://doi.org/10.5194/os-2019-101>, in review (resubmitted), 2019.

Author contributions: TT conducted the sampling. PL developed the instrument and carried out the measurements. PL interpreted the data and analyzed the results based on the discussion with TT. PL wrote the paper with contributions from TT.

Zusammenfassung

Ozeanische transiente Tracer (sog. Spurengase) sind seit mehr als vier Jahrzehnten als wichtig angesehen, da mit ihnen die Ventilation der Ozeane visualisiert und quantifiziert, sowie die Auswirkungen des Klimawandels verstanden werden kann. Sie beschreiben Wege, wenn sie in den Ozean eintreten und sich durch ihn bewegen, und liefern uns wertvolle Zeitinformationen. Wenn solche Zeitinformationen in Abhängigkeit von der Eingabefunktion (zeitverändernde Konzentrationen) interpretiert werden, handelt es sich um chronologische transiente Tracer, wie Dichlordifluormethan (CFC-12) und Schwefelhexafluorid (SF_6). Während der letzten 15 Jahre beschränkte die nicht monotone Veränderung der atmosphärischen Konzentration von CFC-12 seine Fähigkeit als ozeanischer transienter Tracer für kürzlich belüftete Wassermassen, funktioniert aber immer noch für Tiefenwasser. Daher haben wir das Mittelmeer als Beispiel genommen und die jüngsten Veränderungen in der Tiefenbelüftung anhand von Langzeitbeobachtungen von CFC-12 und SF_6 im ersten Manuskript untersucht. Da eine Kombination mehrerer transienter Tracer die Ozeanbelüftung besser interpretieren kann, haben wir im zweiten und dritten Manuskript nach potenziellen neuen ozeanischen transienten Tracern gesucht und diese bewertet: teilhalogenierte Fluorchlorkohlenwasserstoffe (H-FCKW), Fluorkohlenwasserstoffe (HFC) und Perfluorkohlenwasserstoffe (PFC). Die jeweiligen Ergebnisse werden nachstehend beschrieben.

Die erste Studie zeigt eine zeitlich und räumlich sehr variable Tiefenbelüftung im Mittelmeer, die auf einer Kombination von Beobachtungen traditioneller chronologischer transienter Tracer (CFC-12 und SF_6), auf hydrografischen Eigenschaften (Salzgehalt, potenzielle Temperatur und potenzielle Dichte) und auf der Sauerstoffverwertung (apparent oxygen utilization; AOU) von 13 Forschungsfahrten zwischen 1987 und 2018 basiert. Räumlich gesehen zeigen das östliche sowie das westliche Tiefenwasser des Mittelmeeres (EMDW und WMDW) einen West.-Ost-Gradienten mit steigender Salinität und steigender potentieller Temperatur sowie mit sinkender Sauerstoff- und Tracer-Konzentration. Zeitlich gesehen herrscht in den meisten Gebieten des EMDW während der letzten Dekade eine stagnierende bzw. geschwächte Belüftung, obwohl zwischen 2011 und 2016 im Tiefenwasser der Adria eine Belüftung stattfand, welche auf die Schwächung der Intensität der adriatischen Quelle zurückzuführen sein könnte. Es konnte ein größere Belüftung des westlichen Mittelmeers nach dem Ereignis des westlichen Mittelmeerübergangs (Western Mediterranean Transition; WMT) beobachtet werden, gefolgt von einer leichten Abschwächung der Belüftung nach 2016, was ein kombinierter Einfluss des östlichen (für die geschwächte Intensität der adriatischen Quelle) und des westlichen Mittelmeers (wegen des geschwächten Einflusses des WMT-Ereignisses) sein könnte.

In der zweiten und dritten Studie untersuchten und bewerteten wir mögliche neue chronologische transiente Tracer: Chlordifluormethan (HCFC-22), 1,1-Dichlor-1-fluorethan (HCFC-141b), 1-Chlor-1,1-difluorethan (HCFC-142b), 1,1,1,2-Tetrafluorethan (HFC-134a), Pentafluorethan (HFC-125), Fluoroform (HFC-23), Tetrafluoridkohlenstoff (PFC-14, CF₄) und Hexafluorethan (PFC-116) auf vier Aspekte: Eingabefunktion (einschließlich atmosphärischer Geschichte und historischer Oberflächensättigung), Meerwasserlöslichkeit, Durchführbarkeit der Messung und Stabilität im Meerwasser. Die konsistenten mittleren atmosphärischen Jahresverläufe in der nördlichen und südlichen Hemisphäre wurden durch Kombination von In-situ-, Kolben-, archivierter Luft- und Firn-Luftmessungen sowie veröffentlichten Modellberechnungen aus mehreren Netzwerken (einschließlich AGAGE, SIO, CSIRO, NOAA und UEA) rekonstruiert. Die historische Oberflächensättigung wurde mit 94% berechnet, indem die mittlere Meerwassersättigung von jeder einzelnen Forschungsfahrt im Mittelmeer zwischen 1987 und 2018 gemittelt wurde. Die Meerwasserlöslichkeitsfunktionen wurden basierend auf dem Clark-Glew-Weiss-Modell (CGW) konstruiert, welches an die Süßwasserlöslichkeitsfunktionen und Aussalzungskoeffizienten angepasst ist, die durch die linearen Polyparameter-Beziehungen der freien Energie (pp-LFERs) geschätzt werden. Die Messungen von HCFC-22, HCFC-141b, HCFC-142b, HFC-134a und HFC-125 in Tiefenprofilen in Meerwasser wurden erstmals im Mittelmeer gleichzeitig mit dem Medusa-Aqua-System durchgeführt, während HFC-23 und PFCs aufgrund eines Blankwertes bzw. einer niedrigen Nachweisgrenze nicht gemessen werden konnten. Die Stabilität im Meerwasser wurde durch Analyse ihrer Oberflächensättigung, Beobachtungen des inneren Ozeans anhand von CFC-12-Messungen und des Durchschnittsalters im Vergleich zu den aus CFC-12 / SF₆ geschätzten Werten ermittelt.

Nach umfassender Analyse und Bewertung sind die derzeit vielversprechendsten ozeanischen transienten Tracer HCFC-142b und HCFC-141b, da sie aufgrund der gut dokumentierten atmosphärischen Vorgeschichte, der nachgewiesenen Meerwasserlöslichkeit, der Durchführbarkeit der Messungen und ihrer inerten Eigenschaft im Meerwasser mehrere wesentliche Anforderungen erfüllen. Sie werden jedoch wahrscheinlich nur in den nächsten Jahren / Jahrzehnten in dieser Funktion genutzt werden können, da die durch das Montrealer Protokoll auferlegten Beschränkungen die Produktion und den Verbrauch runterregulieren und ihre (künftig) abnehmenden atmosphärischen Konzentrationen sie als transient Tracer unbrauchbar machen. Die Verbindungen, die in Zukunft das größte Potenzial als ozeanische transiente Tracer haben sind PFC-14 und PFC-116 aufgrund ihrer hohen Stabilität im Meerwasser, der langen und gut dokumentierten atmosphärischen Konzentrationshistorie und der gut konstruierten Meerwasserlöslichkeitsfunktionen. Die Herausforderung besteht darin, den Fehler der Messungen aufgrund ihrer geringen Löslichkeit möglichst gering zu halten. Für HFC-134a können wir sein Potenzial als Tracer aufgrund der nicht eindeutigen Ergebnisse, insbesondere hinsichtlich seiner Löslichkeit und Stabilität in Meerwasser, aber auch im Hinblick auf potenzielle analytische Herausforderungen, nicht vollständig bewerten. HFC-125, HFC-23 und HCFC-22 können nicht mehr als transient Tracer berücksichtigt werden, da es

alternative Tracer mit ähnlichen Eingabefunktionen gibt, die sich besser als ozeanische transiente Tracer eignen.

Zusammenfassend hilft diese Arbeit, die Ozeanbelüftung im Mittelmeer in den letzten 30 Jahren (mit Schwerpunkt auf den jüngsten Veränderungen) aus der Perspektive der traditionellen chronologischen transienten Tracer zu verstehen. Außerdem untersucht und bewertet diese Arbeit potenzielle neuartigen chronologischen transiente Tracer im Ozean. Das Ergebnis bildet die Grundlage für die weitere Untersuchung dieser alternativen Tracer, um die Belüftung im globalen Ozean besser interpretieren und die Auswirkungen des Klimawandels verstehen zu können.

Abstract

Oceanic transient tracers have been concerned for more than four decades due to their ability in visualizing and quantifying ocean ventilation and understanding the effects of changing climate. They trace pathways climate anomalies follow as they enter and move through the ocean and provide us with valuable time information. When such time information is interpreted depending on input function (time changing concentrations), they are chronological transient tracers, such as dichlorodifluoromethane (CFC-12) and sulfur hexafluoride (SF_6). During the past ~15 years, the non-monotonous change of atmospheric history of CFC-12 limited its ability as an oceanic transient tracer for recently ventilated water masses, but it still works for deep waters. Therefore, we took the Mediterranean Sea as an example and investigated the recent changes in deep ventilation based on long-term observations of CFC-12 and SF_6 in the first manuscript. Since a combination of multiple transient tracers can better interpret ocean ventilation, we looked for and evaluated potential novel oceanic transient tracers: hydrochlorofluorocarbons (HCFCs), hydrofluorocarbons (HFCs) and perfluorocarbons (PFCs) in the second and third manuscripts. The specific findings are described below.

In the first study, highly variable deep ventilation in the Mediterranean Sea in time and space are reported based on a combination of observations of traditional chronological transient tracers (CFC-12 and SF_6), hydrographic properties (salinity, potential temperature and potential density) and apparent oxygen utilization (AOU) from 13 cruises conducted during 1987-2018. Spatially, both the Eastern and Western Mediterranean Deep Water (EMDW and WMDW) show a general west-to-east gradient of increasing salinity and potential temperature but decreasing oxygen and transient tracer concentrations. Temporally, stagnant and weak ventilation is found in most areas of the EMDW during the last decade in spite of prevailing ventilation in the Adriatic Deep Water between 2011 and 2016, which could be a result of the weakened Adriatic source intensity. In the Western Mediterranean Sea, enhanced ventilation after the Western Mediterranean Transition (WMT) event is observed, and slightly weakened ventilation after 2016 could be a combined influence from the Eastern (for the weakened Adriatic source intensity) and the Western (for the weakened influence from the WMT event) Mediterranean Sea.

In the second and third studies, we explored and evaluated potential novel chronological transient tracers: chlorodifluoromethane (HCFC-22), 1,1-dichloro-1-fluoroethane (HCFC-141b), 1-chloro-1,1-difluoroethane (HCFC-142b), 1,1,1,2-tetrafluoroethane (HFC-134a), pentafluoroethane (HFC-125), fluoroform (HFC-23), carbon tetrafluoride (PFC-14, CF_4) and hexafluoroethane (PFC-116) from four aspects: input function (including atmospheric history and historical surface saturation), seawater solubility, feasibility of measurement and stability in seawater. The consistent annual mean atmospheric histories in the Northern and Southern Hemisphere were reconstructed by combining in

situ, flask, archived air, and firn air measurements as well as published model calculations from multiple networks (including AGAGE, SIO, CSIRO, NOAA, and UEA). The historical surface saturation was calculated to be 94 % by averaging the mean seawater saturation from every single cruise in the Mediterranean Sea during 1987–2018. The seawater solubility functions have been constructed based on the Clark–Glew–Weiss (CGW) model fitted freshwater solubility functions and salting-out coefficients estimated by the poly-parameter linear free-energy relationships (pp-LFERs). The measurements of HCFC-22, HCFC-141b, HCFC-142b, HFC-134a and HFC-125 in depth-profiles in seawater have been simultaneously done in the Mediterranean Sea for the first time by the Medusa-Aqua system, while HFC-23 and PFCs were unable to be measured due to non-zero blank and low detection limit, respectively. The stability in seawater was estimated by analyzing their surface saturation, interior ocean observations against CFC-12 measurements and mean age compared to those estimated from CFC-12/SF₆.

By comprehensive analysis and evaluation, the most promising oceanic transient tracers are HCFC-142b and HCFC-141b currently since they fulfill several essential requirements by virtue of well-documented atmospheric history, established seawater solubility, feasible measurements and inertness in seawater. However, they will likely only work for the next few years/decades considering the restrictions on their production and consumption imposed by the Montreal Protocol and their (future) decreasing atmospheric mole fractions. The compounds that have the greatest potential as oceanic transient tracers in the future are PFC-14 and PFC-116 because of their high stability in seawater, the long and well-documented atmospheric concentration histories and well-constructed seawater solubility functions. The challenge is how to measure them accurately due to their low solubility. For HFC-134a, we are not able to fully evaluate its potential as a tracer due to the inconclusive results, especially on its solubility and stability in seawater, but also with regard to potential analytical challenges. HFC-125, HFC-23, and HCFC-22 can no longer be considered because there are alternative tracers with similar input functions that are better suited as oceanic transient tracers.

In total, this work helps us understand ocean ventilation in the Mediterranean Sea in the past ~30 years (with an emphasis on the recent changes) from the perspective of the traditional chronological transient tracers, as well as explored and evaluated the potential novel chronological transient tracers in the ocean. The outcome sets the base for further investigation of these alternative tracers in order to better interpreting ventilation in the global ocean and understanding the effects of climate change.

Contents

Acknowledgments	V
Manuscript contributions	VII
Zusammenfassung	IX
Abstract	XIII
Contents	XV
Introduction	1
Manuscript I	7
Manuscript II	51
Manuscript III	119
Conclusions and outlook	163
Appendix A Measurement of HCFCs and HFCs in seawater	167
Appendix B Table S2 in Manuscript II	175
Appendix C Table S1 in Manuscript III	193
Curriculum Vitae	203

Introduction

Ocean ventilation, an important process on Earth, is defined by that a water parcel and its carried climatic properties (such as heat, salinity, and dissolved gases, etc.) propagate from the mixed layer into the ocean's interior by advection and diffusion pathways (Fig. 1.1). One important method to analyze the local and global ocean ventilation processes and understand the effects of changing climate is based on the observations of transient tracers (belonging to dissolved gases in the climatic properties mentioned above) in seawater.

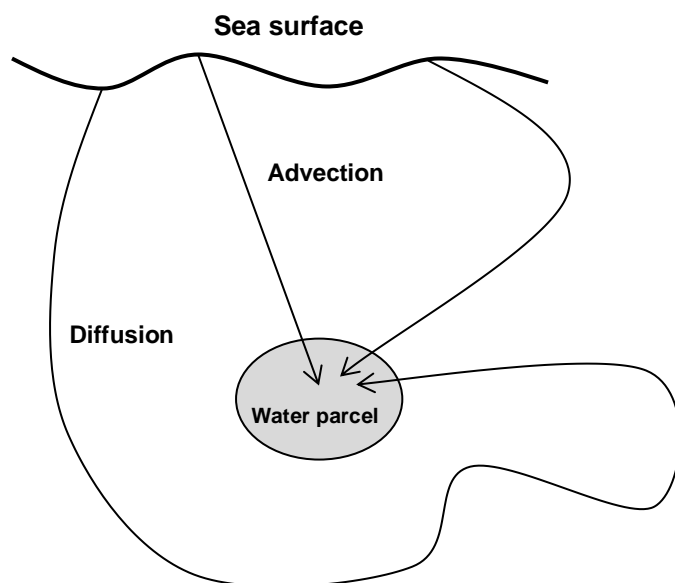


Figure 1.1. Schematic illustrating the “advection” and “diffusion” pathways of ocean ventilation by which fluid properties constituting a water parcel is transported in the ocean (Khatiwala et al., 2001).

Transient tracers can provide time information based on radioactive decay (radioactive transient tracers) or input function (chronological transient tracers). The radioactive transient tracers include tritium (^3H), argon-39 isotope (^{39}Ar) and radiocarbon (^{14}C), etc. Tritium has been applied as a transient tracer in the ocean, especially for shallow waters, since the 1970s but with weak signals recently (Jenkins, 1987, 1998, 1977; Jenkins et al., 2019). Radioactive isotope ^{39}Ar is an ideal tracer for old water masses and recent technological advancements have increased its feasibility of measurement in seawater (Ebser et al., 2018). Radiocarbon is a powerful transient tracer for very old waters, although with complex carbon dynamics (diluted and unstable atmospheric concentrations) and long air-sea equilibrium time (almost 10 years).

The chronological transient tracers include trichlorofluoromethane (CFC-11), dichlorodifluoromethane (CFC-12), 1,1,2-trichloro-1,2,2-trifluoroethane (CFC-113), carbon tetrachloride (CCl_4) and sulfur hexafluoride (SF_6), etc. CFC-11, CFC-113 and CCl_4 have now been

discarded after they were found to be degraded in seawater and/or able to be replaced (Bullister and Lee, 1995; Huhn et al., 2001; Roether et al., 2001). However, CFC-12 and SF₆ have been extensively used to interpret ventilation in the global ocean since the 1980s and the 1990s, respectively (Fine, 2011; Talley et al., 2016) based on their well-documented atmospheric histories (Bullister, 2015; Walker et al., 2000), feasibility of observation in seawater (Bullister and Wisegarver, 2008; Stöven and Tanhua, 2014; Vollmer and Weiss, 2002), well-established seawater solubility functions (Bullister et al., 2002; Warner and Weiss, 1985) and stability in warm seawaters as well as poorly oxygenated seawaters (Tanhua and Olsson, 2005).

CFC-12 and SF₆ have also been used to interpret ventilation in the Mediterranean Sea which is characterized by highly variable ventilation patterns both in time and space. However, most of the previous studies focus on changes in ventilation less than ten years in the Mediterranean Sea (Rhein et al., 1999; Roether et al., 2007; Roether et al., 1996; Schneider et al., 2014). Therefore, in this thesis (Fig. 1.2), temporal and spatial variability in the past three decades, with an emphasis on the recent changes, in deep ventilation of the Mediterranean Sea is interpreted based on long-term observations of CFC-12 and SF₆ (Manuscript I). Since a combination of multiple oceanic transient tracers can better interpret ventilation, hydrochlorofluorocarbons (HCFCs), hydrofluorocarbons (HFCs) and perfluorocarbons (PFCs), as the replacements of CFCs, are explored and evaluated as potential novel chronological transient tracers (HCFCs, HFCs, and PFCs) from four aspects: input function, seawater solubility (Manuscript II), feasibility of measurement and stability in seawater (Manuscript III). After the evaluation, the most promising novel transient tracers have been found. These potential alternative transient tracers need to be further evaluated before they are used to interpret ventilation in the Mediterranean Sea, and even in the global ocean.

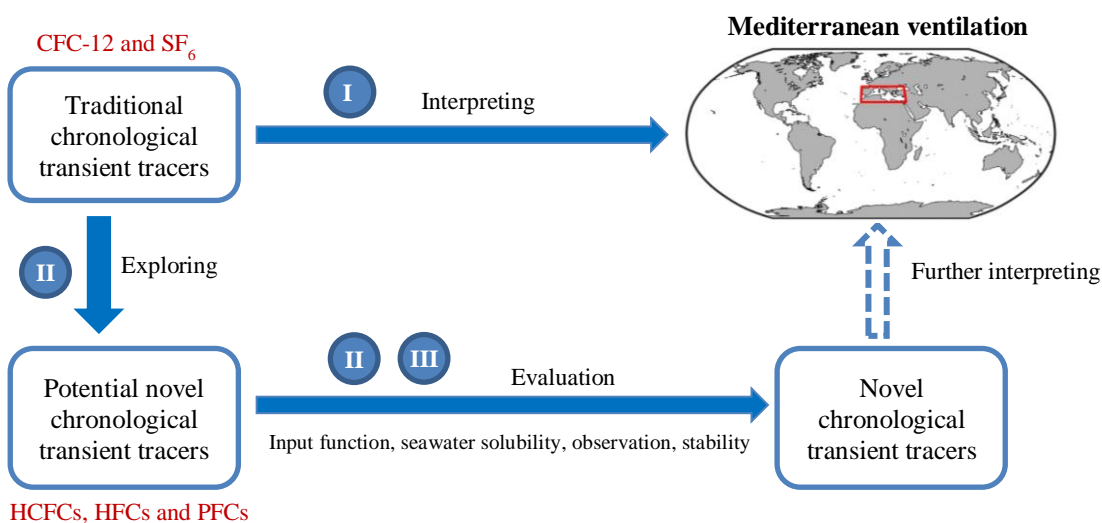


Figure 1.2. Logistic structure of the thesis. I, II and III represent the corresponding manuscripts.

Introductions to the traditional (CFC-12 and SF₆) and potential novel (HCFCs, HFCs and PFCs) chronological transient tracers and their interpreting methods, as well as background information on ocean ventilation and circulation in the Mediterranean Sea are reported in the following manuscripts. The used data sets include CFC-12 and SF₆ observations conducted during cruises M5/6, M31/1, Ura2, P234, Aegaeo98, Ura7, M44/4, M51/2, M84/3, ESAW2, CRELEV2016, TALPro2016, and MSM72 in the Mediterranean Sea, as well as HCFCs, HFCs and PFCs observations conducted during cruise MSM72 in the Mediterranean Sea and during cruise AL516 in the Baltic Sea. The sampling and measurement methodologies, specific data information and statistics are presented in the corresponding manuscripts.

References

- Bullister, J. L.: Atmospheric Histories (1765-2015) for CFC-11, CFC-12, CFC-113, CCl₄, SF₆ and N₂O, NDP-095, 1–23, https://doi.org/10.3334/CDIAC/otg.CFC_ATM_Hist_2015, 2015.
- Bullister, J. L. and Lee, B. S.: Chlorofluorocarbon-11 removal in anoxic marine waters, *Geophys. Res. Lett.*, 22, 1893–1896, <https://doi.org/10.1029/95GL01517>, 1995.
- Bullister, J. L. and Wisegarver, D. P.: The shipboard analysis of trace levels of sulfur hexafluoride, chlorofluorocarbon-11 and chlorofluorocarbon-12 in seawater, *Deep-Sea Res. Pt. I*, 55, 1063–1074, <https://doi.org/10.1016/j.dsr.2008.03.014>, 2008.
- Bullister, J. L., Wisegarver, D. P., and Menzia, F. A.: The solubility of sulfur hexafluoride in water and seawater, *Deep-Sea Res. Pt. I*, 49, 175–187, [https://doi.org/10.1016/S0967-0637\(01\)00051-6](https://doi.org/10.1016/S0967-0637(01)00051-6), 2002.
- Ebser, S., Kersting, A., Stöven, T., Feng, Z., Ringena, L., Schmidt, M., Tanhua, T., Aeschbach, W., and Oberthaler, M. K.: ³⁹Ar dating with small samples provides new key constraints on ocean ventilation, *Nat. Commun.*, 9, 5046, <https://doi.org/10.1038/s41467-018-07465-7>, 2018.
- Fine, R. A.: Observations of CFCs and SF₆ as ocean tracers, *Annu. Rev. Mar. Sci.*, 3, 173–195, <https://doi.org/10.1146/annurev.marine.010908.163933>, 2011.
- Huhn, O., Roether, W., Beining, P., and Rose, H.: Validity limits of carbon tetrachloride as an ocean tracer, *Deep-Sea Res. Pt. I*, 48, 2025–2049, [https://doi.org/10.1016/S0967-0637\(01\)00004-8](https://doi.org/10.1016/S0967-0637(01)00004-8), 2001.
- Jenkins, W. J.: ³H and ³He in the Beta Triangle: Observations of gyre ventilation and oxygen utilization rates, *J. Phys. Oceanogr.*, 17, 763–783, [https://doi.org/10.1175/1520-0485\(1987\)017<0763:AITBTO>2.0.CO;2](https://doi.org/10.1175/1520-0485(1987)017<0763:AITBTO>2.0.CO;2), 1987.
- Jenkins, W. J.: Studying subtropical thermocline ventilation and circulation using tritium and ³He, *J. Geophys. Res.: Oceans*, 103, 15817–15831, <https://doi.org/10.1029/98JC00141>, 1998.
- Jenkins, W. J.: Tritium-helium dating in the Sargasso Sea: A measurement of oxygen utilization rates, *Science*, 196, 291–292, <https://doi.org/10.1126/science.196.4287.291>, 1977.
- Jenkins, W. J., Doney, S. C., Fendrock, M., Fine, R., Gamo, T., Jean-Baptiste, P., Key, R., Klein, B., Lupton, J. E., Newton, R., Rhein, M., Roether, W., Sano, Y., Schlitzer, R., Schlosser, P., and Swift, J.: A comprehensive global oceanic dataset of helium isotope and tritium measurements, *Earth Syst. Sci. Data*, 11, 441–454, <https://doi.org/10.5194/essd-11-441-2019>, 2019.
- Khatiwala, S., Visbeck, M., and Schlosser, P.: Age tracers in an ocean GCM, *Deep-Sea Res. Pt. I*, 48, 1423–1441, [https://doi.org/10.1016/S0967-0637\(00\)00094-7](https://doi.org/10.1016/S0967-0637(00)00094-7), 2001.
- Rhein, M., Send, U., Klein, B., and Krahnemann, G.: Interbasin deep water exchange in the western Mediterranean, *J. Geophys. Res.: Oceans*, 104, 23495–23508, <https://doi.org/10.1029/1999JC900162>, 1999.
- Roether, W., Klein, B., and Bulsiewicz, K.: Apparent loss of CFC-113 in the upper ocean, *J. Geophys. Res.: Oceans*, 106, 2679–2688, <https://doi.org/10.1029/1999JC000079>, 2001.

- Roether, W., Klein, B., Manca, B. B., Theocharis, A., and Kioroglou, S.: Transient Eastern Mediterranean deep waters in response to the massive dense-water output of the Aegean Sea in the 1990s, *Prog. Oceanogr.*, 74, 540–571, <https://doi.org/10.1016/j.pocean.2007.03.001>, 2007.
- Roether, W., Manca, B. B., Klein, B., Bregant, D., Georgopoulos, D., Beitzel, V., Kovačević, V., and Luchetta, A.: Recent changes in eastern Mediterranean deep waters, *Science*, 271, 333–335, <https://doi.org/10.1126/science.271.5247.333>, 1996.
- Schneider, A., Tanhua, T., Roether, W., and Steinfeldt, R.: Changes in ventilation of the Mediterranean Sea during the past 25 year, *Ocean Sci.*, 10, 1–16, <https://doi.org/10.5194/os-10-1-2014>, 2014.
- Stöven, T. and Tanhua, T.: Ventilation of the Mediterranean Sea constrained by multiple transient tracer measurements, *Ocean Sci.*, 10, 439–457, <https://doi.org/10.5194/os-10-439-2014>, 2014.
- Talley, L., Feely, R., Sloyan, B., Wanninkhof, R., Baringer, M., Bullister, J., Carlson, C., Doney, S., Fine, R. A., and Firing, E.: Changes in ocean heat, carbon content, and ventilation: a review of the first decade of GO-SHIP global repeat hydrography, *Annu. Rev. Mar. Sci.*, 8, 185–215, <https://doi.org/10.1146/annurev-marine-052915-100829>, 2016.
- Tanhua, T. and Olsson, K. A.: Removal and bioaccumulation of anthropogenic, halogenated transient tracers in an anoxic fjord, *Mar. Chem.*, 94, 27–41, <https://doi.org/10.1016/j.marchem.2004.07.009>, 2005.
- Vollmer, M. K. and Weiss, R. F.: Simultaneous determination of sulfur hexafluoride and three chlorofluorocarbons in water and air, *Mar. Chem.*, 78, 137–148, [https://doi.org/10.1016/S0304-4203\(02\)00015-4](https://doi.org/10.1016/S0304-4203(02)00015-4), 2002.
- Walker, S. J., Weiss, R. F., and Salameh, P. K.: Reconstructed histories of the annual mean atmospheric mole fractions for the halocarbons CFC-11, CFC-12, CFC-113, and carbon tetrachloride, *J. Geophys. Res.*, 105, 14285–14296, <https://doi.org/10.1029/1999jc900273>, 2000.
- Warner, M. J. and Weiss, R. F.: Solubilities of chlorofluorocarbons 11 and 12 in water and seawater, *Deep Sea Res. Part A. Oceanogr. Res. Pap.*, 32, 1485–1497, [https://doi.org/10.1016/0198-0149\(85\)90099-8](https://doi.org/10.1016/0198-0149(85)90099-8), 1985.

Manuscript I

Recent changes in deep ventilation of the Mediterranean Sea; evidence from long-term transient tracer observations

Pingyang Li and Toste Tanhua: Recent changes in deep ventilation of the Mediterranean Sea; evidence from long-term transient tracer observations, *Frontiers in Marine Science*, in review, 2020.

Abstract. The Mediterranean Sea is a small region of the global ocean but with a very active overturning circulation that allows surface perturbations to be transported to the interior ocean. Understanding of ventilation is important for understanding and predicting climate change and its impact on ocean ecosystems. To quantify changes of deep ventilation, we investigated the spatiotemporal variability of transient tracer (i.e. CFC-12 and SF₆) observations combined with temporal evolution of hydrographic and oxygen observations in the Mediterranean Sea from 13 cruises conducted during 1987-2018, with emphasize on the update from 2011 to 2018. Spatially, both the Eastern and Western Mediterranean Deep Water (EMDW and WMDW) show a general west-to-east gradient of increasing salinity and potential temperature but decreasing oxygen and transient tracer concentrations. Temporally, stagnant and weak ventilation is found in most areas of the EMDW during the last decade despite the prevailing ventilation in the Adriatic Deep Water between 2011 and 2016, which could be a result of the weakened Adriatic source intensity. The EMDW has been a mixture of the older Southern Aegean Sea dense waters formed during the Eastern Mediterranean Transient (EMT) event, and the more recent ventilated deep-water of the Adriatic origin. In the western Mediterranean basin, we found uplifting of old WMDW being replaced by the new deep-water from the Western Mediterranean Transition (WMT) event and uplifting of the new WMDW toward the Alboran Sea. The temporal variability revealed enhanced ventilation after the WMT event but slightly weakened ventilation after 2016, which could be a result of combined influences from the eastern (for the weakened Adriatic source intensity) and western (for the weakened influence from the WMT event) Mediterranean Sea. Additionally, the Mediterranean Sea is characterized by a Tracer Minimum Zone (TMZ) at mid-depth of the water column attributed to the rapid deep ventilation so that the TMZ is the slowest ventilated layer. The TMZ ventilates stronger in the western basin spatially but in the eastern basin during the past ~30 years, which highlights the strong influence of the EMT than the WMT event to the intermediate layer of the Mediterranean Sea.

1 Introduction

Ocean ventilation is an important process in the Earth system that transports ocean surface properties, such as salinity, heat, CO₂ and dissolved gases to the interior ocean. Knowledge of the temporal and spatial variability of ocean ventilation is essential for understanding and predicting the response of the

Earth system to global climate change. As a microcosm of the global ocean where climate change can be observed on a shorter time-scale (Schroeder et al., 2016), the Mediterranean Sea (Fig. S1) is well ventilated but with highly variable ventilation patterns both in time and space. Such ventilation patterns can directly be illustrated by, for instance, long-term observations of transient tracers. Transient tracers are taken up by the ocean at the air-sea interface and transferred into the deep ocean by the Deep/Dense Water Formation (DWF) through convection or subduction processes. There are four main DWF areas in the Mediterranean Sea: the Adriatic Sea, Southern Aegean Sea (Cretan Sea) and the Rhodes Gyre in the eastern Mediterranean basin (EMed), and the Gulf of Lions in the western Mediterranean basin (WMed). The deep water exchanges between the two basins are separated by the Strait of Sicily, which leads to a relative independent deep water circulation in each basin.

In the EMed, the Adriatic Sea used to be the main DWF region prior to the late 1980s (Roether et al., 1996). Interactions between Levantine Intermediate Water (LIW) and water masses from the Northern Adriatic Sea mix and get preconditioned by heat loss and wind stress (Artegiani et al., 1996a; 1996b), creating high saline waters that dense during winter cooling, and leading to the formation of the Adriatic Deep Water (AdDW). After deep convection, the AdDW flows over the Strait of Otranto sill into the Ionian Sea and then spreads southward and eastward to form the Eastern Mediterranean Deep Water (EMDW). However, the formation of the AdDW was in the “stagnation phase” from 1987 to 1999 (Manca et al., 2002; Roether et al., 2007). In the early 1990s, the Eastern Mediterranean Transient (EMT) event took place. The event marked the dominant deep water source shift from the Adriatic Sea to the Aegean Sea and characterized as the massive dense water output from the Aegean Sea (Klein et al., 1999; Roether et al., 1996) triggered by the heat loss from the extremely cold winter in 1992-1993 (Roether et al., 2007) and high salinity (Velaoras et al., 2017). The estimated DWF rate in the Aegean Sea for the period 1989-1995 was three times higher than that of the Adriatic Sea (Lascaratos et al., 1999). Very dense water from the Aegean Sea filled the EMed and blocked the intrusion of the Adriatic-originated water into the Levantine basin (Akpınar et al., 2016). The Aegean-originated water dominated in the Levantine Sea in the 1990s also by shading the DWF in the Rhodes Cyclonic Gyre area (Malanotte-rizzoli and Hecht, 1988). However, in 1999, the water from the Aegean source was not dense enough to reach the bottom of the adjacent Ionian and Levantine basins but ventilated at 1500-2500 m depth (Theocharis et al., 2002). In the 2000s, the Aegean source was still characterized by dense water outflow but getting weak (Velaoras et al., 2014). A reversal of the dominant source for the DWF in the EMed took place between 1999 and 2002 when the Adriatic deep water formation restarted, and the Adriatic Sea returned to be again the major source region in the EMed (Cardin et al., 2015; Hainbucher et al., 2006; Klein et al., 2000; Rubino and Hainbucher, 2007). In 2012, the extremely cold winter triggered another strong deep water formation in the Adriatic Sea (Gačić et al., 2014).

In the WMed, the Western Mediterranean Deep Water (WMDW) forms in the northwestern Mediterranean, mainly in the Gulf of Lions. Open-ocean deep convection, combined with occasional

dense shelf water cascading, is the major contributor to the thermohaline circulation and ventilation in the source regions (Durrieu de Madron et al., 2013; Houpert et al., 2016; Testor et al., 2018). In addition, the EMT event has influenced the DWF processes in the Gulf of Lions in winter (Schroeder et al., 2006). Extensive DWF started from 2004-2006 and is known as the Western Mediterranean Transition (WMT) event (Schroeder et al., 2010; Schroeder et al., 2008). The event is thought to be triggered mainly by the atmospheric forcing in the WMed and the lateral advection of anomalously salty and warm LIW because of increased heating and evaporation in the EMed (Medoc Group, 1970; Schroeder et al., 2016; Schroeder et al., 2010). The WMT event caused the structure of intermediate and deep layers abruptly changed in the WMed and a near-complete renewal of the WMDW (Schneider et al., 2014). In the Tyrrhenian Sea, the situation is a little bit different. Beneath the LIW, the transitional EMDW (tEMDW, a mixture of LIW and EMDW from the EMed) mix with the water in the Tyrrhenian Sea and settles between 600 and 1500 dbar (Sparnocchia et al., 1999). Below the tEMDW, WMDW enters the Tyrrhenian Sea (Schroeder et al., 2016). The mixture of partly tEMDW and WMDW forms the Tyrrhenian Deep Water (TDW) with a core depth deeper than 1500 dbar (Astraldi et al., 2002; Buffett et al., 2017).

As the area separating the EMed and WMed, the Strait of Sicily is composed of the surface Modified Atlantic Water (MAW) flowing eastward, the lower LIW and bottom tEMDW flowing westward (Astraldi et al., 1996; Astraldi et al., 2002; Sparnocchia et al., 1999).

Transient tracers have been used to understand ventilation and circulation processes, and determine water mass characteristics in the Mediterranean Sea in multiple studies. For example, the vertical and spatial distributions of transient tracers have been described in the EMed by studies (2007; Roether et al., 1996) and in the WMed by Rhein et al. (1999) to quantify ventilation timescales. They have also been used to identify the water mass structures and distributions by combined with analysis of hydrographic properties such as salinity and temperature (Cardin et al., 2015; Theocharis et al., 2002), as well as some biogeochemical properties such as dissolved oxygen, silicate and nitrate (Klein et al., 2000; Klein et al., 1999). In addition, transient tracers have been used to estimate the anthropogenic carbon content of the water (Schneider et al., 2010) by applying the Transit Time Distribution (TTD) concept (Stöven and Tanhua, 2014; Waugh et al., 2003). Therefore, a combination of transient tracers (CFC-12, SF₆, etc.), hydrographic properties (salinity, temperature, density, etc.) and oxygen can characterize ventilation processes on the basis of the water mass distributions. Roether et al. (2007) and Cardin et al. (2015) both expressed that the water mass structures of the EMed in 2001 and 2011 were far from the pre-EMT status, but Cardin et al. (2015) also concluded that the 2011 observations possibly indicate a slow return to the pre-EMT status.

The primary goal of this study is to investigate the temporal and spatial variability (with an emphasis on the recent changes) in deep and intermediate ventilation of the Mediterranean Sea based on transient tracer (CFC-12 and SF₆) observations. To the end, we address the spatiotemporal distributions of transient tracer (CFC-12 and SF₆) concentrations as well as the temporal evolution of

potential temperature-salinity (Θ - S) diagrams and depth-profiles of CFC-12 and SF₆ concentrations, salinity, potential temperature, potential density and apparent oxygen utilization in pressure (CFC-12/SF₆/S/PT/ σ_θ /AOU vs. P) between 1987 and 2018. Previously, Schneider et al. (2014) discussed the temporal variability of ventilation in the Mediterranean Sea for the timeframe 1987-2011. The authors studied well-defined boxes in each basin and discussed the averaged vertical profiles of salinity, temperature, oxygen, CFC-12 concentration, CFC-12 tracer age, CFC-12 mean age, tritium/helium age and tritium mean age. In the study by Schneider et al. (2014), they carried out a comparison of averaged profiles from different years within relatively large boxes, whereas, in this study, we compare profiles in specific sampling stations in overlaid or close vicinity to each other (in small boxes). For this approach, there is a risk that small-scale variability, such as eddies, will bias the comparison, whereas for large boxes real variability within the box can bias the comparison.

2 Observations and methods

2.1 Observations from cruises

Table 1 lists the cruises used in this work from which we have transient tracer observations. Sampling sites for each cruise are shown in Fig. 1. Seawater samples for CFC-12 and SF₆ were measured either on board from syringe sampling or ashore from flame-sealed glass ampoules. For cruises in 1987-2001, CFC-12 and CFC-11 were observed, although we focus on the CFC-12 observations due to no recent CFC-11 observations, whereas for cruises in 2011–2018 both CFC-12 and SF₆ data are considered. More details on measurement methods, precisions and accuracies for the observations can be found from the correspondence references and/or cruise reports (Table 1). The observations of CFC-12 and SF₆ from four cruises during the years 2016–2018 are reported here for the first time. The measurement methods can refer to the corresponding cruise reports and/or Stöven and Tanhua (2014).

2.2 Methods for assessing tempo-spatial variability

The Transit Time Distribution (TTD) model describes the propagation of tracer boundary conditions from the ocean surface into the interior based on the Green's function (Hall and Plumb, 1994) and is often used to assess ventilation time-scales. However, the ventilation of the Mediterranean Sea is time-variant, making it difficult to apply the TTD concept. Therefore, in this study, we used (CFC-12 and SF₆) concentrations (in ppt, part per trillions) to assess the historical evolution of ventilation and involved hydrography data to support conclusions of variability in ventilation patterns.

We start by discussing the tempo-spatial distributions of ventilation in the Mediterranean Sea by analyzing CFC-12 and SF₆ concentration sections at roughly the same locations in the EMed and WMed separately. The equilibrium concentrations (in ppt) of the trace gases into the seawater are chosen since their dependence on the salinity and temperature are removed. As a second step, we consider the temporal variability of ventilation by comparing the correlations of potential temperature

and salinity (Θ - S diagrams), as well as depth-profiles of transient tracer concentrations (CFC-12 and SF₆), salinity (S), potential temperature (PT or Θ in °C), potential density (σ_θ in kg m⁻³ referenced to 0 dbar pressure) and apparent oxygen utilization (AOU in $\mu\text{mol kg}^{-1}$) for stations within each box in Fig. 1.

2.3 Tracer age difference

The age of a water parcel is defined as the time elapsed since it left the mixed layer where it was in contact with the atmosphere and was transported into the ocean interior. The concept of tracer age does not consider mixing, which is unrealistic but it provides a framework to compare the ventilation time-scale at one location over time. The atmospheric histories of CFC-12 and SF₆ overlay when the atmospheric history record of SF₆ shifted back 14 years (Tanhua et al., 2013b). Therefore, the tracer age estimated by SF₆ should equal to that by CFC-12 based on measurements of CFC-12 taken 14 years earlier in the same region in a steady-state situation, independent of mixing patterns. Inspired by this, Schneider et al. (2014) compared the tracer ages estimated by SF₆ in 2011 and CFC-12 in 1997/98. However, as seen from the vertical dash line in Fig. S2, the (shifted) atmospheric histories of CFC-12 and SF₆ started to diverge after 2005, which means that the time shift of 14 years doesn't work well for the two tracers after this time. In other words, comparison of tracer age between SF₆ and CFC-12 with a time gap of 14 years still works for deep and intermediate waters, but not so well for more recently ventilated waters.

For this study, we were able to find locations where CFC-12 and SF₆ were measured in 2001 and 2016, respectively in the northern Cretan Passage and the Tyrrhenian Sea. The averaged tracer ages are calculated by first interpolating the individual profiles to standard depths and then by taking the arithmetic mean of the interpolated profiles (Tanhua et al., 2010). The bias created by the changing growth rate of SF₆ from 2015 (time shift of 14 years) and 2016 is expected to be small (the standard deviation is 0.35 %) based on the linear increasing atmospheric mole fraction of SF₆ (Fig. S2).

3 Spatial and temporal distributions of properties in the Mediterranean Sea

3.1 Spatial distributions of CFC-12 and SF₆ in the EMed

We show vertical sections of CFC-12 concentrations for 1987, 1995, 1999, 2001, 2011 and 2018, and SF₆ concentrations for 2011 and 2018 to illustrate the spatial evolution of tracer distributions during the last ~30 years in the Eastern Mediterranean Sea (Fig. 2). For more detailed discussions on individual datasets, we refer the reader to previous studies shown in Table 1. In the following, we describe the observations in relation to the temporal evolution.

1987. This data set represents the only pre-EMT transient tracer observation for the Mediterranean Sea (Fig. 2a). The high CFC-12 concentration in the EMDW in the western Ionian Sea is a signal of recently formed deep water from the Adriatic Sea, with gradually decreasing CFC-12 concentrations

eastward in the EMDW. The layer with the oldest water and CFC-12 concentrations less than ~30 ppt marks the Tracer Minimum Zone (TMZ) at the depth of 1200–2800 dbar. This zone stretches from the Ionian Sea to the central Levantine basin where it reached the near-bottom. The low CFC-12 concentrations indicate an absence of direct ventilation for the deep and intermediate depth ranges in the east. An area of elevated CFC-12 concentration water was centered at ~700 dbar depth in the northern Cretan Passage originated from the Aegean Sea, which implies that newly ventilated Cretan Intermediate Water (CIW) spread into the water below the LIW in the western Levantine basin and the Ionian Sea (Schlitzer et al., 1991). Thus, the EMDW below 1200 dbar depth was mainly fed by the Adriatic-originated water and the intermediate layer between 200 and 1200 dbar fed by CIW and LIW in 1987.

1995. The Meteor cruise in 1995 presents the first comprehensive transient tracer observations after the EMT event (Fig. 2b) conducted in the framework of the POEM (Physical Oceanography in the Eastern Mediterranean) project. The CFC-12 concentrations in 1995 are dramatically different from those in 1987. The youngest water below ~500 dbar was found in the northern Cretan Passage bottom water with a CFC-12 concentration of ~220 ppt, a signal of very strong ventilation since 1987. The EMDW related to the Adriatic-derived water was still found in the western part of the section, with a CFC-12 concentration of ~200 ppt, higher than that in 1987. The CFC-12 concentration in the oldest water (the TMZ) became younger and the TMZ split into two main cores: the western and eastern cores with CFC-12 concentrations of ~90 ppt and ~60 ppt, respectively. The CFC-12 concentration in the TMZ thus increased significantly from 1987 to 1995. The TMZ in 1995 had a narrower depth range and was centred at a shallower depth, which has been interpreted as uplifted bottom waters by intruding Cretan Deep Water (CDW) (Roether et al., 1996). Noting that the oldest water in 1987 was replaced with the younger water, which indicated the strong renewal of water in the EMed in the early 1990s, as reported in previous studies (Roether et al., 2007; Roether et al., 1996; Theocharis et al., 2002).

1999 and 2001. The double core TMZs still exist at the time, but with some changes. In the Ionian Sea, the CFC-12 concentration increased from ~90 ppt in 1995 to ~120 ppt in 1999/2001 (Fig. 2cd). There is also a tendency for the TMZ to displace from the western to the eastern Ionian Sea. In the Levantine basin, the CFC-12 concentrations in the TMZ increased to ~70/80 ppt in 1999/2001 and shoaled from ~2000 dbar to ~1000 dbar. This was accompanied by a diminished thickness of the TMZ in 1999/2001 as the recently formed EMDW from the EMT event advected eastwards along with the deeper layers of the Levantine basin. On the other hand, there is a more obvious signal of high transient tracer concentration on the western sloop in 2001 than in 1999, which may suggest an Adriatic source of deep water.

2011. The spatial distribution of CFC-12 concentrations in 2011 (Fig. 2e) is quite different from the one in 2001. The new Adriatic-derived water is clearly observed in the bottom water of the western Ionian Sea in 2011 with a CFC-12 concentration of ~270 ppt and an SF₆ concentration of ~2.4 ppt (Fig.

2g). The TMZs still existed at roughly the same depth (~1000 dbar) as in 2001, but with significantly higher CFC-12 concentrations: ~160 ppt in the eastern Ionian Sea and ~120 ppt in the Levantine basin. However, the TMZ as defined by the SF₆ concentrations is better defined with ~0.6 ppt in the Levantine basin at slightly larger depth, reflecting the different input functions of the two tracers; SF₆ being more sensitive to more recent changes in ventilation.

2018. Although the 2018 cruise was unable to sample the Levantine basin, there is evidence that the extent of the Adriatic-derived water in the EMDW in the western Ionian Sea expanded eastward and upward from 2011 to 2018 (Fig. 2f). The spatial distribution of SF₆ concentrations in 2018 was generally similar to that of CFC-12 above 500 dbar, but with significant differences below this depth (Fig. 2h). Focusing on the Ionian Sea and the northern Cretan Passage, the CFC-12 concentrations of the two cores of the TMZ in 2018 are ~150 ppt in the northern Cretan Passage and ~170 ppt in the eastern Ionian Sea, which are slightly higher than those in 2011. However, for SF₆, two cores are found with ~0.9 ppt in the north-western and north-eastern Cretan Passage, which are slightly lower than those in 2011. The TMZ is more clearly presented as two cores in 2018 than in 2011; possibly associated with flow well ventilated through the Antikythera strait as the transient tracer profiles just west of the strait (in 2018) show enhanced concentrations at intermediate levels down to 1200 dbar depth. The oldest water was found at ~1500 dbar and 1000-3000 dbar in the northern Cretan Passage defined by CFC-12 and SF₆, respectively in both 2011 and 2018. The transient tracer concentrations in the western Ionian deep Sea decreased from ~270 ppt to ~240 ppt for CFC-12 and from ~2.4 ppt to ~1.9 ppt for SF₆ from 2011 to 2018, implying the weakened Adriatic source intensity. The relative higher SF₆ concentrations shown in the deep layer but not in the bottom layer suggest that the water from the Adriatic source was no longer dense enough to reach the bottom of the Ionian Sea but ventilated the 2000-3000 dbar depth layer between 2011 and 2018. The larger difference of spatial distribution of CFC-12 and SF₆ concentrations took place in 2018 than in 2011, implied the weakened ability of CFC-12 in interpreting ventilation in the Mediterranean Sea considering its decreasing atmospheric history.

3.2 Temporal variability of properties in the EMed

3.2.1 Adriatic Sea

We have a time-series of properties from 1987 to 2016 in the Adriatic Sea (Fig. 3). The time-series show nearly identical CFC-12 concentrations in the deep-water layer (below 600 dbar) dominated by AdDW for the time from 1987 to 1999, while there is a sharp increase in the CFC-12 concentration of ~100 ppt from 1999 to 2011 and another increase of ~100 ppt from 2011 and 2016. A similar increase during 2011-2016 is also found for the SF₆ concentration in the magnitude of ~3 ppt. For other properties in the deep layer, the potential temperature (PT) slightly decreased from 1987 to 1995, and then gradually increased up to 2016. During the same time, the salinity (S) gradually increases, with a rapid increase in salinity of ~0.1 and PT of ~0.5 °C between 1999 and 2011. The high near-bottom

salinities in 2011 are seen through the whole deep layer in 2016. The potential density (σ_θ) generally decreased from 1987 to 1999 and increased to 2011 followed by a decrease to 2016, following mainly compensating trends in S and PT. There is a weak and variable trend for apparent oxygen utilization (AOU) to increase between 1987 and 2016. Compared to the obviously increased salinity and PT (~ 0.15 and ~ 0.5 °C) from 1995 to 2011/16, similar AOU values are found in 1995, 2011 and 2016 in the near-bottom layer. All these changes support strong ventilation in the Adriatic Sea during the last 15-20 years (1999-2016) with the formation of new AdDW with higher S and PT.

3.2.2 Cretan Sea

Figure 4 shows that CFC-12 concentrations, salinity, PT and σ_θ in the Cretan Sea are relatively higher than those in other areas in the Mediterranean Sea. In the deep-water layer (below ~ 1300 dbar), largely increased salinity, σ_θ and CFC-12 concentrations (~ 70 ppt) between 1987 and 1995 are in agreement with the period of enhanced ventilation related to the EMT event, when compared with the nearly unchanged CFC-12 concentrations in the AdDW (Fig. 3) for the same period. From 1995, the Aegean deep-water source was getting weaker as indicated by the continuously decreased salinity, σ_θ and oxygen (increased AOU) in the Cretan Deep Water (CDW) from 1995 to 2018 (Fig. 4). Although with weakened Aegean source intensity, the CDW still ventilated to 2011. The stagnant/weakened ventilation after 2011 can be seen by the fact that CFC-12 concentrations in 2018 are slightly lower than those in 2011, although SF₆ concentrations show the opposite change, related to decreasing CFC-12 and increasing SF₆ atmospheric mole fractions.

Above the CDW, a characteristic Θ -S inversion at 300 – 1300 dbar depth (Fig. 4) is thought to be the core depths of the Transitional Mediterranean Water (TMW). The depth of the inversion is also the depth of “local CFC-12/salinity/PT/oxygen minimum”, indicating infrequent (weak) ventilation (renewal).

3.2.3 Ionian Sea

Northern Ionian Sea. For this area, we show clusters of stations from the western and eastern parts of the basin south of Otranto Strait. For the deep layer (below ~ 1200 dbar) in the north-western Ionian Sea (Fig. 5), CFC-12 concentrations, as well as salinity and PT, continuously increased from 1987 to 2011 but with a small decrease below ~ 2000 dbar from 1997 to 2011 for the latter two properties, while AOU decreased from 1987 to 1995 then increased to 2011. In the deep layer of the north-eastern Ionian Sea, CFC-12 concentrations continuously increased from 1987 to 1997 but with a small decrease to 2018, while salinity and PT increased from 1987 to 1995 but decreased to 2018, and AOU showed the opposite change. The dramatic increase of salinity and PT found between 1987 and 1995 for the north-eastern Ionian Sea, but between 1995 and 1997 for the north-western Ionian Sea could be related to the spreading direction and speed of the Aegean source. There was a large difference of CFC-12 concentrations between the north-western and north-eastern Ionian deep waters in 1987,

indicating a larger Adriatic outflow that tends to follow the western slope. However, the similar CFC-12 concentrations are found between the two deep waters in 1995/97, implying different sources.

Western and Central Ionian Sea. In the western and central Ionian Sea (Fig. 6), CFC-12 concentrations increased significantly from 1987 to 1995, constant levels up to 2001 and another “jump” in concentrations to 2011, that remained essentially constant in 2018, although the SF₆ concentrations slightly decreased from 2011 to 2018 in the layer below ~3000 dbar. Different from the transient tracers, the S/T evolution is characterized by a large increase from 1987 to 1995, the year with the highest S/T of the time-series. In 1999, the S/T decreased significantly but did not reach the pre-EMT levels, and then gradually increased through the time-series up to 2011/18. The AOU story is again slightly different. The AOU decreased from 1987 to 1995, dramatically increased to 1999, decreased to 2001 and then slightly increased to 2018 below 1400 dbar. The stepwise increase and the following decrease occasionally in CFC-12 concentration suggest variable ventilation. For instance, the increased CFC-12 concentrations after 1987 and 2001 indicate enhanced ventilation during the 1987-1995 and 2001-2011 time-periods, stagnated ventilation during 1995-2001 and possibly slightly weakened ventilation in the deep layer from 2011 to 2018 for the western and central Ionian Sea. Similarly, the increase of AOU in 2011-2018 supports the weakened ventilation in the deep layer. The dramatically Θ -S inversion and increased salinity and PT in 1995 found in the central Ionian Sea but not in the western Ionian Sea are related to the EMT event. The difference of properties in the deep layer between the western and central Ionian Sea in 1995 are ~30 ppt for CFC-12 concentrations, ~0.1 for salinity, ~0.3 °C for PT and 10-15 $\mu\text{mol kg}^{-1}$ for AOU.

Eastern Ionian Sea. We have a time-series of 6 occupations from 1987 to 2018 in the eastern Ionian Sea (Fig. 7). The time-series show CFC-12 concentrations with little differences (~50 ppt) for the time from 1995 to 2018 compared to its dramatic increase (~160 ppt) from 1987 to 1995 related to the EMT event. A similar increase took place for other properties, such as salinity, PT and σ_{θ} from 1987 to 1995, but this was followed by a relaxation towards pre-EMT conditions, although this condition is not reached. From 2001 to 2011, salinity and PT continuously decreased but CFC-12 concentrations, σ_{θ} , and AOU increased. As to the time range 2011-2018, properties in the two years showed similar values in general. In summary, dramatically enhanced ventilation is observed from 1987 to 1995 followed by nearly stagnated ventilation up to 2018 in the eastern Ionian Sea.

3.2.4 Northern Cretan Passage

We have a time-series of 8 occupations from 1987 to 2018 in the northern Cretan Passage (Fig. 8). Similar to that in the eastern Ionian Sea, the time-series show CFC-12 concentrations with little differences (~20 ppt) for the time from 1995 to 2018 in the layer below ~2500 dbar compared to its dramatic increase (~200 ppt) from 1987 to 1995 related to the EMT event and strong ventilation. A dramatic increase also took place for other properties, such as salinity (~2.0), PT (~0.55 °C) and σ_{θ} (~0.05 kg m^{-3}) but decrease for AOU (~25 $\mu\text{mol kg}^{-1}$) from 1987 to 1995, as well as salinity, PT and

σ_θ gradually decrease from 1995 to 2011. The gradual but small decrease of CFC-12 concentrations from the 1990s to 2011 indicates nearly stagnant ventilation after 1995. The decreased amplitude of Θ -S inversions between the EMDW of old Adriatic origin and that of Aegean origin from 1995 to 2018 illustrates the weakened Aegean source intensity after 1995 and the erosion of the EMT deep water. Although there is a gradual change in S/T after 1995 towards pre-EMT conditions, there is no change in CFC-12 indicating that the water that mixes with the EMT induced deep water is ventilated at a similar time scale. Similarly, AOU generally increased from 1995 to 2011 after its decrease from 1987 to 1995. For the time range 2011-2018, properties showed various and small changes that can be attributed to local variability. Significantly, AOU increased from 2011 to 2018 supporting slow ventilation.

From the perspective of the tracer age difference (Fig. S3a), the 2001 profile in the northern Cretan Passage represents the post-EMT situation, while the 2016 one represents the combined influence of remnant Aegean and new Adriatic sources. Tracer ages estimated from CFC-12 in 2001 are lower than those estimated from SF₆ in 2016 in the deep layer, supporting the stagnant ventilation in this area during that ~15 years.

3.2.5 Levantine basin

Here we present two areas in the Levantine basin, east of Crete and west of Cyprus, where two Θ -S inversions have developed since 1987. The first inversion appeared in the mid-depth (1000-1800 dbar) in the 1995-2011 time-periods. The second inversion was found near-bottom in 2011, indicating that the influence of the new Adriatic-originated water has been spread to the Levantine basin in 2011.

Increasing CFC-12 concentrations in the EMDW in the Levantine basin below ~1800 dbar from 1987 to 2011 indicates strong ventilation between 1987 and 1999 and slow ventilation after that (Fig. 9). The dramatic change of properties took place between 1987 and 1995 for the western Levantine basin but up to 1999 for the central Levantine basin, consistent with the spreading of the Aegean source. A similar delay of influence took place in the following years. For example, larger differences of CFC-12 concentrations were observed between 1999 and 2001 in the western Levantine but between 2001 and 2011 in the central Levantine. For other properties below ~1800 dbar, salinity, PT and σ_θ also showed increasing trends from 1987 to 1999 with the exception of 1998. After 1999, the trend continued in the deep layer, but with a slight reversal in the near-bottom layer from 2001. As a consequence of the influence of the EMT event, AOU decreased from 1987 to 1995 but increased to 1999, then decreased up to 2001 below ~500 dbar.

3.3 Temporal variability of properties in the Strait of Sicily

The Strait of Sicily is the relatively shallow area connecting the western and eastern Mediterranean basins. In the deep-water layer (below ~600 dbar), the concentration of CFC-12 shows a generally increasing trend after a small decrease between 1987 and 1995 (Fig. 10), as can be expected from the transient of CFC-12 in the atmosphere. The salinity and PT also decreased slightly from 1987 to 1995

and then steadily increased to 2001. Afterward, there is a significant increase in salinity and PT during the rather long time-period up to 2018. The simultaneous changes in both PT and salinity tend to compensate each other in density space, but the overall effect is an increase in density from 1987 to 1995, steady density to 2001 and then decreased density in 2018, which is approaching the lower density found in 1987. The AOU shows a slightly different pattern, with similar concentrations from 1987 to 1995, significantly higher values in 1999 and then lower AOU to 2001/2018.

3.4 Spatial distribution of CFC-12 and SF₆ in the WMed

Sections of the vertical distribution of CFC-12 concentrations in the WMed for 1995, 1997, 2001, 2011 and 2018, and SF₆ concentrations for 2018 are presented in Fig. 11. Similar to the EMed, the main feature of the transient tracer concentration is a TMZ centered at ~1000 dbar depth. In the deeper layer, high concentrations of CFC-12 found in the bottom waters near the Sardinia Channel in 1995 is maybe not that significant considering the limited number of observations, which is supported by the CFC-11 concentrations in 1997 (Rhein et al., 1999). In 2001, the bottom tracer concentrations near the Sardinia Channel have slightly increased to ~200 ppt, but the limited horizontal extent of that section limits the interpretation to the eastern part. Thus, the CFC-12 concentrations in the deep water changed slowly in the second half of the 1990s and the early 2000s attributed to the weak local source, as can be expected from a transient tracer in a steady-state ventilation scenario. Subsequently, due to the influence of the WMT event that started in winter 2004/05, the situations in 2011 and 2018 are different with significantly higher CFC-12 concentrations (260 – 290 ppt) that tend to be higher in the western part of the WMed, as opposed to the higher concentrations in the eastern part in the decade prior to 2001. The elevated CFC-12 concentrations observed in the western WMed bottom water in both 2011 and 2018 revealed the intrusion of the new WMDW toward the Alboran Sea. However, the slightly increased CFC-12 concentrations from 2011 to 2018 in the WMed, especially in the bottom water, are probably a result of the weakened influence of the WMT event during this period. The spatial distributions of CFC-12 and SF₆ concentrations in the WMed deep layer in 2018 (Fig. 11ef) are generally similar with three cores of higher concentrations in the WMed bottom waters.

3.5 Temporal variability of properties in the WMed

3.5.1 Tyrrhenian Sea

Although the Tyrrhenian Sea is influenced by both the EMed and WMed, no Θ -S inversions are observed in the Tyrrhenian Deep Water (TDW) during the last three decades (Fig. 12a), which is significantly different from the cases in the two main basins. The small change in the Θ -S diagrams from 1997 to 2018 indicated the apparent synchronous change of salinity and PT, and the influence of water masses from EMed and WMed to the Tyrrhenian Sea is not strong enough to lead to the inversions.

The CFC-12 concentrations increased dramatically (~100 ppt) between 1987 and 1997 in the deep-water layer (below ~1500 dbar) in the Tyrrhenian Sea (Fig. 12). This was followed by nearly constant concentrations between 1999 and 2001. In 2011, the increased transient tracer (CFC-12 and SF₆) concentrations in the TDW showed enhanced ventilation attributed to the combined influences from the LIW, EMDW, and WMDW, especially the WMT event started from 2004-2006. In the 2010s, the salinity in the TDW is similar in 2011, 2016 and 2018, but with increased CFC-12 concentrations and σ_θ from 2011 to 2016/18. Although the increase of SF₆ concentrations in the TDW below 2000 dbar from 2011 to 2016/18 is consistent with the increased atmospheric SF₆ concentrations, the less obvious increase in CFC-12 concentrations at the same depths can be explained by intense ventilation in the TDW driven by the WMT event considering the decreasing CFC-12 concentrations in the atmosphere. From 2016 to 2018, SF₆ concentrations should increase in the TDW considering the increasing SF₆ atmospheric mole fractions and steady-state ventilation. However, the steady SF₆ concentrations and decreasing CFC-12 concentrations suggest a slowdown of the ventilation, although the changes are small for such a short-time-interval. For other properties, salinity, PT, and σ_θ in the TDW largely increased from 1987 to 1997. Subsequently, σ_θ decreased slightly to 1999 and 2001, and then increased somewhat to 2011 and significantly to 2016/18. This increase in density is mainly driven by increased salinity, and somewhat compensated by increasing PT. AOU increased significantly from 1987 to 1999, decreased to 2001, increased to 2011, slightly decreased to 2016 and then increased to 2018. The changes in AOU support the interpreted results of ventilation by transient tracers.

From the perspective of the tracer age difference (Fig. S3b), minor changed tracer ages in the Tyrrhenian Sea between 2001 and 2016 are found at the depth below ~1700 dbar, which suggests steady-state ventilation. Such a situation may be attributed to the counterbalance of the advective influence of the WMT event, the TDW and the tEMDW. The large 15 years decrease of tracer ages between ~500 and ~1700 dbar may be associated with the input of the LIW and the tEMDW from the EMed because of the influence of the new Adriatic source. A similar tracer age decrease above the deep layer is found in the south Liguro-Provençal basin between 1997 and 2011 (Schneider et al., 2014).

3.5.2 Gulf of Lions and Liguro-Provençal basin

In the northern part of the Western Mediterranean Sea, Gulf of Lions and Liguro-Provençal basin, we have only observations in two years (1997 and 2016), so that only limited information on the temporal evolution can be made. Increased CFC-12 concentration, salinity, PT and σ_θ are observed in the water layer below ~1000 dbar (Fig. S4) indicating the steady to increased ventilation during the period.

3.5.3 Algerian basin

While similar CFC-12 concentrations in 1995, 1997 and 2001 at deep and intermediate depths of the central Algerian basin (Fig. 13) reported the nearly stagnated ventilation before 2001, salinity, PT and σ_θ increased from 1995 to 1997. Following salinity showed similar values in 1997 and 2001, but σ_θ

decreased driven by increased PT. Subsequently, all properties increased significantly from 2001 to 2011 when intense DWF led to strong ventilation in the deep western Mediterranean basin, the WMT event (Schroeder et al., 2008). This trend continued up to 2018, although at a slower pace. The CFC-12 concentrations increased from 2011 to 2016 and then decreased slightly to 2018, although the SF₆ concentration remained relatively constant. The decrease or constant concentration of the transient tracers suggests weakened ventilation in the WMDW after 2016, which is also supported by the increase of AOU from 2011 to 2018. During this time, salinity, PT and σ_θ increased from 2011 to 2016 and showed similar values between 2016 and 2018. In the western Algerian deep layer (Fig. 13), CFC-12 concentrations remain constant from 1995 to 1997 but increased afterward, while salinity, PT and σ_θ continuously increased from 1995 to 2018.

3.5.4 Alboran Sea

In the water layer below ~500 dbar in the Alboran Sea (Fig. 14), trends similar to those in the western Algerian basin are found. That is, CFC-12 concentrations, salinity, PT and σ_θ continuously increased from 1997 to 2018, and AOU increased from 2011 to 2018. The increase of CFC-12 concentrations from 1997 to 2018 depicted the generally enhanced ventilation in the Alboran Sea. Although the influence of the WMT is seen in the Alboran Sea, no Θ -S inversion is observed since the sea is not deep enough (Fig. 11).

4 Discussions

We have compared transient tracer observations from 1987 to 2018 (CFC-12/11 and SF₆) in the Mediterranean Sea, focusing on the layers below the Levantine Intermediate Water (LIW), in order to characterize the temporal evolution of ventilation. Here we discuss trends and variability of the ventilation patterns in the Mediterranean Sea based on the combined observations of transient tracers, salinity, potential temperature, potential density and apparent oxygen utilization described in the previous section. We start with a discussion of the slowly ventilated TMZ and then discuss trends in deep water ventilation for the different basins.

4.1 Tracer Minimum Zone (TMZ)

The Mediterranean Sea is one of few places in the global ocean with a pronounced TMZ at mid-depth of the water column attributed to rapid ventilation in the deep waters so that the TMZ is the slowest ventilated layer. During recent decades, the influences of the EMT and WMT events have led to bottom and deep-water renewal that has modified the TMZ and bottom water ventilation patterns. The TMZ in the contemporary Mediterranean Sea is presented from the Levantine basin to the Alboran Sea, although with a break in the Strait of Sicily. The dominating water mass of the TMZ is the Transitional Mediterranean Water (TMW) in the EMed and the transitional EMDW (tEMDW) in the WMed. The depth of the TMZ has shallowed in both the western and eastern basins before the strong

ventilation episodes of the EMT and WMT events, but has been deepening after these events. For the eastern basin, the TMZ shallows from 1987 to the 1990s and then deepens up to the 2010s. In the western basin, this shift is not so obvious although the TMZ deepens from 1987 to 1995, shallows to the mid-2000s (not shown) and then deepens slightly to the 2010s followed by slow upward motion (Table S1). For instance, the TMZ shallows from ~1400 dbar (1987) to 600-800 dbar (the 1990s) and then deepens to 1000-1300 dbar (2018) in the eastern Ionian Sea, as well as deepens from ~700 dbar (1987) to 900-1000 dbar (1995) and deepens again from 800-1000 dbar (2011) to 1200-1300 dbar (2016/18) in the central Algerian basin. The transient tracer concentrations in the TMZ have increased significantly in the EMed during the past ~30 years. However, the increase of transient tracers in the TMZ of the WMed is less pronounced, indicating that ventilation of the TMZ has been stronger in the EMed than in the WMed temporally. The transient tracer concentration in the TMZ is higher in the WMed than in the EMed for any given year, which highlights that the ventilation of WMed is stronger than the EMed in the same year.

4.2 Eastern Mediterranean basin

We start with the Adriatic Sea as a major source region of deep waters in the Eastern Mediterranean basin. Here we observe no ventilation of the deep-water (below 600 dbar) from 1987 to 1999, but with strong ventilation between 1999 and 2011 that continued in the period 2011-2016. Even though there was no ventilation of the deep water in the Adriatic Sea up to 1999, as seen by constant CFC-12 and increased AOU, it got slightly saltier and warmer. The trend for the intermediate layer (200-600 dbar) is similar, but with a pronounced decrease of transient tracers between 1987 and 1995 and then increased ventilation observed in 1999, indicating how changes in this layer are different from the deep layer. The extremely cold winter in 2012 (Gačić et al., 2014) and increased transient tracer concentrations support strong ventilation in the Adriatic Deep Water between 2011 and 2016, although with decreased bottom density (Chiggiato et al., 2016). The spatial distribution of SF₆ concentrations (Fig. 2h) reveals that the AdDW was no longer dense enough to reach the bottom of the Ionian Sea in 2018, indicating that the Adriatic source intensity weakened during recent years. This is also supported by the decreased transient tracers and dissolved oxygen (i.e. increased AOU) from 2011 to 2018 in the western Ionian bottom water and in 2016 in the Adriatic near-bottom water column (below 1000 dbar). In consequence, the Adriatic Deep Water is currently the dominant deep water source in the EMed, although with weakened intensity during the last decade.

The intensified ventilation in the Adriatic Sea influenced the overflow through the Strait of Otranto sill into the Ionian Sea where the EMDW is formed from the AdDW as it mixes with the remnant deep water from the Aegean source resulted from the EMT event. For the other deep water source of the EMed, the Southern Aegean Sea (i.e. the Cretan Sea), a clear trend is observed with well-ventilated waters in 1995, where after the concentrations remained essentially constant up to 1998, although with considerable variability in the data and slightly higher concentrations in 2011 and 2018. Schneider et

al. (2014) also showed slow ventilation of the Cretan Sea from 1998 to 2011. That is, the Aegean source intensity weakened after 1995 (Fig. 4) and led to the stagnant/weakened ventilation currently observed in the CDW.

For the EMDW in the Ionian Sea where the Aegean and Adriatic sources meet, the temporal increase of CFC-12 concentrations between 1987 and 1995 is larger in the east, which is coincident with the east-to-west gradient of the influence of the dominant Aegean source in the Ionian Sea at that time. This is also illustrated by the amplitude of Θ -S inversion related to the Aegean source, which decreases from the eastern to the western Ionian Sea, as well as from the eastern to the north-western Ionian Sea. In 1999, the influence of the Aegean source was weaker in the eastern and central Ionian deep water but stronger in the western Ionian deep water compared to those in 1995, which describes the delayed influence of the Aegean source to the western Ionian Sea. Subsequently, the amplitude of inversions related to the Aegean source became smaller in the whole Ionian Sea and the extent of the reversal decreased from 2001 to 2018. In 2018, the Θ -S inversions created by the influence of the Aegean source became very small and even invisible. When the influence of the Aegean source to the EMDW in the Ionian Sea became weaker and found at shallower depths (Theocharis et al., 2002), the new Adriatic source started to influence the Ionian Sea from the bottom layer (Cardin et al., 2015; Hainbucher et al., 2006). This is noted by the more pronounced increase of CFC-12 concentrations in the western and central Ionian deep water than in the eastern Ionian deep water between 2001 and 2011, and by the increase of salinity in the water column from ~3000 dbar to the bottom in the western and central Ionian Sea in 2011 (Roether et al., 2014). The new Adriatic source leads to the second Θ -S inversions with decreased salinity and PT observed in the Ionian bottom water in 1999 and 2001. However, the weakened ventilation of the western and central Ionian deep water and nearly stagnated ventilation in the eastern Ionian deep water in 2011-2018, reveal the weakened influence of new Adriatic source to the Ionian Sea, although the AdDW has been the dominant source of deep water in the eastern Mediterranean for the last two decades. Additionally, the CFC-12 concentrations increased more during 2001-2011, and the SF₆ concentrations decreased more during 2011-2018, in the western and central Ionian deep water than those in the eastern Ionian deep water. This implies a high inflow of the new Adriatic source to the western and central Ionian deep water in the 2000s, a signal that is evident in the eastern Ionian deep water in the 2010s.

The water from the Adriatic Sea spreads eastward from the Ionian Sea toward the Cretan Passage, as indicated by the Θ -S inversions (Fig. 8a) in 2011 (Manca et al., 2006; Velaoras et al., 2018), which led to the non-monotonous change of local salinity. The salinity decrease in the water column from ~3000 dbar to the bottom in 2011 is related to the less saline new Adriatic source (Cardin et al., 2015), as is the continued salinity decrease from 2011 to 2016 (Velaoras et al., 2018). The salinity (38.74-38.75) in the northern Cretan Passage in 2016/18 is closer to that in the Adriatic Sea in 2016 (38.72) than that in the Southern Aegean Sea in 2018 (39.05). A similar decrease of salinity from 2015 to 2016 has been reported for the Myrtoan basin, located in the southwestern Aegean Sea (Velaoras et al.,

2017). However, the salinity increased from 2016 to 2018 in the northern Cretan Passage (Fig. 8) and from 2016 to 2017 in the Myrtoan basin (Velaoras et al., 2017), changing the trend.

It is worth noting that the change of physical properties (such as salinity, PT and σ_θ) in the northern Cretan Passage deep water after 1995 is significant while the change of CFC-12 concentrations during the same time is, in practice, small. We see evidence of no new DWF in (the surrounding of) the Aegean/Cretan Sea since the EMT event so that the new Adriatic-originated water could reach into the Levantine basin, where it was detected in 2011.

Although the spatial distribution of CFC-12 concentrations in the EMed in 2018 is different from that in 1987, similar CFC-12 water column gradients (bottom-to-intermediate) were found in 1987, 2011 and 2018 in the western Ionian Sea. However, the distribution of CFC-12 in 2018 is closer to the one in 1987 than that of 2011. Similarly, the distribution pattern of SF₆ in 2018 is closer to that of CFC-12 concentrations in 1987 than that of SF₆ concentrations in 2011. This shows a trend of water mass distributions towards the status of pre-EMT more in 2018 than in 2011. However, it is still far away from the pre-EMT condition in 2018, although the transient tracer relative distributions support a relaxation from the EMT condition to the pre-EMT condition.

4.3 Strait of Sicily

The Strait of Sicily plays a significant role in the communication between EMed and WMed. Due to the data gap, more Θ -S diagrams in 1985, 1986, 1992, 1997, 1998 and 2003 (Astraldi et al., 2002; Gasparini et al., 2005) are combined here to refer three different phases: before the EMT event (1985-1987), during the EMT event (1991-1993) and after the EMT event (after 1995). The deep waters of the Strait are significantly better ventilated in 2018 than in 1995 and 2001 (i.e. significant increase of CFC-12 concentrations), accompanied by increased salinity and PT but decreased density. This reveals that the EMed continuously influences the Strait of Sicily. In 2018, the CFC-12 concentrations, salinity and PT in the Strait of Sicily bottom layer (tEMDW) are higher than those in the Ionian Sea at the same depth (Fig. 6-8, 10) but with lower density. This is an indication of stronger ventilation of the tEMDW in the Strait of Sicily and it influenced more by the LIW than by the EMDW.

4.4 Western Mediterranean basin

The Gulf of Lions is the main source region for deep water in the WMed, but we have only two repeats of transient tracers in this region. The increased transient tracer concentrations indicate intensified ventilation from 1997 to 2016. When combined with more data from the CTD and mooring in 1987, 1988, 1993, 1999 (Pinardi et al., 2015) and 2007-2013 (Houpert et al., 2016; Testor et al., 2018), we found mild Θ -S inversions in the 1990s, but stronger ones and even double inversions starting from the winter 2004/05, which indicates the difference before and after the WMT event in the source region.

The evolution of properties in the deep waters of the Gulf of Lions is comparable to those in the adjacent Algero-Provençal basin, the main basin in the WMed. The WMed deep water is characterized by nearly constant CFC-12 concentrations, i.e. nearly stagnant ventilation, between 1995 and 2001 followed by enhanced ventilation up to 2016 and possibly slower ventilation during the last few years of the time-series up to 2018. The recent slow ventilation could be attributed to the weakened influence of the WMT event that started in winter 2004/05. The Θ -S inversions that are tell-tales of the WMT event were found in 2011, 2016 and 2018 in the central Algerian basin and 2011 and 2018 in the western Algerian basin (Fig. 13). From the mooring data (Schroeder et al., 2016), the near-bottom warm and salty water intruded in 2005, and the layer below the Θ -S inversions became ~600 m thick in 2006, ~1000 m in 2008, >1200 m in 2010, 1400 m in 2013 and >1500 m in 2015, which described the uplifting old WMDW replaced by the new one from near the bottom. From the CTD data (Fig. 13), the depths of inversions were all ~1500 dbar in the central Algerian basin, but ~1250 dbar in 2011 and ~1500 dbar in 2018 in the western Algerian basin. The shallower depths of Θ -S inversions in the western Algerian in 2011 revealed the uplift of the new WMDW toward the Alboran Sea (Schroeder et al., 2010; Schroeder et al., 2008).

There is no direct deep ventilation in the Tyrrhenian Sea but the signal of ventilation is imported by advected water masses. Similar to the Algerian basin, the Tyrrhenian Deep Water (TDW) is characterized by intense signs of ventilation during the 2011-2016 period followed by a possible slowdown of the ventilation after 2016. The increased transient tracer concentrations of the bottom layer around the Sardinia Channel indicate the overflow of WMDW into the Tyrrhenian Sea, which is a sign of intrusion of well-ventilated water resulted from the WMT event to the deep layer that resulted in better-ventilated waters. Another possible sign is the weakened intensity of the EMed influence via the intermediate layer (tEMDW and LIW). This is conducted by the enhanced vertical mixing of intermediate waters into the deep waters derived from the decreased CFC-12 and SF₆ concentrations in the upper waters (above ~1500 dbar) accompanied by the increased tracer concentrations in the deep waters for each year. On the other hand, there are lower CFC-12 concentrations (Fig. 12b) and a less well-developed TMZ (Fig. 11) in the Tyrrhenian Sea than those in the western basin (Fig. 13b). This situation does change with deep-water rich in CFC-12 concentrations coming from the western basin filling the Tyrrhenian Sea near-bottom layer. The differences in CFC-12 concentrations between the TDW and the WMDW are ~10 ppt in 2001, ~60 ppt in 2011 and ~30 ppt in 2018, a development that coincides with the influenced period of the WMT event.

As the shallow sea connected the Algerian basin with the Atlantic Ocean, the Alboran Sea is characterized by well ventilated deep waters with signs of increased ventilation between 1997 and 2011 and constant ventilation up to 2018 due to the influence of the WMT event.

5 Conclusions and outlook

In this study, we report on high spatiotemporal variability of deep and intermediate water ventilation of the Mediterranean Sea using a 30+ year time-series of transient tracer and hydrographic observations. During this period, the effects of two “events” dominate the variability of ventilation, the Eastern Mediterranean Transition (EMT) and the Western Mediterranean Transition (WMT) events. The Mediterranean Sea is one of the best-ventilated bodies of water in the global ocean and is as such characterized by high tracer concentrations in the deep layer below a zone of lower tracer concentrations in the intermediate layer, the Tracer Minimum Zone (TMZ). This zone of weak ventilation stretches across the whole Mediterranean Sea from the Levantine basin into the western basin. In general, the western Mediterranean Sea is better ventilated than the eastern one.

During the last three decades, the EMDW has been formed by the mixing of the dense waters of the Aegean origin with the colder and less saline water of the Adriatic origin, where the dominant source of deep water changed from the Adriatic Sea (before 1990) to the Aegean Sea (in the 1990s) and then back to the Adriatic Sea (in the 2000s and 2010s). Due to the EMT event in the early 1990s, very strong ventilation was found during 1987-1995 in the Aegean Sea and surrounding areas (such as the northern Cretan Passage, eastern Ionian Sea and western Levantine basin). For areas farther away (such as the western Ionian Sea and central Levantine basin), this was manifested for the period 1995-1997/99. For the Adriatic Sea, we see no ventilation of the deep water from 1987 to 1999, but with signs of ventilation up to 2011 and 2016, although weakened during the last decade. Since the restart of the Adriatic deep water source during 1999-2002, the Ionian Sea was well-ventilated whereas the northern Cretan Passage deep water was not ventilated in the 2000s. After 2011, weak ventilation is found in most areas of the EMed. The Eastern Mediterranean shows a general west-to-east gradient of increasing salinity and PT but decreasing oxygen and transient tracer concentrations. The temporal evolution of transient tracer concentrations reveals a trend of water mass distributions toward the status of pre-EMT, and the trend is more obvious in 2018 than in 2011, although with evolving water mass properties.

For the western Mediterranean Sea, the WMDW also shows a general west-to-east gradient of increasing salinity and PT but decreasing oxygen and transient tracer concentrations. A steady-state ventilation scenario with nearly stagnant ventilation is found in the deep-water before 2001. Since the start of the WMT event during the winter 2004/05, strong ventilation is found in the western Mediterranean between 2001 and 2011 and through to 2016 but weakened up to 2018. The latter could be a result of a combined influence from both the WMed (e.g. weakened influence from the WMT event) and the EMed (e.g. weakened Adriatic source intensity). During the past ~15 years, the deep western Mediterranean has been influenced by the new WMDW that moves the old WMDW upward leading to the intrusion of better ventilated deep waters toward the Alboran Sea.

The combination of two transient tracers (e.g. CFC-12 and SF₆) can better constrain the ventilation. In particular, considering the decreasing CFC-12 and increasing SF₆ atmospheric concentrations, the ability of CFC-12 alone in interpreting ventilation in the Mediterranean Sea is decreasing, while SF₆ is

able to deliver information of ventilation and changes in ventilation. The complicated and variable ventilation of the Mediterranean Sea would benefit from an expanding suite of transient tracers. For instance does a range of halogenated CFC replacement compound constitute possible additional tracers (Li et al., 2019; Li and Tanhua, 2019) or the isotope ^{39}Ar (Ebser et al., 2018) that can be used to better constrain TTDs, i.e. constrain ventilation (Stöven and Tanhua, 2014). For the Mediterranean Sea, other models without the assumption of steady-state ventilation (as the TTD does) should be considered in the future based on its high variable ventilation patterns.

Data availability

Cruise data in Table 1 in 1987-2011 are from https://www.nodc.noaa.gov/ocads/oceans/Coastal/Meteor_Med_Sea.html. Observations of CFC-12 and SF_6 from cruises ESAW2, CRELEV2016 are available on request to the corresponding author. Observations of CFC-12 and SF_6 from cruises TALPro2016 and MSM72 are available from <https://cchdo.ucsd.edu/cruise/29AJ20160818> and <https://cchdo.ucsd.edu/cruise/06M220180302>.

Author contributions

PL performed the data processing, contributed figures and tables and wrote the paper. TT conducted the sampling from cruises ESAW2, CRELEV2016, TALPro2016 and MSM72 and supported the writing process.

Competing interests

The authors declare that the research was conducted in the absence of any commercial or financial relationships that could be construed as a potential conflict of interest.

Acknowledgments

We acknowledge the great support by the scientists and crew from expeditions M5/6, M31/1, Ura2, P234, Aegaeo98, Ura7, M44/4, M51/2, M84/3, ESAW2, CRELEV2016, TALPro2016 and MSM72. Special thanks go to Dr. Tim Stöven for his instructions on some MATLAB scripts. The authors also gratefully thank support through the scholarship program from the China Scholarship Council (CSC).

Table 1. Key meta-data for the Mediterranean Sea cruises used in this study. Data of CFC-12 and SF₆ from cruises below the dashed line has not yet been published elsewhere.

Year	Cruise	Research vessel	Cruise period	W/E. Med	CFC-12/SF ₆	References
1987	M5/6	Meteor	1987.08.18–09.24	W, E	CFC-12	(Nellen et al., 1996); (Schlitzer et al., 1991)
1995	M31/1	Meteor	1994.12.30–1995. 03.22	W, E	CFC-12	(Hemleben, 1996); (Roether et al., 1996); (Roether et al., 1998); (Klein et al., 1999)
1997	Ura2	Uranis	1997.08.30–09.08	E	CFC-12	(Manca et al., 2002); (Roether et al., 2007)
1997	P234	Poseidon	1997.10.23–11.10	W	CFC-12	(Rhein et al., 1999)
1998	Aegaeo98	Aegaeo	1998.10.14–10.19	E	CFC-12	(Theocharis et al., 2002)
1999	Ura7	Uranis	1999.02.11–02.17	E	CFC-12	(Manca et al., 2002); (Roether et al., 2007)
1999	M44/4	Meteor	1999.04.10–05.16	W, E	CFC-12	(Pätzold, 2000); (Theocharis et al., 2002)
2001	M51/2	Meteor	2001.10.18–11.11	W, E	CFC-12	(Hemleben et al., 2003); (Roether et al., 2007); (Schneider et al., 2010)
2011	M84/3	Meteor	2011.04.05–04.28	W, E	CFC-12, SF ₆	(Tanhua et al., 2013a); (Cardin et al., 2015); (Stöven and Tanhua, 2014); (Schneider et al., 2014)
2016	ESAW2	Bios Dva	2016.04.05–04.10	E	CFC-12, SF ₆	(Šantić et al., 2019)
2016	CRELEV2016	Aegaeo	2016.06.02–06.10	E	CFC-12, SF ₆	(Velaoras et al., 2018)
2016	TALPro2016	Angeles Alvarino	2016.08.18–08.29	W	CFC-12, SF ₆	(Jullion, 2016)
2018	MSM72	Maria S. Merian	2018.03.02–04.03	W, E	CFC-12, SF ₆	(Hainbucher et al., 2019b)

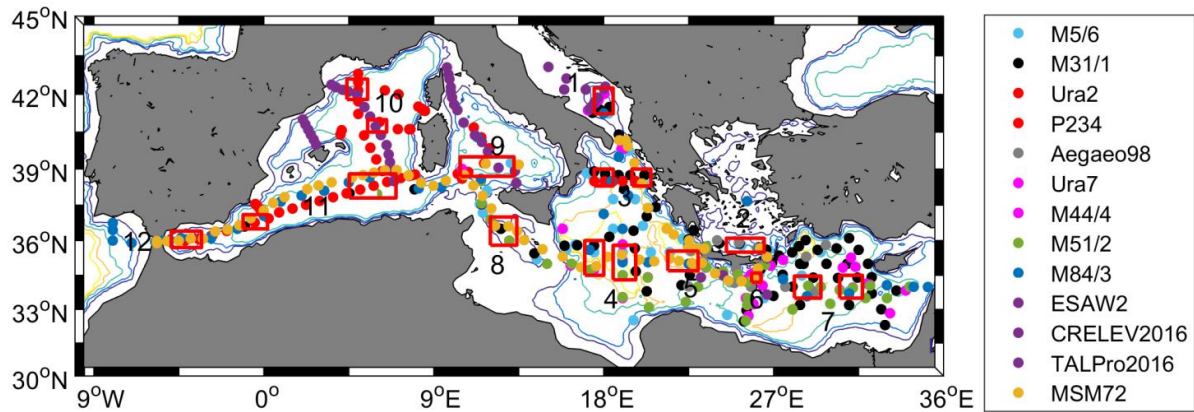


Figure 1. Sampling sites of CFC-12 and SF₆ measurements from historical cruises listed in Table 1 in the Mediterranean Sea; samples from a certain year (rather than cruise) have the same colour, which is used in the plots below. The small red boxes are the areas selected for assessing the temporal variability of ventilation. The areas are located in the (1) Southern Adriatic Sea, (2) Cretan Sea, (3) Northern Ionian Sea, (4) Western and Central Ionian Sea, (5) Eastern Ionian Sea, (6) Northern Cretan Passage, (7) Western and Central Levantine basins, (8) Strait of Sicily, (9) Tyrrhenian Sea, (10) Gulf of Lions and Liguro-Provençal basin, (11) Eastern and Western Algerian basin and (12) Alboran Sea. The depth contours are 500 m, 1000 m, 2000 m, 3000 m and 3500 m.

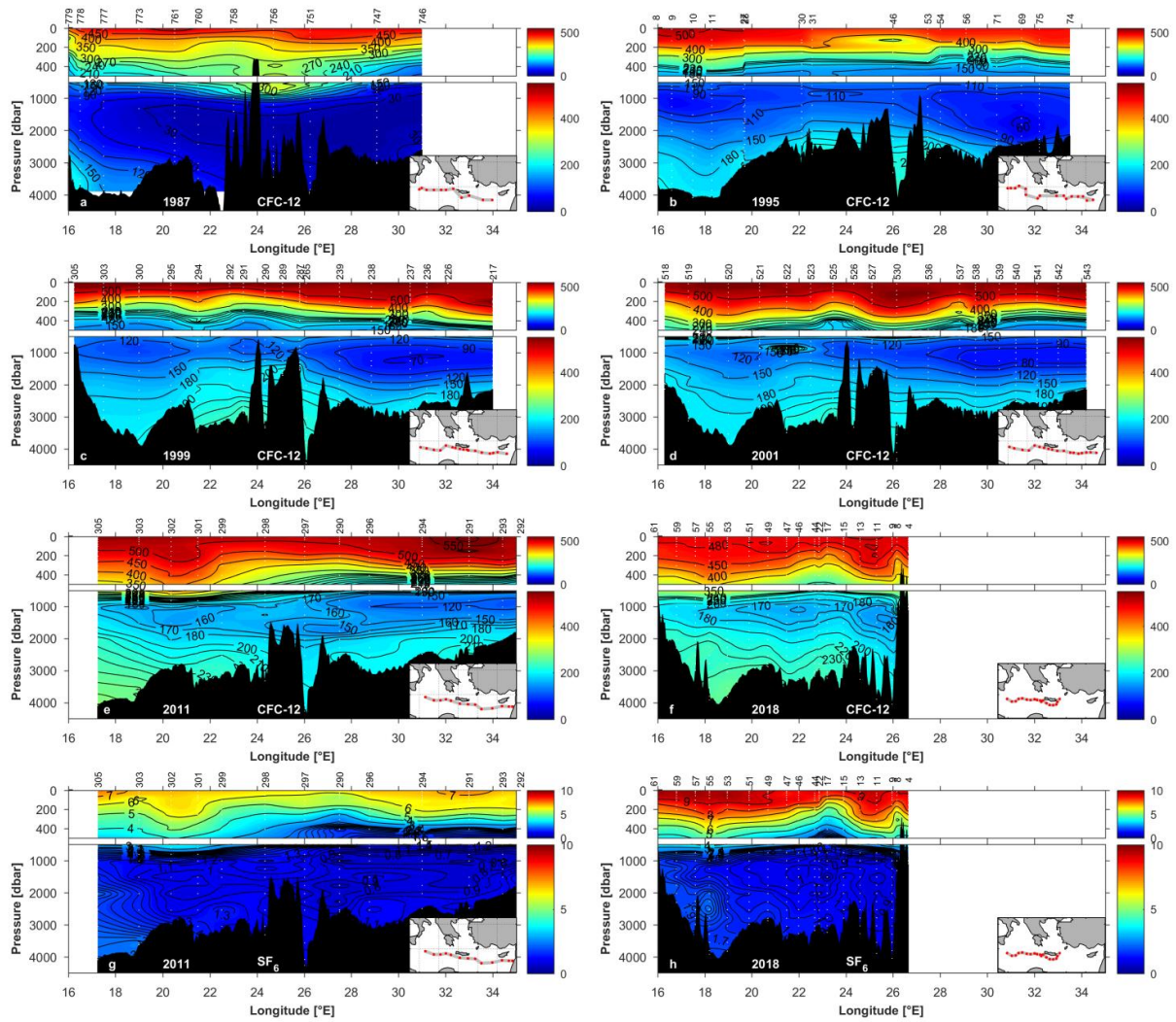


Figure 2. Vertical sections of CFC-12 concentration (in ppt) in the Eastern Mediterranean Sea (see inset map for station locations) in (a) 1987 (Meteor M5/6), (b) 1995 (Meteor M31/1), (c) 1999 (Meteor M44/4), (d) 2001 (Meteor M51/2), (e) 2011 (Meteor M84/3) and (f) 2018 (Maria S. Merian MSM72) and vertical sections of SF₆ concentration (in ppt) in the EMed in (g) 2011 (Meteor M84/3) and (h) 2018 (Maria S. Merian MSM72). The same scales of longitude and pressure are used for all figures, while the same colour bars are separately used for CFC-12 and SF₆ sections. The upper panels highlight the top 500 dbar. The markers on the top x-axis stand for the station number.

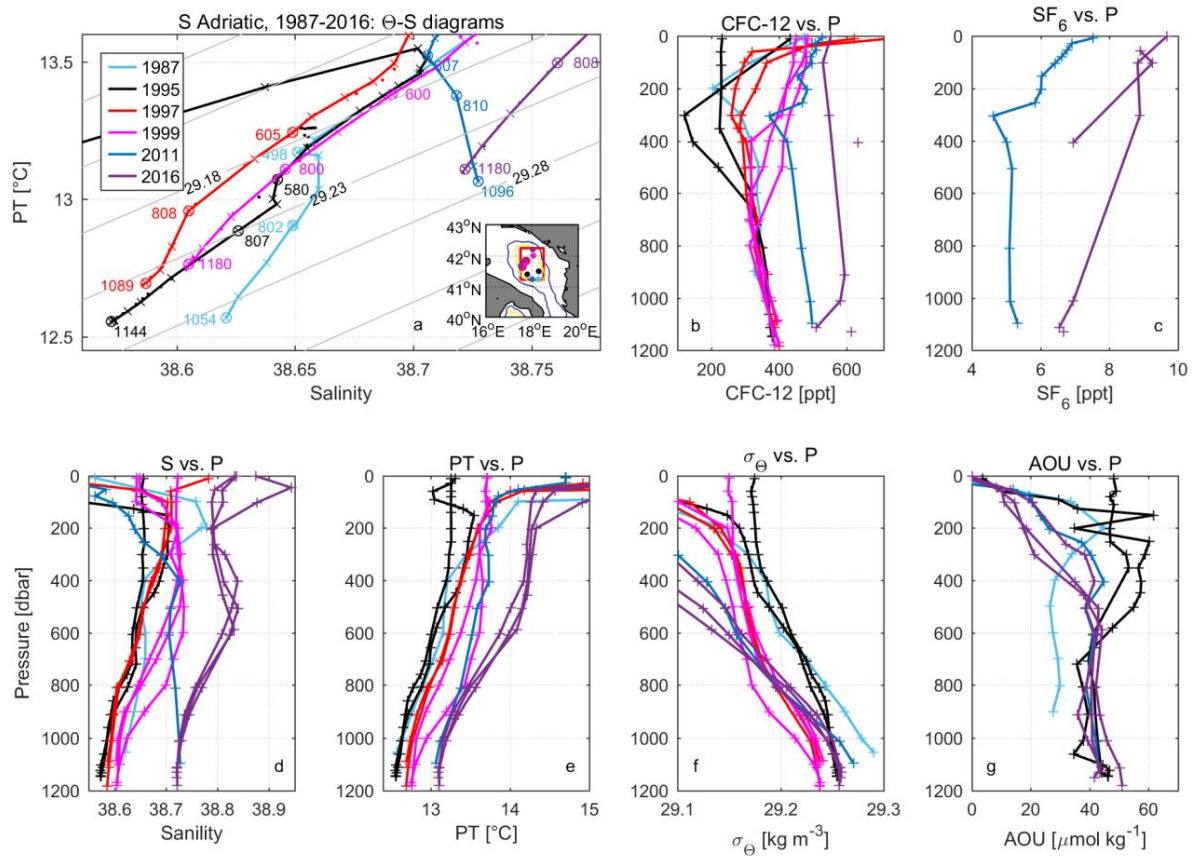


Figure 3. Temporal variability of the Southern Adriatic Sea illustrated with (a) Θ -S diagrams with σ_{Θ} isolines, (b) CFC-12 concentration vs. pressure, (c) SF_6 concentration vs. pressure, (d) salinity vs. pressure, (e) potential temperature (PT) vs. pressure, (f) potential density (σ_{Θ}) vs. pressure and (g) apparent oxygen utilization (AOU) vs. pressure. For site numbers see the legend and for site positions see inset map (isolines are 500, 1000, 2000, 3000 and 3500 m). The stations shown are (in the sequence of the legend) M5/6 766, M31/1 16 and 17, Ura2 18 and 11, Ura7 8, 7 and 5, M84/3 313 and ESAW2 29, 8 and 7. Bottle data is indicated by crosses (for the first station from each cruise) and dots (for the rest stations from each cruise) in Θ -S diagrams and pluses in other plots (for all stations from each cruise).

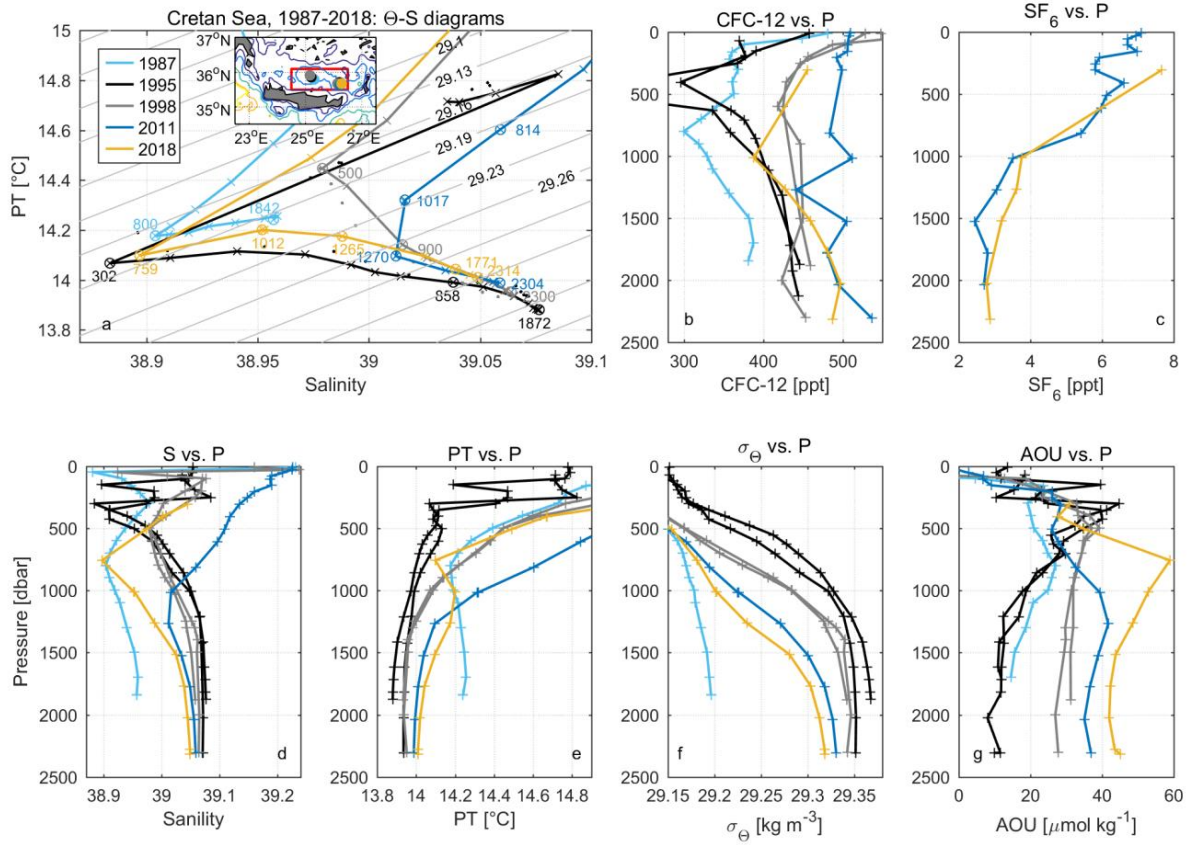


Figure 4. Similar to Fig. 3 but in the Cretan Sea. The stations shown are M5/6 753, M31/1 41 and 42, Aegaeo98 10 and 13, M84/3 288 and MSM72 2.

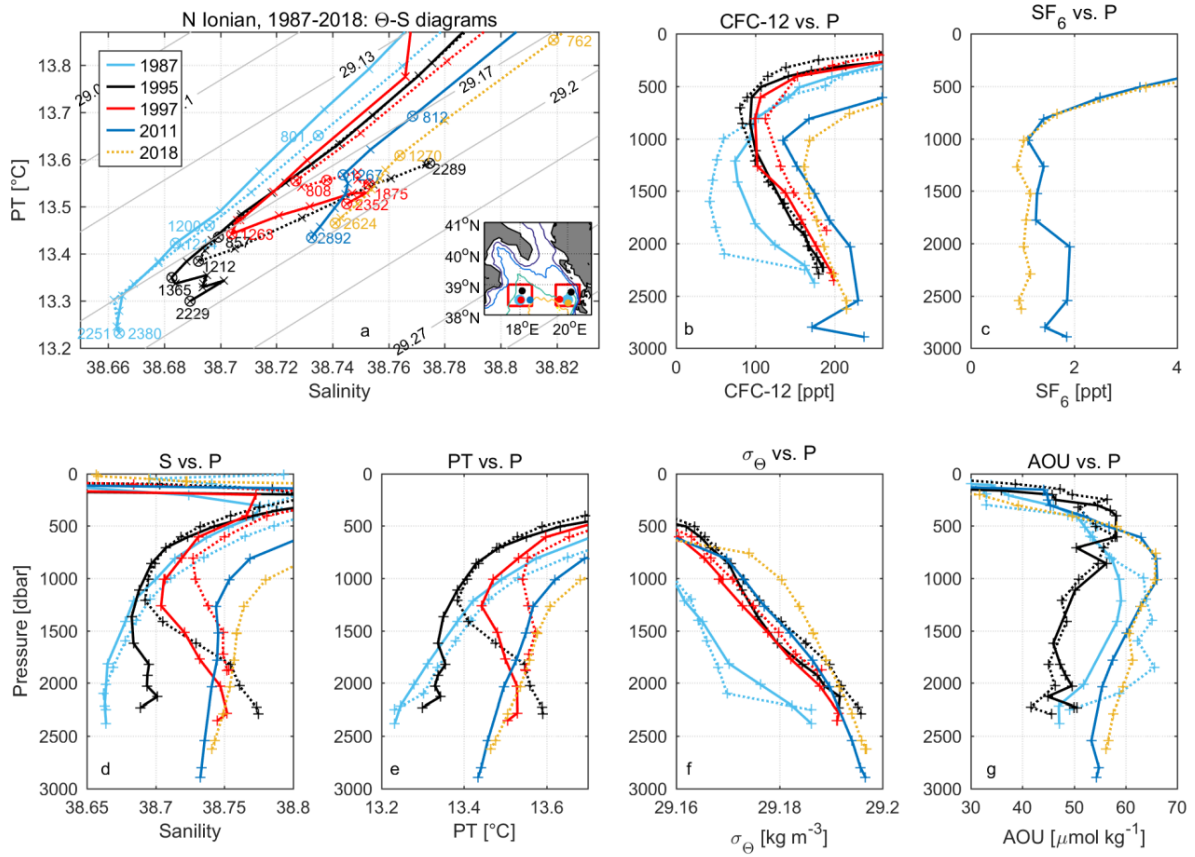


Figure 5. Similar to Fig. 3 but in the northern Ionian Sea. The stations shown in the north-western Ionian Sea are M5/6 770, M31/1 13, Ura2 21 and M84/3 314 and shown by continuous lines. The stations shown in the north-eastern Ionian Sea are M5/6 764, M31/1 23, Ura2 46 and MSM72 34 and shown by dotted lines.

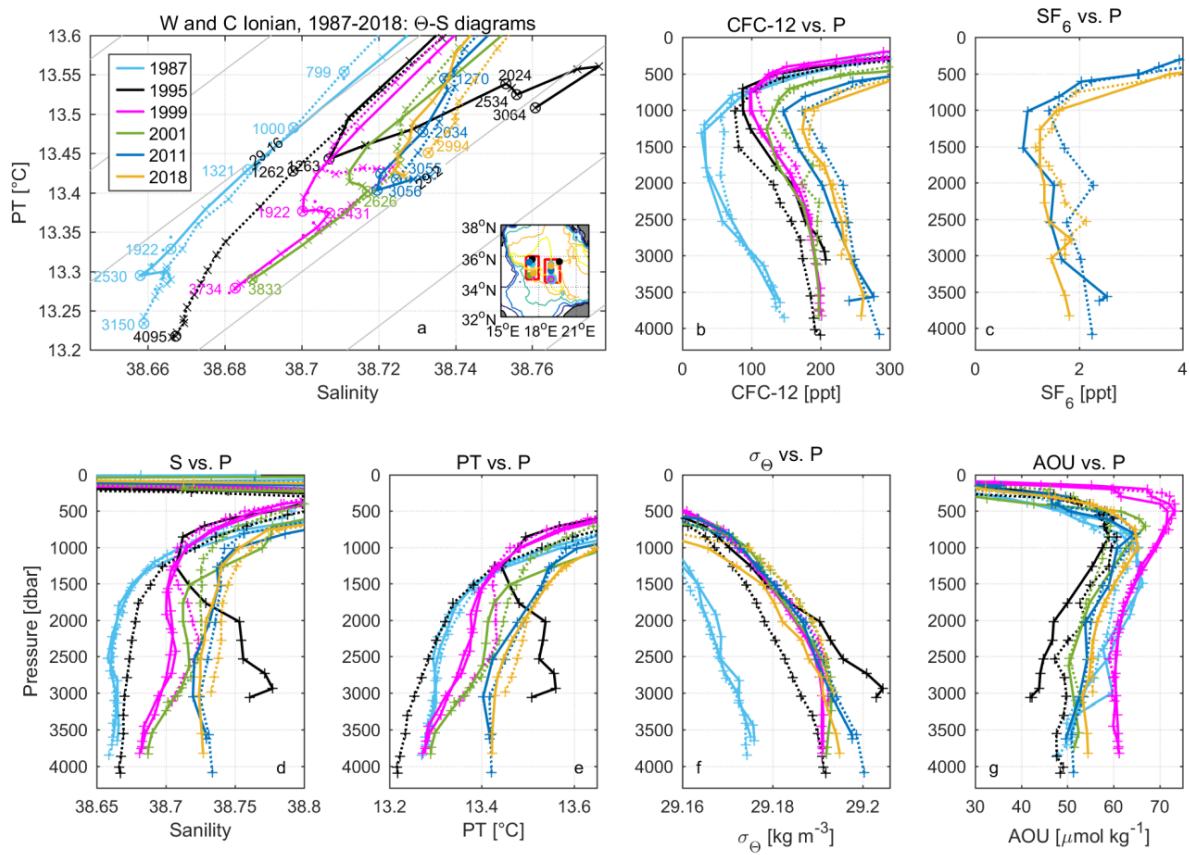


Figure 6. Similar to Fig. 3 but in the western and central Ionian Sea. The stations shown in the western Ionian Sea are M5/6 777, M31/1 10, M44/4 303, M51/2 519, M84/3 305 and MSM72 57 and shown by dotted lines. The stations in the central Ionian Sea are M5/6 773 and 774, M31/1 27, M44/4 301 and 300, M51/2 520, M84/3 303 and MSM72 53 and shown by continuous lines.

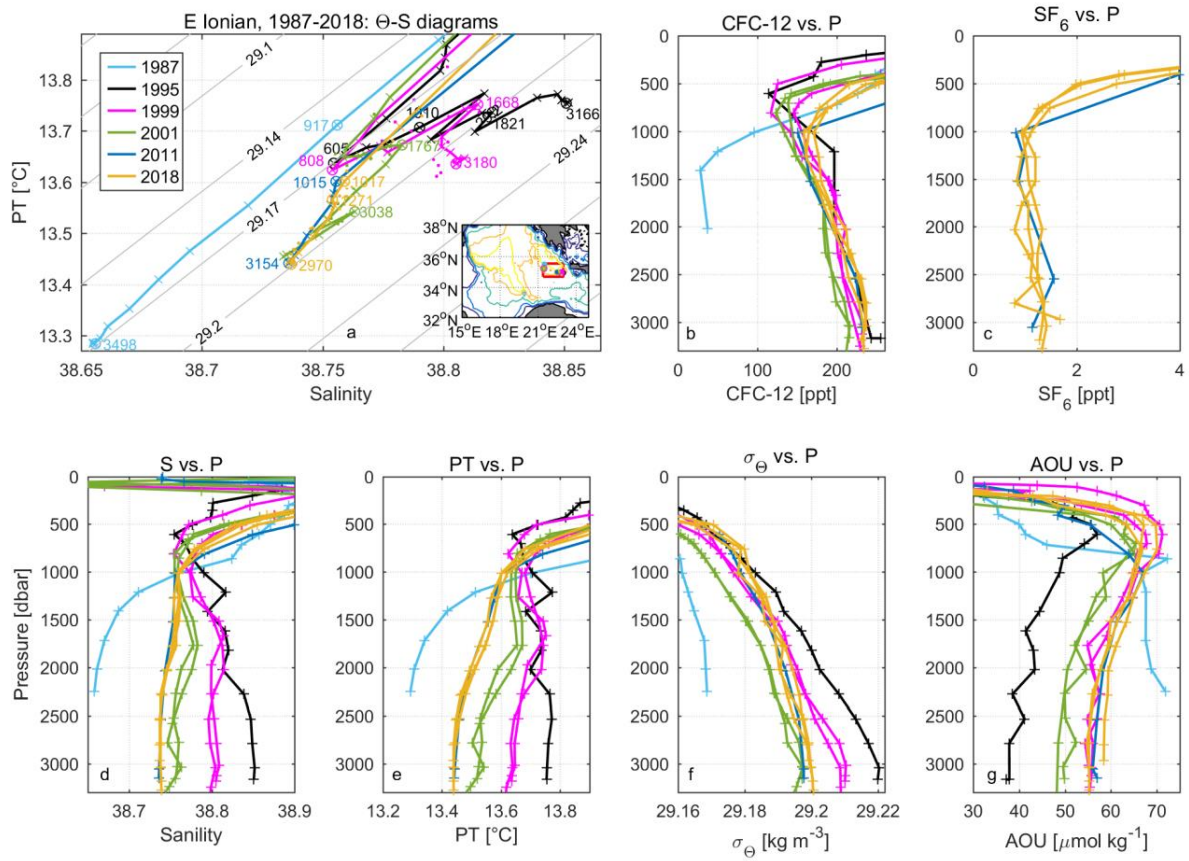


Figure 7. Similar to Fig. 3 but in the eastern Ionian Sea. The stations shown are M5/6 760, M31/1 32, M44/4 292 and 294, M51/2 522 and 523, M84/3 299 and MSM72 22, 44, 46 and 47.

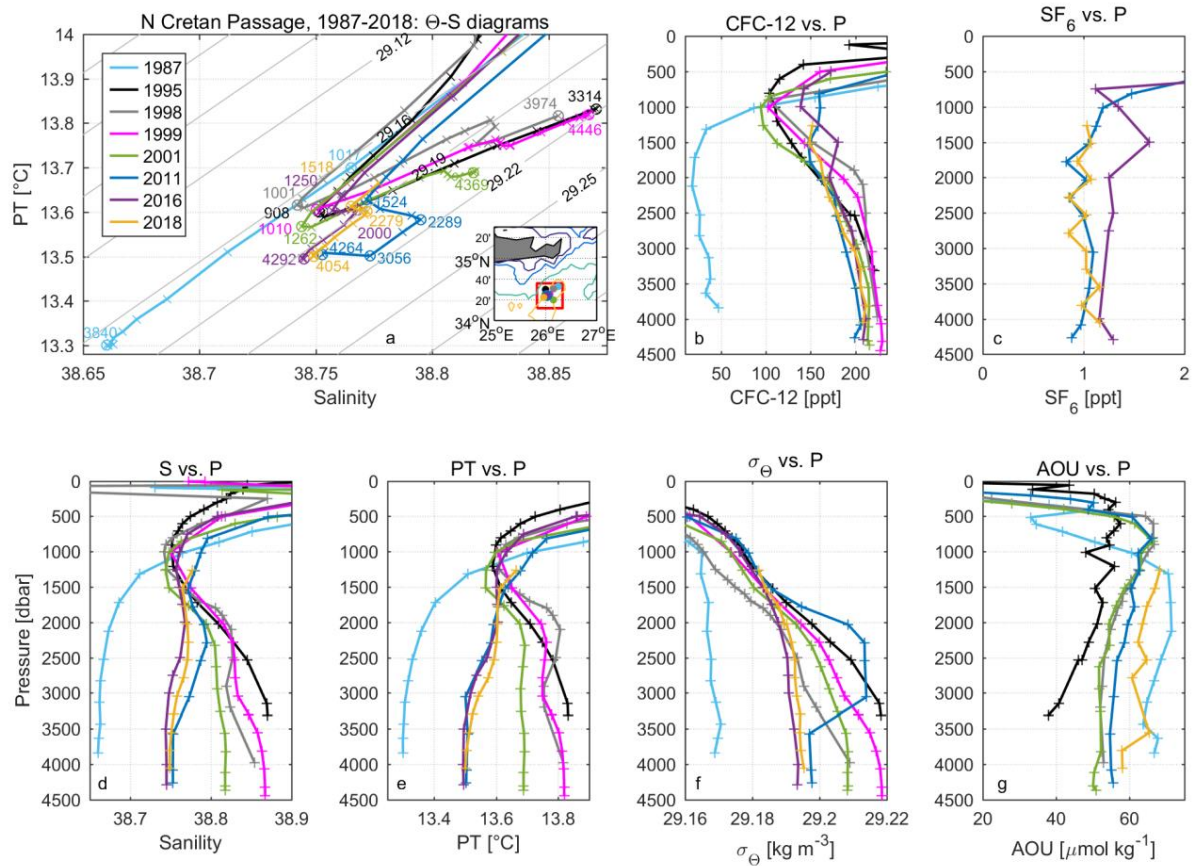


Figure 8. Similar to Fig. 3 but in the northern Cretan Passage. The stations shown are M5/6 751, M31/1 46, Aegaeo98 40, M44/4 265, M51/2 530, M84/3 297, CRELEV2016 18 and MSM72 9. The structures of Θ -S diagrams in the northern Cretan Passage can be generally separated as three patterns: the one in 1987 with low salinity and PT (38.66, 13.3) in the deep water (EMDW of old Adriatic origin); the one in 1995-2001 with an inversion at 900-1300 dbar core depth (EMDW of old Adriatic origin) and the near-bottom water (EMDW of Aegean origin) with high salinity and PT (38.87, 13.8); the one in 2011-2018 with an inversion at 1250-1500 dbar core depth (EMDW of old Adriatic origin) followed by another inversion at 2000-2300 dbar (EMDW of Aegean origin) and the near-bottom water (EMDW of new Adriatic origin) with medium salinity and PT (38.75, 13.5).

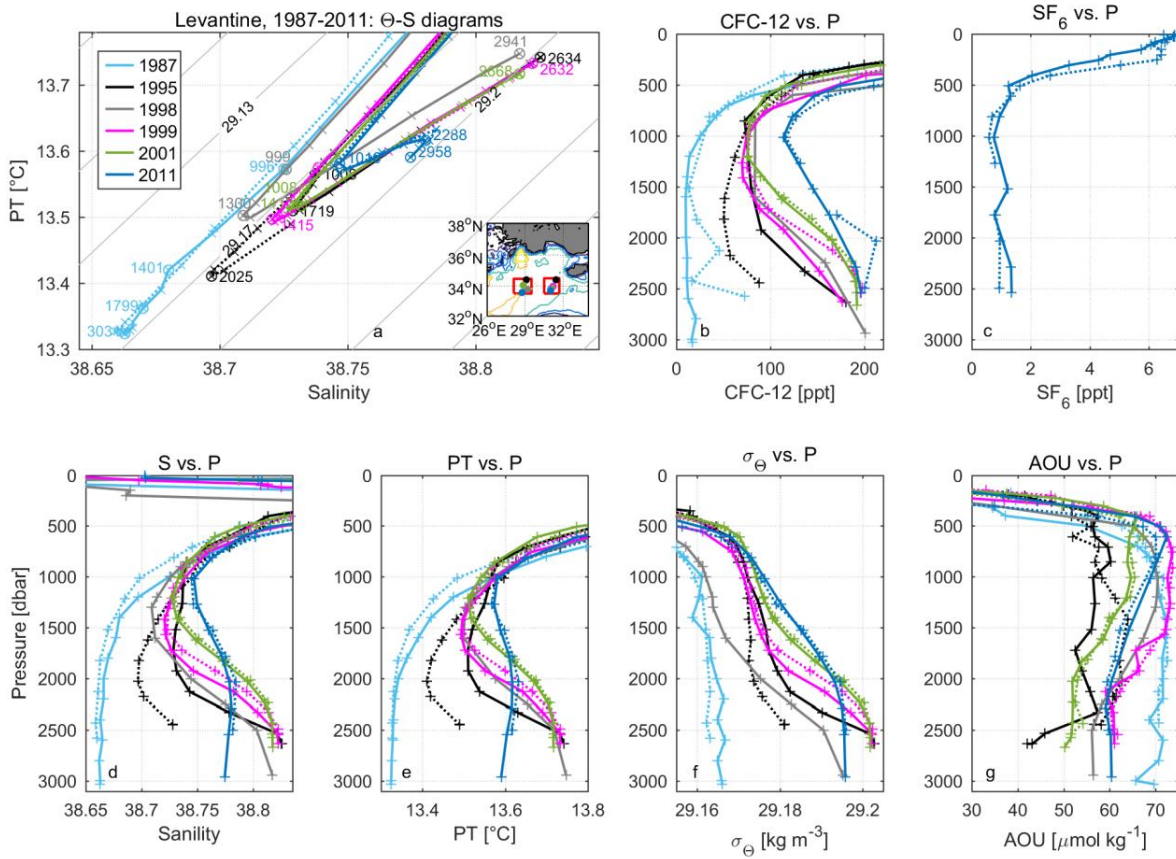


Figure 9. Similar to Fig. 3 but in the western and central Levantine basin. The stations shown in the western Levantine basin are M5/6 747, M31/1 56, Aegaeo98 441, M44/4 238, M51/2 537 and M84/3 296 and shown by continuous lines. The stations shown in the central Levantine basin are M5/6 746, M31/1 69, M44/4 236, M51/2 540 and M84/3 294 and shown by dotted lines.

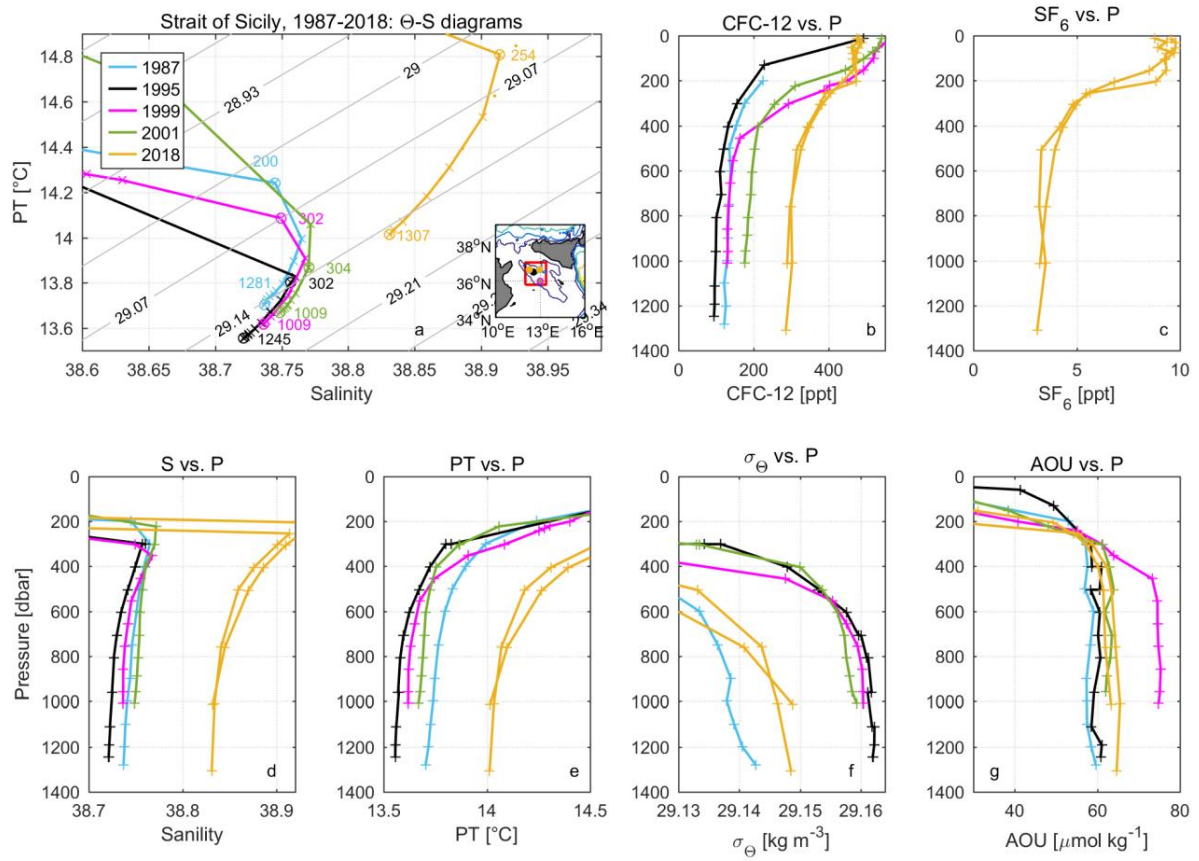


Figure 10. Similar to Fig. 3 but in the Strait of Sicily. The stations shown are M5/6 781, M31/1 6, M44/4 307, M51/2 516 and MSM72 72 and 70.

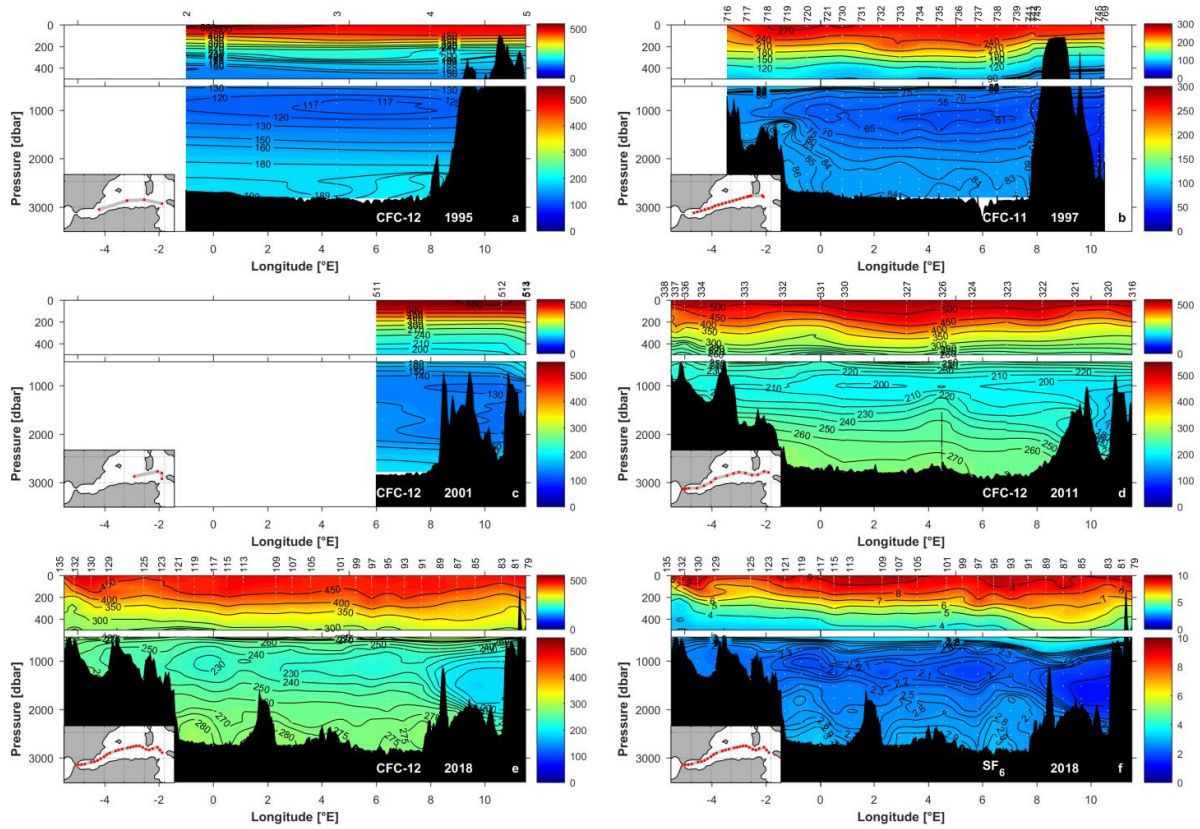


Figure 11. Vertical sections of CFC-12/CFC-11 concentration (in ppt) in the Western Mediterranean Sea (see inset maps for station locations) in (a) 1995 (Meteor M31/1), (b) 1997 (Meteor 234), (c) 2001 (Meteor M51/2), (d) 2011 (Meteor M84/3) and (e) 2018 (Maria S. Merian MSM72) and vertical section of SF₆ concentrations (in ppt) in the WMed in (f) 2018 (Maria S. Merian MSM72). The vertical section of CFC-12 concentrations in 1997 is replaced by that of CFC-11 concentration due to the higher quality of CFC-11 data (Rhein et al., 1999). The same scales of longitude and pressure are used for all figures, while the same colour bars are separately used for CFC-12, CFC-11 and SF₆ sections. The upper panels highlight the top 500 dbar. The markers on the top x-axis stand for the station number.

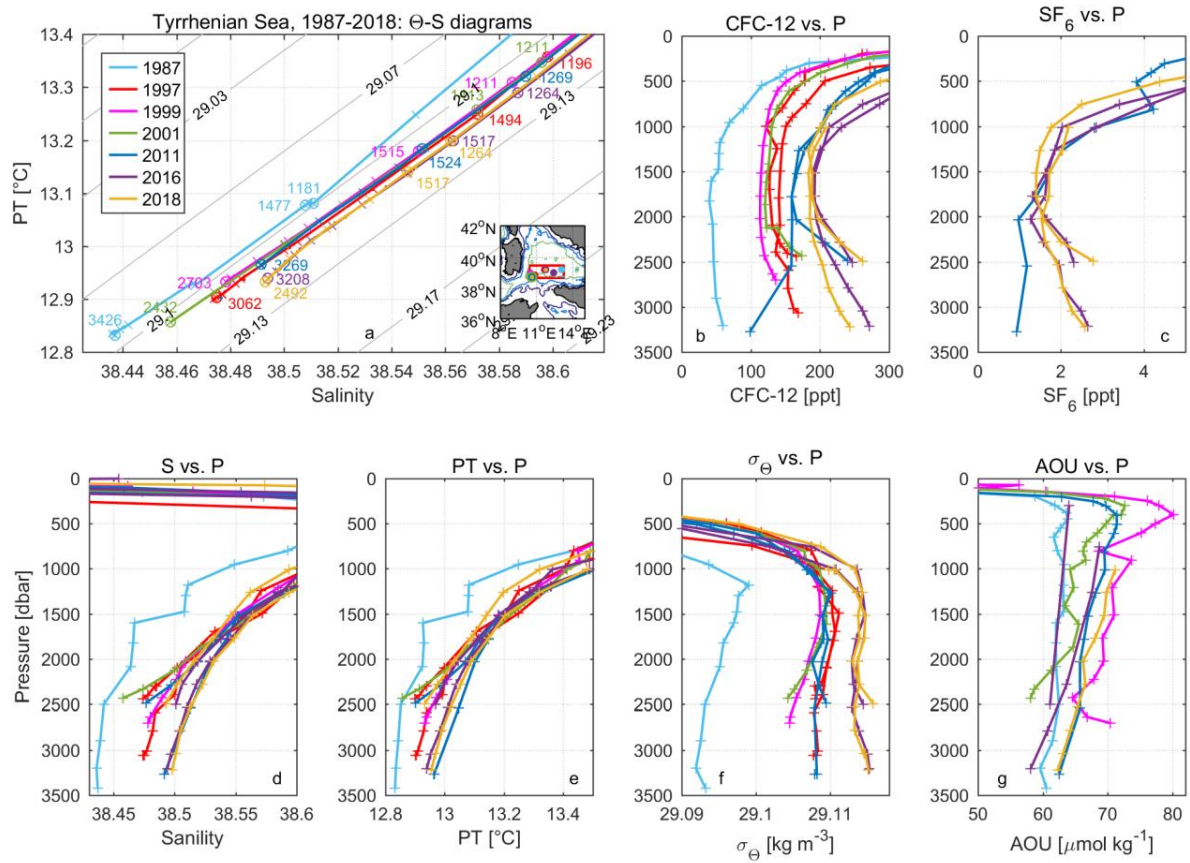


Figure 12. Similar to Fig. 3 but in the Tyrrhenian Sea. The stations shown are M5/6 786, P234 767 and 768, M44/4 310, M51/2 512, M84/3 317 and 320, TALPro2016 6 and 5, and MSM72 83 and 77.

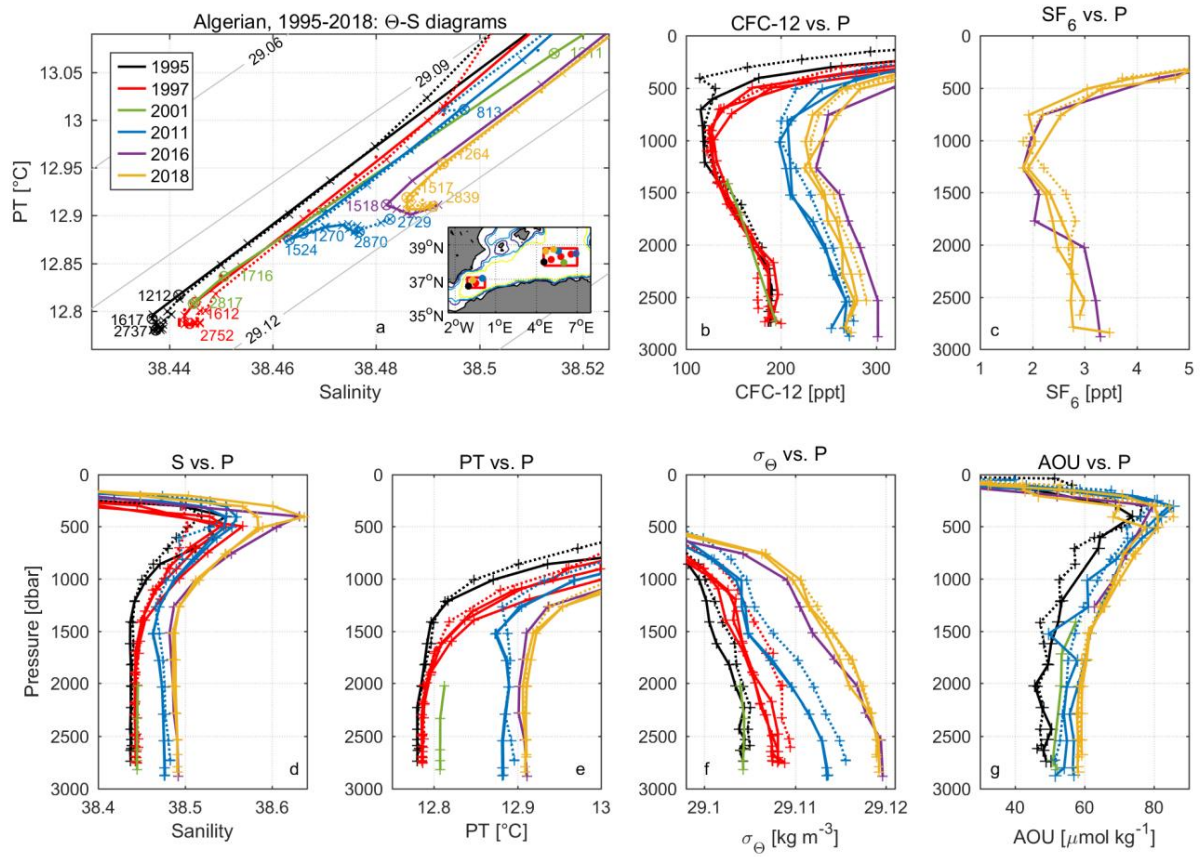


Figure 13. Similar to Fig. 3 but in the central and western Algerian basin. The stations shown in the central Algerian basin are M31/1 3, P234 736, 737 and 738, M51/2 511, M84/3 324 and 323, TALPro2016 19 and MSM72 99 and 101 and shown by continuous lines. The stations in the western Algerian basin are M31/1 2, P234 720, M84/3 331 and MSM72 119 and shown by dotted lines.

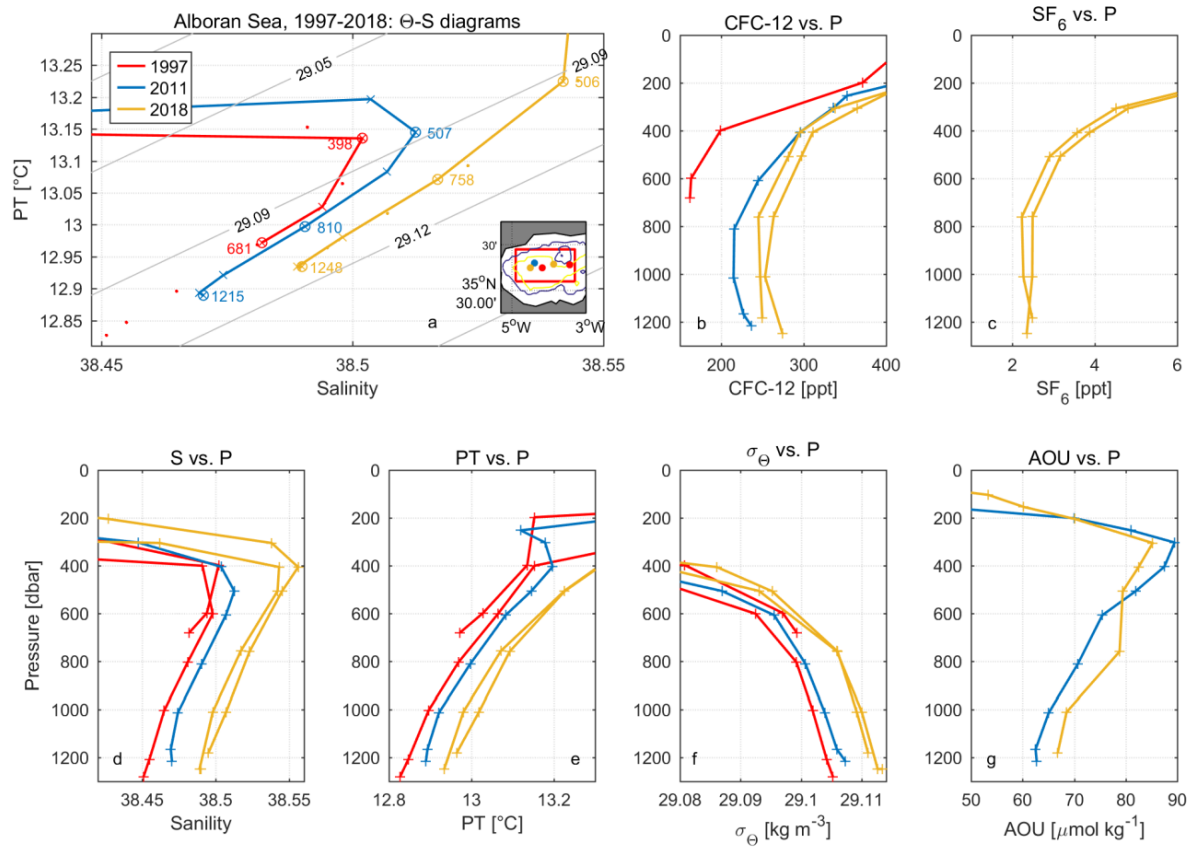


Figure 14. Similar to Fig. 3 but in the Alboran Sea. The stations shown are P234 716 and 715, M84/3 334 and MSM72 130 and 129.

References

- Akpinar, A., Yilmaz, E., Fach, B., and Salihoglu, B.: Physical Oceanography of the Eastern Mediterranean Sea, *The Turkish Part of the Mediterranean Sea*, 1–14, 2016.
- Artegiani, A., Paschini, E., Russo, A., Bregant, D., Raicich, F., and Pinardi, N.: The Adriatic Sea general circulation. Part I: Air–sea interactions and water mass structure, *J. Phys. Oceanogr.*, *27*, 1492–1514, [https://doi.org/10.1175/1520-0485\(1997\)027<1492:TASGCP>2.0.CO;2](https://doi.org/10.1175/1520-0485(1997)027<1492:TASGCP>2.0.CO;2), 1996a.
- Artegiani, A., Paschini, E., Russo, A., Bregant, D., Raicich, F., and Pinardi, N.: The Adriatic Sea general circulation. Part II: baroclinic circulation structure, *J. Phys. Oceanogr.*, *27*, 1515–1532, [https://doi.org/10.1175/1520-0485\(1997\)027<1515:TASGCP>2.0.CO;2](https://doi.org/10.1175/1520-0485(1997)027<1515:TASGCP>2.0.CO;2), 1996b.
- Astraldi, M., Gasparini, G., Sparnocchia, S., Moretti, M., and Sansone, E.: The characteristics of the water masses and the water transport in the Sicily Strait at long time scales, *Bulletin de l'Institut océanographique, Monaco. Numéro spécial*, 95–116, 1996.
- Astraldi, M., Gasparini, G., Vetrano, A., and Vignudelli, S.: Hydrographic characteristics and interannual variability of water masses in the central Mediterranean: a sensitivity test for long-term changes in the Mediterranean Sea, *Deep-Sea Res. Pt. I*, *49*, 661–680, [https://doi.org/10.1016/S0967-0637\(01\)00059-0](https://doi.org/10.1016/S0967-0637(01)00059-0), 2002.
- Buffett, G. G., Krahnemann, G., Klaeschen, D., Schroeder, K., Sallares, V., Papenberg, C., Ranero, C. R., and Zitellini, N.: Seismic oceanography in the Tyrrhenian Sea: Thermohaline staircases, eddies, and internal waves, *J. Geophys. Res.: Oceans*, *122*, 8503–8523, <https://doi.org/10.1002/2017JC012726>, 2017.
- Cardin, V., Civitarese, G., Hainbucher, D., Bensi, M., and Rubino, A.: Thermohaline properties in the Eastern Mediterranean in the last three decades: is the basin returning to the pre-EMT situation?, *Ocean Sci.*, *11*, 53–66, <https://doi.org/10.5194/os-11-53-2015>, 2015.
- Chiggiato, J., Bergamasco, A., Borghini, M., Falcieri, F. M., Falco, P., Langone, L., Miserocchi, S., Russo, A., and Schroeder, K.: Dense-water bottom currents in the Southern Adriatic Sea in spring 2012, *Mar. Geol.*, *375*, 134–145, <https://doi.org/10.1016/j.margeo.2015.09.005>, 2016.
- Durrieu de Madron, X., Houpert, L., Puig, P., Sanchez-Vidal, A., Testor, P., Bosse, A., Estournel, C., Somot, S., Bourrin, F., and Bouin, M.-N.: Interaction of dense shelf water cascading and open-sea convection in the northwestern Mediterranean during winter 2012, *Geophys. Res. Lett.*, *40*, 1379–1385, <https://doi.org/10.1002/grl.50331>, 2013.
- Ebser, S., Kersting, A., Stöven, T., Feng, Z., Ringena, L., Schmidt, M., Tanhua, T., Aeschbach, W., and Oberthaler, M.: ³⁹Ar dating with small samples provides new key constraints on ocean ventilation. *Nat. Commun.* *9*, 5046. <https://doi.org/10.1038/s41467-018-07465-7>, 2018.
- Gačić, M., Civitarese, G., Kovačević, V., Ursella, L., Bensi, M., Menna, M., Cardin, V., Poulain, P.-M., Cosoli, S., and Notarstefano, G.: Extreme winter 2012 in the Adriatic: an example of climatic effect on the BiOS rhythm, *Ocean Sci.*, *10*, 513–522, <https://doi.org/10.5194/os-10-513-2014>, 2014.

- Gasparini, G., Ortona, A., Budillon, G., Astraldi, M., and Sansone, E.: The effect of the Eastern Mediterranean Transient on the hydrographic characteristics in the Strait of Sicily and in the Tyrrhenian Sea, *Deep-Sea Res. Pt. I*, 52, 915–935, <https://doi.org/10.1016/j.dsr.2005.01.001>, 2005.
- Hainbucher, D., Álvarez, M., Astray, B., Bachi, G., Cardin, V., Celentano, P., Chaikakis, S., Montero, M. C., Civitarese, G., Hassoun, A. E. R., Fajar, N. M., Fripiat, F., Gerke, L., Gogou, A., Gualart, E., Gülk, B., Lange, N., Rochner, A., Santinelli, C., Schroeder, K., Steinhoff, T., Tanhua, T., Urbini, L., Velaoras, D., Wolf, F., and Welsch, A.: Variability and Trends in Physical and Biogeochemical Parameters of the Mediterranean Sea, Cruise No. MSM72, March 02, 2018 - April 03, 2018, Iraklion (Greece) - Cádiz (Spain), MED-SHIP2. Bremen: Gutachterpanel Forschungsschiffe, 2019.
- Hainbucher, D., Rubino, A., and Klein, B.: Water mass characteristics in the deep layers of the western Ionian Basin observed during May 2003, *Geophys. Res. Lett.*, 33, L05608, <https://doi.org/10.1029/2005GL025318>, 2006.
- Hall, T. M. and Plumb, R. A.: Age as a diagnostic of stratospheric transport, *J. Geophys. Res.: Atmos.*, 99, 1059–1070, <https://doi.org/10.1029/93JD03192>, 1994.
- Hemleben, C.: Oestliches Mittelmeer, Rotes Meer, Arabisches Meer: Cruise No. 31; 30 December 1994-22 March 1995, Leitstelle Meteor, 1996.
- Hemleben, C., Hoernle, K., Jørgensen, B., and Roether, W.: Ostatlantik, Mittelmeer, Schwarzes Meer, Cruise No. 51, 12 September-28 December 2001, METEOR-Berichte, Universität Hamburg, 2003.
- Houpert, L., Durrieu de Madron, X., Testor, P., Bosse, A., d'Ortenzio, F., Bouin, M.-N., Dausse, D., Le Goff, H., Kunesch, S., and Labaste, M.: Observations of open-ocean deep convection in the northwestern Mediterranean Sea: Seasonal and interannual variability of mixing and deep water masses for the 2007–2013 Period, *J. Geophys. Res.: Oceans*, 121, 8139–8171, <https://doi.org/10.1002/2016JC011857>, 2016.
- Jullion, L.: A Tyrrhenian Sea & Alger-provencal component of the MedSHIP Programme, RV Angeles Alvaríño, 18/08/16 - 29/08/16, Palermo (Italy) - Barcelona (Spain), Bremerhaven, EUROFLEETS2 Cruise Summary Report. [Online]. Available: [hdl:10013/epic.5a866780-1f8a-45cf-8111-47b2b5dc29db](https://hdl.handle.net/10013/epic.5a866780-1f8a-45cf-8111-47b2b5dc29db) [Accessed 20 September 2019], 2016.
- Klein, B., Roether, W., Civitarese, G., Gacic, M., Manca, B. B., and d'Alcala, M. R.: Is the Adriatic returning to dominate the production of Eastern Mediterranean Deep Water?, *Geophys. Res. Lett.*, 27, 3377–3380, <https://doi.org/10.1029/2000GL011620>, 2000.
- Klein, B., Roether, W., Manca, B. B., Bregant, D., Beitzel, V., Kovacevic, V., and Luchetta, A.: The large deep water transient in the Eastern Mediterranean, *Deep-Sea Res. Pt. I*, 46, 371–414, [https://doi.org/10.1016/S0967-0637\(98\)00075-2](https://doi.org/10.1016/S0967-0637(98)00075-2), 1999.
- Lascaratos, A., Roether, W., Nittis, K., and Klein, B.: Recent changes in deep water formation and spreading in the eastern Mediterranean Sea: a review, *Prog. Oceanogr.*, 44, 5–36, [https://doi.org/10.1016/S0079-6611\(99\)00019-1](https://doi.org/10.1016/S0079-6611(99)00019-1), 1999.

- Li, P., Mühle, J., Montzka, S.A., Oram, D.E., Miller, B.R., Weiss, R.F., Fraser, P.J., and Tanhua, T.: Atmospheric histories, growth rates and solubilities in seawater and other natural waters of the potential transient tracers HCFC-22, HCFC-141b, HCFC-142b, HFC-134a, HFC-125, HFC-23, PFC-14 and PFC-116. *Ocean Sci.*, 33–60. <https://doi.org/10.5194/os-15-33-2019>, 2019.
- Li, P., and Tanhua, T.: Medusa-Aqua system: simultaneous measurement and evaluation of novel potential halogenated transient tracers HCFCs, HFCs and PFCs in the ocean. *Ocean Sci. Discuss.*, 1–34. <https://doi.org/10.5194/os-2019-101>, 2019.
- Malanotte-rizzoli, P. and Hecht, A.: Large-scale properties of the Eastern Mediterranean: a review, *Oceanol. Acta*, 11, 323–335, 1988.
- Manca, B., Kovačević, V., Gačić, M., and Viezzoli, D.: Dense water formation in the Southern Adriatic Sea and spreading into the Ionian Sea in the period 1997-1999, *J. Mar. Syst.*, 33-34, 133–154, [https://doi.org/10.1016/S0924-7963\(02\)00056-8](https://doi.org/10.1016/S0924-7963(02)00056-8), 2002.
- Manca, B. B., Ibello, V., Pacciaroni, M., Scarazzato, P., and Giorgetti, A.: Ventilation of deep waters in the Adriatic and Ionian Seas following changes in thermohaline circulation of the Eastern Mediterranean, *Clim. Res.*, 31, 239–256, <https://doi.org/10.3354/cr031239>, 2006.
- Medoc Group: Observation of formation of deep water in the Mediterranean Sea, 1969, *Nature*, 227, 1037, <https://doi.org/10.1038/2271037a0>, 1970.
- Nellen, W., Bettac, W., Roether, W., Schnack, D., Thiel, H., Weikert, H., and Zeitschel, B.: MINDIK (Band II), Reise Nr. 5, 2 January-24 September 1987, METEOR-Berichte, Universität Hamburg, 1996.
- Pätzold, J.: Östliches Mittelmeer-Nördliches Rotes Meer 1999: Cruise No. 44, 22 January-16 May 1999, Leitstelle Meteor, 2000.
- Pinardi, N., Zavatarelli, M., Adani, M., Coppini, G., Fratianni, C., Oddo, P., Simoncelli, S., Tonani, M., Lyubartsev, V., and Dobricic, S.: Mediterranean Sea large-scale low-frequency ocean variability and water mass formation rates from 1987 to 2007: A retrospective analysis, *Prog. Oceanogr.*, 132, 318–332, <https://doi.org/10.1016/j.pocean.2013.11.003>, 2015.
- Rhein, M., Send, U., Klein, B., and Krahnemann, G.: Interbasin deep water exchange in the western Mediterranean, *J. Geophys. Res.: Oceans*, 104, 23495–23508, <https://doi.org/10.1029/1999JC900162>, 1999.
- Roether, W., Klein, B., Beitzel, V., and Manca, B. B.: Property distributions and transient-tracer ages in Levantine Intermediate Water in the Eastern Mediterranean, *J. Mar. Syst.*, 18, 71–87, [https://doi.org/10.1016/S0924-7963\(98\)00006-2](https://doi.org/10.1016/S0924-7963(98)00006-2), 1998.
- Roether, W., Klein, B., and Hainbucher, D.: The Eastern Mediterranean Transient: evidence for similar events previously, *The Mediterranean Sea: Temporal variability and spatial patterns*, 75–83, 2014.

- Roether, W., Klein, B., Manca, B. B., Theocharis, A., and Kioroglou, S.: Transient Eastern Mediterranean deep waters in response to the massive dense-water output of the Aegean Sea in the 1990s, *Prog. Oceanogr.*, 74, 540-571, <https://doi.org/10.1016/j.pocean.2007.03.001>, 2007.
- Roether, W., Manca, B. B., Klein, B., Bregant, D., Georgopoulos, D., Beitzel, V., Kovačević, V., and Luchetta, A.: Recent changes in eastern Mediterranean deep waters, *Science*, 271, 333–335, <https://doi.org/10.1126/science.271.5247.333>, 1996.
- Rubino, A. and Hainbucher, D.: A large abrupt change in the abyssal water masses of the eastern Mediterranean, *Geophys. Res. Lett.*, 34, L23607, <https://doi.org/10.1029/2007GL031737>, 2007.
- Šantić, D., Kovačević, V., Bensi, M., Giani, M., Vrdoljak Tomaš, A., Ordulj, M., Santinelli, C., Šestanović, S., Šolić, M., and Grbec, B.: Picoplankton Distribution and Activity in the Deep Waters of the Southern Adriatic Sea, *Water*, 11, 1655, <https://doi.org/10.3390/w11081655>, 2019.
- Schlitzer, R., Roether, W., Oster, H., Junghans, H.-G., Hausmann, M., Johannsen, H., and Michelato, A.: Chlorofluoromethane and oxygen in the Eastern Mediterranean, *Deep Sea Res. Part A. Oceanogr. Res. Pap.*, 38, 1531–1551, [https://doi.org/10.1016/0198-0149\(91\)90088-W](https://doi.org/10.1016/0198-0149(91)90088-W), 1991.
- Schneider, A., Tanhua, T., Körtzinger, A., and Wallace, D. W. R.: High anthropogenic carbon content in the eastern Mediterranean, *J. Geophys. Res.*, 115, C12050, <https://doi.org/10.1029/2010jc006171>, 2010.
- Schneider, A., Tanhua, T., Roether, W., and Steinfeldt, R.: Changes in ventilation of the Mediterranean Sea during the past 25 year, *Ocean Sci.*, 10, 1–16, <https://doi.org/10.5194/os-10-1-2014>, 2014.
- Schroeder, K., Chiggiato, J., Bryden, H., Borghini, M., and Ismail, S. B.: Abrupt climate shift in the Western Mediterranean Sea, *Sci. Rep.*, 6, 23009, <https://doi.org/10.1038/srep23009>, 2016.
- Schroeder, K., Gasparini, G., Tangherlini, M., and Astraldi, M.: Deep and intermediate water in the western Mediterranean under the influence of the Eastern Mediterranean Transient, *Geophys. Res. Lett.*, 33, L21607, <https://doi.org/10.1029/2006GL027121>, 2006.
- Schroeder, K., Josey, S., Herrmann, M., Grignon, L., Gasparini, G., and Bryden, H.: Abrupt warming and salting of the Western Mediterranean Deep Water after 2005: Atmospheric forcings and lateral advection, *J. Geophys. Res.: Oceans*, 115, C08029, <https://doi.org/10.1029/2009JC005749>, 2010.
- Schroeder, K., Ribotti, A., Borghini, M., Sorgente, R., Perilli, A., and Gasparini, G.: An extensive western Mediterranean deep water renewal between 2004 and 2006, *Geophys. Res. Lett.*, 35, L18605, <https://doi.org/10.1029/2008GL035146>, 2008.
- Sparnocchia, S., Gasparini, G., Astraldi, M., Borghini, M., and Pistek, P.: Dynamics and mixing of the Eastern Mediterranean outflow in the Tyrrhenian basin, *J. Mar. Syst.*, 20, 301–317, [https://doi.org/10.1016/S0924-7963\(98\)00088-8](https://doi.org/10.1016/S0924-7963(98)00088-8), 1999.
- Stöven, T. and Tanhua, T.: Ventilation of the Mediterranean Sea constrained by multiple transient tracer measurements, *Ocean Sci.*, 10, 439–457, <https://doi.org/10.5194/os-10-439-2014>, 2014.

- Tanhua, T., Hainbucher, D., Schroeder, K., Cardin, V., Álvarez, M., and Civitarese, G.: The Mediterranean Sea system: a review and an introduction to the special issue, *Ocean Sci.*, 9, 789–803, <https://doi.org/10.5194/os-9-789-2013>, 2013a.
- Tanhua, T., Van Heuven, S., Key, R. M., Velo, A., Olsen, A., and Schirnick, C.: Quality control procedures and methods of the CARINA database, *Earth Syst. Sci. Data*, 2, 35–49, <https://doi.org/10.5194/essd-2-35-2010>, 2010.
- Tanhua, T., Waugh, D. W., and Bullister, J. L.: Estimating changes in ocean ventilation from early 1990s CFC-12 and late 2000s SF₆ measurements, *Geophys. Res. Lett.*, 40, 927–932, <https://doi.org/10.1002/grl.50251>, 2013b.
- Testor, P., Bosse, A., Houpert, L., Margirier, F., Mortier, L., Legoff, H., Dausse, D., Labaste, M., Karstensen, J., and Hayes, D.: Multiscale observations of deep convection in the northwestern Mediterranean Sea during winter 2012–2013 using multiple platforms, *J. Geophys. Res.: Oceans*, 123, 1745–1776, <https://doi.org/10.1002/2016JC012671>, 2018.
- Theocharis, A., Klein, B., Nittis, K., and Roether, W.: Evolution and status of the Eastern Mediterranean Transient (1997–1999), *J. Mar. Syst.*, 33, 91–116, [https://doi.org/10.1016/S0924-7963\(02\)00054-4](https://doi.org/10.1016/S0924-7963(02)00054-4), 2002.
- Velaoras, D., Krokos, G., Nittis, K., and Theocharis, A.: Dense intermediate water outflow from the Cretan Sea: A salinity driven, recurrent phenomenon, connected to thermohaline circulation changes, *J. Geophys. Res.: Oceans*, 119, 4797–4820, <https://doi.org/10.1002/2014JC009937>, 2014.
- Velaoras, D., Papadopoulos, V. P., Kontoyiannis, H., Cardin, V., and Civitarese, G.: Water masses and hydrography during April and June 2016 in the Cretan Sea and Cretan Passage (Eastern Mediterranean Sea), *Deep-Sea Res. Pt. II*, 164, 25–40, <https://doi.org/10.1016/j.dsr2.2018.09.005>, 2018.
- Velaoras, D., Papadopoulos, V. P., Kontoyiannis, H., Papageorgiou, D. K., and Pavlidou, A.: The response of the Aegean Sea (eastern Mediterranean) to the extreme 2016–2017 winter, *Geophys. Res. Lett.*, 44, 9416–9423, <https://doi.org/10.1002/2017GL074761>, 2017.
- Waugh, D. W., Hall, T. M., and Haine, T. W.: Relationships among tracer ages, *J. Geophys. Res.: Oceans*, 108, 3138, <https://doi.org/10.1029/2002JC001325>, 2003.

Supplement of

Recent changes in deep ventilation of the Mediterranean Sea; evidence from long-term transient tracer observations

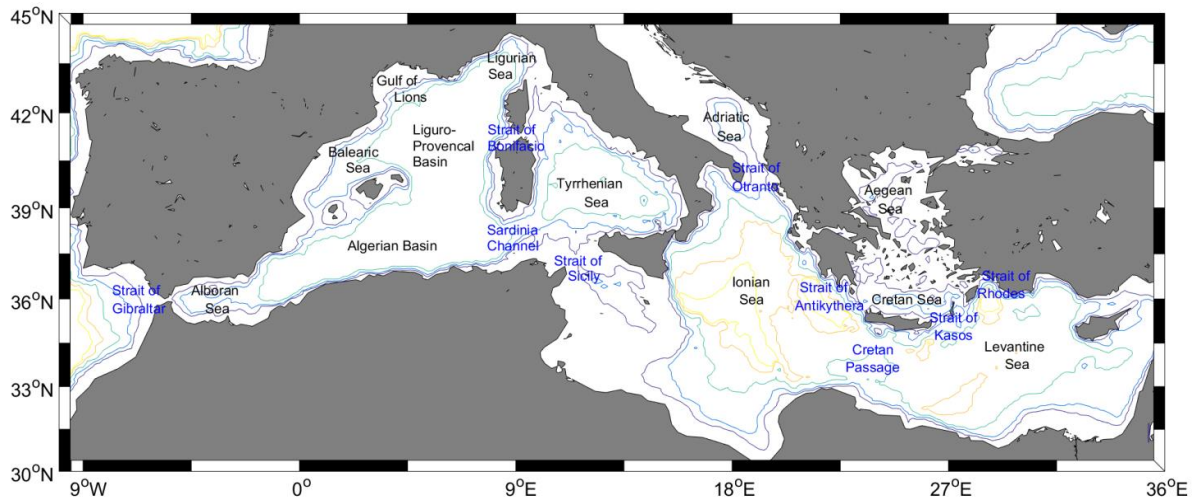


Figure S1. Map of the Mediterranean Sea. The depth contours are 500 m, 1000 m, 2000 m, 3000 m and 3500 m.

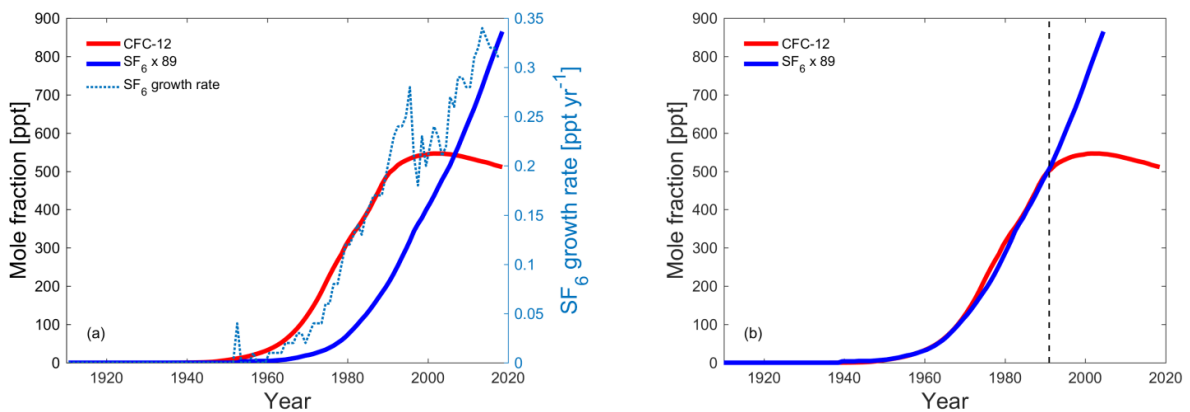


Figure S2. (a) Atmospheric mole fractions of CFC-12 and SF₆ and growth rate of SF₆ in the Northern Hemisphere; (b) Atmospheric mole fractions of CFC-12 and SF₆ but with the SF₆ record shifted back 14 years; the vertical dash line shows 2005 for SF₆ and 1991 for CFC-12.

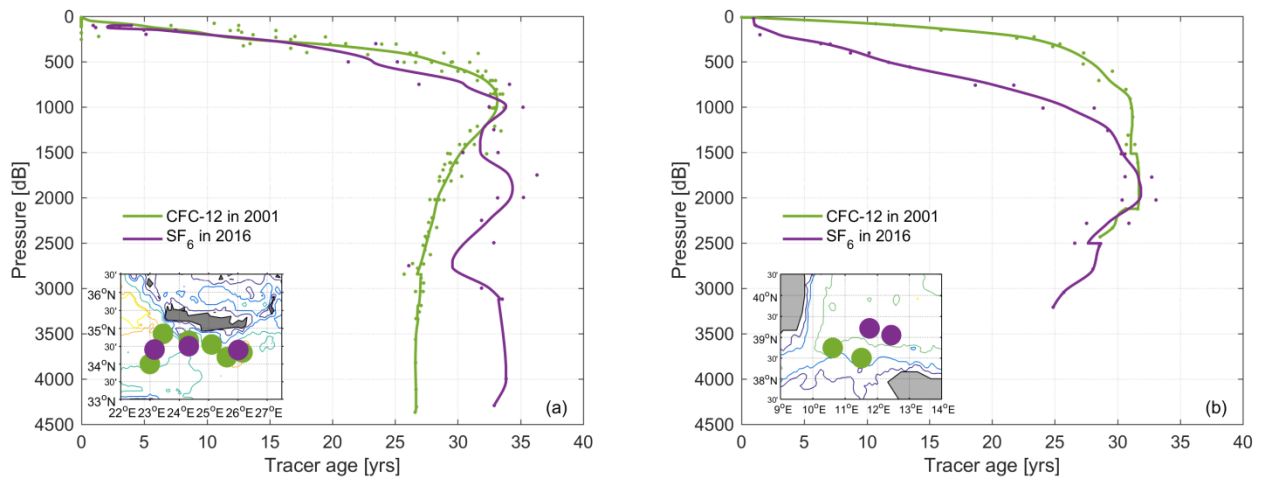


Figure S3. Comparison of averaged tracer age profiles of CFC-12 in 2001 and SF₆ in 2016 in the (a) northern Cretan Passage and (b) the Tyrrhenian Sea. CFC-12 and SF₆ at the stations are shown by dots on the map. CFC-12 data in 2001 is from cruise M51/2; SF₆ data in 2016 is from (a) cruise CERLEV2016 and (b) cruise TalPro2016, respectively.

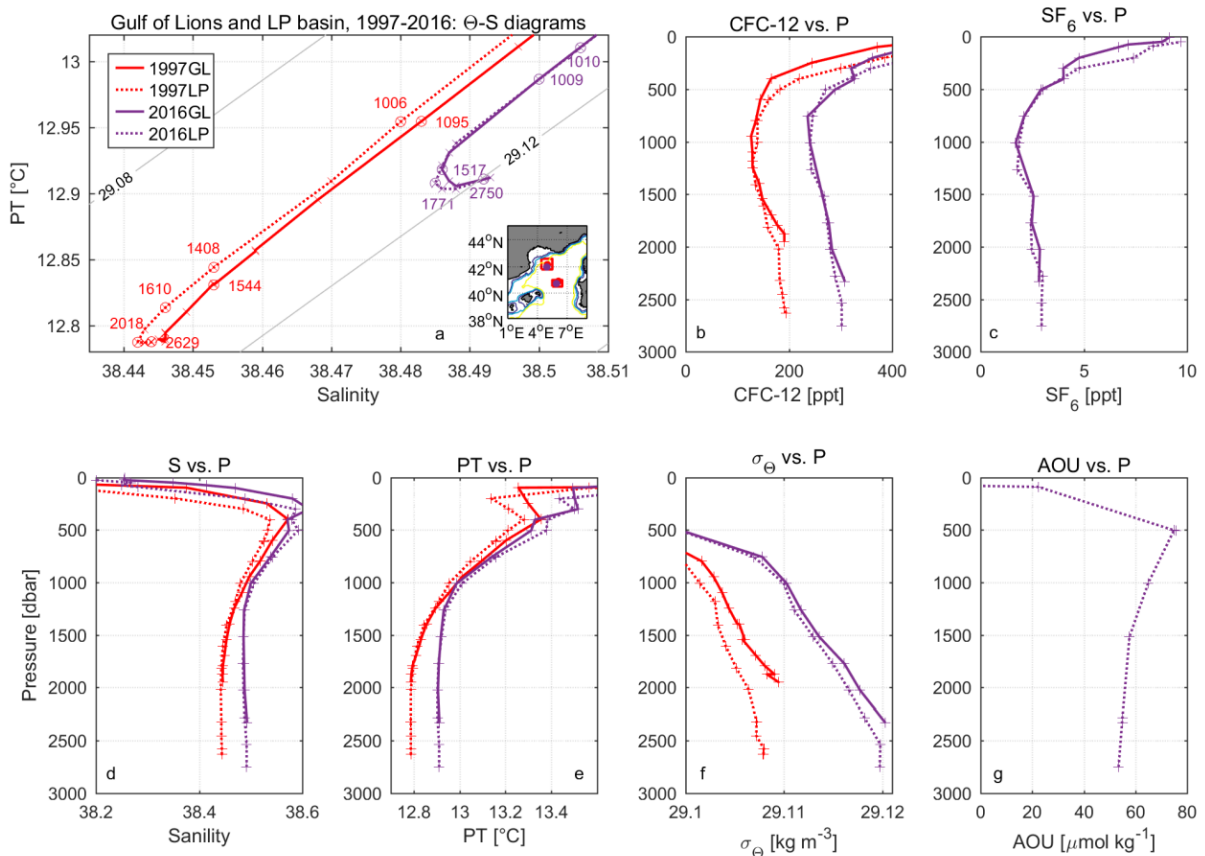


Figure S4. Similar to Fig. 3 but in the Gulf of Lions (GL) and Liguro-Provençal (LP) basin. The stations shown in the Gulf of Lions are P234 756 and TALPro2016 28 and shown by continuous lines. The stations shown in the Liguro-Provençal basin are P234 750 and TALPro2016 25 and shown by dotted lines.

Table S1. Pressure (dbar) of the Tracer Minimum Zone (TMZ) during 1987-2018 based on CFC-12 (black) and SF₆ (blue) observations.

Basin/Sea	1987	1995	1997	1999	2001	2011	2016	2018
Adriatic Sea	~200	300-400	300-400	500-800		~300 ~300	not present not present	
Cretan Sea	~800	400-500				1200-1500 ~1500	1000-2000 ~2000	
North-western Ionian Sea	1200-1300	800-900	~800			~1000 ~1000		
North-eastern Ionian Sea	~1600	~700	~800					1200-1300 1200-1300
Western Ionian Sea	~1900	~1000		700-800	~1000	~1000 ~1000		~1500 ~1500
Central Ionian Sea	1200-1400	~700		700-800	1200-1300	~1000 1000-1500		1200-1300 1200-1300
Eastern Ionian Sea	~1400	~600		~800	700-800	~1000 ~1000		1000-1300 1000-1500
Northern Cretan Passage	2100-2200	~800		~1000	~1000	1500-1600 1700-1800	1000 700-800	1500-1600 2700-2800
Western Levantine basin	~1600	800-900		1200-1300	~1200	~1000 ~1000		
Central Levantine basin	1500-1600	1800-1900		~1300	~1200	~1000 ~1000		
Tyrrhenian Sea	1800-1900		1000-2400	2000-2100	1800-1900	1700-1800 not present	1700-1800 1700-2000	1200-1600 1700-2000
Gulf of Lion			900-1000				700-800 ~1000	
LP basin			1100-1200				~1000 1200-1300	
Central Algerian basin	~700	900-1000				800-1000	1200-1300 1200-1300	1000-1300 1200-1300
Western Algerian basin	800-900	~1100				~1000		1200-1300 ~1000
Alboran Sea			600-700			~1000		700-1000 700-1300

Manuscript II



Atmospheric histories, growth rates and solubilities in seawater and other natural waters of the potential transient tracers HCFC-22, HCFC-141b, HCFC-142b, HFC-134a, HFC-125, HFC-23, PFC-14 and PFC-116

Pingyang Li¹, Jens Mühle², Stephen A. Montzka³, David E. Oram⁴, Benjamin R. Miller³, Ray F. Weiss², Paul J. Fraser⁵, and Toste Tanhua¹

¹GEOMAR Helmholtz Centre for Ocean Research Kiel, Marine Biogeochemistry, 24105 Kiel, Germany

²Scripps Institution of Oceanography, University of California, San Diego, La Jolla, California 92093, USA

³Earth System Research Laboratory, National Oceanic and Atmospheric Administration, Boulder, Colorado 80305, USA

⁴National Centre for Atmospheric Science, Centre for Ocean and Atmospheric Sciences, School of Environmental Sciences, University of East Anglia, Norwich, NR4 7TJ, UK

⁵Climate Science Centre, Commonwealth Scientific and Industrial Research Organization Oceans and Atmosphere, Aspendale, Victoria, 3195, Australia

Correspondence: Toste Tanhua (ttanhua@geomar.de)

Received: 23 July 2018 – Discussion started: 3 August 2018

Revised: 29 November 2018 – Accepted: 10 December 2018 – Published: 11 January 2019

Abstract. We present consistent annual mean atmospheric histories and growth rates for the mainly anthropogenic halogenated compounds HCFC-22, HCFC-141b, HCFC-142b, HFC-134a, HFC-125, HFC-23, PFC-14 and PFC-116, which are all potentially useful oceanic transient tracers (tracers of water transport within the ocean), for the Northern and Southern Hemisphere with the aim of providing input histories of these compounds for the equilibrium between the atmosphere and surface ocean. We use observations of these halogenated compounds made by the Advanced Global Atmospheric Gases Experiment (AGAGE), the Scripps Institution of Oceanography (SIO), the Commonwealth Scientific and Industrial Research Organization (CSIRO), the National Oceanic and Atmospheric Administration (NOAA) and the University of East Anglia (UEA). Prior to the direct observational record, we use archived air measurements, firn air measurements and published model calculations to estimate the atmospheric mole fraction histories. The results show that the atmospheric mole fractions for each species, except HCFC-141b and HCFC-142b, have been increasing since they were initially produced. Recently, the atmospheric growth rates have been decreasing for the HCFCs (HCFC-22, HCFC-141b and HCFC-142b), increasing for the HFCs

(HFC-134a, HFC-125, HFC-23) and stable with little fluctuation for the PFCs (PFC-14 and PFC-116) investigated here. The atmospheric histories (source functions) and natural background mole fractions show that HCFC-22, HCFC-141b, HCFC-142b, HFC-134a, HFC-125 and HFC-23 have the potential to be oceanic transient tracers for the next few decades only because of the recently imposed bans on production and consumption. When the atmospheric histories of the compounds are not monotonically changing, the equilibrium atmospheric mole fraction (and ultimately the age associated with that mole fraction) calculated from their concentration in the ocean is not unique, reducing their potential as transient tracers. Moreover, HFCs have potential to be oceanic transient tracers for a longer period in the future than HCFCs as the growth rates of HFCs are increasing and those of HCFCs are decreasing in the background atmosphere. PFC-14 and PFC-116, however, have the potential to be tracers for longer periods into the future due to their extremely long lifetimes, steady atmospheric growth rates and no explicit ban on their emissions. In this work, we also derive solubility functions for HCFC-22, HCFC-141b, HCFC-142b, HFC-134a, HFC-125, HFC-23, PFC-14 and PFC-116 in water and seawater to facilitate their use as oceanic tran-

sient tracers. These functions are based on the Clark–Glew–Weiss (CGW) water solubility function fit and salting-out coefficients estimated by the poly-parameter linear free-energy relationships (pp-LFERs). Here we also provide three methods of seawater solubility estimation for more compounds. Even though our intention is for application in oceanic research, the work described in this paper is potentially useful for tracer studies in a wide range of natural waters, including freshwater and saline lakes, and, for the more stable compounds, groundwaters.

1 Introduction

Oceanic and natural water transient tracers have time-varying sources and/or sinks. Chlorofluorocarbons (CFCs) were used traditionally as oceanographic transient tracers because of their continuously increasing atmospheric mole fractions until some years ago. They are powerful tools in oceanography for which they are used to, for instance, deduce transport times, estimate mixing rates between water masses, study formation rates of new water masses and determine the anthropogenic carbon (C_{ant}) content of seawater (Weiss et al., 1985; Waugh et al., 2006; Fine, 2011; Schneider et al., 2012; Stöven et al., 2016). The production and consumption of CFCs have been phased out as a consequence of the implementation of the Montreal Protocol (MP) on Substances that Deplete the Ozone Layer (first in developed nations by 1996, followed by developing nations by 2010) designed to halt the degradation of the Earth's protective ozone layer (Fig. 1). The atmospheric mole fractions of the major CFCs have been decreasing since the mid-1990s to early 2000s (Carpenter et al., 2014; Bullister, 2015), and although CFCs are valuable indices to quantify deep water transport, the use of CFCs as oceanographic transient tracers has become more difficult for recently ventilated water masses. During recent decades sulfur hexafluoride (SF_6) has been added to the suite of transient tracers measured in the ocean (Tanhua et al., 2004; Bullister et al., 2006). Its atmospheric mole fractions are still increasing and its atmospheric distribution is measured widely. However, SF_6 is also facing restrictions; for example, in Europe it has been banned for release as a tracer gas and in all applications except high-voltage switchgear since 1 January 2006 (Fig. 1). Since a combination of transient tracers is needed to constrain ventilation (Waugh et al., 2002; Stöven et al., 2015), it is necessary to explore other transient tracers with positive growth rates for the study of mixing and transport processes in the oceans and in other natural waters.

1.1 Potential transient tracers

Generally, several requirements for a useful oceanic transient tracer can be defined: the tracer should have a well-established, transient source function (or well-defined decay function); have a low or well-known natural background; be

conservative (not produced or destroyed) in the marine environment; and be measured relatively inexpensively, accurately and rapidly. Potential candidates as transient tracers that fulfill at least some of the requirements listed above include hydrochlorofluorocarbons (HCFCs) such as HCFC-22, HCFC-141b and HCFC-142b, hydrofluorocarbons (HFCs) such as HFC-134a, HFC-125 and HFC-23, and perfluorocarbons (PFCs) such as PFC-14 and PFC-116. As a first step in evaluating the usefulness of these compounds as oceanic transient tracers, we synthesize their atmospheric mole fraction histories and review their solubilities. An upcoming work will evaluate the in-field data on these compounds.

HCFC-22. Chlorodifluoromethane (CHClF_2) is the most abundant HCFC in the global atmosphere. It was first synthesized in 1928 and commercial use started in 1936 (Calm and Domanski, 2004). It has been used dispersedly in domestic and commercial refrigeration, as a spray-can propellant, and in extruded polystyrene foam industries (McCulloch et al., 2003; Jacobson, 2012) and nondispersedly as the feedstock in fluoropolymer production (Miller et al., 2010). HCFC-22 was first measured in the atmosphere in 1979 (Rasmussen et al., 1980); a pronounced increase in its abundance in the 1990s was found in both hemispheres as HCFC-22 became an interim replacement for CFC-12 since the late 1980s (Xiang et al., 2014). There are no known natural emission sources for HCFC-22 (Saikawa et al., 2012). A considerable amount of literature has been published on the atmospheric histories of HCFC-22. Montzka et al. (1993) presented the NOAA network measurements and historic mole fractions from a two-box model for HCFC-22 from 1980 to 1993, and these have since been updated and augmented with measurements from Antarctic firn air and box models to construct an atmospheric history and emissions for HCFC-22 from 1944 to 2014 (Montzka et al., 2010a, 2015). Sturrock et al. (2002) presented CSIRO HCFC-22 data from 1940 to 2000 based on an analysis of Antarctic firn air samples using the AGAGE instrumentation. In 2012, Saikawa et al. (2012) reported observations and archived air measurements from multiple networks, combined with the Model for Ozone And Related chemical Tracers (MOZART), to present the atmospheric mole fractions for HCFC-22 from 1995 to 2009.

HCFC-141b. 1,1-Dichloro-1-fluoroethane ($\text{CH}_3\text{CCl}_2\text{F}$) has been widely used as a foam-blowing agent in rigid polyurethane foams for insulation purposes and in integral skin foams as a replacement for CFC-11. It was also employed as a solvent for lubricants, coatings and cleaning fluids for aircraft maintenance and electrical equipment as a replacement for CFC-113 (Derwent et al., 2007). The industrial production and use of HCFC-141b have greatly increased since the early 1990s, as have its global mole fractions and emissions (Oram et al., 1995; Sturrock et al., 2002; Montzka et al., 2015; Prinn et al., 2018a).

HCFC-142b. 1-Chloro-1,1-difluoroethane (CH_3CClF_2) has largely been emitted from extruded polystyrene board stock as a foam-blowing agent combined with small emis-

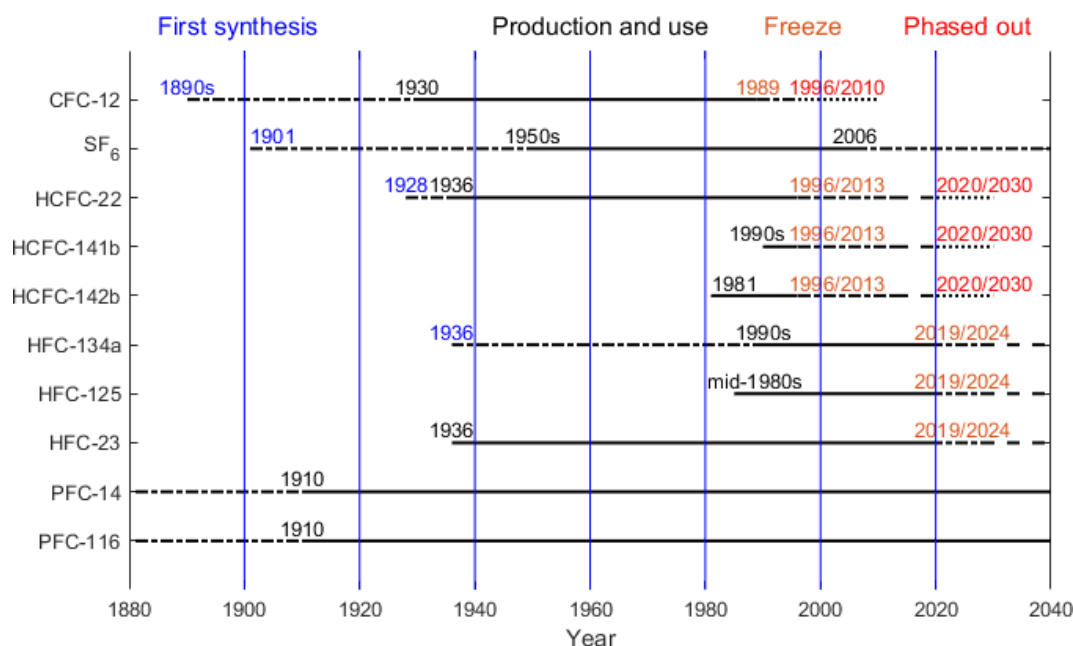


Figure 1. Comparison of production and use histories of CFC-12, SF₆, HCFCs, HFCs and PFCs.

sions from refrigeration applications as a replacement for CFC-12 (TEAP, 2003). Previous studies described measurements of HCFC-141b and HCFC-142b from the AGAGE network, UEA and CSIRO including measurements of the Cape Grim Air Archive (CGAA) and Antarctic firm air (Oram et al., 1995; Sturrock et al., 2002; Simmonds et al., 2017; Prinn et al., 2018a). NOAA flask and firm air measurements for both compounds have also been reported (Montzka et al., 1994, 2009, 2015).

HFC-134a. 1,1,1,2-Tetrafluoroethane (CH₂FCF₃) is the most abundant HFC in the Earth's atmosphere. It was first synthesized by Albert Henne in 1936 (Matsunaga, 2002). Extensive production and emission of HFC-134a began in the early 1990s. It was used as a preferred refrigerant in domestic, commercial and automotive air conditioning and refrigeration to replace CFC-12. It is also used to a lesser extent as a foam-blowing agent, cleaning solvent, fire suppressant and propellant in metered-dose inhalants and aerosols (Simmonds et al., 2015, 2017). Continuous and substantially increasing atmospheric levels of HFC-134a were found over the past 2 decades (Xiang et al., 2014). A number of researchers have reported the atmospheric history of HFC-134a. The observational record of HFC-134a started from near-zero levels in the background atmosphere (Oram et al., 1996). Montzka et al. (1996) reported initial measurements from the NOAA network for HFC-134a from the late 1980s to mid-1995, which have since been updated (Montzka et al., 2015). Simmonds et al. (1998) presented AGAGE observations for HFC-134a from 1994 to 1997, updated by O'Doherty et al. (2004) from 1998 to 2002, by Rigby et al. (2014) and by Prinn et al. (2018a) to recent times.

HFC-125. Pentafluoroethane (CHF₂CF₃) is currently the third most abundant HFC. It is used primarily in refrigerant blends for commercial refrigeration applications and has a minor use in fire-fighting equipment as a replacement for halons. Atmospheric mole fractions of HFC-125 are also rising consistently as one of the substitutes for CFCs (O'Doherty et al., 2009; Rigby et al., 2014; Prinn et al., 2018a). In 2009, O'Doherty et al. (2009) reported in situ and archived air measurements from Mace Head and Cape Grim, combined with the AGAGE 2-D 12-box model results for HFC-125 from 1977 to 2009. In 2015, Montzka et al. (2015) reported results of flask measurements of HFC-125 spanning from 2007 to 2013.

HFC-23. Fluoroform or trifluoromethane (CHF₃) is a by-product from the industrial production of HCFC-22. Historically it has been considered as waste and simply vented to the atmosphere, although process optimization and abatement can eliminate most or all emissions. HFC-23 was also used as a feedstock for halon-1301 (CBrF₃) production. Small amounts are reportedly used in semiconductor (plasma etching) fabrication, in very low-temperature refrigeration (dispersive) and in specialty fire-suppressant systems (dispersive) (McCulloch and Lindley, 2007). HFC-23 was first reported in the background atmosphere by Oram et al. (1998) in samples dating back to 1978. It continued to increase in the atmosphere (Miller et al., 2010; Rigby et al., 2014; Simmonds et al., 2018) despite the voluntary and regulatory efforts in developed nations and abatement measures in developing nations financially supported by the United Nations Framework Convention on Climate Change (UNFCCC) Clean Development Mechanism (CDM). In the past 3 decades, a

number of researchers have reported the atmospheric mole fractions of HFC-23. In 1998, Oram et al. (1998) reported measured and model-generated mole fractions of HFC-23 at Cape Grim from 1978 to 2005. Updated in situ AGAGE measurements and results from the AGAGE 2-D atmospheric 12-box chemical transport model for HFC-23 from 1978 to 2010 and from 1950 to 2016 have been presented by Miller et al. (2010) and Simmonds et al. (2018), respectively. A history derived from multiple firn air sample collections was also published in 2010 (Montzka et al., 2010a).

PFC-14. Tetrafluoromethane or carbon tetrafluoride (CF_4) is the most abundant perfluorocarbon (PFC) in the Earth's atmosphere and is one of the most long-lived tracer gases with an atmospheric lifetime of more than 50 000 years. The presence of carbon tetrafluoride in the atmosphere was first deduced by Gassmann (1974) from an analysis of contaminant levels of PFC-14 in high-purity krypton samples. The first atmospheric measurements of PFC-14 were made by Rasmussen et al. (1979). It has a background atmospheric mole fraction due to its natural source from the rocks and soils, especially tectonic activity (Deeds et al., 2015). The preindustrial level was 34.05 ± 0.33 ppt for PFC-14 (Trudinger et al., 2016). The primary anthropogenic sources of PFC-14 are aluminum production, the semiconductor industry (Khalil et al., 2003; Mühle et al., 2010; Fraser et al., 2013) and perhaps the production of rare earth elements. Consequently, atmospheric mole fractions have approximately doubled since the early 20th century (Mühle et al., 2010; Trudinger et al., 2016; Prinn et al., 2018a).

PFC-116. Hexafluoroethane (C_2F_6) is another long-lived tracer gas with an atmospheric lifetime of at least 10 000 years. The tropospheric abundance of PFC-116 was first determined by Penkett et al. (1981). It has a small natural abundance (Mühle et al., 2010; Trudinger et al., 2016); the preindustrial level has been estimated to be 0.002 ppt (Trudinger et al., 2016). Like CF_4 it is also emitted as a by-product of aluminum production (Fraser et al., 2013) and during semiconductor manufacturing.

1.2 Production and ban histories

The major atmospheric degradation pathway of HCFCs and HFCs is through reaction with hydroxyl radicals (OH) in the troposphere (Montzka et al., 2010b). Combustion in thermal power stations has been pointed out as a tropospheric sink of PFCs (Cicerone, 1979; Ravishankara et al., 1993; Morris et al., 1995). The atmospheric lifetimes, ocean partial lifetimes, ozone depletion potentials (ODPs) and global warming potentials (GWPs) for HCFC-22, HCFC-141b, HCFC-142b, HFC-23, HFC-134a, HFC-125, PFC-14 and PFC-116 are listed in the Table 1. As shown Table 1, the atmospheric lifetimes of HCFCs and HFCs with respect to hydrolysis in seawater are very long (Yvon-Lewis and Butler, 2002; Carpenter et al., 2014), ranging from thousands to millions of years, indicating that HCFCs and HFCs are relatively stable

in seawater. PFCs have atmospheric lifetimes on the order of thousands of years and very low solubilities in seawater. The production and use histories of CFC-12, SF_6 , HCFCs, HFCs and PFCs are plotted in Fig. 1. HCFCs have been regulated with the aim of ceasing production and consumption by 2020 for non-Article 5 (developed) countries and 2030 for Article 5 (developing) countries (although this only covers dispersive applications) and phaseout beginning with a freeze in 1996 for developed nations and in 2013 for developing nations under the MP and its more recent amendments. Because of the high GWP of HFCs, 197 countries recently committed to cutting the production and consumption of HFCs by more than 80 % over the next 30 years under the Kigali Amendment of the MP, although not all of these countries have ratified this amendment. The reductions in HFC production and consumption are based on GWP-weighted quantities. Developed countries that have ratified the amendment have agreed to reduce HFC consumption beginning in 2019. Most developing countries will freeze consumption in 2024, some in 2028. This measure will most likely slow down HFC growth rates, eventually leading to a decline in their atmospheric mole fraction, similar to what is observed for CFCs.

In order to explore if these halogenated compounds can be used as transient ocean tracers, their atmospheric histories (source functions) and natural background should be established. Previous work has reconstructed annually averaged atmospheric mole fraction histories for some trace gases for use in tracer oceanographic applications. For example, Walker et al. (2000) reported annual mean atmospheric mole fractions for CFC-11, CFC-12, CFC-113 and CCl_4 for the period 1910–1998 and updated the data to 2008 on the website (<http://bluemoon.ucsd.edu/pub/cfchist/>, last access: 20 December 2018). On the basis of Walker's work, Bullister (2015) reported atmospheric histories for CFC-11, CFC-12, CFC-113, CCl_4 , SF_6 and N_2O for the period 1765–2015. Previous work related to our target compounds has mainly focused on the atmospheric history over specific periods, often at a high temporal resolution. We have listed these works above. For our purposes, we are interested in a consistent record of the full atmospheric history at annual temporal resolution. As Trudinger et al. (2016) presented the consistent atmospheric histories of PFC-14 and PFC-116 from 1900 to 2014, we only study the growth rates for these two compounds and evaluate their utility as oceanic transient tracers.

In this study, drawing on previous literature and published data, we present atmospheric mole fractions (JFM means, annual means and JAS means) and growth rates for HCFC-22, HCFC-141b, HCFC-142b, HFC-134a, HFC-125, HFC-23, PFC-14 and PFC-116 for both the Northern (NH) and Southern Hemisphere (SH). The JFM means (the average of monthly means in January, February and March) and JAS means (the average of monthly means in July, August and September) are chosen to coincide with the coldest part of the year in the NH and SH, respectively, i.e., the time of (deep) water mass formation when ambient trace gases are

Table 1. Atmospheric lifetimes, ocean partial lifetimes, ozone depletion and global warming potentials of HCFC-22, HCFC-141b, HCFC-142b, HFC-134a, HFC-125, HFC-23, PFC-14 and PFC-116.

Compound	Molecular formula	Atmospheric lifetimes ^a (years)	Ocean partial lifetimes ^b (years)	ODP ^c	GWP ^d 100-year horizon
HCFC-22	CHClF ₂	12	1174	0.025	1765
HCFC-141b	C ₂ H ₃ Cl ₂ F	9.4	9190	0.082	782
HCFC-142b	C ₂ H ₃ ClF ₂	18	122 200	0.025	1982
HFC-134a	CH ₂ FCF ₃	14	5909	0	1301
HFC-125	C ₂ HF ₅	31	10 650	0	3169
HFC-23	CHF ₃	228	–	0	12 398
PFC-14	CF ₄	> 50 000	–	0	6626
PFC-116	C ₂ F ₆	> 10 000	–	0	11 123

^a See SPARC (2013). ^b Partial atmospheric lifetimes with respect to oceanic uptake; see Yvon-Lewis and Butler (2002) and Carpenter et al. (2014). ^c ODP: ozone depletion potential; see Laube et al. (2013). ^d GWP: global warming potential; see Hodnebrog et al. (2013).

carried from the surface to the interior ocean. The reconstructed atmospheric histories have been compiled from a combination of air measurements and model calculations. In order to provide a comprehensive and consistent view of halogenated compound atmospheric distribution and changes over time, ambient air measurements published by the Advanced Global Atmospheric Gases Experiment (AGAGE), the Scripps Institution of Oceanography (SIO), the Commonwealth Scientific and Industrial Research Organization (CSIRO), the National Oceanic and Atmospheric Administration (NOAA) and the University of East Anglia (UEA) are considered in this study. The calibration scale differences of these networks in the form of scale conversion factors are determined. SIO and CSIRO data are reported on AGAGE scales. NOAA and UEA data are converted to AGAGE scales by these conversion factors. For years prior to atmospheric observations, the reconstructed dry mole fractions for each species were provided by a combination of atmospheric models, firm air measurements and the analysis of archived air samples. The aim of this work is to synthesize existing data and model results into one consistent data product of atmospheric history with annual values useful for ocean tracer applications; it is not intended to replace more detailed atmospheric studies. All reported values in this study are dry air mole fractions. In a similar work, Meinshausen et al. (2017) provided consolidated datasets of historical atmospheric mole fractions of 43 greenhouse gases (GHGs). Compared with this earlier study, the differences and added value of this study are that we (1) incorporated UEA data not included in the Meinshausen et al. (2017) study, (2) report data on a common calibration scale (AGAGE) by converting NOAA and UEA data to AGAGE scales, (3) estimated annual means based on baseline data with local pollution events removed, (4) estimated the propagated uncertainties based on the original standard deviations of monthly means or data points, (5) used a different method for data fitting, and (6) presented the atmospheric histories for winter (JFM

means in the NH and JAS means in the SH), which is especially useful for oceanic transient tracers studies.

In addition, we explore whether these compounds can be used as oceanic transient tracers by reporting on the solubility characteristics of each of the gases. We are not aware of any published estimates that directly provide solubility functions of all target compounds in seawater, and only very limited studies (with several data points) on the solubility of these compounds in seawater have been reported. Scharlin and Battino (1995) published four solubility data points in the temperature range 15–30 °C and a salinity of 35.086 for PFC-14 in seawater. In the present analysis, the water and seawater solubility functions of HCFC-22, HCFC-141b, HCFC-142b, HFC-134a, HFC-125, HFC-23, PFC-14 and PFC-116 are derived by the combined method based on the combination of the Clark–Glew–Weiss (CGW) fit to estimate their water solubility function and the poly-parameter linear free-energy relationships (pp-LFERs) to estimate their salting-out coefficients. Three concluded methods (the (revised) method II only based on the pp-LFERs, the combined method and the experimental method) for seawater solubility estimation are also provided for more compounds. Although the atmospheric histories and solubility functions in water and seawater of the target compounds are intended for oceanic research, the work described in this paper is potentially useful for studying a range of natural waters, including freshwater, saline lakes and groundwaters.

2 Data and methods

2.1 Data from the AGAGE network

2.1.1 AGAGE in situ measurements and instrumentation

In situ atmospheric measurements have been made by the Advanced Global Atmospheric Gases Experiment (AGAGE) (Prinn et al., 2000; O'Doherty et al., 2004,

2009; Miller et al., 2010; Mühle et al., 2010; Prinn et al., 2018a, b). The data are available on the AGAGE website (<http://agage.eas.gatech.edu/>, last access: 20 December 2018) where historic and the newest atmospheric measurements are reported. AGAGE provides measurements of more than 40 compounds, whereas we focus only on HCFC-22, HCFC-141b, HCFC-142b, HFC-134a, HFC-125, HFC-23, PFC-14 and PFC-116 (Table S1 in the Supplement). There are more than 10 AGAGE and affiliated stations globally, mostly located at coastal or mountain sites. Here we exclude all AGAGE stations at tropical latitudes that are periodically subjected to air masses originating in the other hemisphere (Prinn et al., 1992, 2000; Walker et al., 2000). Observations at the AGAGE remote stations Mace Head, Ireland (MHD; 53° N, 10° W), and Trinidad Head, California (THD; 41° N, 124° W), were assumed to represent 30–90° N atmospheric mole fractions, whereas observations at Cape Grim, Tasmania (CGO; 41° S, 145° E), represent 30–90° S mole fractions. Small latitudinal gradients in the AGAGE Mace Head and Trinidad Head observations of different compounds are present but assumed to be of minor importance to this work. These stations, their locations and the date ranges of the samples used in this study are listed in Table S1. The “pollution-free” monthly mean atmospheric mole fractions and standard deviations for all target compounds are used in this study.

All ambient air measurements were carried out using two similar measurement technologies over time based on the cryogenic pre-concentration with gas chromatography separation and mass spectrometry detection (GC-MS). The initial instrument used was the ADS (adsorption–desorption system) with GC-MS, but in the early to mid-2000s this was replaced by the Medusa GC-MS with a doubled sampling frequency, upgraded sample pre-concentration methodologies, extended compound selection and improved measurement precisions. For more information on the instrumentation and the working standards, see Simmonds et al. (1995), Miller et al. (2008), Arnold et al. (2012) and Prinn et al. (2018a). For the measurement precision, see Prinn et al. (2018a).

2.1.2 AGAGE measurements of CSIRO and SIO archived air

To extend the available mole fraction records back in time, NH and SH air archive samples collected by CSIRO and SIO were measured using AGAGE instrumentation for target compounds. Southern Hemisphere Cape Grim Air Archive (CGAA) samples, which are background or “baseline” air, were collected at the Baseline Air Pollution Station, Cape Grim, Tasmania, by CSIRO and the Bureau of Meteorology. The samples have been cryogenically collected into 34 L electropolished stainless-steel canisters (Langenfelds et al., 1996; Fraser et al., 2017) since 1978. The CGAA samples were analyzed on Medusa-9 in the CSIRO laboratory at Aspendale (Miller et al., 2010). Northern Hemisphere (NH) samples used for this paper were filled during background

conditions mostly at Trinidad Head, but also at La Jolla, California, Cape Meares, Oregon (courtesy of the Oregon Graduate Center via CSIRO, Aspendale, and the Norwegian Institute for Air Research, Oslo, Norway), and Point Barrow, Alaska (courtesy of Robert Rhew, University of California, Berkeley), and analyzed at SIO, La Jolla, on laboratory-based Medusa GC-MS instruments (Medusa-1, Medusa-7) (O’Doherty et al., 2009). A stepwise tightening filtering algorithm was applied based on their deviations from a fit through all data from each semi-hemisphere (including pollution-free monthly mean *in situ* data) to remove outliers (Mühle et al., 2010; Vollmer et al., 2016).

HFC-134a air archive data obtained using AGAGE instrumentation at CSIRO and SIO are reported here for the first time (Table S1d). The archived air measurements for HFC-125 reported by O’Doherty et al. (2009) are used in this study (Table S1e) and have been updated to include more present data. The CGAA archived air measurements for HCFC-22 reported by Miller et al. (1998) are used here. CGAA Medusa-3 and Medusa-9 measurements for HFC-23 from AGAGE reported by Miller et al. (2010) are also reported here (Table S1f). CSIRO SH and SIO NH archived air samples have been analyzed on AGAGE GC-MS instrumentation at CSIRO, Aspendale and at SIO, La Jolla, for PFC-14 and PFC-116 (Mühle et al., 2010).

2.1.3 AGAGE measurements of CSIRO firn air

The firn layer is unconsolidated snow overlaying an ice sheet. Large volumes (hundreds of liters) of air trapped in firn can be extracted for subsequent analysis. From the measured firn depth profiles, atmospheric histories can be derived using firn diffusion models. Firn air histories typically cover the period from the present day (or drilling date) to up to 100 years ago.

The firn air samples for HCFC-141b and HCFC-142b were collected from six depths at Law Dome, Antarctic, in 1997–1998 at the DSSW20K site (Table S1b and c) (Sturrock et al., 2002). The firn air samples were measured on the AGAGE ADS–GC-MS instrument at Cape Grim. Antarctic firn air samples have also been used for the reconstruction of the atmospheric histories of PFC-14 and PFC-116 (Trudinger et al., 2016).

2.2 Data from the NOAA network

2.2.1 NOAA flask measurements

Flask air measurements of the compounds considered in this study have been made by the National Oceanic and Atmospheric Administration (NOAA) as early as 1992 (Montzka et al., 1994, 1996, 2009, 2015). The data are available on the NOAA website (<ftp://ftp.cmdl.noaa.gov/hats/>, last access: 20 December 2018) where the latest atmospheric measurements are reported. There are many NOAA and affiliated stations globally. In order to be consistent with the chosen

AGAGE stations, NOAA observations at only Mace Head, Ireland (MHD; 42 m above sea level; m a.s.l.), for HCFC-22, HCFC-141b, HCFC-142b and HFC-134a as well as Trinidad Head, USA (THD; 120 m a.s.l.), for HCFC-22, HCFC-141b, HCFC-142b, HFC-134a and HFC-125 are used to represent atmospheric mole fractions from 30–90° N. The observations at Cape Grim, Australia (CGO; 164 m a.s.l.), represent the 30–90° S mole fractions. These stations, their locations and the sampling dates of the samples used in this study are listed in Table S1 and are essentially identical to the corresponding AGAGE stations.

Air samples are analyzed in the NOAA/ESRL/GMD Boulder laboratory by GC-MS techniques for HCFC-22, HCFC-141b, HCFC-142b, HFC-134a and HFC-125. More details are given by Montzka et al. (1993, 1994, 1996, 2015). The working standards and measurement precision are also reported in these studies.

2.2.2 NOAA measurements of archived and shipborne air samples

Archived air and shipborne air measurements from both hemispheres for HCFC-141b and HCFC-142b are given in Thompson et al. (2004). The archived air samples for HCFC-141b and HCFC-142b have been obtained at Niwot Ridge (NWR; 40° N, 106° W) since 1986. The cruise air samples were collected during the Soviet–American Gas and Aerosol Experiment (SAGA) II cruise in the Pacific Ocean in 1987 (37° N–30° S, 160–170° W).

Archived air and shipborne air measurements for HFC-134a were presented by Montzka et al. (1996). Samples were collected at NWR. Samples were obtained shipboard during two cruises, one in the Pacific Ocean in 1987 (SAGA II above) and in 1994 (41° N–47° S, 127–76° W) and another in the Atlantic Ocean in 1994 (46° N–48° S, 14–60° W).

2.2.3 NOAA measurements of firn air

The first measurements of HCFC-141b and HFC-134a in firn air were made by Butler et al. (1999) and showed that there are no natural sources for these compounds.

2.3 Data from the UEA network

UEA archived air

University of East Anglia (UEA) measurements on Cape Grim Air Archive subsamples (since 1978) and flask samples collected at Cape Grim are updated following the original publications for HCFC-141b, HCFC-142b (Oram et al., 1995) and HFC-134a (Oram et al., 1996). The Cape Grim archived air contains trace gas records known to be representative of background air in the Southern Hemisphere. UEA has analyzed subsamples of the Cape Grim Air Archive, whereas the CGAA has been analyzed directly on AGAGE

instrumentation at Cape Grim, CSIRO, Aspendale and at the SIO, La Jolla (Sect. 2.1.2).

The Cape Grim archived air, which is located at CSIRO, Aspendale, was subsampled for the UEA at Aspendale and the UEA flask air samples were collected directly at Cape Grim; both were analyzed by GC-MS at the UEA for HCFC-141b, HCFC-142b and HFC-134a (Oram et al., 1995, 1996) (Table S1b and c). The working standards and measurement uncertainties were also shown in the abovementioned studies.

2.4 Data from models

In order to estimate atmospheric mole fractions before direct atmospheric measurements commenced, the results from published models, a two-box model for HCFC-22 (Montzka et al., 2010a) and the AGAGE 2-D atmospheric 12-box chemical transport model for HFC-23 (Cunnold et al., 1983, 1994; Miller et al., 2010; Rigby et al., 2011), PFC-14 and PFC-116 (Trudinger et al., 2016), are also included in this study (Table S1g and h).

The two-box model for HCFC-22 from Montzka et al. (2010a) considers the atmosphere as two boxes – one box representing each hemisphere. Each hemisphere is assumed to be well mixed and a standing vertical gradient is assumed. Using the two-box model, Montzka et al. (2010a) derived the atmospheric mole fractions from 1944 to 2009 for HCFC-22 by assuming a constant 0.95 scaling of global emissions estimated by the Alternative Fluorocarbons Environmental Acceptability Study (AFEAS).

The AGAGE two-dimensional atmospheric 12-box chemical transport model, used here for HFC-23, PFC-14 and PFC-116 mole fractions, contains four lower tropospheric boxes, four upper tropospheric boxes and four stratospheric boxes, with boundaries at 30° N, 0 and 30° S in the horizontal and 500 and 200 hPa in the vertical (Cunnold et al., 1983, 1994; Rigby et al., 2011). It has previously used to estimate mole fractions and emissions of CFC-11, CFC-12 and various other trace gases. Miller et al. (2010) derived mole fractions for HFC-23 for the period 1978–2009 through an inversion technique using this 2-D 12-box model, but not back to zero atmospheric mole fraction. Trudinger et al. (2016) calculated the atmospheric mole fractions of PFC-14 and PFC-116 in each semi-hemisphere since 1900 by combining the data from ice core, firn, air archive and in situ measurements, thus extending the work of Mühle et al. (2010).

2.5 AGAGE, NOAA and UEA calibration scales

The latest AGAGE absolute calibration scales for various trace gases are displayed on the AGAGE website (<https://agage.mit.edu/>, last access: 20 December 2018 and <http://agage.eas.gatech.edu/data>, last access: 20 December 2018). AGAGE in situ measurements have been reported on the latest SIO absolute calibration scales for HCFC-

Table 2. Primary calibration scale conversion factors for HCFC-22, HCFC-141b, HCFC-142b, HFC-134a, HFC-125 and HFC-23 between AGAGE (UB and SIO) and NOAA^a.

HCFC-22	SIO-93	SIO-98	SIO-05	NOAA-1992
SIO-98	1.0053 ^b	–	–	–
NOAA-1992	0.997 ± 0.004 ^c	0.993 ± 0.007 ^b	–	–
NOAA-2006	–	–	0.9971 ± 0.0027 ^d	1.005 ^e
HCFC-141b		UB-98	SIO-05	
NOAA-1994		1.006 ± 0.003 ^b	0.9941 ± 0.0049 ^d	
HCFC-142b		UB-98	SIO-05	
NOAA-1994		0.937 ± 0.003 ^b	0.9743 ± 0.0052 ^d	
HFC-134a		UB-98	SIO-05	
NOAA-1995		1.035 ± 0.004 ^b	1.0015 ± 0.0048 ^d	
HFC-125		UB-98	SIO-14	
SIO-14		1.0826 ^f	–	
NOAA-2008		–	0.946 ± 0.008 ^g	

^a Example: for HCFC-22 measurement results reported on the SIO-98 scale, multiply 1.0053 to convert to the SIO-93 scale. AGAGE: Advanced Global Atmospheric Gases Experiment, UB: University of Bristol, SIO: Scripps Institution of Oceanography, NOAA: National Oceanic and Atmospheric Administration. ^b Prinn et al. (2000). ^c Miller et al. (1998). ^d Prinn et al. (2018a). ^e NOAA calibration scales for various trace gases (<https://www.esrl.noaa.gov/gmd/ccl/scales.html>, last access: 20 December 2018). ^f AGAGE calibration scale (http://agage.eas.gatech.edu/data_archive/agage/AGAGE_scale_2018_v1.pdf, last access: 20 December 2018). ^g Simmonds et al. (2017).

22 (SIO-05), HCFC-141b (SIO-05), HCFC-142b (SIO-05), HFC-134a (SIO-05), HFC-125 (SIO-14), HFC-23 (SIO-07), PFC-14 (SIO-05) and PFC-116 (SIO-07), as have archived air measurements for HFC-134a and HFC-23. The archived air measurements for HFC-125 reported by O'Doherty et al. (2009) on the calibration scale UB-98 (UB: University of Bristol) were converted to the latest scale SIO-14 by the conversion factor SIO-14 / UB-98 = 1.0826 (see Table 2). The archived air measurements for HCFC-22 reported by Miller et al. (1998) on the calibration scale SIO-93 were converted to the latest scale SIO-05 by the combined conversion factors NOAA-1992 / SIO-93 = 0.997 ± 0.004, NOAA-2006 / NOAA-1992 = 1.005 and NOAA-2006 / SIO-05 = 0.9971 ± 0.0027 (see Table 2). The firm air measurements for HCFC-141b and HCFC-142b were reported on the calibration scale UB-98. Conversion factors NOAA-1994 / UB-98 = 1.006 ± 0.003 and NOAA-1994 / SIO-05 = 0.9941 ± 0.0049 are used to transfer data to the latest calibration scale SIO-05 for HCFC-141b (Prinn et al., 2000; Simmonds et al., 2017). For HCFC-142b, the data can be converted from scale UB-98 to the latest calibration scale SIO-05 by conversion factors NOAA-1994 / UB-98 = 0.937 ± 0.003 and NOAA-1994 / SIO-05 = 0.9743 ± 0.0052 (Prinn et al., 2000; Simmonds et al., 2017).

All NOAA absolute calibration scales for various trace gases are shown at <https://www.esrl.noaa.gov/gmd/ccl/scales.html> (last access: 20 December 2018). NOAA flask measurements were reported on the latest NOAA calibration scale for HCFC-22 (NOAA-2006), HCFC-141b (NOAA-

1994), HCFC-142b (NOAA-1994), HFC-134a (NOAA-1995) and HFC-125 (NOAA-2008). NOAA archived air measurements for HCFC-141b and HCFC-142b were also reported on the latest scale. All data reported on NOAA scales are converted here to AGAGE calibration scale for both compounds. The conversion factors between AGAGE and NOAA are shown in Table 2 and were derived on the basis of Table 12 from Prinn et al. (2000), Table S4 from Simmonds et al. (2017) and Table 5 from Prinn et al. (2018a). The scale conversions between NOAA-1994 and SIO-98 for HCFC-22 in Prinn et al. (2000) were based on the comparison of gas mole fractions in air samples in 1994–1995, and the scale conversions between NOAA-1994 and UB-98 for HCFC-141b and HCFC-142b were based on the measurements against the NOAA standard and UB standard in 1997–1998. In the recent studies, the scale conversions between NOAA and AGAGE were based on the comparison of gas mole fractions in air samples in 1998–2017 for HCFC-22, HCFC-141b, HCFC-142b, and HFC-134 at CGO, SMO, THD and MSD (Prinn et al., 2018a). For HFC-125, the NOAA / AGAGE ratio was based on the comparison in 2007–2015 at CGO, SMO and THD (Simmonds et al., 2017).

Archived air measurements from UEA are obtained on the NOAA-1994 scale for HCFC-141b and HCFC-142b and on the NOAA-1995 scale for HFC-134a. It is important to note that the original UEA calibration scale for HCFC-141b, HCFC-142b and HFC-134a (Oram et al., 1995, 1996) has been superseded by the NOAA scale. All UEA measurements obtained on the NOAA scale are converted to the

AGAGE calibration scale by the conversion factors shown in Table 2.

2.6 Hemispheric annual mean and uncertainty estimation

We assembled data from in situ, flask, archived air and firn air measurements from the AGAGE, SIO, CSIRO, NOAA and UEA networks and/or laboratories as well as from AGAGE and NOAA model calculations (Table S1a–h). As the AGAGE baseline monthly means are nominally pollution-free data, the flask measurements from the NOAA network were processed by a statistical procedure to identify measurements that may have been influenced by regional pollution. Briefly, monthly means were calculated by averaging around four values for each month. Then the resultant standard deviations for each month were estimated by error propagation. For each month, values exceeding 3 standard deviations above the monthly mean were rejected as polluted. Afterwards, the monthly means for flask measurements were recalculated without pollution events, combined with UEA data and converted to AGAGE scales. The combined data from all networks and/or laboratories then formed the database used here.

The initial database containing replicate times has been converted into values without such replicates by using the number of measurement-weighted averages at each replicate time. That is to say, when measurements from different networks and sites are combined, hemispheric monthly averages were first calculated by weighted averages to give monthly means more weight as they are based on many individual measurements.

Hemispheric monthly means for each compound were estimated by a smoothing spline fit to the combined and sorted data. The inverses of the square of the standard deviations $((\delta y_i)^{-2})$ of each monthly mean or data points are used as the weights for the spline fit. Although there are no significant differences between the AGAGE and the NOAA monthly means in the same hemisphere, the hemispheric monthly means are closer to the AGAGE monthly means due to the much higher number of measurements in a given month from the AGAGE network (every 2 h, around 100–300 pollution-free samples per month for each site) compared to the NOAA network (weekly flask, around four samples per month for each site).

Hemispheric annual means were calculated by averaging the monthly means of the corresponding 12 months. The JFM means and JAS means are estimated by averaging monthly means of January, February and March and monthly means of July, August and September of the same year.

The smoothing spline fit method discussed above was based on previous studies (Reinsch, 1967; Craven and Wahba, 1978; Wahba, 1983, 1990; Hutchinson and De Hoog, 1985). The method is briefly described below. For more details, see Sect. S1 in the Supplement.

For a set of n data points taking values y_i at times t_i , the smoothing spline fit $g(t)$ of the function $g(t_i)$ is defined to be the minimizer of

$$p \sum_{i=1}^n \left[\frac{g(t_i) - y_i}{\delta y_i} \right]^2 + \int g''(t)^2 dt. \quad (1)$$

Generally, the function is given an initial guess by sampling various values of the smoothing parameter p from 10^{-4} , 10^{-3} , ..., 10^{10} . The initial guess is the first local maximum. If it does not exist, the minimum location is used instead. The generalized cross-validation is used to estimate the smoothing parameter p . After estimating the optimal smoothing parameter, the estimated variance (VAR) and 95 % Bayesian confidence intervals (CI) are calculated. The weights (W) are assumed to be the inverse of the square of standard deviations $((\delta y_i)^{-2})$ associated with the observed variables. The spline is calculated as specified by Reinsch (1967).

The uncertainties of the final annual means are calculated based on the original uncertainties of the monthly means (e.g., for AGAGE in situ data, a standard deviation from 100–300 pollution-free measurements per month for each site) or the measurement precisions for individual data points. The uncertainties in the pollution-free AGAGE monthly means and the calculated NOAA monthly means include uncertainties in the measurements themselves (precision), scale propagation errors and sampling frequency errors. When the monthly means of the NOAA and UEA measurements were converted to AGAGE scales, scale conversion errors were also propagated. Following error propagation, the errors of the hemispheric monthly means were first calculated by the number of measurement-weighted root mean squares (RMSs) of the standard deviation of replicate values. The final uncertainties of hemispheric monthly means are calculated based on the misfit between the smoothing spline fit and the observed values. The uncertainties of hemispheric annual means were calculated as the square root of the squared errors from each of the 12 months.

2.7 Seawater solubility estimation method

Solubility has been reported in terms of the Henry's law solubility coefficient H ($\text{mol L}^{-1} \text{atm}^{-1}$), the mole fraction solubility x (mol mol^{-1}), the Bunsen solubility coefficient β (L L^{-1} , in STP condition), the Ostwald solubility coefficient L (L L^{-1}), the weight solubility coefficient c_w ($\text{mol kg}^{-1} \text{atm}^{-1}$) or the K unen solubility coefficient S (L g^{-1}). The definitions of solubility are shown in Young et al. (1982) and Gamsj ager et al. (2008, 2010). The relationship between different solubility terms is

$$H = \frac{x}{(1-x) \cdot p^\ominus \cdot V_m} = \frac{\beta}{R \cdot T^\ominus} = \frac{L}{R \cdot T} = \frac{c_w \cdot M_l}{V_m} = \frac{S \cdot M_g}{R \cdot T^\ominus \cdot V_m}, \quad (2)$$

where $T^\ominus = 273.15$ K and $p^\ominus = 101.325$ kPa = 1 atm are the standard temperature and pressure (STP); V_m is the molar volume of the solvent, $V_m = 18.01528 \times 10^{-3}$ L mol⁻¹ is the molar volume of water; R is the ideal gas constant, 8.314459848 L kPa K⁻¹ mol⁻¹ (or 0.08205733847 L atm K⁻¹ mol⁻¹); T is the temperature in Kelvin; and M_l is the molar mass of the solvent, which is 18.01528 g mol⁻¹ for water. Next, we present three methods to estimate the solubility of compounds in freshwater and seawater.

2.7.1 Method I: the CGW model

The following method to estimate the solubility of gases in seawater was reported in Deeds (2008) and is briefly described here. The Clark–Glew–Weiss (CGW) solubility equation can be used to calculate the solubility of gases in freshwater and seawater. It is derived from the integrated van 't Hoff equation and the Setschenow salinity dependence (Weiss, 1970, 1974) and expressed as a function of temperature and salinity.

$$\ln L = a_1 + a_2 \cdot \left(\frac{100}{T}\right) + a_3 \cdot \ln\left(\frac{T}{100}\right) + S \left[b_1 + b_2 \cdot \left(\frac{T}{100}\right) + b_3 \cdot \left(\frac{T}{100}\right)^2 \right], \quad (3)$$

where L is the Ostwald solubility coefficient in L L⁻¹ of a gas in seawater, T is the absolute temperature in Kelvin, S is the salinity in ‰ (or g kg⁻¹), and a_i and b_i are constants.

When $S = 0$, this equation becomes the freshwater solubility equation for a gas:

$$\ln L_0 = a_1 + a_2 \cdot \left(\frac{100}{T}\right) + a_3 \cdot \ln\left(\frac{T}{100}\right), \quad (4)$$

where L_0 is the Ostwald solubility in L L⁻¹ of a gas in freshwater.

We did not find complete studies on the solubility of our target gases in seawater based on experiments. Fortunately, the solubility of a gas in seawater can be determined from its freshwater solubility, which can be represented by a modified Setschenow equation (Masterton, 1975).

$$\ln(L_0/L) = k_s \cdot I_v \quad (5)$$

Here L_0 is the freshwater solubility, L is the solubility in a mixed electrolyte solution, such as seawater, k_s is the salting-out coefficient and I_v is the ionic strength of the solution. k_s is an empirically derived, temperature-dependent constant. It can be estimated as a function of temperature using the freshwater and seawater solubility data by a least-square fit with a second-order polynomial (Masterton, 1975).

$$k_s = c_1 t^2 + c_2 t + c_3 = c_1 (T - 273.15)^2 + c_2 (T - 273.15) + c_3, \quad (6)$$

where t is the temperature in Celsius, T is the temperature in Kelvin and c_i represents the constants.

The ionic strength of seawater I_v (g L⁻¹) can be calculated from its salinity (S) (Deeds, 2008):

$$I_v = \frac{0.03600}{1.80655} \times S \times \rho(T, S), \quad (7)$$

where $\rho(T, S)$ is the density of seawater in kg L⁻¹ estimated using the equation of state of seawater (Millero and Poisson, 1981). This equation is suitable for temperature (T) from 273.15 K (0 °C) to 313.15 K (40 °C) and salinities (S) from 0.5 to 43.

The seawater solubility of the target compounds based on method I can therefore be estimated by combining Eqs. (4), (5), (6) and (7).

$$\ln L = \left[a_1 + a_2 \cdot \left(\frac{100}{T}\right) + a_3 \cdot \ln\left(\frac{T}{100}\right) \right] \cdot \exp[-(c_1(T - 273.15)^2 + c_2(T - 273.15) + c_3)] \times \frac{0.03600}{1.80655} \times S \times \rho(T, S) \quad (8)$$

2.7.2 Method II: the pp-LFER model

The solubility estimation of compounds is based on a cavity model: the poly-parameter linear free-energy relationships (pp-LFERs) in Abraham (1993). The pp-LFER model has been applied and validated for many types of partition coefficients (Abraham et al., 2004, 2012). In this model, the process of dissolution of a gaseous or liquid solute in a solvent involves setting up various exoergic solute–solvent interactions. Each of these interactions is presented in relevant solute parameters or descriptors. The selected Abraham model solute descriptors are the excess molar refraction (E) in cm³ mol⁻¹/10, the solute dipolarity–polarizability (S), the overall solute hydrogen-bond acidity (A) and basicity (B), the McGowan's characteristic molar volume (V) in cm³ mol⁻¹/100, and the gas–hexadecane partition coefficient ($\log L^{16}$) at 298.15 K.

$$\log SP = c + eE + sS + aA + bB + vV \tag{9}$$

$$\log SP = c + eE + sS + aA + bB + l \log L^{16} \tag{10}$$

In these equations, the dependent variable logSP is some property of a series of solutes in a given system. Therefore, SP could be the partition coefficient, P , for a series of solutes in a given water–solvent system in Eq. (9) or L for a series of solutes in a given gas–solvent system in Eq. (10).

In this work, logSP refers to some solubility-related property of a series of gaseous solutes in water. SP is the gas–water partition coefficient K_w , which can be defined in terms of the equilibrium mole fractions of the solute through Eq. (11).

$$K_w = \frac{\text{Conc. of solute in water, in mol dm}^{-3}}{\text{Conc. of solute in the gas phase, in mol dm}^{-3}} \tag{11}$$

The Ostwald solubility coefficient L_0 (in $L L^{-1}$) is usually expressed as the gas–water partition coefficients K_w , which can be estimated by Eq. (10). But L_0 can be determined by both Eqs. (9) and (10) because the “solvent” in the “water–solvent partition coefficient” could also be gas phase (Abraham et al., 1994, 2001, 2012). Based on the definition of gas–water partition coefficients in Eq. (11), the values calculated from Eq. (9), the water–gas partition coefficients, should be the reciprocal of the real solubility coefficients. But they are not. When Abraham dealt with this in his work (Abraham et al., 1994, 2001, 2012), he already treated the SP in Eq. (9) as the Ostwald solubility coefficients L_0 . So L_0 can be determined by both Eqs. (12) and (13) by rewriting Eqs. (9) and (10).

$$\log L_0 = c + eE + sS + aA + bB + vV \tag{12}$$

$$\log L_0 = c + eE + sS + aA + bB + l \log L^{16} \tag{13}$$

Inspired by Endo et al. (2012) and Goss et al. (2006), using the pp-LFER model to estimate the salting-out coefficients based on corrected V (V_c) (described afterwards), V_c , replaced V in Eq. (12) with the same coefficients and other descriptors. It was also used to calculate the Ostwald solubility coefficient in water, expressed as Eq. (14), for comparison.

$$\log L_0 = c + eE + sS + aA + bB + vV_c \tag{14}$$

L_0 values estimated by Eqs. (12), (13) and (14) based on V , $\log L^{16}$ and V_c were compared with the observed values. The estimated L_0 closest to the observed values will be chosen as the one to estimate the Ostwald solubility coefficients in water for the pp-LFER model method.

Table 3. Regression coefficients in equations for partition.

Equation	Coefficient	Process	T (K)	c	e	s	a	b	v/l	n ^a	r ^b	SD ^c	F ^d
Eqs. (12), (14)	L_0	Water–gas	298.15	−0.994	0.577	2.549	3.813	4.841	−0.869	408	0.9976	0.151	16810
Eqs. (12), (14)	L_0	Water–gas	310.15	−0.966	0.698	2.412	3.393	4.577	−1.072	82	0.9945	0.156	1270.8
Eq. (13)	L_0	Gas–water	298.15	−1.271	0.822	2.743	3.904	4.814	−0.213	392	0.9962	0.185	10229
Eq. (13)	L_0	Gas–water	310.15	−1.328	1.058	2.568	3.658	4.533	−0.248	84	0.9920	0.188	863
Eq. (17)	K_s	Salting-out	298.15 ± 2	0.112 ± 0.021	−0.020 ± 0.013	−0.042 ± 0.020	−0.047 ± 0.018	−0.060 ± 0.022	0.171 ± 0.017	43	0.83	0.031	–

^a n is the number of data points. ^b r is the correlation coefficient. ^c SD is the standard deviation. ^d F is the F statistic.

The set of coefficients, c , e , s , a , b , v and l characterize a solvent phase in terms of specific solute–solvent interactions. They are determined by multiple linear regression (MLR) analysis. The coefficients c , e , s , a , b , v and l for Eqs. (12), (13) and (14) at 298.15 and 310.15 K are shown in Table 3 (Abraham et al., 1994, 2001, 2012). The Abraham model solute descriptors E , S , A , B , V , V_c and $\log L^{16}$ are calculated based on different methods and shown in Table 4. E for target compounds except HCFC-22 and PFC-116 can be obtained from Abraham et al. (2001). For HCFC-22, the value of the E descriptor was calculated by Eq. (15) on the basis of the number of iodine, bromine, chlorine and fluorine atoms (nI, nBr, nCl and nF) in a halocarbon (Abraham et al., 2012) obtained from a regression analysis of 221 compounds. The methods of determining S , A , B descriptors are reported in previous studies (Abraham et al., 1989, 1991, 1993). The V descriptor, which is the measure of the size of a solute, is the molar volume of a solute calculated from McGowan's approach (McGowan and Mellors, 1986; Abraham and McGowan, 1987). The V_c descriptor is the corrected McGowan's characteristic molar volume with the characteristic atomic volume for a fluorine atom (Goss et al., 2006). L^{16} is the solute gas–hexadecane partition coefficient or the Oswald solubility coefficient in hexadecane at 298.15 K, which can be obtained from previous studies (Abraham et al., 1987, 2001, 2012).

$$E = 0.641nI + 0.328nBr + 0.140nCl - 0.0984nF$$

$$n = 221, \text{SD} = 0.083 \quad (15)$$

The solubility of a compound in salt solution can be determined from its solubility in water by Eq. (16). This equation is also the method for the quantitative description of the salting-out effect in neutral organic solutes, expressed in the following form using a modified Setschenow relationship (Sander, 1999; Schwarzenbach et al., 2003; Endo et al., 2012):

$$\log(L_0/L) = K_S \cdot [\text{salt}], \quad (16)$$

where L_0 is the Ostwald solubility coefficient in pure water (in L L^{-1}), L is the Ostwald solubility coefficient in the salt solution (in L L^{-1}), K_S is the molality-based Setschenow (or salting-out) coefficient (M^{-1}) for the salinity- and common-logarithm-based Setschenow equation and is independent of [salt], and [salt] is the molality of the salt in mol L^{-1} . The relationship between [salt] and salinity (S , g L^{-1}) in seawater is $[\text{salt}] = S/M_{\text{NaCl}}$. M_{NaCl} is the molar mass of sodium chloride (NaCl , 58.44 g mol^{-1}). So the salt mole fraction in seawater is approximately equivalent to 0.6 M NaCl (i.e., $[\text{NaCl}] = \text{ca. } 0.6 \text{ M}$). It is best to define the salt solution based on molality. Adding dry salt to a solution does not change the molality of other solutes as the molality is the mass of the solvent rather than the solution (Sander, 1999).

The salting-out coefficient K_S should be estimated to calculate the solubility of a compound in a salt solution. K_S can be estimated by the poly-parameter linear free-energy relationships (pp-LFERs) since K_S is formally comparable with the common logarithm of the partition coefficient between the 1 M NaCl solution and freshwater (Abraham et al., 2012; Endo et al., 2012).

$$K_S = c + eE + sS + aA + bB + vV_c \quad (17)$$

The coefficients c , e , s , a , b and v for Eq. (17) at $298.15 \pm 2 \text{ K}$ are shown in Table 3 (Endo et al., 2012). E , S , A , B and V_c are the same as the ones described above. It is not easy to calculate the error in the descriptors as all the descriptors are calculated simultaneously (Abraham et al., 2001). E is calculated without error. V_c is the McGowan's characteristic molar volume without error. The general errors of S , A , B are thought to be 0.03 (Abraham et al., 1998, 2001). We assume that the error for each is 0.01 when S , A and B are all not zero and that the error is 0.03 for S and 0 for A and B when S is not zero but A and B are both zero. So the uncertainties of salting-out coefficients could be calculated by error propagation based on different functions. Using the above pp-LFER model, the Setschenow coefficient K_S can be estimated for numerous compounds with various functional groups (Endo et al., 2012).

The solubility of compounds in seawater based on the pp-LFER model can be estimated by combining one of the Eqs. (12), (13), (14) with Eqs. (16) and (17).

$$L = L_0 \cdot 10^{-K_S \cdot \frac{S}{M_{\text{NaCl}}}} \quad (18)$$

In order to distinguish between Abraham's original method and the revised method based on his method in estimating Ostwald solubility coefficients in water, we name it "method II" when L_0 is calculated by Eqs. (12) or (13) and "revised method II" when L_0 is calculated by Eq. (14).

2.7.3 Combined method: combined CGW model and pp-LFER model

The main difference between the two methods described above to estimate the solubility of compounds in seawater is the different methods to estimate the water solubility and salting-out coefficients. Method I, reported in Deeds (2008), is mainly based on the Clark–Glew–Weiss (CGW) solubility model. The water solubility functions of compounds are constructed based on the CGW model and the salting-out coefficients are estimated as a function of temperature using the freshwater and seawater solubility data by the least-square fit with a second-order polynomial. In method I, more solubility measurements in water and seawater are needed and the chemical properties of compounds are considered. Method II is based on the poly-parameter linear free-energy relationships (pp-LFERs). The water solubility of compounds

Table 4. E , S , A , B , V , V_c and $\log L^{16}$ descriptors of HCFC-22, HCFC-141b, HCFC-142b, HFC-134a, HFC-125, HFC-23, PFC-14, PFC-116 and CFC-12 for the pp-LFER model.

Species	Chemical formula	E	S	A	B	V	V_c	$\log L^{16}$
HCFC-22	CHClF ₂	−0.056	0.380	0.040	0.050	0.4073	0.4473	0.692
HCFC-141b	C ₂ H ₃ Cl ₂ F	0.084	0.430	0.005	0.054	0.6530	0.6729	1.920
HCFC-142b	C ₂ H ₃ ClF ₂	−0.080	0.240	0.060	0.056	0.5482	0.5882	1.081
HFC-134a	CH ₂ FCF ₃	−0.410	0.342	0.060	0.040	0.4612	0.5412	0.318
HFC-125	C ₂ HF ₅	−0.510	−0.019	0.105	0.064	0.4789	0.6445	0.100
HFC-23	CHF ₃	−0.427	0.183	0.110	0.034	0.3026	0.3626	−0.274
PFC-14	CF ₄	−0.550	−0.250	0.000	0.000	0.3203	0.4003	−0.819
PFC-116	C ₂ F ₆	−0.590	−0.350	0.000	0.000	0.4966	0.6166	−
CFC-12	CCl ₂ F ₂	0.027	0.125	0.000	0.000	0.5297	0.5697	1.124

and salting-out coefficients are both estimated based on the pp-LFERs. Consideration of the physical properties of compounds is more important in method II. Both methods have shortages and advantages. For method I, there are frequently too few seawater solubility measurements for target compounds in order to construct the second-order polynomial between the salting-out coefficient and temperature. For method II, the water solubility functions for target compounds are only constructed at 298.15 and 310.15 K (Abraham et al., 2001, 2012).

The best approach is a combination of methods I and II to construct the solubility of compounds in water and seawater. The freshwater solubility functions of compounds can be constructed based on the Clark–Glew–Weiss (CGW) solubility model (method I) with the advantage of validity over a larger temperature range. The seawater solubility functions of compounds can be constructed on the basis of the pp-LFERs in estimating the salting-out coefficients (method II) with the advantage of working for more compounds. By combining Eqs. (4), (16) and (17), the solubility of compounds in seawater (L , Ostwald solubility coefficient in $L L^{-1}$) based on the combined method can be estimated by the following equation. This equation is used to estimate the seawater solubility of the target compounds in this paper.

$$L = 10^{-K_S \cdot S / M_{NaCl}} \cdot \exp \left[a_1 + a_2 \cdot \left(\frac{100}{T} \right) + a_3 \cdot \ln \left(\frac{T}{100} \right) \right] \quad (19)$$

3 Results and discussion

3.1 Atmospheric histories and growth rates

During late winter, typically January, February and March in the Northern Hemisphere and July, August and September in the Southern Hemisphere, heat is lost from the surface seawater, which results in an increased density of the surface seawater. During this process, the mixed layer deepens and

older water (usually with lower transient tracer mole fractions) is brought in contact with the atmosphere. The mixed layer gains density and tends to be transported towards the ocean interior through diffusive, advective and/or convective processes. This water then carries with it a signature of the atmospheric mole fraction, pending the saturation state of the water as it leaves the surface layer. For tracers with rapidly increasing atmospheric mole fractions and for deep mixed layers, under-saturation of the tracers has frequently been reported (e.g., Tanhua et al., 2008). Since we are interested in reporting the annual means for the compounds for their use as oceanic tracers of water masses, it is useful to know the atmospheric mole fractions of these compounds in late winter compared to annual means. JFM and JAS are nominally the coldest times in the Northern and Southern Hemisphere, respectively, and normally the main periods when water masses are formed. Therefore, we reconstructed JFM mean and JAS mean atmospheric mole fractions for all species in the Northern and the Southern Hemisphere. The annual mean atmospheric mole fractions of these compounds are mainly given to allow for comparison to the annual mean atmospheric mole fractions for CFC-11, CFC-12, CFC-113 and CCl₄ given in previous studies (Walker et al., 2000; Bullister, 2015).

As described in Sect. 2, there are a number of datasets available for HCFC-22, HCFC-141b, HCFC-142b, HFC-134a, HFC-125, HFC-23, PFC-14 and PFC-116 (Table S1, Fig. S1a–h in the Supplement). Once consolidated into a single dataset via a common calibration scale, all data were fitted by a smoothing spline to determine the monthly means for each compound. The hemispheric annual mean, JFM mean (NH) and JAS mean (SH) atmospheric dry air mole fractions in parts per trillion (ppt) are then estimated and shown in Fig. S1a–h and the top of Fig. 2a–h. The associated uncertainties were estimated by error propagation and are shown at the top of Fig. 2a–h. The mole fractions and associated uncertainties are also given with JFM means (e.g., 2000.125), annual means (e.g., 2000.500) and JAS means (e.g., 2000.625) and shown in Table S2. Annual growth

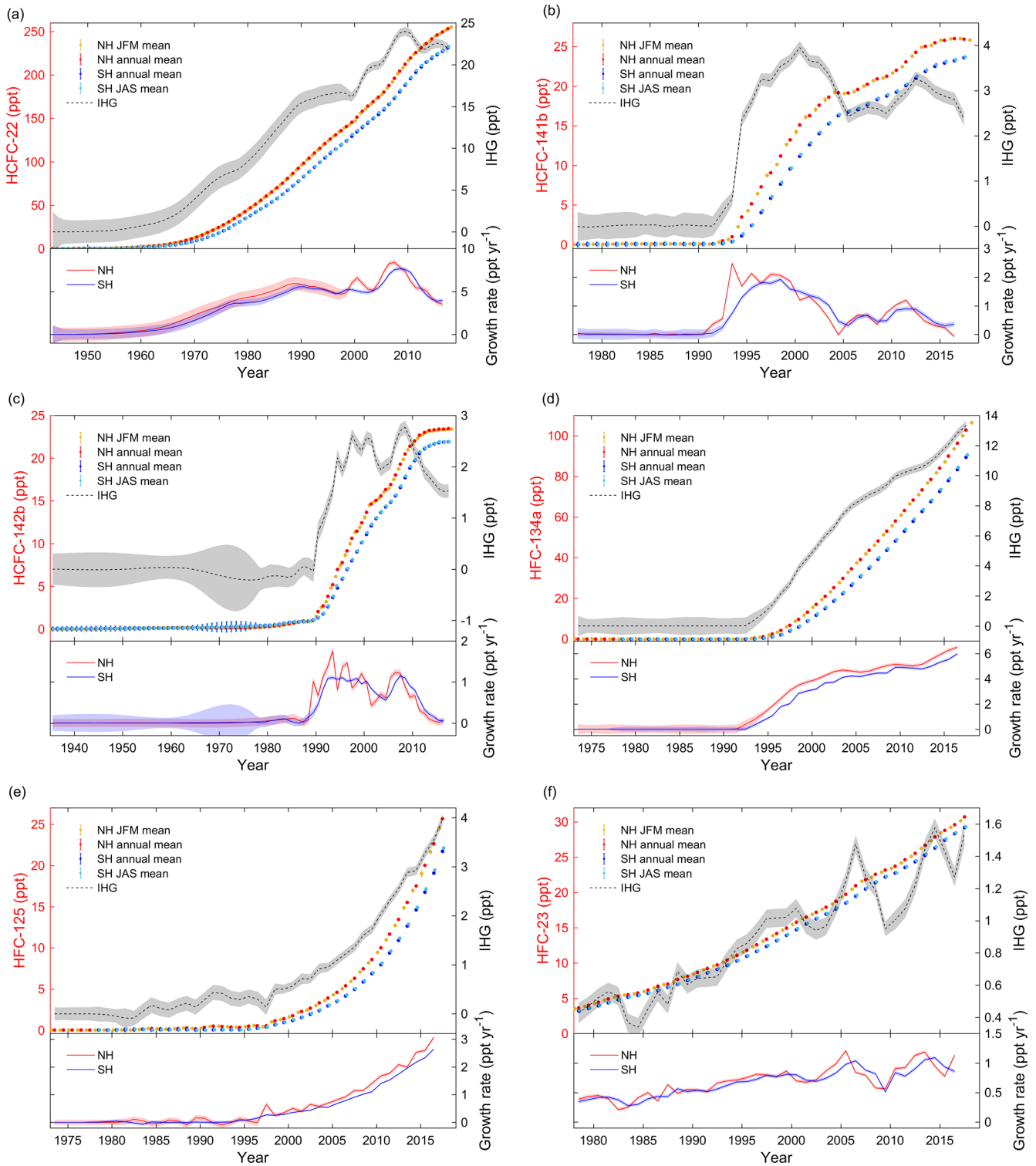


Figure 2.

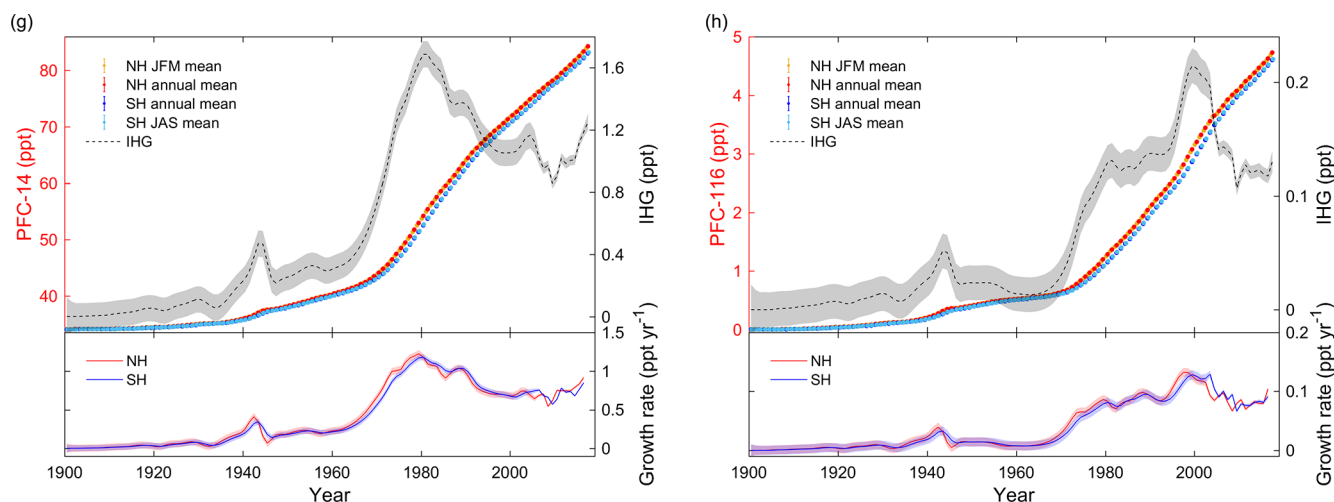


Figure 2. (a) HCFC-22: the top of the panel shows the JFM means (NH), annual means (NH and SH) and JAS means (SH) of atmospheric mole fractions and the interhemispheric gradients (IHG, in black, using the right axes). The lower section shows the annual growth rates in ppt yr^{-1} . Shadings in the figure reflect the uncertainties. (b) Similar to Fig. 2a, but for HCFC-141b. (c) Similar to Fig. 2a, but for HCFC-142b. (d) Similar to Fig. 2a, but for HFC-134a. (e) Similar to Fig. 2a, but for HFC-125. (f) Similar to Fig. 2a, but for HFC-23. (g) Similar to Fig. 2a, but for PFC-14. (h) Similar to Fig. 2a, but for PFC-116.

rates were calculated based on the annual means combined with their associated errors and are shown at the bottom of Fig. 2a–h. Interhemispheric gradients (IHGs) are estimated from the annual mean atmospheric mole fractions of a gas in the NH minus the annual mean in the SH in the same year (Fig. 2a–h). Errors of the IHG were estimated based on error propagation of the annual means in the NH and the SH in the same year (Fig. 2a–h).

3.1.1 HCFC-22

Annual mole fractions of HCFC-22 (Figs. 2a, S1a, Table S2) were 253.2 ± 0.4 ppt (NH) and 231.2 ± 0.3 ppt (SH) in 2017, which is a 23 % increase from 2009 (Montzka et al., 2010a). The interhemispheric gradient (IHG) initially increased but has been diminishing since 2010 because of a decline in emissions (growth rates). Growth rates for HCFC-22 rose steadily until 1990, followed by a slight decrease, which coincides with the large production and consumption reported between the 1950s and 1990s (Fig. 1) and a freeze of production magnitudes in developed countries in 1996. A rapid increase occurred between 2005 and 2008. Corresponding step changes were also seen in 2005 in both observations (upper panel in Fig. 2a) and emissions (Xiang et al., 2014) in response to the United Nations Environment Programme (UNEP) production changes (UNEP, 2018). The growth rate peaked in 2007 (NH) at 8.4 ppt yr^{-1} and in 2008 (SH) at 7.6 ppt yr^{-1} before a sharp 91 % decline to 2016 at an annual average rate of 0.8 ppt yr^{-2} (NH) and 0.7 ppt yr^{-2} (SH). This suggests that global emissions are not growing as rapidly as before 2008, as reported by Montzka et al. (2015) and Graziosi et al. (2015), consistent with the phaseout in the

dispersive application of HCFCs since 2007 (Graziosi et al., 2015).

3.1.2 HCFC-141b

HCFC-141b (Figs. 2b, S1b, Table S2) annual mole fractions increased from 1990, and a slowdown occurred in the second half of the 2000s, corresponding to a sharp drop in production and consumption in 2005 (Montzka et al., 2015). HCFC-141b annual mole fractions have increased to a maximum of 26.0 ± 0.1 ppt (NH) in 2016 and 23.6 ± 0.1 ppt (SH) in 2017, representing 36 % (NH) and 41 % (SH) increases from 2005 and 7 % (NH) and 12 % (SH) increases from 2012. This also suggests that the annual mole fractions in the NH began to decrease. Rapid growth rates were seen before 1993 (NH) and 1995 (SH), coinciding with intensified industrial production and consumption of HCFCs in the 1990s. This is followed by a comparatively stable plateau period, 1994–1999 (NH) and 1995–1999 (SH), consistent with UNEP production (Montzka et al., 2015) and consumption changes (UNEP, 2018). Subsequently, the growth rate declined until around 2005. Since 2005, production has increased substantially in developing countries, so growth rates recovered to higher values in 2006–2007. Growth rates in 2012 appear to represent a 109 % (NH) and 59 % (SH) decline to 2016 of $-0.07 \text{ ppt yr}^{-1}$ (NH) and 0.36 ppt yr^{-1} (SH). The growth rates in 2016 are very close to the growth rates seen in the 1980s. This decline coincides with the global production and consumption of HCFCs being capped in 2013 in developing countries (Montzka et al., 2015).

3.1.3 HCFC-142b

Annual mean mole fractions for HCFC-142b (Figs. 2c, S1c, Table S2) show a slow initial increase until 1989 followed by a sharp increase in the 1990s, the same slowdown in the mid-2000s as seen with HCFC-141b, and finally a plateau in recent years. Annual mole fractions reached a maximum of 23.4 ± 0.1 ppt (NH) and 21.9 ± 0.1 ppt (SH) in 2017 at the end of the time series, representing a 39 % (NH) and 48 % (SH) increase since 2005. Annual mole fractions in the NH show a declining trend. The IHG and growth rates exhibit two peaks, one in the 1990s and another in 2007–2008, followed by a substantial drop. There are minima in growth rates around 2005 for all three HCFCs. The peak–valley–peak distribution patterns of HCFCs are consistent with the UNEP consumption changes (UNEP, 2018). For HCFC-142b, this is followed by a dramatic 99 % (NH) and 94 % (SH) decline to 2015 from 2007–2008 at an annual average rate of 0.14 ppt yr^{-2} for both hemispheres. This decline in both atmospheric mole fractions and emissions follows reduced production and consumption in developed countries and a leveling-off of production and consumption in developing countries (Carpenter et al., 2014). The current growth rates for HCFC-142b are similar to those seen in the 1980s before the rapid increase in emissions.

3.1.4 HFC-134a

Annual mean mole fractions of HFC-134a (Figs. 2d, S1d, Table S2) have increased continuously since the 1990s. The monotonical increase is reflected in emissions (Xiang et al., 2014; Montzka et al., 2015; Simmonds et al., 2017). HFC-134a annual mole fractions reached a maximum of 102.7 ± 0.2 ppt (NH) and 89.4 ± 0.2 ppt (SH) by the end of the current time series, representing 163 % (NH) and 191 % (SH) increases since 2005 and 40 % (NH) and 42 % (SH) increases since 2012. IHG and growth rates started to increase around 1992, then rapidly increased in 1995–2004, followed by a stabilization of growth rate in 2009–2012 and then an increase since 2012. The maximum growth rates are shown at the end of the time series of 6.5 ppt yr^{-1} (NH) and 6.0 ppt yr^{-1} (SH), representing a 3.7–3.8 % per year increase from 2005 and a 6.3–6.5 % per year increase from 2012.

3.1.5 HFC-125

Annual mean mole fractions, IHG and growth rates of HFC-125 (Figs. 2e, S1e, Table S2) increased throughout the atmospheric history record, which reflects a continuing increase in emissions (O'Doherty et al., 2009; Montzka et al., 2015; Simmonds et al., 2017). Annual mole fractions reached a maximum of 25.7 ± 0.1 ppt (NH) and 21.7 ± 0.05 ppt (SH) at the end of the time series, representing 199 % (NH) and 216 % (SH) increases since 2009 (O'Doherty et al., 2009). The growth rate reached a peak of 3.1 ppt yr^{-1} (NH) and

2.6 ppt yr^{-1} (SH) by the end of the time series, representing 117 % (NH) and 138 % (SH) increases from 2009. The increase in the growth rate of HFC-125 is more than 3 times the growth rate increase for HFC-134a.

3.1.6 HFC-23

Annual mean mole fractions of HFC-23 (Figs. 2f, S1f, Table S2) have increased since 1978. HFC-23 atmospheric mole fractions peaked at 30.7 ± 0.05 ppt (NH) and 29.2 ± 0.06 ppt (SH) by the end of the time series (in 2017), representing a 4–4.1 % per year increase since 2009 (Miller et al., 2010). IHG and growth rates exhibit an increasing trend with large fluctuations over the time series, with local maxima in the growth rate in 2006 and 2013 and a minimum in 2009, which reflect changes in emissions (Carpenter et al., 2014; Simmonds et al., 2018). The slowing in growth rate was in response to emission reductions in developed countries that began in the late 1990s, combined with the UNFCCC CDM destruction program for developing countries that started around 2007 (Miller and Kuijpers, 2011; Carpenter et al., 2014). The higher values in growth rates could be attributed to the increase in production of HCFC-22 with no subsequent incineration of HFC-23 (Miller and Kuijpers, 2011; Carpenter et al., 2014). The current annual growth rates are 1.1 ppt yr^{-1} (NH) and 0.86 ppt yr^{-1} (SH), representing 100 % (NH) and 68 % (SH) increases since 2009. The increase in the growth rates for HFC-23 is between the ones for HFC-134a and for HFC-125.

3.1.7 PFC-14 (CF₄)

Trudinger et al. (2016) used a firm diffusion model to determine the atmospheric abundance of PFC-14 (Figs. 2g, S1g, Table S2) since 1900 from ice core, firm air, archived air and in situ measurements. Here we updated and extended the time series assembled by Trudinger et al. (2016). PFC-14 has a natural background of 34.05 ± 0.33 ppt (Trudinger et al., 2016). Annual mean mole fractions and growth rates began to increase around 1900, with a local maximum in growth rate around 1943. The maximum reflects changing emissions from increasing aluminium production during World War II (Barber and Tabereaux, 2014; Trudinger et al., 2016), for example for the construction of aircraft. Mole fractions of PFC-14 began to increase rapidly in the 1970s. Since then it has continued to grow, reaching a maximum of 84.30 ± 0.04 ppt (NH) and 83.05 ± 0.03 ppt (SH) at the end of the time series (in 2017), representing 8 % (NH) and 7 % (SH) increases from 2009. The growth rates began to increase from the 1950s and peaked in 1980 before declining. The decline is attributed to a concerted effort by the aluminium and semiconductor industries to reduce their emissions (Trudinger et al., 2016). The growth rate minimum in 2009 could be related to the global financial crisis (Trudinger et al., 2016). PFC-14 growth rates have increased again during the last

5 years probably due to increased aluminium production and perhaps rare earth element production in developing countries (Vogel and Friedrich, 2018). The current growth rates are 0.91 ppt yr^{-1} (NH) and 0.85 ppt yr^{-1} (SH), representing 48 % (NH) and 49 % (SH) increases from 2009.

3.1.8 PFC-116

We updated and extended the time series previously shown in Trudinger et al. (2016). PFC-116 (Figs. 2h, S1h, Table S2) has a preindustrial background of 0.002 ppt (Trudinger et al., 2016). PFC-116 shows a similar atmospheric trend to PFC-14. Annual mean mole fractions have increased since ~ 1900 , with a step-up around 1943 (discussed above; PFC-116 is coproduced with PFC-14 during aluminium production), and increased significantly in the 1970s, reaching $4.73 \pm 0.007 \text{ ppt}$ (NH) and $4.06 \pm 0.007 \text{ ppt}$ (SH) by the end of the record, representing 16 % increases from 2009. PFC-116 growth rates began to increase slowly, followed by maxima around 1943 (discussed above for PFC-14). Then they declined and stayed relatively stable until 1965 when they started to climb to a maximum at the end of the 1990s. Subsequently, they declined and stayed relatively stable at $0.104 \text{ ppt yr}^{-1}$ (NH) and 0.09 ppt yr^{-1} (SH).

Global annual mean mole fractions of HCFCs, HFCs and PFCs, except HCFC-141b and HCFC-142b, have increased continuously in the background atmosphere throughout the whole atmospheric history record (Fig. 2a–h). Recent growth rates are decreasing for HCFCs, increasing for HFCs and stable for PFCs. From Fig. 2a–h, it is clear that the mole fractions for target compounds in the NH are always larger than those in the SH but follow similar trends; the growth rates in both hemispheres are also similar (lagged in the SH) and the trends in IHG and in emissions and growth rates are very similar. This behavior is because the majority of the emissions (typically $> 95 \%$) occur in the NH extratropics (O'Doherty et al., 2009; Saikawa et al., 2012; Carpenter et al., 2014; UNEP, 2018) and the interhemispheric mixing time is around 1 or 2 years. Thus, the larger the increase in emissions in the NH, the higher the resultant IHG. If all emissions stop, long-lived compounds would expect to reach near-identical mole fractions in both hemispheres.

3.2 Growth patterns

The atmospheric history trends of target compounds generally follow expected patterns based on the history of their known industrial applications and production bans. We can make out three distinct behavioral patterns with which we could predict the trend of annual mean mole fractions of these compounds. In pattern I, the annual mean mole fractions show sigmoidal (S-shaped) growth and the annual growth rates exhibit the shape of Gaussian distribution over the whole time period, such as HCFC-141b and HCFC-142b. This means that the annual mole fractions of these com-

pounds are going to decrease or are decreasing. In pattern II, the annual mean mole fractions show initial exponential growth followed by a period of linear increase, while the growth rates show a sigmoidal pattern but a slight increase recently, such as HFC-134a and HFC-23 (combined with the modeled mole fraction output of HFC-23 from 1950 to 2016 shown in Fig. 1 in Simmonds et al., 2018). This means that the mole fractions of these compounds are going to continuously increase with relatively slower growth rates in the near future. Afterward, they will likely experience a plateau phase, followed by a decline following the restrictions imposed by the 2016 Kigali Amendment to the Montreal Protocol. Since the atmospheric lifetime of HFC-23 is much longer than that of HFC-134a, time profiles and IHG change are expected to be a little different between HFC-134a and HFC-23. In pattern III, the annual mean mole fractions and growth rates both show exponential (J-shaped) growth, such as HFC-125. So the atmospheric history and growth rates of HFC-125 are going to increase for a longer period of time than HFC-134a and HFC-23, and then will likely follow a similar path to the compounds in pattern II as they are subjected to the same regulations.

The annual mean mole fractions of the remaining halogenated compounds, HCFC-22, PFC-14 and PFC-116, have also increased throughout the time series and continue to increase today. The growth rates of these compounds initially increased and experienced a peak before declining. The growth trend for HCFC-22 is more likely to experience a plateau and then a decrease, following the trends of HCFC-141b and HCFC-142b as they are subjected to the same regulations. Different from all other target compounds, the annual mean growth rates of PFC-14 and PFC-116 have stabilized after a short decline without specific restrictions on emissions. This could be attributed to the changing sources of both PFC-14 and PFC-116. PFC emissions from the aluminium industry dominated for a long time but have likely been declining for the past decade or so, while emissions by the electronics industry (Kim et al., 2014) and probably the rare earth elements industry became more important. The very long lifetimes of PFCs in the atmosphere makes a decrease in the atmospheric mole fraction unlikely in the foreseeable future.

Considering the combined growth patterns and the production and consumption histories for these gases (Fig. 1), the sequence of atmospheric change in HCFCs and HFCs coincides with the replacement sequence of CFCs. In the 1980s, CFCs were found to be a threat to the ozone layer (Molina and Rowland, 1974; Rowland and Molina, 1975). To facilitate the phaseout of the more potent ozone-depleting CFCs, HCFC production and consumption increased rapidly in developed countries in the 1990s and in developing countries in the mid-2000s as industrial and domestic usage of CFCs was curtailed. Thus, atmospheric growth rates of HCFCs reached a peak in the 1990s and/or 2000s. Following the 2007 amendment to the Montreal Protocol, the production and consump-

tion of HCFCs was phased out sooner than originally mandated. With a large emission source of HCFC-22 existing in refrigeration systems and stockpiling, emissions are expected to continue (Carpenter et al., 2014). The atmospheric mole fractions of HCFCs tend toward stable values or decline as a consequence of the freeze of HCFC production and consumption for dispersive uses in 2013 in Article 5 countries. Moreover, the growth rates of HCFCs are decreasing. HFCs have been developed as potential substitutes for both CFCs and HCFCs because they pose no harm to the ozone layer. Their production and consumption has increased rapidly over the past decade or so. This accounts for the rapid growth of the atmospheric mole fractions of many HFCs and the J-shaped or S-shaped patterns of their growth rates.

3.3 Solubility in seawater

The seawater solubility functions for HCFC-22, HCFC-141b, HCFC-142b, HFC-134a, HFC-125, HFC-23, PFC-14 and PFC-116 are estimated based on their freshwater solubilities as no direct studies of the solubility functions of the target compounds in seawater have been published.

3.3.1 Solubility in freshwater

Available freshwater solubility data for HCFC-22, HCFC-141b, HCFC-142b, HFC-134a, HFC-125, HFC-23, PFC-14 and PFC-116 from previous studies were compiled. These data were converted to a common solubility unit (Ostwald solubility, L_0 , in LL^{-1}) and fitted with the Clark–Glew–Weiss (CGW) function of temperature to construct the freshwater solubility equations shown in Fig. S2a–h. For data from Abraham et al. (2001), only the observed values of water solubility are involved in the fits; those calculated values using the (revised) method II (described below) are shown only for comparison. The water solubility functions in Ostwald solubility units for HCFC-22, HFC-134a, HFC-125, HFC-23 and PFC-116 (Fig. S2a, d, e, f, h) are compared with the results from Deeds (2008) and agree well. Except for HFC-125, the results for other compounds match well with each other.

For HFC-125, three fitted curves are shown in Fig. S2e, reflecting the fact that data obtained by different methods do not agree with each other. Curve 1 includes data from Miguel et al. (2000), in which the $\phi - \phi$ approach (the fugacity coefficient–fugacity coefficient method) has been used to predict the experimental results and the fugacity coefficients were calculated using a modified version of the Peng–Robinson equation of state, and Battino et al. (2011), in which the data were collected from the International Union of Pure and Applied Chemistry (IUPAC) Solubility Data Series, in some cases as averages or estimates. Curve 2 includes data from Mclinden (1990) obtained from the vapor pressure of the pure substance divided by aqueous solubility (sometimes called VP / AS) and HSDB (2015), in which the data

were calculated with the quantitative structure–property relationship (QSPR) or a similar theoretical method. Curve 3 includes data from Reichl (1996) and Abraham et al. (2001), which are both measured values from original publications. Considering that the data based on measurements match with our results (Fig. S2e) calculated by method II (only based on the physical properties of compounds), curve 3 (the curve in the bottom) is chosen as the water solubility fit.

For PFC-14, the freshwater solubility curve in Ostwald solubility units (Fig. S2h) was compared with the ones from both Clever (2005) and Deeds (2008). The curve in this study matches better with the one from Clever (2005). In Fig. S2a–h, the fits for water solubility functions agree within 4.0 %, 7.8 %, 2.5 %, 6.8 %, 5.9 %, 2.3 %, 0.95 % and 3.5 % with the majority (two-thirds) of the data for HCFC-22, HCFC-141b, HCFC-142b, HFC-134a, HFC-125, HFC-23, PFC-14 and PFC-116, respectively. The constants a_1 , a_2 , a_3 for the solubility functions of the target compounds in water are given in Table 5.

In order to validate the calculation method of water solubility, the solubilities for CFC-12 in water calculated by the combined method and by the method from Warner and Weiss (1985) were compared. Warner and Weiss (1985) estimated the freshwater and seawater solubility function of CFC-12 through experiments and a different model fit without using a salting-out coefficient. The freshwater solubility function of CFC-12 calculated by the combined method was constructed by collecting freshwater solubility data from the literature (Fig. S2i). The freshwater solubilities of CFC-12 from Warner and Weiss (1985) match data from other studies very well (the root mean square of misfit is 0.006). Moreover, the fits based on the function in Warner and Weiss (1985) and the CGW model in this study match very well (Fig. S2i). The average relative standard deviation (RSD) of water solubility estimated by the two methods for CFC-12 in the range of 273.15–313.15 K (0–40 °C) is 0.17 %. This means that our method for estimating freshwater solubility is valid.

3.3.2 Salting-out coefficient

The salting-out coefficient K_S is independent of salinity and is a function only of temperature, which can be obtained from method I and method II in Sect. 2.7. In order to validate this, K_S was calculated by Eq. (16) (method II) based on the experimental results of the freshwater and seawater solubility of CFC-12 from Warner and Weiss (1985). The average of K_S is $0.229 \pm (1.41 \times 10^{-15}) L g^{-1}$ at 298.15 K when the salinity is in the range of 0–40. The RSD is $6.16 \times 10^{-13} \%$, which is minor enough to be neglected. Thus, K_S is independent of salinity. In Fig. S3, a quadratic relationship between the salting-out coefficient and temperature was found. K_S is in the range of 0.229 – $0.249 L g^{-1}$ (at a mean of $0.235 \pm 0.005 L g^{-1}$) at a salinity of 35 when the temperature is in the range of 273.15–313.15 K (0–40 °C). The RSD

Table 5. Ostwald solubility coefficients of HCFC-22, HCFC-141b, HCFC-142b, HFC-134a, HFC-125, HFC-23, PFC-14, PFC-116 and CFC-12 in seawater estimated based on the combined method.

Compound	a_1	a_2	a_3	K_S	T_{\min} (K)	T_{\max} (K)	L_0 at 1 atm, 25 °C (LL ⁻¹)	L at 1 atm, 25 °C, 35.0‰ (LL ⁻¹)
HCFC-22	-66.9256	109.8625	27.3778	0.169 ± 0.022	278.15	353.15	0.844	0.669
HCFC-141b	-85.6439	138.0940	35.6875	0.204 ± 0.023	278.15	353.15	0.711	0.537
HCFC-142b	-73.3682	118.3104	29.8797	0.198 ± 0.022	278.15	353.15	0.352	0.268
HFC-134a	-67.1680	109.1227	27.0984	0.193 ± 0.022	278.15	353.15	0.381	0.292
HFC-125	-51.8823	84.5045	19.3067	0.224 ± 0.021	283.15	343.15	0.086	0.063
HFC-23	30.0046	-31.6631	-18.8072	0.168 ± 0.021	278.15	348.15	0.313	0.249
PFC-14	-113.8218	162.6686	49.4215	0.202 ± 0.022	273.15	328.15	0.00513	0.00388
PFC-116	-102.0437	147.9210	41.9999	0.244 ± 0.022	278.15	328.15	0.00143	0.00102
CFC-12	-101.3445	156.4709	42.2833	0.204 ± 0.021	273.15	348.15	0.069	0.052

$$L = 10^{-K_S \cdot S / M_{\text{NaCl}}} \cdot \exp \left[a_1 + a_2 \cdot \left(\frac{100}{T} \right) + a_3 \cdot \ln \left(\frac{T}{100} \right) \right]$$

is 2.3 %. This means that the effect of temperature on the salting-out coefficient is also very small.

In order to estimate the solubility functions for target compounds in seawater, their salting-out coefficients (K_S) should be estimated. As shown in Eq. (17), K_S is estimated based on the descriptors of all target compounds. With the exception of PFC-116, E , S , A , B and V_c values for the target compounds were obtained from Abraham et al. (2001, 2012). For PFC-116, the excess molar refraction (E) was calculated by Eq. (15). The dipolarity–polarizability (S) for PFC-116 (C_2F_6) was estimated as -0.350 based on the S of PFC-14 (CF_4 , -0.250) and PFC-218 (C_3F_8 , -0.450) (Abraham et al., 2001) and the error for the estimate of S is estimated to be 0.02 based on the error propagation. A and B for PFC-116 (C_2F_6) are both zero since it includes only carbon–halogen atom bonds and no carbon–hydrogen bonds. V_c of PFC-116 was obtained from Abraham and McGowan (1987) and Goss et al. (2006). The values of all descriptors for the target compounds are shown in Table 4. The errors in calculating the descriptors were estimated as 0.088, 0.047, 0.128, 0.081, 0.095, 0.051, 0.071 and 0.088 for HCFC-22, HCFC-141b, HCFC-142b, HFC-134a, HFC-125, HFC-23, PFC-14 and PFC-116, respectively (Abraham et al., 2001). On the basis of the E , S , A , B , V_c descriptors, salting-out coefficients (K_S) were estimated at 298.15 ± 2 K and are shown in Table 5.

As shown in Sect. 2.7.2, K_S changes with temperature, which is described by the coefficients c , e , s , a , b and v in Eq. (17). The salting-out coefficient is a second-order polynomial function of temperature as we described for method I in Sect. 2.7.1 and discussed above for CFC-12 (Fig. S3). Based on the discussion for CFC-12, the effect of temperature on the salting-out coefficient is small. Also, very limited studies of K_S have been reported and we assume that the salting-out coefficient K_S does not change with temperature (i.e., it is a constant). Thus, the final salting-out coefficients are calculated using Eq. (17) at 298.15 K for the target compounds and shown in Table 5.

3.3.3 Solubility in seawater based on the combined method

Following the calculation method shown in Sect. 2.7.3, seawater solubility functions for HCFC-22, HCFC-141b, HCFC-142b, HFC-134a, HFC-125, HFC-23, PFC-14 and PFC-116 were constructed in the corresponding temperature range (Table 5) based on Eq. (19). Ostwald solubility coefficients in seawater at 1 atm, 25 °C and 35 g kg⁻¹ were estimated to be 0.669 LL⁻¹ for HCFC-22, 0.537 (HCFC-141b), 0.268 (HCFC-142b), 0.292 (HFC-134a), 0.063 (HFC-125), 0.249 (HFC-23), 0.00388 (PFC-14) and 0.00102 (PFC-116), respectively (Table 5). For comparison, the solubilities of CFC-12, CFC-11, CFC-113, CCl_4 and SF_6 in seawater are converted to the Ostwald solubility unit at 1 atm, 25 °C and 35 g kg⁻¹. They are 0.0504, 0.177, 0.0518, 0.568 and 0.00401 LL⁻¹, respectively. In previous studies, Mackay et al. (2006) reported that many hydrocarbons have a solubility in seawater ~ 75 % of their solubility in distilled water. Moore et al. (1995) reported that the solubility of short-lived halocarbons (e.g., CH_3I , CHBr_3 , CH_2Br_2 , CHBr_2Cl and CHCl_3) in seawater is 80 % of their solubility in freshwater. For comparison, the solubility of CFC-12 in seawater is 73 % of its solubility in freshwater (Warner and Weiss, 1985). The percentages are 72 % for CFC-11 (Warner and Weiss, 1985), 74 % for CFC-113 (Bu and Warner, 1995), 78 % for CCl_4 (Bullister and Wisegarver, 1998) and 73 % for SF_6 (Bullister et al., 2002). For our target compounds, the percentages of seawater solubility for freshwater solubility at 298.15 K and a salinity of 35 ‰ are 79 % for HCFC-22 and HFC-23, 77 % for HFC-134a, 76 % for HCFC-141b, HCFC-142b and PFC-14, 73 % for HFC-125, and 71 % for PFC-116. Similar to the CFCs and SF_6 , the percentages for HCFCs, HFCs and PFCs are also in the range of around 70 %–80 %.

The temperature dependence of the Ostwald solubility coefficients of the target compounds in seawater at a salinity of 35 is shown in Fig. 3. The dependence on salinity at 298.15 K

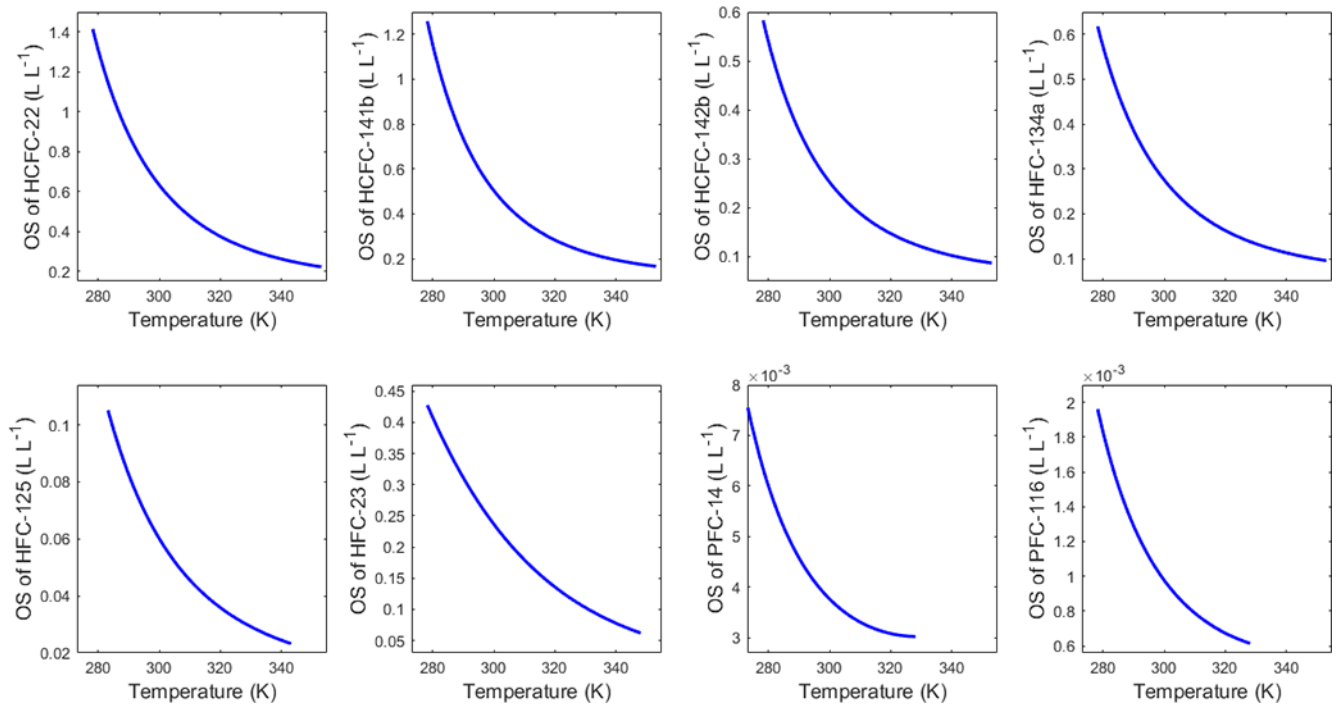


Figure 3. Temperature dependence of the Ostwald solubility (OS) coefficients in seawater for HCFC-22, HCFC-141b, HCFC-142b, HFC-134a, HFC-125, HFC-23, PFC-14 and PFC-116 at a salinity of 35.

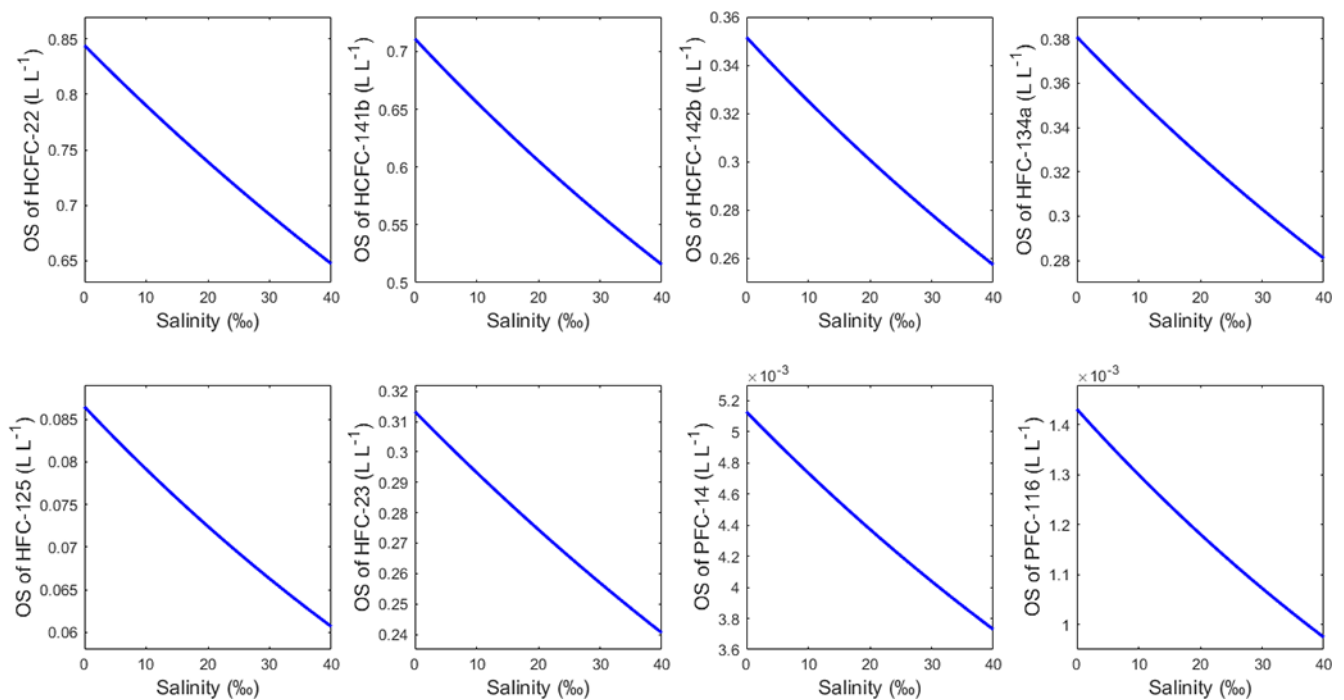


Figure 4. Salinity dependence of the Ostwald solubility (OS) coefficients in seawater for HCFC-22, HCFC-141b, HCFC-142b, HFC-134a, HFC-125, HFC-23, PFC-14 and PFC-116 at a temperature of 298.15 K.

is shown in Fig. 4. Seawater solubilities fall monotonically with increasing temperature and salinity. The latter shows a near-linear decline.

Overall uncertainties of water solubility estimates for the target compounds are calculated as the root mean square of the misfit between the measurements and the fitted values. They are 0.0352 LL^{-1} for HCFC-22, 0.0283 (HCFC-141b), 0.0065 (HCFC-142b), 0.0141 (HFC-134a), 0.0016 (HFC-125), 0.0132 (HFC-23), 9.0695×10^{-5} (PFC-14) and 9.1858×10^{-5} (PFC-116). The uncertainties of seawater solubility of the target compounds at different salinities (0–40) and a temperature of 298.15 K are estimated by the propagation of uncertainty from water solubility and salting-out coefficients. They are 0.034 LL^{-1} for HCFC-22, 0.032 (HCFC-141b), 0.031 (HCFC-142b), 0.031 (HFC-134a), 0.030 (HFC-125), 0.031 (HFC-23), 0.030 (PFC-14) and 0.029 (PFC-116). The uncertainties of seawater solubility at different temperatures (273.15–313.15 K) and a salinity of 35 are also estimated by the same method. They are 0.041 LL^{-1} for HCFC-22, 0.037 (HCFC-141b), 0.029 (HCFC-142b), 0.030 (HFC-134a), 0.026 (HFC-125), 0.029 (HFC-23), 0.027 for (PFC-14) and 0.025 (PFC-116).

In order to evaluate the effectiveness of the combined method, the Ostwald solubility coefficients of PFC-14 in seawater estimated by the combined method were compared with the observed values (Table 6) because only the seawater solubilities of PFC-14 have been measured (Scharlin and Battino, 1995). The estimated solubility of PFC-14 in seawater at 293.15 K is the closest to the measured values. The RSD of the calculated value and the measured value is only 0.79 %.

3.3.4 Comparison of solubility in seawater based on three methods

In order to validate the possibility of method I and method II, and to find out the advantages of the combined method, we estimated seawater solubilities of the target compounds based on method I and method II and compared them to the results from the combined method.

For method I, only the seawater solubility function of PFC-14 was constructed (Table S3) as only the seawater solubilities of PFC-14 have been reported (Scharlin and Battino, 1995). The advantage of the constructed seawater solubility function is that it can be used over a greater temperature range rather than only for a few selected temperatures.

The only difference between method II and the combined method is the difference in estimating water solubility. For water solubility calculations, method II uses the pp-LFERs based only on the physical properties of compounds, whereas the combined method uses the CGW model based on measurements. For water solubility based on the pp-LFERs, the water solubilities L_0 estimated by Eqs. (12), (13) and (14) based on V , $\log L^{16}$ and V_c were compared to the observed values (Table S4). As shown in Table S4, the water solu-

bilities of most compounds calculated based on V_c (revised method II) are closer to both the observed values (Abraham et al., 2001) and the CGW fitted values than when they are calculated based on V or $\log L^{16}$ (method II). So the revised method II is more suitable for the target compounds except for HFC-125 for which the pp-LFER model method is used. The calculated water solubilities based on the (revised) method II are shown in Fig. S2a–i for comparison. Small differences in water solubility calculated by the (revised) method II and the combined method (CGW model) verify the reliability of both methods. Compared with the pp-LFER model method, the water solubility estimated by the CGW model method is closer to the observed values (Table S4). This is also the reason why the CGW model method from method I is chosen for the combined method in estimating water solubility coefficients. The final seawater solubility functions of the target compounds and CFC-12 based on (revised) method II are shown in Table S5.

Until now, seawater solubility functions for the target compounds and CFC-12 based on (revised) method II and the combined method have been constructed. In order to better understand the difference between experimental results and model estimations, we compared the seawater solubility of CFC-12 calculated from Warner and Weiss (1985), from revised method II, and from the combined method. The results are shown in Fig. 5. The RSDs of the seawater solubility for CFC-12 estimated by the revised method II and by Warner and Weiss (1985) are 3.4 % at 298.15 K and 13.5 % at 310.15 K. The average RSDs of the seawater solubilities estimated by Warner and Weiss (1985) and by the combined method are 1.4 ± 0.9 % in the coincidental temperature range of 278.15–313.15 K at the same salinity of 35 and 2.9 ± 0.4 % in the coincidental salinity range of 0–40 at the same temperature of 298.15 K. These results show that the seawater solubility estimated by the combined method is very close to measured values in Warner and Weiss (1985). Without measurements of the seawater solubility of these compounds, the combined method is a good way to estimate the seawater solubility.

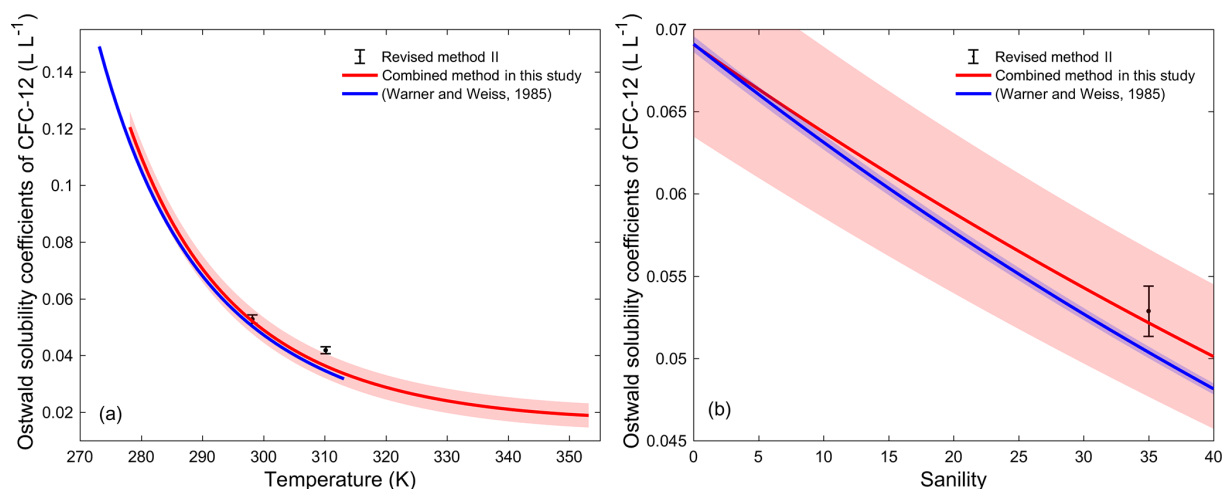
Based on the discussion above we make the following recommendations with respect to the calculation of the seawater solubilities of halogenated compounds.

- i. The (revised) method II could be used to estimate the seawater solubilities of compounds when neither water solubility data nor seawater solubility data have been obtained. This method is only based on the physical properties of compounds. The water solubility values and the salting-out coefficients are both estimated using the pp-LFERs.
- ii. The combined method is a better way to estimate the seawater solubility of compounds when water solubility, but not seawater solubility, has been measured. This is the case for the current study. The water solubility

Table 6. Comparison of the Ostwald solubility coefficients (L , $L L^{-1}$) of PFC-14 in seawater with previous results.

T (K)	t ($^{\circ}\text{C}$)	S (‰)	L , this study	L , (Scharlin and Battino, 1995)	RSD* (%)
288.15	15	35.086	0.005052	0.005169	1.62
293.15	20	35.086	0.004578	0.004527	0.79
298.15	25	35.086	0.004217	0.004027	3.26
303.15	30	35.086	0.003944	0.003635	5.77

* Relative standard deviation (RSD) of the Ostwald solubility coefficients estimated by the combined method and measured in Scharlin and Battino (1995).

**Figure 5.** Comparison of the Ostwald solubility coefficients in seawater for CFC-12 (a) in the available temperature range at a salinity of 35 and (b) in the salinity range of 0–40 at a temperature of 298.15 K calculated from revised method II, from the combined method, and from Warner and Weiss (1985). Error bars and shadings in the figure reflect the uncertainties.

function is constructed based on the CGW fit and the salting-out coefficient is estimated using the pp-LFERs.

- iii. The method in published studies (Warner and Weiss, 1985; Bu and Warner, 1995; Bullister and Wisegarver, 1998; Bullister et al., 2002) is the best way to estimate seawater solubilities. Here, both the water solubility values and seawater solubility values are experimentally determined.

It is worth noting that these methods can potentially be applied to many more compounds.

3.4 Transient tracer potential and comparison with CFC-12

The production and consumption history of CFC-12 is shown in Fig. 1. The history of CFC-12 used as an oceanic transient tracer is also presented here. In 1973, Lovelock et al. (1973) first proposed that CFC-12 can be used as a transient tracer to study water masses in the ocean. Subsequently, large numbers of studies (Gammon et al., 1982; Weiss et al., 1985; Smethie et al., 1988; Körtzinger et al., 1999; Tanhua et al., 2008; Smith et al., 2016; Fine et al., 2017) using CFC-12

as an oceanic transient tracer have been published. In the 1990s, the World Ocean Circulation Experiments (WOCE) used CFC-12 as the normal tracer to investigate global ocean circulation and mixing. CFC-12 is still used as a tracer, although its production was prohibited in 1996; its atmospheric mole fraction subsequently peaked in the early 2000s and is now in slow decline.

As one of the requirements to be a useful oceanic tracer, transient source functions (i.e., atmospheric mole fraction histories) have been established for HCFC-22, HCFC-141b, HCFC-142b, HFC-134a, HFC-125, HFC-23, PFC-14 and PFC-116 here. With the exception of HCFC-141b (Fig. S1b) and HCFC-142b (Fig. S1c), the discussed compounds are still steadily increasing in the atmosphere. Therefore, they have the potential to be used as oceanic transient tracers if only considering their source functions.

For HCFCs, only mole fractions of HCFC-22 are continuing to increase in the global atmosphere. All three HCFCs show declining growth rates since 2007. Combined with the ban on HCFCs in 2007, freezing in 1996 (developed) to 2013 (developing) and the phaseout in 2020–2030 (Fig. 1), HCFCs can likely be used as oceanic transient tracers for the next several decades for recently ventilated waters. Due to a fall in

emissions of HCFC-141b and HCFC-142b, the use of these two compounds will be more limited than HCFC-22 considering that atmospheric mole fractions of HCFC-141b have already begun to decrease and mole fractions of HCFC-142b are likely to decrease quite soon. Therefore, the atmospheric lifetimes of compounds are quite important, particularly once emissions have fallen. When atmospheric mole fractions of a given compound start to decrease, they are obviously no longer monotonically increasing, and the resultant calculated equilibrium atmospheric mole fraction in the ocean is no longer unique. Consequently, there will be two possible apparent ages for water masses so that this compound will have limited use as an oceanic tracer.

The mole fractions of HFCs are continuously increasing in the atmosphere, as are their growth rates. Restrictions on HFC consumption in the 2016 Kigali Amendment, with reduction of consumption beginning in 2019 in developed countries and freezing of consumption in 2024–2028 in developing countries (Fig. 1), mean that HFCs can likely be used as oceanic transient tracers for young waters for the next several decades. Moreover, HFCs have a higher potential to be oceanic transient tracers than HCFCs considering the increasing growth rates in the background atmosphere.

PFCs are increasing in the atmosphere over well-known natural background mole fractions. Combined with an atmospheric lifetime of over 50 000 years for PFC-14 and 10 000 years for PFC-116, PFCs have greater potential than HCFCs and HFCs to be oceanic transient tracers. PFC-14 has the potential to be a tracer for a longer period thanks to its longer lifetime, steady atmospheric growth rate and no current ban, as discussed by Deeds et al. (2008). However, PFC-14 is difficult to measure because it is extremely volatile and difficult to trap and separate chromatographically. PFC-116 can also be used as a transient tracer similar to PFC-14. The challenges for PFC-116 as an oceanic tracer are that it is a significant analytical challenge (low mole fractions in the atmosphere) with low solubility in seawater.

Well-established source functions and solubility functions in seawater are only two of the many requirements for an oceanic tracer. To be an oceanic transient tracer, the compound should also be conservative in the marine environment and be capable of rapid, relatively inexpensive and accurate measurement. The conservative nature of target compounds is briefly discussed in Sect. 1.2 by estimating the oceanic partial lifetimes of compounds with respect to hydrolysis in seawater. As we discussed for CFC-12, it is still used as an oceanic transient tracer though its production was phased out in the 1990s. For our target compounds, they have opportunities to be tracers once they are stable in seawater, can be measured in the ocean and have potential while atmospheric mole fractions continue to increase. This work provides two of the requirements for potential new oceanic transient tracers, while additional studies on compound conservation in seawater (comprehensive and detailed discussion) and mea-

surement methods of target compounds are needed to qualify these compounds as suitable tracers.

4 Conclusions

This work has established the source functions for HCFC-22, HCFC-141b, HCFC-142b, HFC-134a, HFC-125, HFC-23, PFC-14 and PFC-116 based on a synthesis of available data and models optimized for transient tracer work in two ways: (1) the atmospheric mole fractions are calculated at the time of water mass formation (late winter in each hemisphere) and (2) the seawater solubility of these compounds is reviewed for the first time. In general, the mole fractions of most compounds have been continuously rising over the past 3 decades and are still increasing today (though HCFC-141b and 142b rise rates have slowed down significantly). For HCFC-141b and HCFC-142b the annual mean mole fractions show sigmoidal growth and the growth rates have the shape of a normal distribution. For HFC-134a and HFC-23, the annual mean mole fractions show initial exponential growth followed by linear increase and the growth rates show a sigmoidal pattern. For HFC-125, the annual mean mole fractions and growth rates both show an exponential increase. To a certain extent, these growth patterns could predict the trends of annual mole fractions in the near future. The source functions and natural background mole fractions for all compounds show that HCFC-22, HCFC-141b, HCFC-142b, HFC-134a, HFC-125 and HFC-23 have the potential to be oceanic transient tracers for the next few decades, though their growth rates are expected to reverse, particularly for the HCFCs, due to the restriction on production and consumption imposed by the Montreal Protocol. HFCs have a higher potential to be oceanic transient tracers than HCFCs due to the increasing growth rates in the atmosphere, though these are likely to fall as a result of the recent Kigali Amendment. PFC-14 and PFC-116 have the potential to be tracers for a longer period due to their longer lifetimes, more consistent atmospheric growth rates and lack of direct production or emission bans currently in place, though they are listed in the Kyoto Protocol and industrial practices are changing to try to reduce or minimize emissions. In addition, we have used three different methods to estimate the seawater solubilities of the compounds of interest based on available theoretical concepts and experimental data. The seawater solubility functions of these compounds were subsequently constructed, completing the input functions of these potentially useful oceanic transient tracers.

Data availability. Data described in Table S1 are available at http://agage.eas.gatech.edu/data_archive/agage/ (last access: 20 December 2018) and <ftp://ftp.cmdl.noaa.gov/hats/> (last access: 20 December 2018) or from the corresponding author upon reasonable request. The calculated hemispheric annual mean mole fractions, JFM mean and JAS mean for target compounds can be found in Table S2.

Supplement. The supplement related to this article is available online at: <https://doi.org/10.5194/os-15-33-2019-supplement>.

Author contributions. The work was carried out by PL as a PhD candidate under the supervision of TT. JM, SAM, DEO, BRM, RW and PJF provided the atmospheric mole fraction data. PL collected the solubility data. PL analyzed and interpreted all the data based on discussion with TT. All authors worked on the paper.

Competing interests. The authors declare that they have no conflict of interest.

Acknowledgements. We acknowledge the Advanced Global Atmospheric Gases Experiment (AGAGE) programs, the Scripps Institution of Oceanography (SIO), the Commonwealth Scientific and Industrial Research Organization (CSIRO) Oceans and Atmosphere, the National Oceanic and Atmospheric Administration Earth System Research Laboratory Global Monitoring Division (NOAA/ESRL/GMD), and the University of East Anglia (UEA) for making their atmospheric data available. We thank the station operators, managers and support staff at the different monitoring sites of the AGAGE, the NOAA, the UEA and the CSIRO/Bureau of Meteorology, especially Gerry Spain, Randy Dickau, Paul B. Krummel, Paul Steele, Martin K. Vollmer, Caroline Siso, Bradley D. Hall, James W. Elkins and Ray Wang. In particular, we thank SIO, Diane Ivy (MIT) and Ray L. Langenfelds (CSIRO) for measuring and supplying the archived air samples. We are especially thankful to Simon O'Doherty (University of Bristol) and Johannes C. Laube (UEA) for providing data. We thank Arne Körtzinger for his instruction on this work. The authors are greatly indebted to Matthew Taliaferro for providing useful MATLAB code. We also appreciate the financial support from the China Scholarship Council (CSC). We dedicate this work to John Bullister whose tireless work in updating and establishing the source functions for the more traditional transient tracer was a great inspiration to us and served as a role model for our work.

Edited by: Piers Chapman

Reviewed by: four anonymous referees

References

- Abraham, M., Enrique Cometto-Mu, J., Cain, W., and Díaz, M.: The determination of solvation descriptors for terpenes, and the prediction of nasal pungency thresholds, *J. Chem. Soc. Perk. T.* 2, 2405–2412, <https://doi.org/10.1039/A805665J>, 1998.
- Abraham, M. H.: Scales of solute hydrogen-bonding: their construction and application to physicochemical and biochemical processes, *Chem. Soc. Rev.*, 22, 73–83, 1993.
- Abraham, M. H. and McGowan, J. C.: The use of characteristic volumes to measure cavity terms in reversed phase liquid chromatography, *Chromatographia*, 23, 243–246, 1987.
- Abraham, M. H., Grellier, P. L., and McGill, R. A.: Determination of olive oil-gas and hexadecane-gas partition coefficients, and calculation of the corresponding olive oil-water and hexadecane-water partition coefficients, *J. Chem. Soc. Perk. T.*, 2, 797–803, <https://doi.org/10.1039/P29870000797>, 1987.
- Abraham, M. H., Grellier, P. L., Prior, D. V., Duce, P. P., Morris, J. J., and Taylor, P. J.: Hydrogen bonding. Part 7. A scale of solute hydrogen-bond acidity based on logK values for complexation in tetrachloromethane, *J. Chem. Soc. Perk. T.*, 2, 699–711, <https://doi.org/10.1039/P29890000699>, 1989.
- Abraham, M. H., Whiting, G. S., Doherty, R. M., and Shuely, W. J.: Hydrogen bonding: XVI. A new solute solvation parameter, $\pi 2H$, from gas chromatographic data, *J. Chromatogr. A*, 587, 213–228, 1991.
- Abraham, M. H., Andonian-Haftvan, J., Whiting, G. S., Leo, A., and Taft, R. S.: Hydrogen bonding. Part 34. The factors that influence the solubility of gases and vapours in water at 298 K, and a new method for its determination, *J. Chem. Soc. Perk. T.*, 2, <https://doi.org/10.1039/P29940001777>, 1777–1791, 1994.
- Abraham, M. H., Gil-Lostes, J., Corr, S., and Acree, W. E.: Determination of partition coefficients of refrigerants by gas liquid chromatographic headspace analysis, *J. Chromatogr. A*, 1265, 144–148, 2012.
- Abraham, M. H., Gola, J. M., Cometto-Muñiz, J. E., and Cain, W. S.: Solvation properties of refrigerants, and the estimation of their water-solvent and gas-solvent partitions, *Fluid Phase Equilib.*, 180, 41–58, 2001.
- Abraham, M. H., Ibrahim, A., and Zissimos, A. M.: Determination of sets of solute descriptors from chromatographic measurements, *J. Chromatogr. A*, 1037, 29–47, 2004.
- Arnold, T., Mühle, J., Salameh, P. K., Harth, C. M., Ivy, D. J., and Weiss, R. F.: Automated Measurement of Nitrogen Trifluoride in Ambient Air, *Anal. Chem.*, 84, 4798–4804, 2012.
- Barber, M. and Tabereaux, A. T.: The Evolution of Søderberg Aluminum Cell Technology in North and South America, *JOM*, 66, 223–234, 2014.
- Battino, R., Seybold, P. G., and Campanell, F. C.: Correlations Involving the Solubility of Gases in Water at 298.15 K and 101325 Pa, *J. Chem. Eng. Data*, 56, 727–732, 2011.
- Bu, X. and Warner, M. J.: Solubility of chlorofluorocarbon 113 in water and seawater, *Deep-Sea Res. Pt. I*, 42, 1151–1161, [https://doi.org/10.1016/0967-0637\(95\)00052-8](https://doi.org/10.1016/0967-0637(95)00052-8), 1995.
- Bullister, J. L.: Atmospheric Histories (1765–2015) for CFC-11, CFC-12, CFC-113, CCl₄, SF₆ and N₂O, NDP-095, https://doi.org/10.3334/CDIAC/otg.CFC_ATM_Hist_2015, 2015.
- Bullister, J. L. and Wisegarver, D. P.: The solubility of carbon tetrachloride in water and seawater, *Deep-Sea Res. Pt. I*, 45, 1285–1302, 1998.
- Bullister, J. L., Wisegarver, D. P., and Menzia, F. A.: The solubility of sulfur hexafluoride in water and seawater, *Deep-Sea Res. Pt. I*, 49, 175–187, 2002.
- Bullister, J. L., Wisegarver, D. P., and Sonnerup, R. E.: Sulfur hexafluoride as a transient tracer in the North Pacific Ocean, *Geophys. Res. Lett.*, 33, L18603, <https://doi.org/10.1029/2006GL026514>, 2006.
- Butler, J. H., Battle, M., Bender, M. L., Montzka, S. A., Clarke, A. D., Saltzman, E. S., Sucher, C. M., Severinghaus, J. P., and Elkins, J. W.: A record of atmospheric halocarbons during the twentieth century from polar firn air, *Nature*, 399, 749–755, 1999.

- Calm, J. M. and Domanski, P. A.: R-22 replacement status, *EcoLibrium*TM, 3, 18–24, 2004.
- Carpenter, L. J., Reimann, S., Burkholder, J. B., Clerbaux, C., Hall, B. D., Hossaini, R., Laube, J. C., and Yvon-Lewis, S. A.: Scientific Assessment of Ozone Depletion: 2014, World Meteorological Organization Geneva, 2014.
- Cicerone, R. J.: Atmospheric carbon tetrafluoride: A nearly inert gas, *Science*, 206, 59–61, <https://doi.org/10.1126/science.206.4414.59>, 1979.
- Clever, H. L.: IUPAC-NIST Solubility Data Series. 80. Gaseous Fluorides of Boron, Nitrogen, Sulfur, Carbon, and Silicon and Solid Xenon Fluorides in all Solvents, *J. Phys. Chem. Ref. Data*, 34, 201, <https://doi.org/10.1063/1.1794762>, 2005.
- Craven, P. and Wahba, G.: Smoothing noisy data with spline functions: Estimating the Correct Degree of Smoothing by the Method of Generalized Cross-Validation, *Numer. Math.*, 31, 377–403, 1978.
- Cunnold, D. M., Prinn, R. G., Rasmussen, R. A., Simmonds, P. G., Alyea, F. N., Cardelino, C. A., Crawford, A. J., Fraser, P. J., and Rosen, R. D.: The Atmospheric Lifetime Experiment: 3. Lifetime methodology and application to three years of CFC1₃ data, *J. Geophys. Res.*, 88, 8379–8400, <https://doi.org/10.1029/JC088iC13p08379>, 1983.
- Cunnold, D. M., Fraser, P. J., Weiss, R. F., Prinn, R. G., Simmonds, P. G., Miller, B. R., Alyea, F. N., and Crawford, A. J.: Global trends and annual releases of CCl₃F and CCl₂F₂ estimated from ALE/GAGE and other measurements from July 1978 to June 1991, *J. Geophys. Res.-Atmos.*, 99, 1107–1126, 1994.
- Deeds, D. A.: The Natural Geochemistry of Tetrafluoromethane and Sulfur Hexafluoride : Studies of Ancient Mojave Desert Groundwaters, North Pacific Seawaters and the Summit Emissions of Kilauea Volcano, PhD thesis, 2008.
- Deeds, D. A., Mühle, J., and Weiss, R. F.: Tetrafluoromethane in the deep North Pacific Ocean, *Geophys. Res. Lett.*, 35, L14606, <https://doi.org/10.1029/2008GL034355>, 2008.
- Deeds, D. A., Kulongoski, J. T., Mühle, J., and Weiss, R. F.: Tectonic activity as a significant source of crustal tetrafluoromethane emissions to the atmosphere: Observations in groundwaters along the San Andreas Fault, *Earth. Planet. Sc. Lett.*, 412, 163–172, 2015.
- Derwent, R. G., Simmonds, P. G., Grealley, B. R., O’Doherty, S., McCulloch, A., Manning, A., Reimann, S., Folini, D., and Vollmer, M. K.: The phase-in and phase-out of European emissions of HCFC-141b and HCFC-142b under the Montreal Protocol: Evidence from observations at Mace Head, Ireland and Jungfraujoch, Switzerland from 1994 to 2004, *Atmos. Environ.*, 41, 757–767, 2007.
- Endo, S., Pfennigsdorff, A., and Goss, K.-U.: Salting-out effect in aqueous NaCl solutions: Trends with size and polarity of solute molecules, *Environ. Sci. Technol.*, 46, 1496–1503, 2012.
- Fine, R. A.: Observations of CFCs and SF₆ as ocean tracers, *Annu. Rev. Mar. Sci.*, 3, 173–195, 2011.
- Fine, R. A., Peacock, S., Maltrud, M. E., and Bryan, F. O.: A new look at ocean ventilation time scales and their uncertainties, *J. Geophys. Res.-Oceans*, 3771–3798, <https://doi.org/10.1002/2016JC012529>, 2017.
- Fraser, P., Steele, P., and Cooksey, M.: PFC and carbon dioxide emissions from an Australian aluminium smelter using time-integrated stack sampling and GC-MS, GC-FID analysis, in: *Light Metals 2013*, Springer, 2013.
- Fraser, P. J., Pearman, G. I., and Derek, N.: CSIRO Non-carbon Dioxide Greenhouse Gas Research. Part 1: 1975–90, *Hist. Rec. Aust. Sci.*, 29, 1–13, 2017.
- Gammon, R. H., Cline, J., and Wisegarver, D.: Chlorofluoromethanes in the northeast Pacific Ocean: Measured vertical distributions and application as transient tracers of upper ocean mixing, *J. Geophys. Res.-Oceans*, 87, 9441–9454, 1982.
- Gamsjäger, H., Lorimer, J. W., Scharlin, P., and Shaw, D. G.: Glossary of terms related to solubility (IUPAC Recommendations 2008), *Pure Appl. Chem.*, 80, 233–276, 2008.
- Gamsjäger, H., Lorimer, J. W., Salomon, M., Shaw, D. G., and Tomkins, R.: The IUPAC-NIST Solubility Data Series: A guide to preparation and use of compilations and evaluations (IUPAC Technical Report), *Pure Appl. Chem.*, 82, 1137–1159, 2010.
- Gassmann, M.: Freon 14 im “Krypton reinst” und in der Atmosphäre, *Naturwissenschaften*, 61, 127–127, 1974.
- Goss, K.-U., Bronner, G., Harner, T., Hertel, M., and Schmidt, T. C.: The partition behavior of fluorotelomer alcohols and olefins, *Environ. Sci. Technol.*, 40, 3572–3577, 2006.
- Graziosi, F., Arduini, J., Furlani, F., Giostra, U., Kuijpers, L. J. M., Montzka, S. A., Miller, B. R., O’Doherty, S. J., Stohl, A., Bonasoni, P., and Maione, M.: European emissions of HCFC-22 based on eleven years of high frequency atmospheric measurements and a Bayesian inversion method, *Atmos. Environ.*, 112, 196–207, 2015.
- Hodnebrog, Ø., Etmann, M., Fuglestedt, J. S., Marston, G., Myhre, G., Nielsen, C. J., Shine, K. P., and Wallington, T. J.: Global warming potentials and radiative efficiencies of halocarbons and related compounds: A comprehensive review, *Rev. Geophys.*, 51, 300–378, 2013.
- HSDB: Hazardous Substances Data Bank, TOXicology data NETWORK (TOXNET), National Library of Medicine (US), available at: <https://toxnet.nlm.nih.gov/newtoxnet/hsdb.htm>, last access: 10 April 2015.
- Hutchinson, M. F. and De Hoog, F.: Smoothing noisy data with spline functions, *Numer. Math.*, 47, 99–106, 1985.
- Jacobson, M. Z.: Air pollution and global warming: history, science, and solutions, Cambridge University Press, 2012.
- Khalil, M. A. K., Rasmussen, R. A., Culbertson, J. A., Prins, J. M., Grimsrud, E. P., and Shearer, M. J.: Atmospheric perfluorocarbons, *Environ. Sci. Technol.*, 37, 4358–4361, 2003.
- Kim, J., Fraser, P. J., Li, S., Mühle, J., Ganesan, A. L., Krummel, P. B., Steele, L. P., Park, S., Kim, S. K., and Park, M. K.: Quantifying aluminum and semiconductor industry perfluorocarbon emissions from atmospheric measurements, *Geophys. Res. Lett.*, 41, 4787–4794, 2014.
- Körtzinger, A., Rhein, M., and Mintrop, L.: Anthropogenic CO₂ and CFCs in the North Atlantic Ocean – A comparison of man-made tracers, *Geophys. Res. Lett.*, 26, 2065–2068, 1999.
- Langenfelds, R., Steele, P. F. R. F. L., and Allison, L. P. C.: The Cape Grim Air Archive: the first seventeen years, 1978–1995, Baseline Atmospheric Program (Australia) 1994–95, 53–70, 1996.
- Laube, J. C., Keil, A., Bönisch, H., Engel, A., Röckmann, T., Volk, C. M., and Sturges, W. T.: Observation-based assessment of stratospheric fractional release, lifetimes, and ozone depletion potentials of ten important source gases, *Atmos.*

- Chem. Phys., 13, 2779–2791, <https://doi.org/10.5194/acp-13-2779-2013>, 2013.
- Lovelock, J. E., Maggs, R. J., and Wade, R. J.: Halogenated Hydrocarbons in and over the Atlantic, *Nature*, 241, 194–196, 1973.
- Mackay, D., Shiu, W., Ma, K., and Lee, S. C.: *Handbook of physical-chemical properties and environmental fate for organic chemicals*, CRC press, 2006.
- Masterton, W. L.: Salting coefficients for gases in seawater from scaled-particle theory, *J. Solut. Chem.*, 4, 523–534, 1975.
- Matsunaga, K. O.: *Comparison of Environmental Impacts and Physical Properties of Refrigerants*, PhD thesis, New York: Columbia University, 2002.
- McCulloch, A. and Lindley, A. A.: Global emissions of HFC-23 estimated to year 2015, *Atmos. Environ.*, 41, 1560–1566, 2007.
- McCulloch, A., Midgley, P. M., and Ashford, P.: Releases of refrigerant gases (CFC-12, HCFC-22 and HFC-134a) to the atmosphere, *Atmos. Environ.*, 37, 889–902, 2003.
- McGowan, J. C. and Mellors, A.: *Molecular volumes in chemistry and biology*, E. Horwood, 1986.
- Mclinden, M. O.: *Physical properties of alternatives to the fully halogenated chlorofluorocarbons*, United States, 1990.
- Meinshausen, M., Vogel, E., Nauels, A., Lorbacher, K., Meinshausen, N., Etheridge, D. M., Fraser, P. J., Montzka, S. A., Rayner, P. J., Trudinger, C. M., Krummel, P. B., Beyerle, U., Canadell, J. G., Daniel, J. S., Enting, I. G., Law, R. M., Lunder, C. R., O'Doherty, S., Prinn, R. G., Reimann, S., Rubino, M., Velders, G. J. M., Vollmer, M. K., Wang, R. H. J., and Weiss, R.: Historical greenhouse gas concentrations for climate modelling (CMIP6), *Geosci. Model Dev.*, 10, 2057–2116, <https://doi.org/10.5194/gmd-10-2057-2017>, 2017.
- Miguel, A. A. F., Ferreira, A. G. M., and Fonseca, I. M. A.: Solubilities of some new refrigerants in water, *Fluid Phase Equilib.*, 173, 97–107, 2000.
- Miller, B. R. and Kuijpers, L. J. M.: Projecting future HFC-23 emissions, *Atmos. Chem. Phys.*, 11, 13259–13267, <https://doi.org/10.5194/acp-11-13259-2011>, 2011.
- Miller, B. R., Huang, J., Weiss, R. F., Prinn, R. G., and Fraser, P. J.: Atmospheric trend and lifetime of chlorodifluoromethane (HCFC-22) and the global tropospheric OH concentration, *J. Geophys. Res.*, 103, 13237–13248, <https://doi.org/10.1029/98JD00771>, 1998.
- Miller, B. R., Weiss, R. F., Salameh, P. K., Tanhua, T., Grealley, B. R., Mühle, J., and Simmonds, P. G.: Medusa: A sample preconcentration and GC/MS detector system for in situ measurements of atmospheric trace halocarbons, hydrocarbons, and sulfur compounds, *Anal. Chem.*, 80, 1536–1545, 2008.
- Miller, B. R., Rigby, M., Kuijpers, L. J. M., Krummel, P. B., Steele, L. P., Leist, M., Fraser, P. J., McCulloch, A., Harth, C., Salameh, P., Mühle, J., Weiss, R. F., Prinn, R. G., Wang, R. H. J., O'Doherty, S., Grealley, B. R., and Simmonds, P. G.: HFC-23 (CHF₃) emission trend response to HCFC-22 (CHClF₂) production and recent HFC-23 emission abatement measures, *Atmos. Chem. Phys.*, 10, 7875–7890, <https://doi.org/10.5194/acp-10-7875-2010>, 2010.
- Millero, F. J. and Poisson, A.: International one-atmosphere equation of state of seawater, *Deep-Sea Res. Pt. I*, 28, 625–629, 1981.
- Molina, M. J. and Rowland, F. S.: Stratospheric sink for chlorofluoromethanes: chlorine atom-catalysed destruction of ozone, *Nature*, 249, 810–812, 1974.
- Montzka, S. A., Myers, R. C., Butler, J. H., Elkins, J. W., and Cummings, S. O.: Global tropospheric distribution and calibration scale of HCFC-22, *Geophys. Res. Lett.*, 20, 703–706, 1993.
- Montzka, S. A., Myers, R. C., Butler, J. H., and Elkins, J. W.: Early trends in the global tropospheric abundance of hydrochlorofluorocarbon-141b and 142b, *Geophys. Res. Lett.*, 21, 2483–2486, 1994.
- Montzka, S. A., Myers, R. C., Butler, J. H., Elkins, J. W., Lock, L. T., Clarke, A. D., and Goldstein, A. H.: Observations of HFC-134a in the remote troposphere, *Geophys. Res. Lett.*, 23, 169–172, 1996.
- Montzka, S. A., Hall, B. D., and Elkins, J. W.: Accelerated increases observed for hydrochlorofluorocarbons since 2004 in the global atmosphere, *Geophys. Res. Lett.*, 36, L03804, <https://doi.org/10.1029/2008GL036475>, 2009.
- Montzka, S. A., Kuijpers, L., Battle, M. O., Aydin, M., Verhulst, K. R., Saltzman, E. S., and Fahey, D. W.: Recent increases in global HFC-23 emissions, *Geophys. Res. Lett.*, 37, L02808, <https://doi.org/10.1029/2009GL041195>, 2010a.
- Montzka, S. A., Reimann, S. C. L. A., O'Doherty, S., Engel, A., Krüger, K., and Sturges, W. T.: Ozone-Depleting Substances (ODSs) and Related Chemicals, in: *Scientific Assessment of Ozone Depletion: 2010*, Chapter 1, World Meteorological Organization, Geneva, Switzerland, 1–112, 2010b.
- Montzka, S. A., McFarland, M., Andersen, S. O., Miller, B. R., Fahey, D. W., Hall, B. D., Hu, L., Siso, C., and Elkins, J. W.: Recent trends in global emissions of hydrochlorofluorocarbons and hydrofluorocarbons: Reflecting on the 2007 adjustments to the Montreal Protocol, *J. Phys. Chem. A*, 119, 4439–4449, 2015.
- Moore, R. M., Geen, C. E., and Tait, V. K.: Determination of Henry's law constants for a suite of naturally occurring halogenated methanes in seawater, *Chemosphere*, 30, 1183–1191, 1995.
- Morris, R. A., Miller, T. M., Viggiano, A., Paulson, J. F., Solomon, S., and Reid, G.: Effects of electron and ion reactions on atmospheric lifetimes of fully fluorinated compounds, *J. Geophys. Res.-Atmos.*, 100, 1287–1294, 1995.
- Mühle, J., Ganesan, A. L., Miller, B. R., Salameh, P. K., Harth, C. M., Grealley, B. R., Rigby, M., Porter, L. W., Steele, L. P., Trudinger, C. M., Krummel, P. B., O'Doherty, S., Fraser, P. J., Simmonds, P. G., Prinn, R. G., and Weiss, R. F.: Perfluorocarbons in the global atmosphere: tetrafluoromethane, hexafluoroethane, and octafluoropropane, *Atmos. Chem. Phys.*, 10, 5145–5164, <https://doi.org/10.5194/acp-10-5145-2010>, 2010.
- O'Doherty, S., Cunnold, D. M., Manning, A. J., Miller, B. R., Wang, R. H. J., Krummel, P. B., Fraser, P. J., Simmonds, P. G., McCulloch, A., and Weiss, R. F.: Rapid growth of hydrofluorocarbon 134a and hydrochlorofluorocarbons 141b, 142b, and 22 from Advanced Global Atmospheric Gases Experiment (AGAGE) observations at Cape Grim, Tasmania, and Mace Head, Ireland, *J. Geophys. Res.*, 109, D06310, <https://doi.org/10.1029/2003JD004277>, 2004.
- O'Doherty, S., Cunnold, D. M., Miller, B. R., Mühle, J., McCulloch, A., Simmonds, P. G., Manning, A. J., Reimann, S., Vollmer, M. K., Grealley, B. R., Prinn, R. G., Fraser, P. J., Steele, L. P., Krummel, P. B., Dunse, B. L., Porter, L. W., Lunder, C. R., Schmidbauer, N., Hermansen, O., Salameh, P. K., Harth, C. M., Wang, R. H. J., and Weiss, R. F.: Global and regional emissions of HFC-125 (CHF₂CF₃) from in situ and air archive atmospheric obser-

- vations at AGAGE and SOGE observatories, *J. Geophys. Res.*, 114, D23304, <https://doi.org/10.1029/2009JD012184>, 2009.
- Oram, D. E., Reeves, C. E., Penkett, S. A., and Fraser, P. J.: Measurements of HCFC-142b and HCFC-141b in the Cape Grim air Archive: 1978–1993, *Geophys. Res. Lett.*, 22, 2741–2744, 1995.
- Oram, D. E., Reeves, C. E., Sturges, W. T., Penkett, S. A., Fraser, P. J., and Langenfelds, R. L.: Recent tropospheric growth rate and distribution of HFC-134a (CF₃CH₂F), *Geophys. Res. Lett.*, 23, 1949–1952, 1996.
- Oram, D. E., Sturges, W. T., Penkett, S. A., McCulloch, A., and Fraser, P. J.: Growth of fluoroform (CHF₃, HFC-23) in the background atmosphere, *Geophys. Res. Lett.*, 25, 35–38, 1998.
- Penkett, S. A., Prosser, N. J. D., Rasmussen, R. A., and Khalil, M. A. K.: Atmospheric measurements of CF₄ and other fluorocarbons containing the CF₃ grouping, *J. Geophys. Res.-Oceans*, 86, 5172–5178, 1981.
- Prinn, R., Cunnold, D., Simmonds, P., Alyea, F., Boldi, R., Crawford, A., Fraser, P., Gutzler, D., Hartley, D., and Rosen, R.: Global average concentration and trend for hydroxyl radicals deduced from ALE/GAGE trichloroethane (methyl chloroform) data for 1978–1990, *J. Geophys. Res.-Atmos.*, 97, 2445–2461, 1992.
- Prinn, R. G., Weiss, R. F., Fraser, P. J., Simmonds, P. G., Cunnold, D. M., Alyea, F. N., O'Doherty, S., Salameh, P., Miller, B. R., Huang, J., Wang, R. H. J., Hartley, D. E., Harth, C., Steele, L. P., Sturrock, G., Midgley, P. M., and McCulloch, A.: A history of chemically and radiatively important gases in air deduced from ALE/GAGE/AGAGE, *J. Geophys. Res.*, 105, 17751–17792, <https://doi.org/10.1029/2000JD900141>, 2000.
- Prinn, R. G., Weiss, R. F., Arduini, J., Arnold, T., DeWitt, H. L., Fraser, P. J., Ganesan, A. L., Gasore, J., Harth, C. M., Hermansen, O., Kim, J., Krummel, P. B., Li, S., Loh, Z. M., Lunder, C. R., Maione, M., Manning, A. J., Miller, B. R., Mitrevski, B., Mühle, J., O'Doherty, S., Park, S., Reimann, S., Rigby, M., Saito, T., Salameh, P. K., Schmidt, R., Simmonds, P. G., Steele, L. P., Vollmer, M. K., Wang, R. H., Yao, B., Yokouchi, Y., Young, D., and Zhou, L.: History of chemically and radiatively important atmospheric gases from the Advanced Global Atmospheric Gases Experiment (AGAGE), *Earth Syst. Sci. Data*, 10, 985–1018, <https://doi.org/10.5194/essd-10-985-2018>, 2018a.
- Prinn, R. G., Weiss, R. F., Arduini, J., Arnold, T., Fraser, P. J., Ganesan, A. L., Gasore, J., Harth, C. M., Hermansen, O., Kim, J., Krummel, P. B., Li, S., Loh, Z. M., Lunder, C. R., Maione, M., Manning, A. J., Miller, B. R., Mitrevski, B., Mühle, J., O'Doherty, S., Park, S., Reimann, S., Rigby, M., Salameh, P. K., Schmidt, R., Simmonds, P. G., Steele, L. P., Vollmer, M. K., Wang, R. H., and Young, D.: The ALE/GAGE/AGAGE Network (DB 1001), <https://doi.org/10.3334/CDIAC/atg.db1001>, 2018b.
- Rasmussen, R. A., Penkett, S. A., and Prosser, N.: Measurement of carbon tetrafluoride in the atmosphere, *Nature*, 277, 549–551, 1979.
- Rasmussen, R. A., Khalil, M. A. K., Penkett, S. A., and Prosser, N. J. D.: CHClF₂ (F-22) in the Earth's atmosphere, *Geophys. Res. Lett.*, 7, 809–812, 1980.
- Ravishankara, A., Solomon, S., Turnipseed, A. A., and Warren, R.: Atmospheric lifetimes of long-lived halogenated species, *Science*, 259, 194–199, <https://doi.org/10.1126/science.259.5092.194>, 1993.
- Reichl, A.: Messung und Korrelierung von Gaslöslichkeiten halogenierter Kohlenwasserstoffe, PhD thesis, Shaker, 1996.
- Reinsch, C. H.: Smoothing by spline functions, *Numer. Math.*, 10, 177–183, 1967.
- Rigby, M., Ganesan, A. L., and Prinn, R. G.: Deriving emissions time series from sparse atmospheric mole fractions, *J. Geophys. Res.-Atmos.*, 116, D08306, <https://doi.org/10.1029/2010JD015401>, 2011.
- Rigby, M., Prinn, R., O'Doherty, S., Miller, B., Ivy, D., Mühle, J., Harth, C., Salameh, P., Arnold, T., and Weiss, R.: Recent and future trends in synthetic greenhouse gas radiative forcing, *Geophys. Res. Lett.*, 41, 2623–2630, 2014.
- Rowland, F. S. and Molina, M. J.: Chlorofluoromethanes in the environment, *Rev. Geophys.*, 13, 1–35, 1975.
- Saikawa, E., Rigby, M., Prinn, R. G., Montzka, S. A., Miller, B. R., Kuijpers, L. J. M., Fraser, P. J. B., Vollmer, M. K., Saito, T., Yokouchi, Y., Harth, C. M., Mühle, J., Weiss, R. F., Salameh, P. K., Kim, J., Li, S., Park, S., Kim, K.-R., Young, D., O'Doherty, S., Simmonds, P. G., McCulloch, A., Krummel, P. B., Steele, L. P., Lunder, C., Hermansen, O., Maione, M., Arduini, J., Yao, B., Zhou, L. X., Wang, H. J., Elkins, J. W., and Hall, B.: Global and regional emission estimates for HCFC-22, *Atmos. Chem. Phys.*, 12, 10033–10050, <https://doi.org/10.5194/acp-12-10033-2012>, 2012.
- Sander, R.: Modeling atmospheric chemistry: Interactions between gas-phase species and liquid cloud/aerosol particles, *Surv. Geophys.*, 20, 1–31, 1999.
- Scharlin, P. and Battino, R.: Solubility of CCl₂F₂, CClF₃, CF₄, and CH₄ in Water and Seawater at 288.15–303.15 K and 101.325 kPa, *J. Chem. Eng. Data*, 40, 167–169, 1995.
- Schneider, A., Tanhua, T., Körtzinger, A., and Wallace, D. W. R.: An evaluation of tracer fields and anthropogenic carbon in the equatorial and the tropical North Atlantic, *Deep-Sea Res. Pt. I*, 67, 85–97, 2012.
- Schwarzenbach, R. P., Gschwend, P. M., and Imboden, D. M.: *Environmental Organic Chemistry*, 2. ed, John Wiley & Sons: Hoboken, NJ, 2003.
- Simmonds, P. G., O'Doherty, S., Huang, J., Prinn, R., Derwent, R. G., Ryall, D., Nickless, G., and Cunnold, D.: Calculated trends and the atmospheric abundance of 1, 1, 1, 2-tetrafluoroethane, 1, 1-dichloro-1-fluoroethane, and 1-chloro-1, 1-difluoroethane using automated in-situ gas chromatography-mass spectrometry measurements recorded at Mace Head, Ireland, from October 1994 to March 1997, *J. Geophys. Res.-Atmos.*, 103, 16029–16037, 1998.
- Simmonds, P. G., Derwent, R. G., Manning, A. J., McCulloch, A., and O'Doherty, S.: USA emissions estimates of CH₃CHF₂, CH₂FCF₃, CH₃CF₃ and CH₂F₂ based on in situ observations at Mace Head, *Atmos. Environ.*, 104, 27–38, 2015.
- Simmonds, P. G., O'Doherty, S., Nickless, G., Sturrock, G. A., Swaby, R., Knight, P., Ricketts, J., Woffendin, G., and Smith, R.: Automated gas chromatograph/mass spectrometer for routine atmospheric field measurements of the CFC replacement compounds, the hydrofluorocarbons and hydrochlorofluorocarbons, *Anal. Chem.*, 67, 717–723, 1995.
- Simmonds, P. G., Rigby, M., McCulloch, A., O'Doherty, S., Young, D., Mühle, J., Krummel, P. B., Steele, P., Fraser, P. J., Manning, A. J., Weiss, R. F., Salameh, P. K., Harth, C. M., Wang, R. H. J., and Prinn, R. G.: Changing trends and emissions

- of hydrochlorofluorocarbons (HCFCs) and their hydrofluorocarbon (HFCs) replacements, *Atmos. Chem. Phys.*, 17, 4641–4655, <https://doi.org/10.5194/acp-17-4641-2017>, 2017.
- Simmonds, P. G., Rigby, M., McCulloch, A., Vollmer, M. K., Henne, S., Mühle, J., O'Doherty, S., Manning, A. J., Krummel, P. B., Fraser, P. J., Young, D., Weiss, R. F., Salameh, P. K., Harth, C. M., Reimann, S., Trudinger, C. M., Steele, L. P., Wang, R. H. J., Ivy, D. J., Prinn, R. G., Mitrevski, B., and Etheridge, D. M.: Recent increases in the atmospheric growth rate and emissions of HFC-23 (CHF₃) and the link to HCFC-22 (CHClF₂) production, *Atmos. Chem. Phys.*, 18, 4153–4169, <https://doi.org/10.5194/acp-18-4153-2018>, 2018.
- Smethie, W., Chipman, D., Swift, J., and Koltermann, K.: Chlorofluoromethanes in the Arctic Mediterranean seas: evidence for formation of bottom water in the Eurasian Basin and deep-water exchange through Fram Strait, *Deep-Sea Res. Pt. A.*, 35, 347–369, 1988.
- Smith, J. N., Smethie, W. M., Yashayev, I., Curry, R., and Azetsu-Scott, K.: Time series measurements of transient tracers and tracer-derived transport in the Deep Western Boundary Current between the Labrador Sea and the subtropical Atlantic Ocean at Line W, *J. Geophys. Res.-Oceans*, 121, 8115–8138, 2016.
- SPARC: Lifetimes of Stratospheric Ozone-Depleting Substances, Their Replacements, and Related Species, 2013.
- Stöven, T., Tanhua, T., Hoppema, M., and Bullister, J. L.: Perspectives of transient tracer applications and limiting cases, *Ocean Sci.*, 11, 699–718, <https://doi.org/10.5194/os-11-699-2015>, 2015.
- Stöven, T., Tanhua, T., Hoppema, M., and von Appen, W.-J.: Transient tracer distributions in the Fram Strait in 2012 and inferred anthropogenic carbon content and transport, *Ocean Sci.*, 12, 319–333, <https://doi.org/10.5194/os-12-319-2016>, 2016.
- Sturrock, G. A., Etheridge, D. M., Trudinger, C. M., Fraser, P. J., and Smith, A. M.: Atmospheric histories of halocarbons from analysis of Antarctic firn air: Major Montreal Protocol species, *J. Geophys. Res.-Atmos.*, 107, 4765, <https://doi.org/10.1029/2002JD002548>, 2002.
- Tanhua, T., Anders Olsson, K., and Fogelqvist, E.: A first study of SF₆ as a transient tracer in the Southern Ocean, *Deep-Sea Res. Pt. II*, 51, 2683–2699, 2004.
- Tanhua, T., Olsson, K. A., and Jeansson, E.: Tracer evidence of the origin and variability of Denmark Strait Overflow Water, in: *Arctic-Subarctic Ocean Fluxes*, Springer, 2008.
- TEAP: Report of the Technology and Economic Assessment Panel. HCFC Task Force Report, United Nations Environment Programme, Ozone Secretariat, P. O. Box 30552, Nairobi, Kenya, 2003.
- Thompson, T. M., Butler, J. H., Daube, B. C., Dutton, G. S., Elkins, J. W., Hall, B. D., Hurst, D. F., King, D. B., Kline, E. S., and Lafleur, B. G.: Halocarbons and other Atmospheric Trace Species, Section 5, in *Climate Monitoring and Diagnostics Laboratory: Summary Report No. 27, 2002–2003*, edited by: Schnell, R., Buggle, A. M., and Rosson, R., 115–135, NOAA/Climate Monitoring and Diagnostics Laboratory, Boulder, Colo., 2004.
- Trudinger, C. M., Fraser, P. J., Etheridge, D. M., Sturges, W. T., Vollmer, M. K., Rigby, M., Martinerie, P., Mühle, J., Worton, D. R., Krummel, P. B., Steele, L. P., Miller, B. R., Laube, J., Mani, F. S., Rayner, P. J., Harth, C. M., Witrant, E., Blunier, T., Schwander, J., O'Doherty, S., and Battle, M.: Atmospheric abundance and global emissions of perfluorocarbons CF₄, C₂F₆ and C₃F₈ since 1800 inferred from ice core, firn, air archive and in situ measurements, *Atmos. Chem. Phys.*, 16, 11733–11754, <https://doi.org/10.5194/acp-16-11733-2016>, 2016.
- UNEP: United Nations Environment Programme, available at: <https://www.ozone.unep.org/countries/data>, last access: 22 July 2018.
- Vogel, H. and Friedrich, B.: An Estimation of PFC Emission by Rare Earth Electrolysis, in: *Light Metals 2018*, edited by: Martin, O., TMS 2018, The Minerals, Metals & Materials Series, Springer, Cham, 1507–1517, 2018.
- Vollmer, M. K., Mühle, J., Trudinger, C. M., Rigby, M., Montzka, S. A., Harth, C. M., Miller, B. R., Henne, S., Krummel, P. B., and Hall, B. D.: Atmospheric histories and global emissions of halons H-1211 (CBrClF₂), H-1301 (CBrF₃), and H-2402 (CBrF₂CBrF₂), *J. Geophys. Res.-Atmos.*, 121, 3663–3686, 2016.
- Wahba, G.: Bayesian “confidence intervals” for the cross-validated smoothing spline, *J. Roy. Stat. Soc. B*, 45, 133–150, 1983.
- Wahba, G.: *Spline models for observational data*, SIAM, Society for industrial and applied mathematics, Philadelphia, Pennsylvania, 1990.
- Walker, S. J., Weiss, R. F., and Salameh, P. K.: Reconstructed histories of the annual mean atmospheric mole fractions of the halocarbons CFC-11 CFC-12, CFC-113, and carbon tetrachloride, *J. Geophys. Res.*, 105, 14285–14296, <https://doi.org/10.1029/1999JC900273>, 2000.
- Warner, M. J. and Weiss, R. F.: Solubilities of chlorofluorocarbons 11 and 12 in water and seawater, *Deep-Sea Res. Pt. I*, 32, 1485–1497, [https://doi.org/10.1016/0198-0149\(85\)90099-8](https://doi.org/10.1016/0198-0149(85)90099-8), 1985.
- Waugh, D. W., Vollmer, M. K., Weiss, R. F., Haine, T. W., and Hall, T. M.: Transit time distributions in Lake Issyk-Kul, *Geophys. Res. Lett.*, 29, 2231, <https://doi.org/10.1029/2002GL016201>, 2002.
- Waugh, D. W., Abraham, E. R., and Bowen, M. M.: Spatial variations of stirring in the surface ocean: A case study of the Tasman Sea, *J. Phys. Oceanogr.*, 36, 526–542, 2006.
- Weiss, R. F.: The solubility of nitrogen, oxygen and argon in water and seawater, *Deep-Sea Res. Pt. II*, 17, 721–735, 1970.
- Weiss, R. F.: Carbon Dioxide in Water and Seawater: the Solubility of a Non-ideal Gas, *Mar. Chem.*, 2, 203–215, [https://doi.org/10.1016/0304-4203\(74\)90015-2](https://doi.org/10.1016/0304-4203(74)90015-2), 1974.
- Weiss, R. F., Bullister, J. L., Gammon, R. H., and Warner, M. J.: Atmospheric chlorofluoromethanes in the deep equatorial Atlantic, *Nature*, 314, 608–610, <https://doi.org/10.1038/314608a0>, 1985.
- Xiang, B., Patra, P. K., Montzka, S. A., Miller, S. M., Elkins, J. W., Moore, F. L., Atlas, E. L., Miller, B. R., Weiss, R. F., Prinn, R. G., and Wofsy, S. C.: Global emissions of refrigerants HCFC-22 and HFC-134a: Unforeseen seasonal contributions, *P. Natl. Acad. Sci. USA*, 111, 17379–17384, 2014.
- Young, C. L., Battino, R., and Clever, H. L.: *The Solubility of Gases in Liquids: Introductory Information*, IUPAC SDS, 27/28, 1982.
- Yvon-Lewis, S. A. and Butler, J. H.: Effect of oceanic uptake on atmospheric lifetimes of selected trace gases, *J. Geophys. Res.-Atmos.*, 107, 4414, <https://doi.org/10.1029/2001JD001267>, 2002.

Supplement of

Atmospheric histories, growth rates and solubilities in seawater and other natural water of the potential transient tracers HCFC-22, HCFC-141b, HCFC-142b, HFC-134a, HFC-125, HFC-23, PFC-14 and PFC-116

Content:

Section S1. Smoothing spline fit method

Table S1 (a-h). Collected data used for HCFC-22, HCFC-141b, HCFC-142b, HFC-134a, HFC-125, HFC-23, PFC-14 and PFC-116

Table S2. Atmospheric mole fractions for HCFC-22, HCFC-141b, HCFC-142b, HFC-134a, HFC-125, HFC-23, PFC-14 and PFC-116 (see Appendix B)

Table S3. Ostwald solubility function of PFC-14 in seawater estimated by the method I

Table S4. Comparison among the calculated Ostwald solubility coefficients (L_0 , L L^{-1}) by the poly-parameter linear free energy relationships (pp-LFERs) based on V , V_c and $\log L^{16}$, observed ones and calculated ones by the Clark-Glew-Weiss (CGW) model fit of target compounds and CFC-12 in the water at 298.15 K and 310.15 K

Table S5. Ostwald solubility functions of target compounds and CFC-12 in water estimated by the (revised) method II at 298.15 K and 310.15 K

Figure S1 (a-h). HCFC-22, HCFC-141b, HCFC-142b, HFC-134a, HFC-125, HFC-23, PFC-14 and PFC-116: Atmospheric mole fractions in the NH and SH estimated from collected data (Table S1a-h)

Figure S2 (a-i). HCFC-22, HCFC-141b, HCFC-142b, HFC-134a, HFC-125, HFC-23, PFC-14, PFC-116 and CFC-12 freshwater solubility (Ostwald solubility coefficients) as a function of temperature based on previous studies

Figure S3. The relationship between salting-out coefficients (SOC) and temperature calculated by Eq. (16) for CFC-12 based on the data from Warner and Weiss (1985).

Section S1. Smoothing spline fit method

After the data containing replicate times have been converted into a value at each replicate time, the data were sorted as $x_1 < x_2 < \dots < x_i < \dots < x_n$.

Set $x_i, y_i, \delta y_i$ ($i = 1, 2, \dots, n$) to be the decimal time, the corresponding atmospheric mole fractions and the standard deviation.

Normalize the x vector

$$t_i = (x_i - \min(x_i)) / (\max(x_i) - \min(x_i)) \quad (1)$$

The smoothing function $f(t)$ to be constructed shall

$$\text{Minimize } p \sum_{i=1}^n \left[\frac{g(t_i) - y_i}{\delta y_i} \right]^2 + \int g''(t)^2 dt \quad (2)$$

The solution of the minimum principle is a spline. By introducing the auxiliary variable z together with the Lagrangian parameter p , we have to look for the minimum of the function

$$\int_{t_1}^{t_n} g''(t)^2 dt + p \left[\sum_{i=1}^n \left(\frac{g(t_i) - y_i}{\delta y_i} \right)^2 + z^2 \right] \quad (3)$$

From the corresponding Euler-Lagrange equations, we determine the optimal function $f(t)$.

$$f(t) = a_i + b_i(t - t_i) + c_i(t - t_i)^2 + d_i(t - t_i)^3, \quad t_i \leq t < t_{i+1} \quad (4)$$

We obtain the spline coefficients (Reinsch, 1967).

$$c_i = \frac{pQ^T y}{B}, \quad c = [0; c_i; 0]^T \quad (5)$$

$$a = y - W^2 Q c / p \quad (6)$$

$$d_i = (c_{i+1} - c_i) / (3h_i) \quad (7)$$

$$b_i = (a_{i+1} - a_i) / h_i - c_i h_i - d_i h_i^2 \quad (8)$$

$$\text{coeffs} = [d, c, b, a] \quad (9)$$

Here, the following notation is used:

$$h_i = t_{i+1} - t_i, \quad (10)$$

$$W = \text{diag}(\delta y_1, \dots, \delta y_n), \quad (11)$$

T is the $(n-1) \times (n-1)$ dimensional positive tridiagonal matrix with entries t_{ij} ($i, j = 1, 2, \dots, n-1$) given by

$$t_{ii} = 2(h_{i-1} + h_i) / 3, \quad t_{i,i+1} = t_{i+1,i} = h_i / 3 \quad (12)$$

Q is the $(n) \times (n-2)$ dimensional tridiagonal matrix with entries q_{ij} ($i = 1, 2, \dots, n; j = 1, 2, \dots, n-2$) given by

$$q_{i-1,i} = 1/h_{i-1}, \quad q_{i,i} = -1/h_{i-1} - 1/h_i, \quad q_{i+1,i} = 1/h_i \quad (13)$$

The elements in the i^{th} column of Q given by the coefficients of the 2nd order divided differences based on t_i, \dots, t_{i+2} . Let the coefficient matrix be denoted by

$$B_p = Q^T W^2 Q + pT \quad (14)$$

The *influence matrix* associated with the smoothing spline is the unique $n \times n$ symmetric matrix A_p satisfying

$$a = A_p y \quad (15)$$

The error

$$\text{error} = y - a = W^2 Q B_p^{-1} Q^T y \quad (16)$$

So that

$$I - A_p = W^2 Q B_p^{-1} Q^T \quad (17)$$

The weighted residual sum of squares

$$RSS = \|(I - A_p)y/W\|^2 = \|W^2 Q B_p^{-1} Q^T y\|^2 \quad (18)$$

The estimated value of the generalized cross-validation (GCV) minimization function V of p used in the experiments below is the minimizer of the GCV function V_p defined

$$V_p = \frac{n \|(I - A_p)y/W\|^2}{[Tr(I - A_p)]^2} \quad (19)$$

The estimated degrees of freedom (Hutchinson and De Hoog, 1985)

$$Tr(I - A_p) = n - 2 - p Tr(T/B) \quad (20)$$

The estimated variance

$$VAR = RSS / Tr(I - A_p) \quad (21)$$

The estimated 95% Bayesian confidence intervals (CI) for the cross-validated smoothing spline (Wahba, 1983) are given by

$$CI = 1.96 \sqrt{VAR * diag(A_p)} \quad (22)$$

Table S1a. Collected data used for HCFC-22

Data	Network	Station	Latitude °N	Longitude °E	Instrument	Data availability	Scale	Reference
NH								
<i>In situ</i>	AGAGE	Mace Head	53.3	-9.9	ADS	1999.01-2004.12	SIO-05	(Prinn et al., 2018a; Prinn et al., 2018b)
<i>In situ</i>	AGAGE	Mace Head	53.3	-9.9	Medusa	2003.11-2017.09	SIO-05	(Prinn et al., 2018a; Prinn et al., 2018b)
Flask	NOAA	Mace Head	53.3	-9.9	GC-MS	1998.10-2018.08	NOAA-2006	(Montzka et al., 1996a; Montzka et al., 2015)
<i>In situ</i>	AGAGE	Trinidad Head	41	-124.1	Medusa	2005.05-2017.09	SIO-05	(Prinn et al., 2018a; Prinn et al., 2018b)
Flask	NOAA	Trinidad Head	41	-124.1	GC-MS	2002.03-2018.08	NOAA-2006	(Montzka et al., 1996a; Montzka et al., 2015)
Model	NOAA	NH	30-90	-	2-D box	1944-2009	NOAA-2006	(Montzka et al., 2010)
SH								
<i>In situ</i>	AGAGE	Cape Grim	-40.7	144.7	ADS	1998.03-2004.12	SIO-05	(Prinn et al., 2018a; Prinn et al., 2018b)
<i>In situ</i>	AGAGE	Cape Grim	-40.7	144.7	Medusa	2004.01-2017.09	SIO-05	(Prinn et al., 2018a; Prinn et al., 2018b)
Flask	NOAA	Cape Grim	-40.7	144.7	GC-MS	1991.11-2018.08	NOAA-2006	(Montzka et al., 1996a; Montzka et al., 2015)
Archived air	AGAGE	Cape Grim	-40.7	144.7	Medusa	1978.04-1996.12	SIO-93	(Miller et al., 1998)
Model	NOAA	SH	-30 ~ -90	-	2-D box	1944-2009	NOAA-2006	(Montzka et al., 2010)

Table S1b. Collected data used for HCFC-141b

Data	Network	Station	Latitude °N	Longitude °E	Instrument	Data availability	Scale	Reference
NH								
Archived air	NOAA	Niwot Ridge	40	-	GC-MS	1987.01-1994.03	NOAA-1994	(Thompson et al., 2004)
<i>In situ</i>	AGAGE	Mace Head	53.3	-9.9	ADS	1994.11-2004.12	SIO-05	(Prinn et al., 2018a; Prinn et al., 2018b)
<i>In situ</i>	AGAGE	Mace Head	53.3	-9.9	Medusa	2003.11-2017.09	SIO-05	(Prinn et al., 2018a; Prinn et al., 2018b)
Flask	NOAA	Mace Head	53.3	-9.9	GC-MS	1998.10-2018.08	NOAA-1994	(Montzka et al., 1996a; Montzka et al., 2015)
<i>In situ</i>	AGAGE	Trinidad Head	41	-124.1	Medusa	2005.03-2017.09	SIO-05	(Prinn et al., 2018a; Prinn et al., 2018b)
Flask	NOAA	Trinidad Head	41	-124.1	GC-MS	2002.02-2018.08	NOAA-1994	(Montzka et al., 1996a; Montzka et al., 2015)
SH								
Firn air	AGAGE	Antarctic	-90	-4.8	ADS	1935.06-1991.11	UB-98	(Sturrock et al., 2002)
Archived air	NOAA	-	-29.4	-	GC-MS	1987.06	NOAA-1994	(Thompson et al., 2004)
Archived air	UEA	Cape Grim	-40.7	144.7	GC-MS	1978.04-2011.06	NOAA-1994	(Oram et al., 1995);
<i>In situ</i>	AGAGE	Cape Grim	-40.7	144.7	ADS	1998.03-2004.12	SIO-05	(Prinn et al., 2018a; Prinn et al., 2018b)
<i>In situ</i>	AGAGE	Cape Grim	-40.7	144.7	Medusa	2004.01-2017.09	SIO-05	(Prinn et al., 2018a; Prinn et al., 2018b)
Flask	NOAA	Cape Grim	-40.7	144.7	GC-MS	1994.10-2018.08	NOAA-1994	(Montzka et al., 1996a; Montzka et al., 2015)

Table S1c. Collected data used for HCFC-142b

Data	Network	Station	Latitude °N	Longitude °E	Instrument	Data availability	Scale	Reference
NH								
Archived air	NOAA	Niwot Ridge	40	-	GC-MS	1987.01-1994.03	NOAA-1994	(Thompson et al., 2004)
<i>In situ</i>	AGAGE	Mace Head	53.3	-9.9	ADS	1994.10-2004.12	SIO-05	(Prinn et al., 2018a; Prinn et al., 2018b)
<i>In situ</i>	AGAGE	Mace Head	53.3	-9.9	Medusa	2003.11-2017.09	SIO-05	(Prinn et al., 2018a; Prinn et al., 2018b)
Flask	NOAA	Mace Head	53.3	-9.9	GC-MS	1998.10-2018.07	NOAA-1994	(Montzka et al., 1996a; Montzka et al., 2015)
<i>In situ</i>	AGAGE	Trinidad Head	41	-124.1	Medusa	2005.03-2017.09	SIO-05	(Prinn et al., 2018a; Prinn et al., 2018b)
Flask	NOAA	Trinidad Head	41	-124.1	GC-MS	2002.02-2018.08	NOAA-1994	(Montzka et al., 1996a; Montzka et al., 2015)
SH								
Firn air	AGAGE	Antarctic	-90	-4.8	ADS	1936.06-1992.05	UB-98	(Sturrock et al., 2002)
Archived air	NOAA	-	-29.4	-	GC-MS	1987.06	NOAA-1994	(Thompson et al., 2004)
Archived air	UEA	Cape Grim	-40.7	144.7	GC-MS	1978.04-2011.06	NOAA-1994	(Oram et al., 1995);
<i>In situ</i>	AGAGE	Cape Grim	-40.7	144.7	ADS	1998.03-2004.12	SIO-05	(Prinn et al., 2018a; Prinn et al., 2018b)
<i>In situ</i>	AGAGE	Cape Grim	-40.7	144.7	Medusa	2004.01-2017.09	SIO-05	(Prinn et al., 2018a; Prinn et al., 2018b)
Flask	NOAA	Cape Grim	-40.7	144.7	GC-MS	1992.01-2018.08	NOAA-1994	(Montzka et al., 1996a; Montzka et al., 2015)

Table S1d. Collected data used for HFC-134a

Data	Network	Station	Latitude °N	Longitude °E	Instrument	Data availability	Scale	Reference
NH								
Archived air	AGAGE	La Jolla and other	32.87	-117.25	Medusa	1973.06-2016.04	SIO-05	this study
Archived air	NOAA	Niwot Ridge	40	-	GC-MS	1976.01-1999.04	NOAA-1995	(Montzka et al., 1996b)
<i>In situ</i>	AGAGE	Mace Head	53.3	-9.9	ADS	1994.10-2004.12	SIO-05	(Prinn et al., 2018a; Prinn et al., 2018b)
<i>In situ</i>	AGAGE	Mace Head	53.3	-9.9	Medusa	2003.11-2017.09	SIO-05	(Prinn et al., 2018a; Prinn et al., 2018b)
Flask	NOAA	Mace Head	53.3	-9.9	GC-MS	1998.10-2018.06	NOAA-1995	(Montzka et al., 1996a; Montzka et al., 2015)
<i>In situ</i>	AGAGE	Trinidad Head	41	-124.1	Medusa	2005.03-2017.09	SIO-05	(Prinn et al., 2018a; Prinn et al., 2018b)
Flask	NOAA	Trinidad Head	41	-124.1	GC-MS	2002.02-2018.06	NOAA-1995	(Montzka et al., 1996a; Montzka et al., 2015)
SH								
Archived air	AGAGE	Cape Grim	-40.7	144.7	Medusa	1978.04-2011.06	SIO-05	this study
Archived air	NOAA	-	-29.4	-	GC-MS	1987.06	NOAA-1995	(Montzka et al., 1996b)
Archived air	UEA	Cape Grim	-40.7	144.7	GC-MS	1990.05-2012.12	NOAA-1995	(Oram et al., 1996)
<i>In situ</i>	AGAGE	Cape Grim	-40.7	144.7	ADS	1998.02-2004.12	SIO-05	(Prinn et al., 2018a; Prinn et al., 2018b)
<i>In situ</i>	AGAGE	Cape Grim	-40.7	144.7	Medusa	2004.01-2017.09	SIO-05	(Prinn et al., 2018a; Prinn et al., 2018b)
Flask	NOAA	Cape Grim	-40.7	144.7	GC-MS	1994.10-2018.08	NOAA-1995	(Montzka et al., 1996a; Montzka et al., 2015)

Table S1e. Collected data used for HFC-125

Data	Network	Station	Latitude °N	Longitude °E	Instrument	Data availability	Scale	Reference
NH								
Archived air	AGAGE	La Jolla and other	32.87	-117.25	Medusa	1973.06-2015.11	SIO-14	(O'Doherty et al., 2009)
Archived air	AGAGE	La Jolla and other	32.87	-117.25	Medusa	1973.06-2011.06	UB-98	(O'Doherty et al., 2009)
<i>In situ</i>	AGAGE	Mace Head	53.3	-9.9	ADS	1998.02-2004.12	SIO-14	(Prinn et al., 2018a; Prinn et al., 2018b)
<i>In situ</i>	AGAGE	Mace Head	53.3	-9.9	Medusa	2003.11-2017.09	SIO-14	(Prinn et al., 2018a; Prinn et al., 2018b)
<i>In situ</i>	AGAGE	Trinidad Head	41	-124.1	Medusa	2005.03-2017.09	SIO-14	(Prinn et al., 2018a; Prinn et al., 2018b)
Flask	NOAA	Trinidad Head	41	-124.1	GC-MS_M2	2007.01-2015.04	NOAA-2008	(Montzka et al., 2015)
SH								
Archived air	AGAGE	Cape Grim	-40.7	144.7	Medusa	1978.04-2011.06	SIO-14	(O'Doherty et al., 2009)
Archived air	AGAGE	Cape Grim	-40.7	144.7	Medusa	1995.02-2001.09	UB-98	(O'Doherty et al., 2009)
<i>In situ</i>	AGAGE	Cape Grim	-40.7	144.7	ADS	1998.02-2004.12	SIO-14	(Prinn et al., 2018a; Prinn et al., 2018b)
<i>In situ</i>	AGAGE	Cape Grim	-40.7	144.7	Medusa	2004.02-2017.09	SIO-14	(Prinn et al., 2018a; Prinn et al., 2018b)
Flask	NOAA	Cape Grim	-40.7	144.7	GC-MS_M2	2007.01-2015.04	NOAA-2008	(Montzka et al., 2015)

Table S1f. Collected data used for HFC-23

Data	Network	Station	Latitude °N	Longitude °E	Instrument	Data availability	Scale	Reference
NH								
<i>In situ</i>	AGAGE	Mace Head	53.3	-9.9	Medusa	2007.10-2017.09	SIO-07	(Prinn et al., 2018a; Prinn et al., 2018b)
<i>In situ</i>	AGAGE	Trinidad Head	41	-124.1	Medusa	2007.09-2017.09	SIO-07	(Prinn et al., 2018a; Prinn et al., 2018b)
Model	AGAGE	NH	30-90	-	2-D 12-box	1978.01-2009.12	SIO-07	(Miller et al., 2010)
SH								
Archived air	AGAGE	Cape Grim	-40.7	144.7	Medusa3	2005.04-2009.11	SIO-07	(Miller et al., 2010)
Archived air	AGAGE	Cape Grim	-40.7	144.7	Medusa9	1978.04-2006.12	SIO-07	(Miller et al., 2010)
<i>In situ</i>	AGAGE	Cape Grim	-40.7	144.7	Medusa	2007.01-2017.09	SIO-07	(Prinn et al., 2018a; Prinn et al., 2018b)
Model	AGAGE	SH	-30 ~ -90	-	2-D 12-box	1978.01-2009.12	SIO-07	(Miller et al., 2010)

Table S1g. Collected data used for PFC-14

Data	Network	Station	Latitude °N	Longitude °E	Instrument	Data availability	Scale	Reference
NH								
<i>In situ</i>	AGAGE	Mace Head	53.3	-9.9	Medusa	2006.05-2017.09	SIO-05	(Prinn et al., 2018a; Prinn et al., 2018b)
<i>In situ</i>	AGAGE	Trinidad Head	41	-124.1	Medusa	2006.04-2017.09	SIO-05	(Prinn et al., 2018a; Prinn et al., 2018b)
Model	AGAGE	NH	30-90	-	2-D 12-box	1900-2015	SIO-05	(Trudinger et al., 2016)
SH								
<i>In situ</i>	AGAGE	Cape Grim	-40.7	144.7	Medusa	2006.05-2017.09	SIO-05	(Prinn et al., 2018a; Prinn et al., 2018b)
Model	AGAGE	SH	-30 ~ -90	-	2-D 12-box	1900-2015	SIO-05	(Trudinger et al., 2016)

Table S1h. Collected data used for PFC-116

Data	Network	Station	Latitude °N	Longitude °E	Instrument	Data availability	Scale	Reference
NH								
<i>In situ</i>	AGAGE	Mace Head	53.3	-9.9	Medusa	2003.11-2017.09	SIO-07	(Prinn et al., 2018a; Prinn et al., 2018b)
<i>In situ</i>	AGAGE	Trinidad Head	41	-124.1	Medusa	2005.05-2017.09	SIO-07	(Prinn et al., 2018a; Prinn et al., 2018b)
Model	AGAGE	NH	30-90	-	2-D 12-box	1900-2015	SIO-07	(Trudinger et al., 2016)
SH								
<i>In situ</i>	AGAGE	Cape Grim	-40.7	144.7	Medusa	2004.04-2017.09	SIO-07	(Prinn et al., 2018a; Prinn et al., 2018b)
Model	AGAGE	SH	-30 ~ -90	-	2-D 12-box	1900-2015	SIO-07	(Trudinger et al., 2016)

Table S3. Ostwald solubility function of PFC-14 in seawater estimated by the method I

Compound	a_1	a_2	a_3	c_1	c_2	c_3	T_{\min} (K)	T_{\max} (K)	L_0 at 1 atm, 25 °C (L L ⁻¹)	L at 1 atm, 25 °C, 35.0 ‰ (L L ⁻¹)
PFC-14	-113.822	162.669	49.422	$6.60 \cdot 10^{-5}$	0.00334	0.2131	273.15	328.15	0.00513	0.004027
$\ln L = \left[a_1 + a_2 \cdot \left(\frac{100}{T} \right) + a_3 \cdot \ln \left(\frac{T}{100} \right) \right] \times \exp \left[- (c_1 (T - 273.15)^2 + c_2 (T - 273.15) + c_3) \times \frac{0.03600}{1.80655} \times S \times \rho(T, S) \right]$										

Table S4. Comparison among the calculated Ostwald solubility coefficients (L_0 , L , L^{-1}) by the poly-parameter linear free energy relationships (pp-LFERs) based on V_c and $\log L^{16}$, observed ones and calculated ones by the Clark-Glew-Weiss (CGW) model fit of target compounds and CFC-12 in the water at 298.15 K and 310.15 K

Species	T (K)	Calculated $\log L_{0,V}$ by the pp-LFERs ^a	Calculated $L_{0,V}$ by the pp-LFERs ^a	Calculated $\log L_{0,V_c}$ by the pp-LFERs ^b	Calculated L_{0,V_c} by the pp-LFERs ^b	Calculated $\log L_{0,L^{16}}$ by the pp-LFERs ^c	Calculated $L_{0,L^{16}}$ by the pp-LFERs ^c	Observed $\log L_{0,d}$	Observed $L_{0,d}$	Calculated $L_{0,d}$ by the CGW fit ^e
HCFC-22	298.2	-0.017	0.961	-0.052	0.888	-0.025	0.944	-0.091	0.811	0.844
HCFC-141b	298.2	-0.136	0.731	-0.154	0.702	-0.152	0.705	-0.148	0.711	0.711
HCFC-142b	298.2	-0.405	0.394	-0.44	0.363	-0.405	0.394	-0.449	0.356	0.352
HFC-134a	298.2	-0.326	0.472	-0.407	0.392	-0.326	0.472	-0.408	0.391	0.381
HFC-125	298.2	-1.003	0.099	-1.13	0.074	-0.989	0.103	-1.059	0.087	0.086
HFC-23	298.2	-0.453	0.352	-0.505	0.313	-0.469	0.34	-0.51	0.309	0.313
PFC-14	298.2	-2.241	0.00574	-2.296	0.00505	-0.25	0.00562	-2.306	0.00494	0.00513
PFC-116	298.2	-2.658	0.0022	-2.763	0.00173	-2.716	-	-	-	0.00143
CFC-12	298.2	-1.12	0.076	-1.155	0.07	-1.145	0.072	-1.129	0.074	0.069
HCFC-22	310.2	-0.161	0.691	-0.203	0.626	-0.21	0.617	-	-	0.598
HCFC-141b	310.2	-0.306	0.494	-0.327	0.471	-0.348	0.449	-0.336	0.461	0.484
HCFC-142b	310.2	-0.571	0.269	-0.614	0.243	-0.591	0.256	-0.605	0.248	0.246
HFC-134a	310.2	-0.563	0.274	-0.621	0.239	-0.636	0.231	-0.547	0.284	0.269
HFC-125	310.2	-1.208	0.062	-1.339	0.046	-0.241	0.057	-1.203	0.063	0.062
HFC-23	310.2	-0.618	0.241	-0.683	0.208	-0.685	0.207	-0.622	0.239	0.225
PFC-14	310.2	-2.31	0.0049	-2.382	0.00415	-2.413	0.00386	-2.386	0.00411	0.00437
PFC-116	310.2	-2.755	0.00176	-2.883	0.00131	-2.851	-	-	-	0.0011
CFC-12	310.2	-1.213	0.061	-1.256	0.055	-1.257	0.055	-1.275	0.053	0.048

- ^a Calculated $\log L_0$, V and L_0 , V are calculated by the pp-LFERS, which are obtained from Table 6,7,9,12-15 in Abraham et al. (2001) and Table 2 in Abraham et al. (2012)
- ^b Calculated $\log L_0$, V_c and L_0 , V_c are calculated by the pp-LFERS based on the V_c
- ^c Calculated $\log L_0$, L^{16} and L_0 , L^{16} are calculated by the pp-LFERS, which are obtained from Table 6,7,9,12-15 in Abraham et al. (2001) and Table 2 in Abraham et al. (2012)
- ^d Observed $\log L_0$ and L_0 are measured by experiments, which are also obtained from Table 6,7,9,12-15 in Abraham et al. (2001) and Table 2 in Abraham et al. (2012)
- ^e Calculated L_0 by the CGW fit is calculated based on the combined method for water solubility

Table S5. Ostwald solubility functions of target compounds and CFC-12 in seawater estimated by the (revised) method II at 298.15 K and 310.15 K

Species	Chemical Formula	T (K)	c	e	s	a	b	v	K_s	L_0 at 1 atm, 25 °C (L.L ⁻¹)	L at 1 atm, 25 °C, 35.0‰ (L.L ⁻¹)
HCFC-22	CHClF ₂	298.2	-0.99	0.58	2.55	3.81	4.84	-0.87	0.169 ± 0.022	0.888	0.703
HCFC-141b	C ₂ H ₃ Cl ₂ F	298.2	-0.99	0.58	2.55	3.81	4.84	-0.87	0.204 ± 0.023	0.702	0.53
HCFC-142b	C ₂ H ₃ ClF ₂	298.2	-0.99	0.58	2.55	3.81	4.84	-0.87	0.198 ± 0.022	0.363	0.277
HFC-134a	CH ₂ FCF ₃	298.2	-0.99	0.58	2.55	3.81	4.84	-0.87	0.193 ± 0.022	0.392	0.3
HFC-125	C ₃ HF ₅	298.2	-0.99	0.58	2.55	3.81	4.84	-0.87	0.224 ± 0.021	0.091	0.067
HFC-23	CHF ₃	298.2	-0.99	0.58	2.55	3.81	4.84	-0.87	0.168 ± 0.021	0.313	0.248
PFC-14	CF ₄	298.2	-0.99	0.58	2.55	3.81	4.84	-0.87	0.202 ± 0.022	0.00505	0.00382
PFC-116	C ₃ F ₆	298.2	-0.99	0.58	2.55	3.81	4.84	-0.87	0.244 ± 0.022	0.00173	0.00123
CFC-12	CCl ₂ F ₂	298.2	-0.99	0.58	2.55	3.81	4.84	-0.87	0.204 ± 0.021	0.07	0.053
HCFC-22	CHClF ₂	310.2	-0.97	0.7	2.41	3.39	4.58	-1.07	0.169 ± 0.022	0.626	0.53
HCFC-141b	C ₂ H ₃ Cl ₂ F	310.2	-0.97	0.7	2.41	3.39	4.58	-1.07	0.204 ± 0.023	0.471	0.385
HCFC-142b	C ₂ H ₃ ClF ₂	310.2	-0.97	0.7	2.41	3.39	4.58	-1.07	0.198 ± 0.022	0.243	0.2
HFC-134a	CH ₂ FCF ₃	310.2	-0.97	0.7	2.41	3.39	4.58	-1.07	0.193 ± 0.022	0.239	0.198
HFC-125	C ₃ HF ₅	310.2	-0.97	0.7	2.41	3.39	4.58	-1.07	0.224 ± 0.021	0.059	0.047
HFC-23	CHF ₃	310.2	-0.97	0.7	2.41	3.39	4.58	-1.07	0.168 ± 0.021	0.208	0.176
PFC-14	CF ₄	310.2	-0.97	0.7	2.41	3.39	4.58	-1.07	0.202 ± 0.022	0.00415	0.0034
PFC-116	C ₃ F ₆	310.2	-0.97	0.7	2.41	3.39	4.58	-1.07	0.244 ± 0.022	0.00131	0.00103
CFC-12	CCl ₂ F ₂	310.2	-0.97	0.7	2.41	3.39	4.58	-1.07	0.204 ± 0.021	0.055	0.045

$$L = 10^{\left[-K_s \cdot \frac{s}{M_{NaCl}} + c + eE + sS + aA + bB + vV_c \right]}, \quad (V \text{ for HFC-125, } V_c \text{ for other compounds})$$

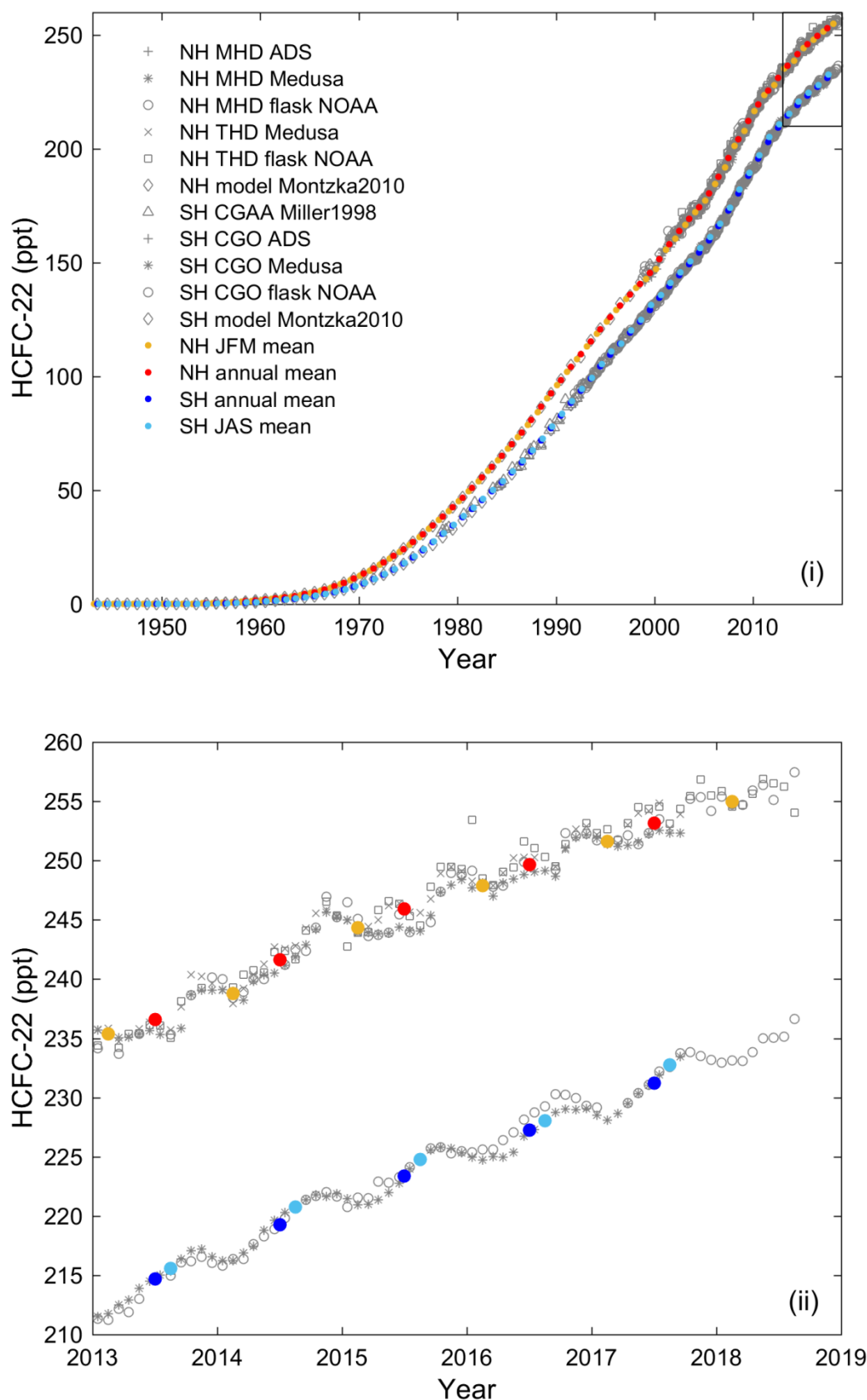


Figure S1a. HCFC-22: Atmospheric mole fractions in the NH and SH based on collected data (Table S2a) in the range of (i) 1943-2019; (ii) 2013-2019. Fig. (ii) is the enlarged figure of the square in Fig. (i).

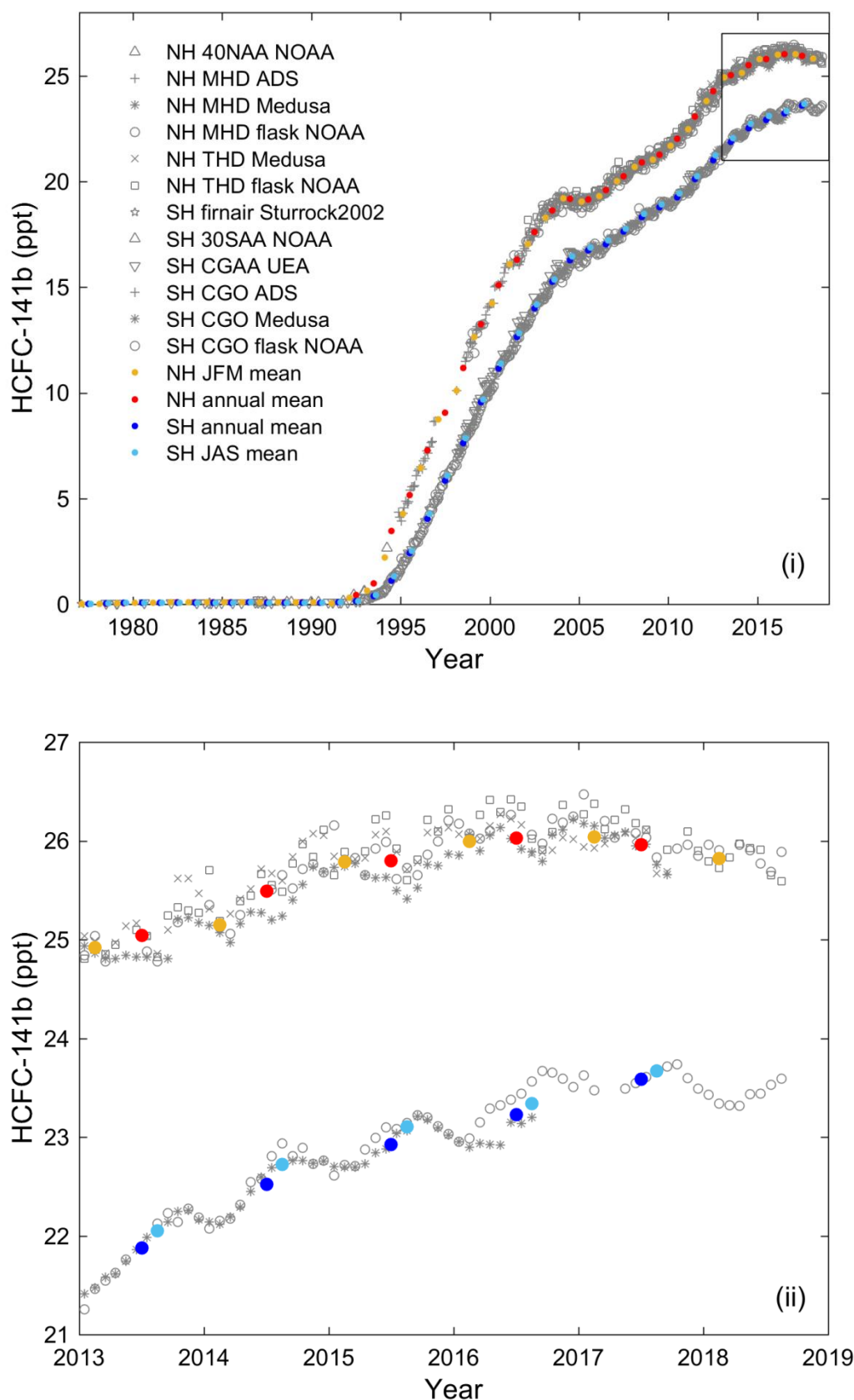


Figure S1b. HCFC-141b: Atmospheric mole fractions in the NH and SH based on collected data (Table S2b) in the range of (i) 1977-2019; (ii) 2013-2019. Fig. (ii) is the enlarged figure of the square in Fig. (i).

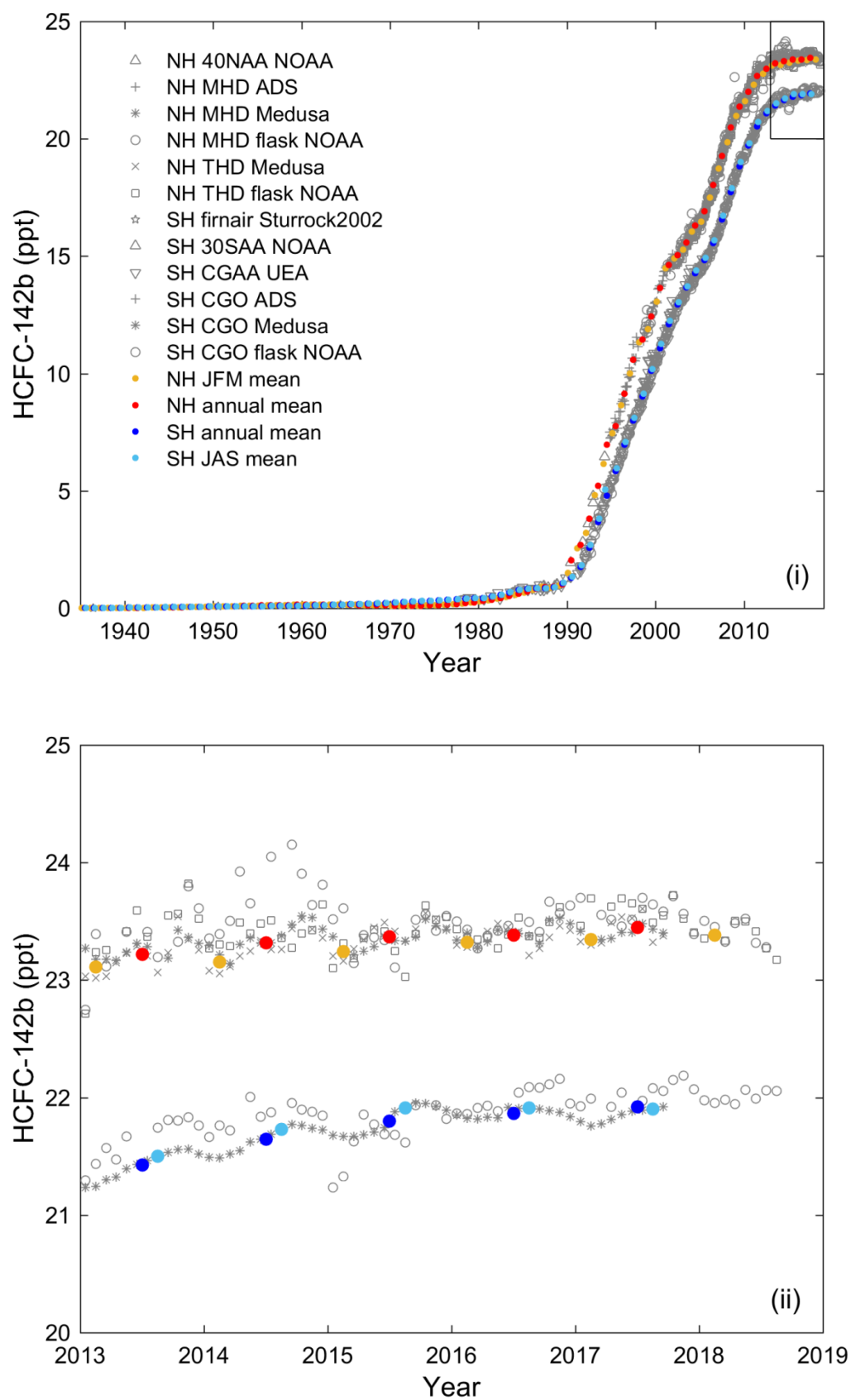


Figure S1c. HCFC-142b: Atmospheric mole fractions in the NH and SH based on collected data (Table S2c) in the range of (i) 1935-2019; (ii) 2013-2019. Fig. (ii) is the enlarged figure of the square in Fig. (i).

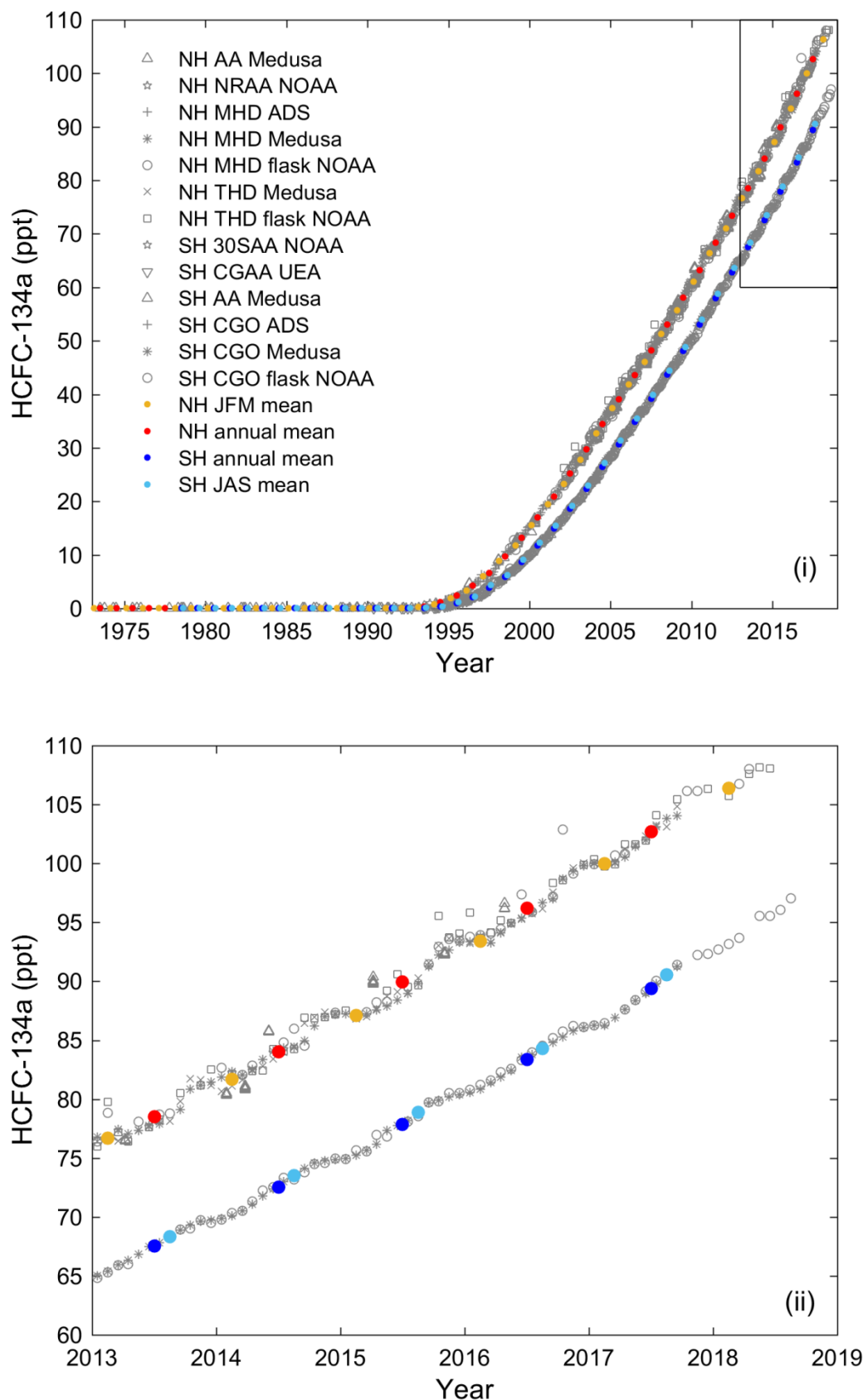


Figure S1d. HFC-134a: Atmospheric mole fractions in the NH and SH based on collected data (Table S2d) in the range of (i) 1973-2019; (ii) 2013-2019. Fig. (ii) is the enlarged figure of the square in Fig. (i).

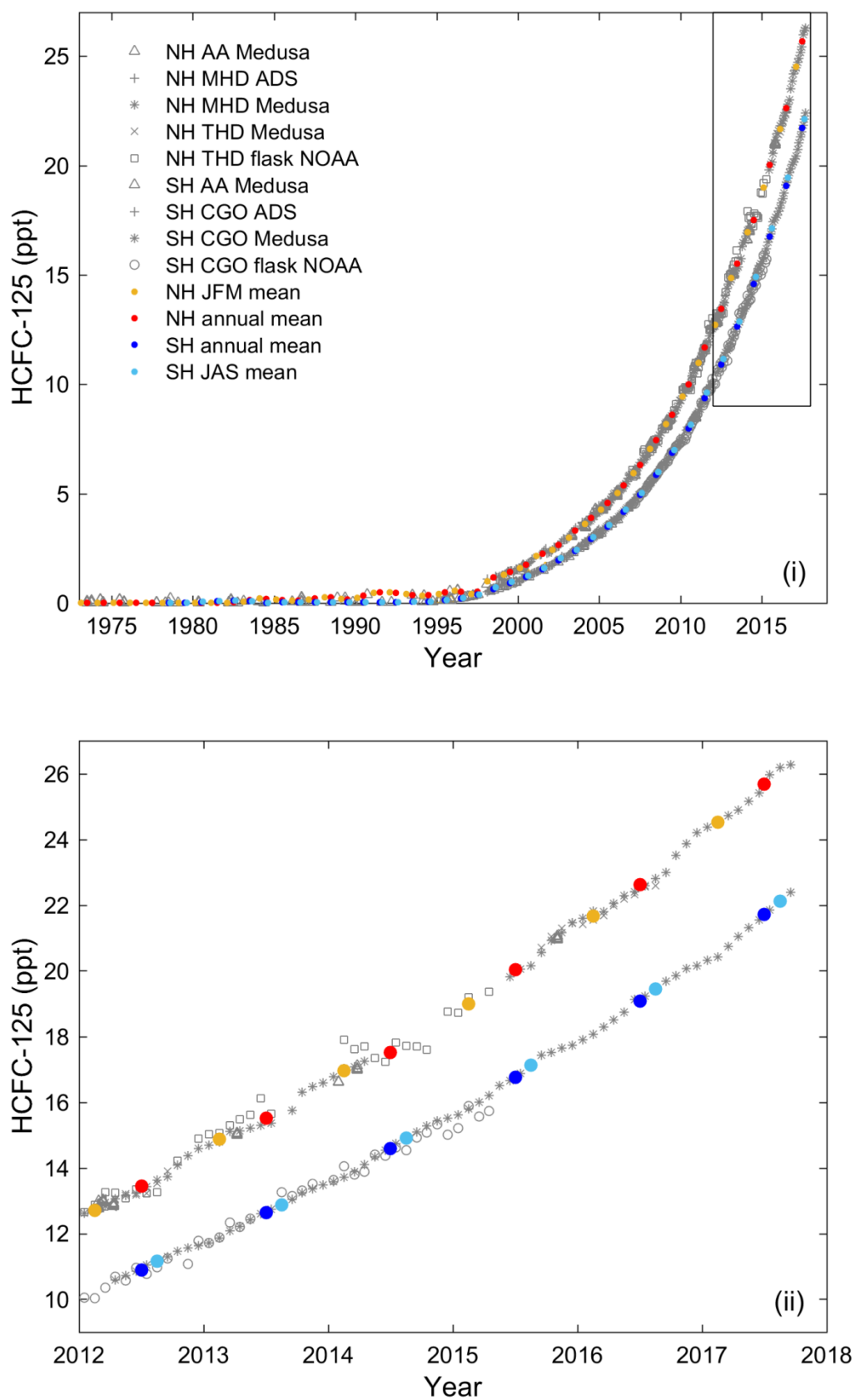


Figure S1e. HFC-125: Atmospheric mole fractions in the NH and SH based on collected data (Table S2e) in the range of (i) 1973-2018; (ii) 2012-2018. Fig. (ii) is the enlarged figure of the square in Fig. (i).

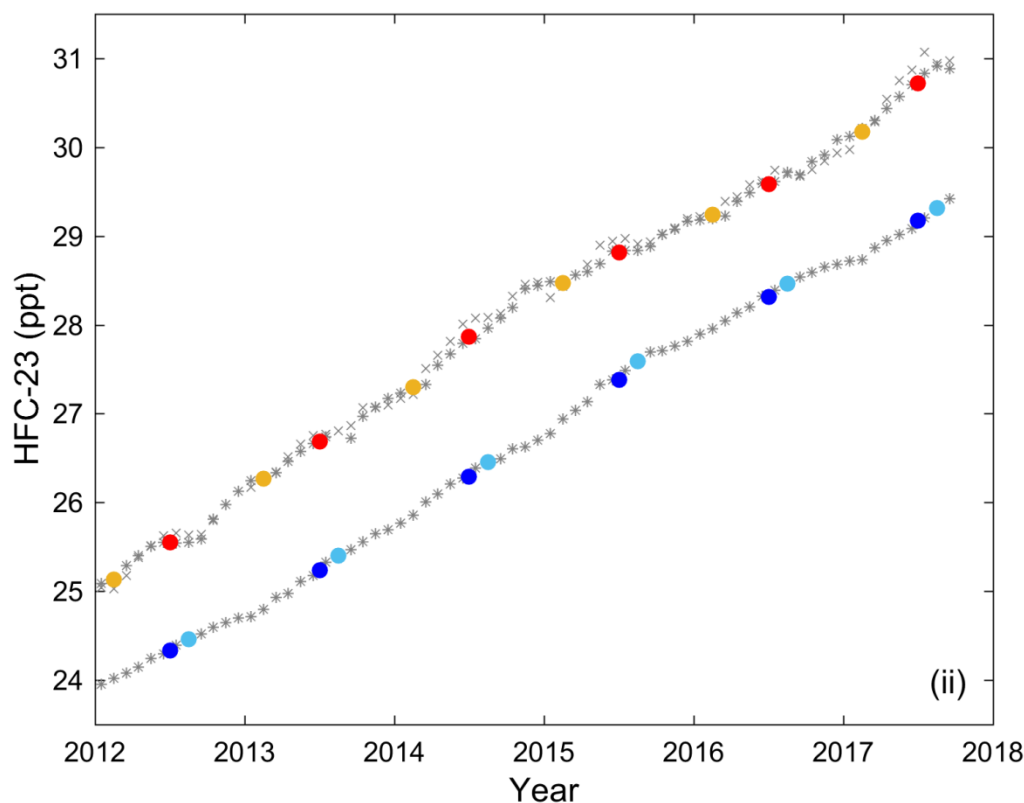
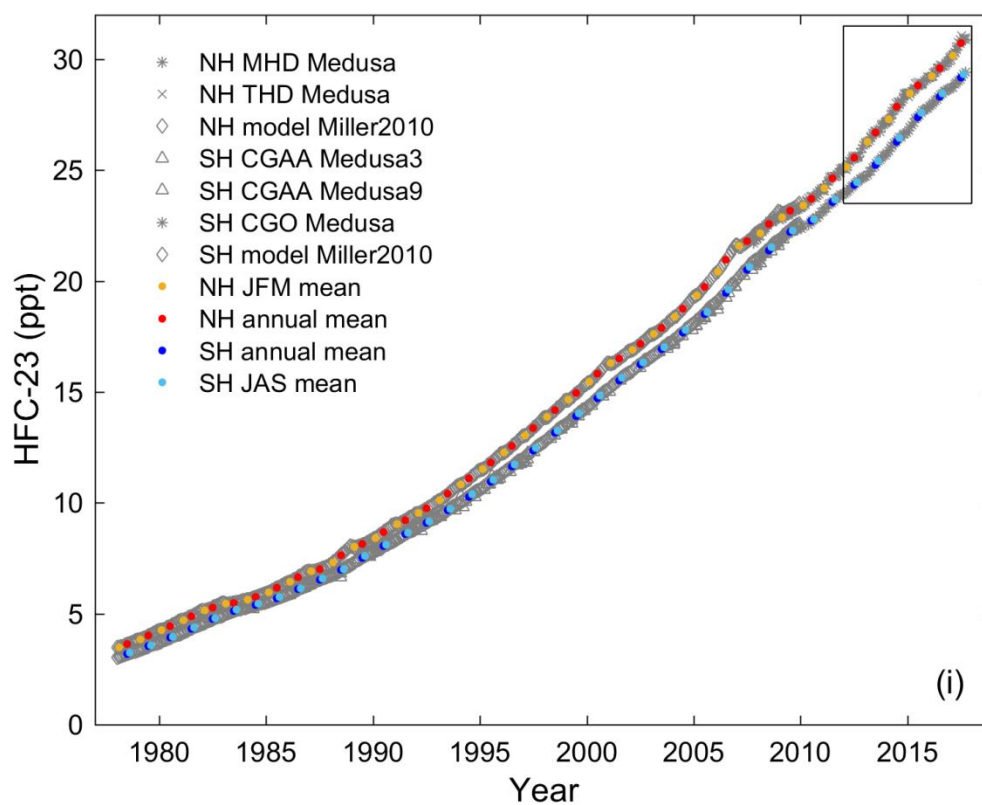


Figure S1f. HFC-23: Atmospheric mole fractions in the NH and SH based on collected data (Table S2f) in the range of (i) 1978-2018; (ii) 2012-2018. Fig. (ii) is the enlarged figure of the square in Fig. (i).

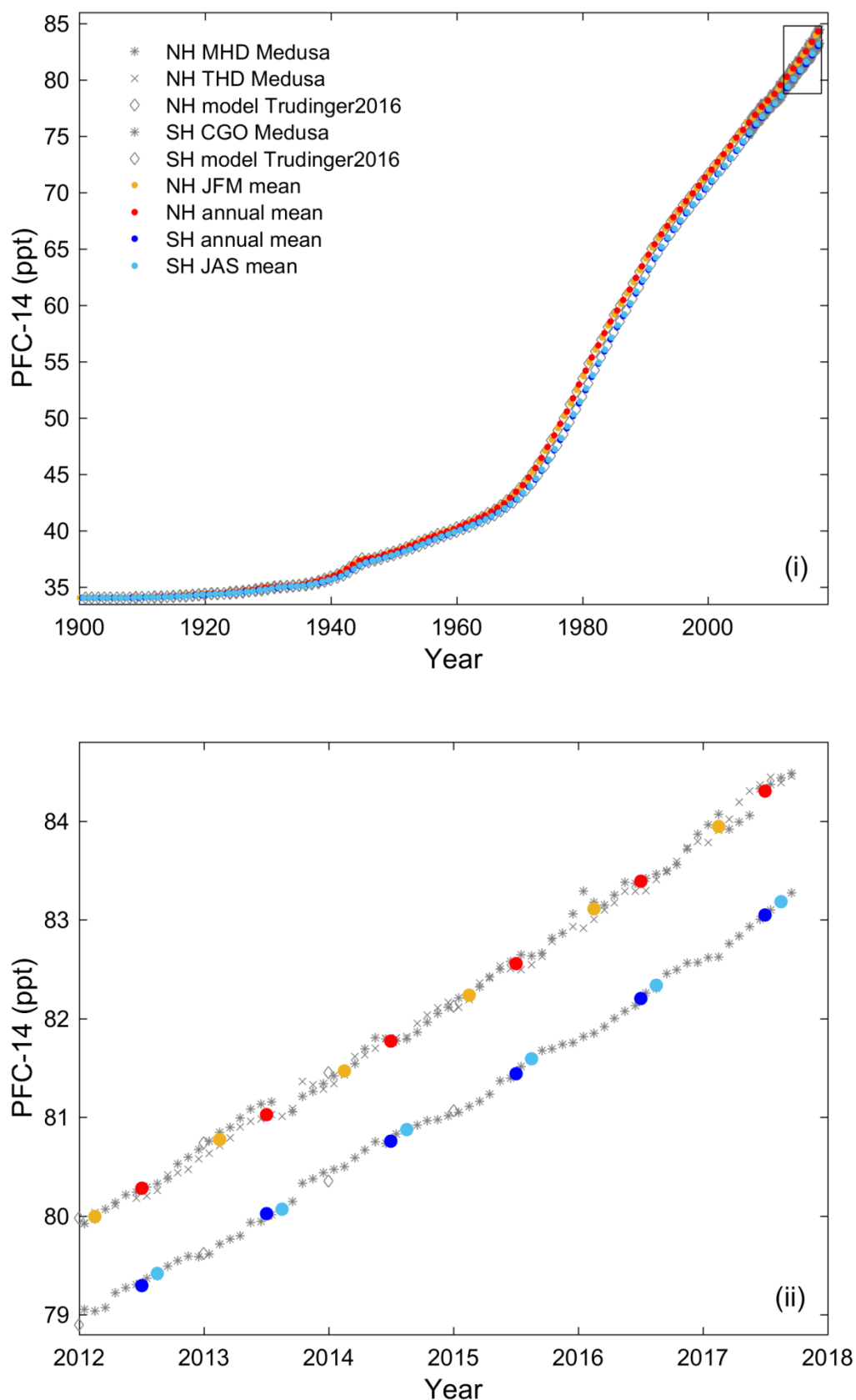


Figure S1g. PFC-14: Atmospheric mole fractions in the NH and SH based on collected data (Table S2g) in the range of (i) 1900-2018; (ii) 2012-2018. Fig. (ii) is the enlarged figure of the square in Fig. (i).

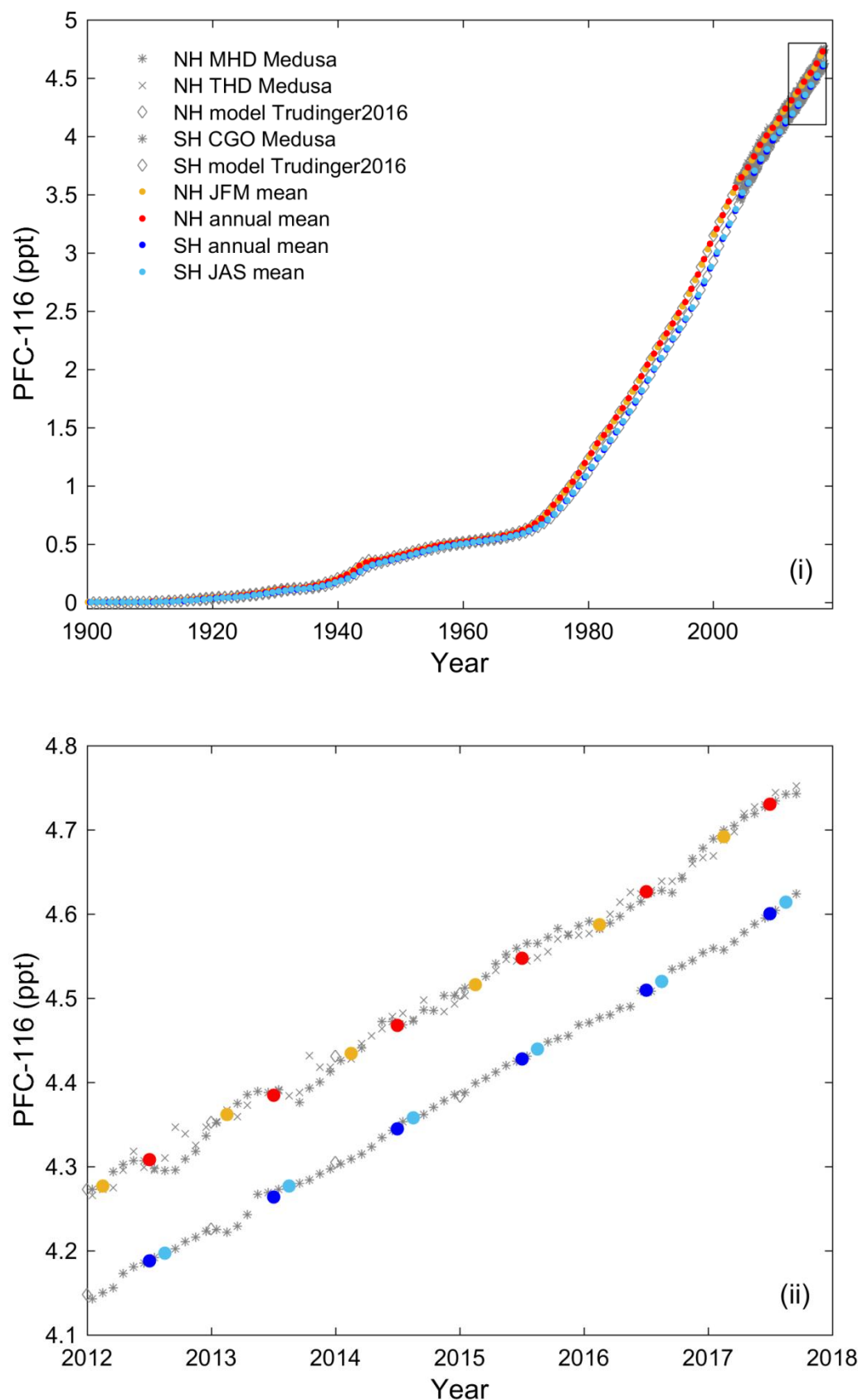


Figure S1h. PFC-116: Atmospheric mole fractions in the NH and SH based on collected data (Table S2h) in the range of (i) 1900-2018; (ii) 2012-2018. Fig. (ii) is the enlarged figure of the square in Fig. (i).

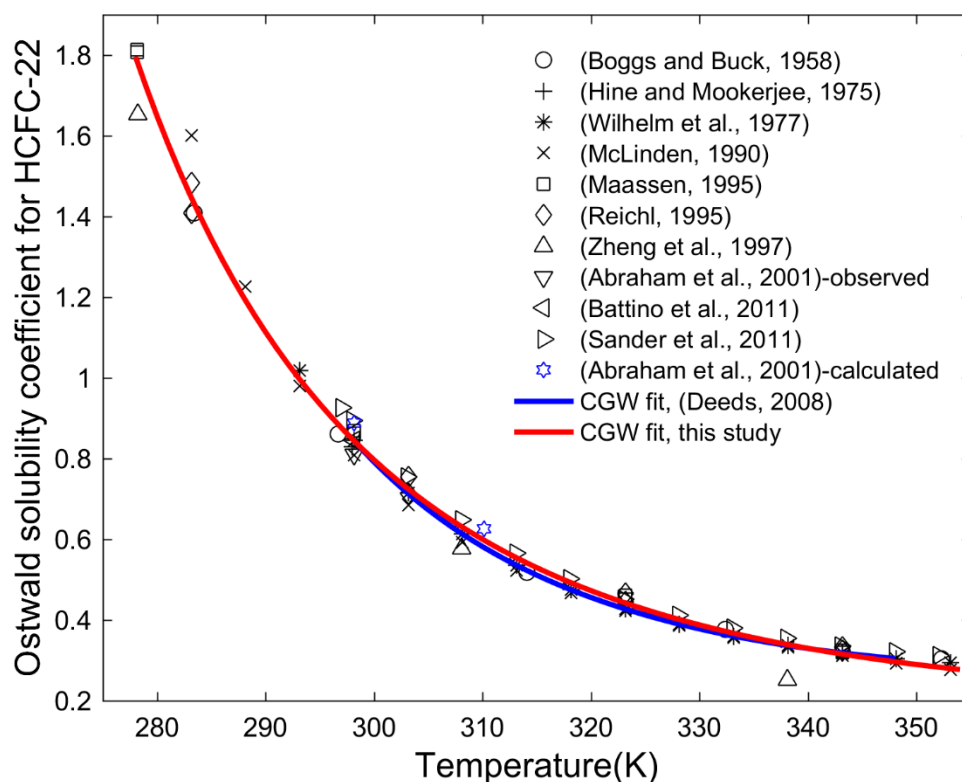


Figure S2a. HCFC-22 freshwater solubility (Ostwald solubility coefficients) as a function of temperature based on previous studies (Abraham et al., 2001; Battino et al., 2011; Boggs and Buck Jr, 1958; Hine and Mookerjee, 1975; Maaßen, 1995; McLinden, 1990; Reichl, 1996; Sander et al., 2011; Wilhelm et al., 1977; Zheng et al., 1997). The Clarke-Glew-Weiss (CGW) model is used to fit the data (black markers) and compared with the results from Deeds (2008) and from (Abraham et al., 2001)-calculated (blue Hexagram, calculated by the revised method II). The CGW fit in this study agrees to within 4.0 % with two-thirds of the data.

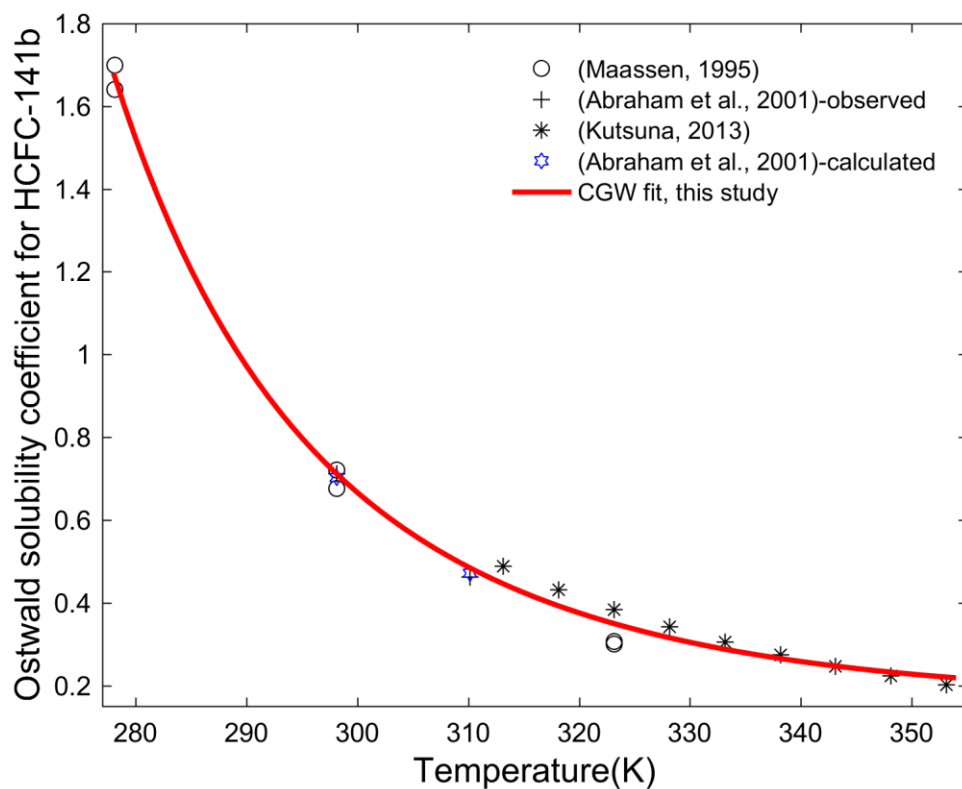


Figure S2b. HCFC-141b freshwater solubility (Ostwald solubility coefficients) as a function of temperature based on previous studies (Abraham et al., 2001; Kutsuna, 2013; Maaßen, 1995). The Clarke-Glew-Weiss (CGW) model is used to fit the data (black markers) and compared with the results from (Abraham et al., 2001)-calculated (blue Hexagram, calculated by the revised method II). The CGW fit in this study agrees to within 7.8 % with two-thirds of the data.

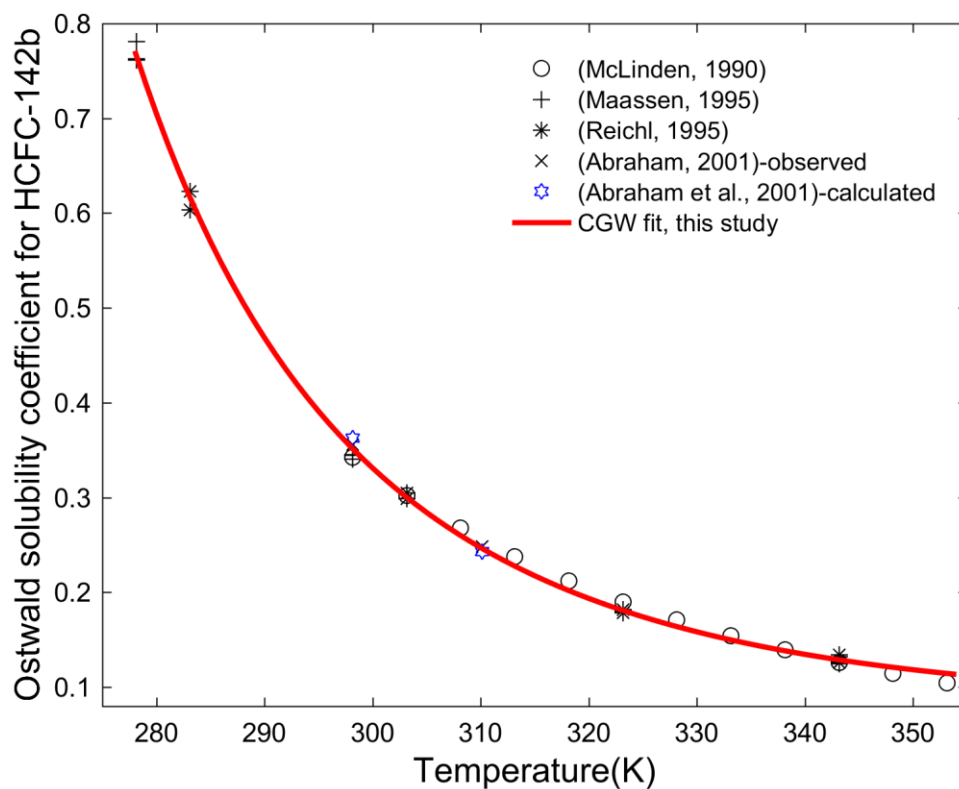


Figure S2c. HCFC-142b freshwater solubility (Ostwald solubility coefficients) as a function of temperature based on previous studies (Abraham et al., 2001; Maassen, 1995; McLinden, 1990; Reichl, 1996). The Clarke-Glew-Weiss (CGW) model is used to fit the data (black markers) and compared with the results from (Abraham et al., 2001)-calculated (blue Hexagram, calculated by the revised method II). The CGW fit in this study agrees to within 2.5 % with two-thirds of the data.

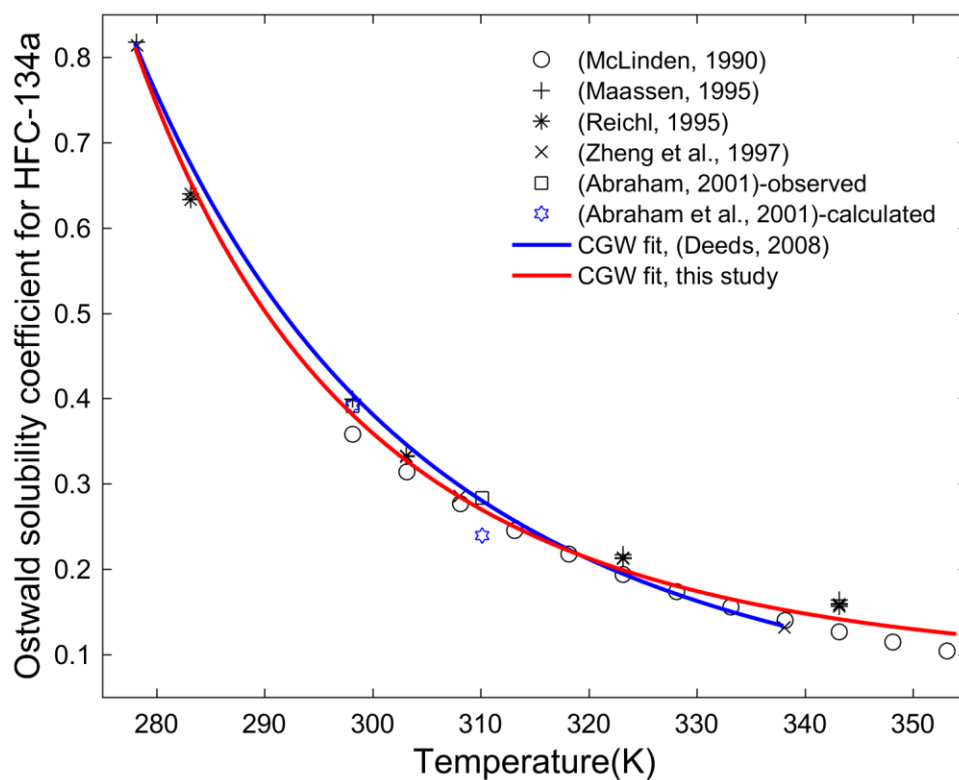


Figure S2d. HFC-134a freshwater solubility (Ostwald solubility coefficients) as a function of temperature based on previous studies (Abraham et al., 2001; Maaßen, 1995; McLinden, 1990; Reichl, 1996; Zheng et al., 1997). The Clarke-Glew-Weiss (CGW) model is used to fit the data (black markers) and compared with the results from Deeds (2008) and from (Abraham et al., 2001)-calculated (blue Hexagram, calculated by the revised method II). The CGW fit in this study agrees to within 6.8 % with two-thirds of the data.

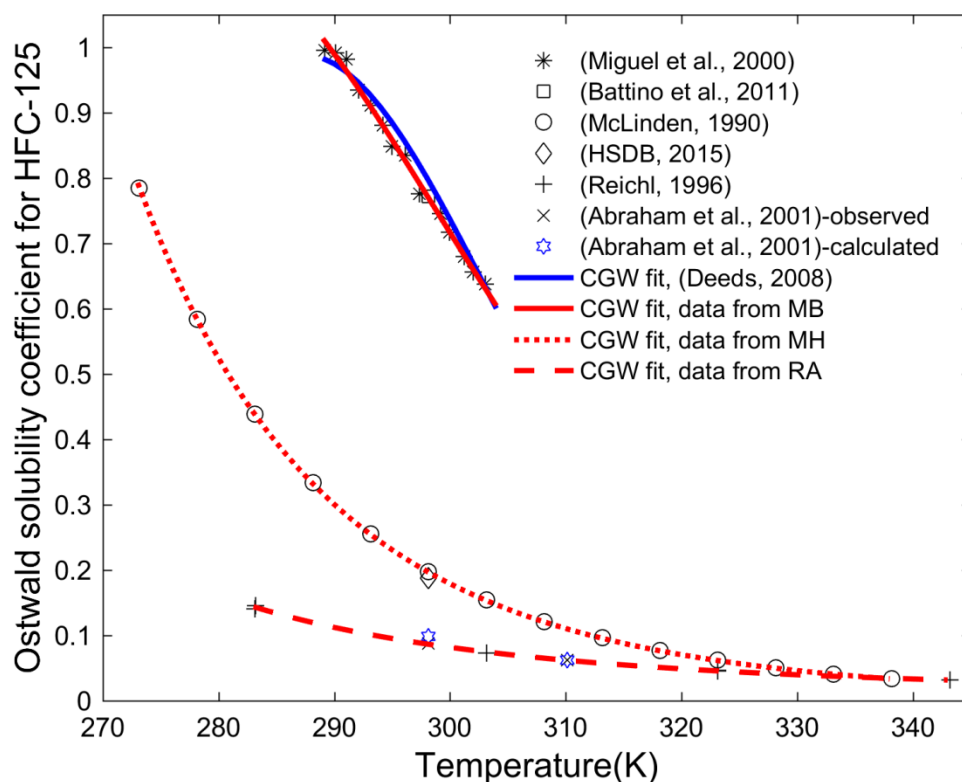


Figure S2e. HFC-125 freshwater solubility (Ostwald solubility coefficients) as a function of temperature based on previous studies (Abraham et al., 2001; Battino et al., 2011; HSDB, 2015; McLinden, 1990; Miguel et al., 2000; Reichl, 1996). The Clarke-Glew-Weiss (CGW) model is used to fit the data (black markers) and compared with the results from Deeds (2008) and from Abraham et al. (2001)-calculated (blue Hexagram, calculated by the method II based on Eq. (12)). The CGW fit in this study agrees to within 2.1 % with all data. Unfortunately, the data from previous studies are not described by one CGW fit, but by three. Curve 1 is the upper and red solid line fitted the data (Battino et al., 2011; Miguel et al., 2000) in the temperature range of 289.15-303.15 K. This fit agrees to within 1.0 % with 2/3 data. Curve 2 is the middle and red dotted line fitted the data (HSDB, 2015; McLinden, 1990) from 273.15 K to 338.15 K. This fit agrees to within 0.75 % with 2/3 data. Curve 3 is the bottom and red dashed line fitted the data (Abraham et al., 2001; Reichl, 1996) in the temperature range of 283.15-343.15 K. This fit agrees to within 3.3 % with two-thirds of the data. The discrepancy of the three fits is discussed in the text.

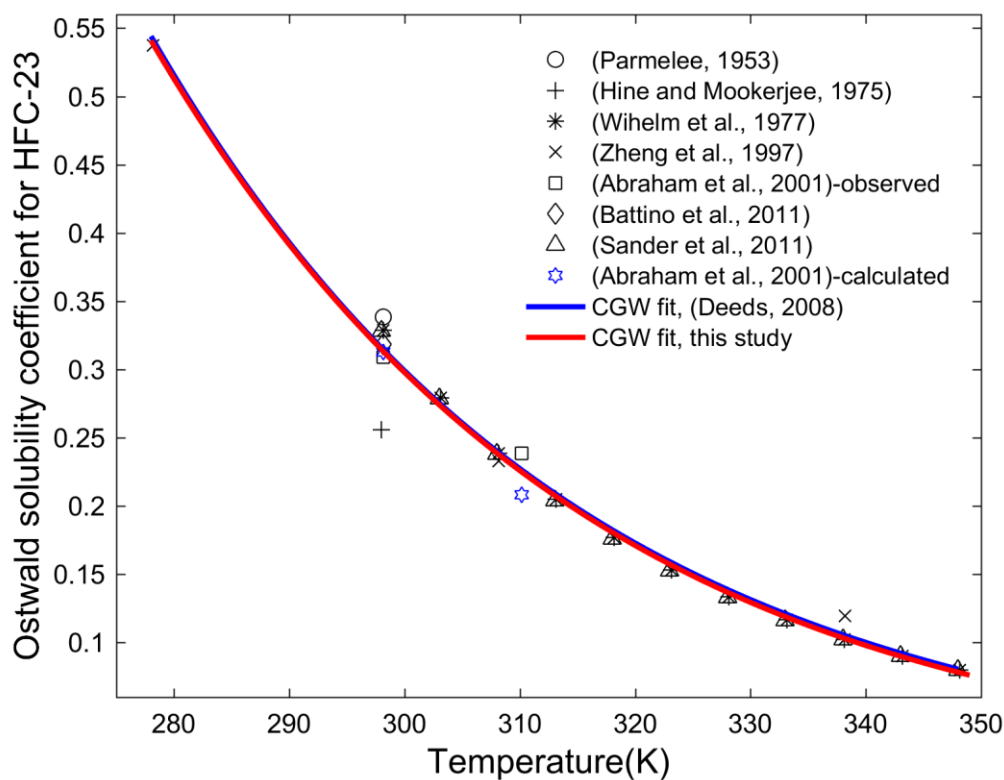


Figure S2f. HFC-23 freshwater solubility (Ostwald solubility coefficients) as a function of temperature based on previous studies (Abraham et al., 2001; Battino et al., 2011; Hine and Mookerjee, 1975; Parmelee, 1953; Sander et al., 2011; Wilhelm et al., 1977; Zheng et al., 1997). The Clarke-Glew-Weiss (CGW) model is used to fit the data (black markers) and compared with the results from Deeds (2008) and from (Abraham et al., 2001)-calculated (blue Hexagram, calculated by the revised method II). The CGW fit in this study agrees to within 2.3 % with two-thirds of the data.

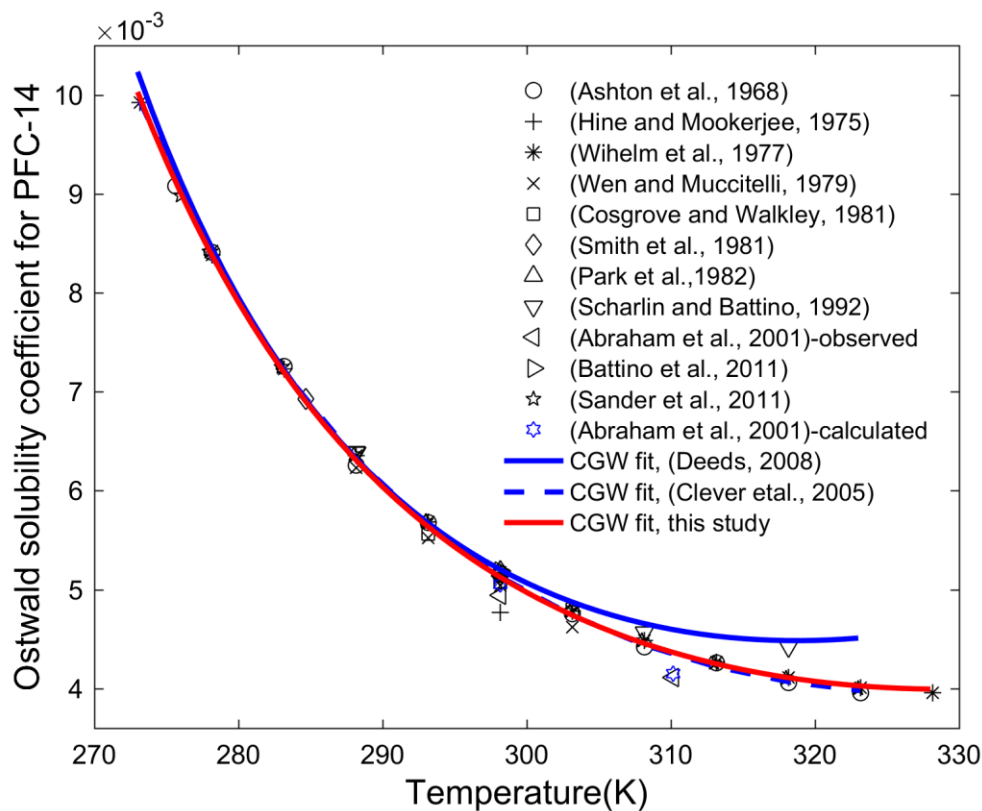


Figure S2g. PFC-14 freshwater solubility (Ostwald solubility coefficients) as a function of temperature based on previous studies (Smith et al., 1981; Park et al., 1982; Scharlin and Battino, 1992; Abraham et al., 2001; Battino et al., 2011; Sander et al., 2011). The Clarke-Glew-Weiss (CGW) model is used to fit the data (black markers) and compared with the results from Deeds (2008), from Clever et al. (2005) and from (Abraham et al., 2001)-calculated (blue Hexagram, calculated by the revised method II). The CGW fit in this study agrees to within 0.95 % with two-thirds of the data.

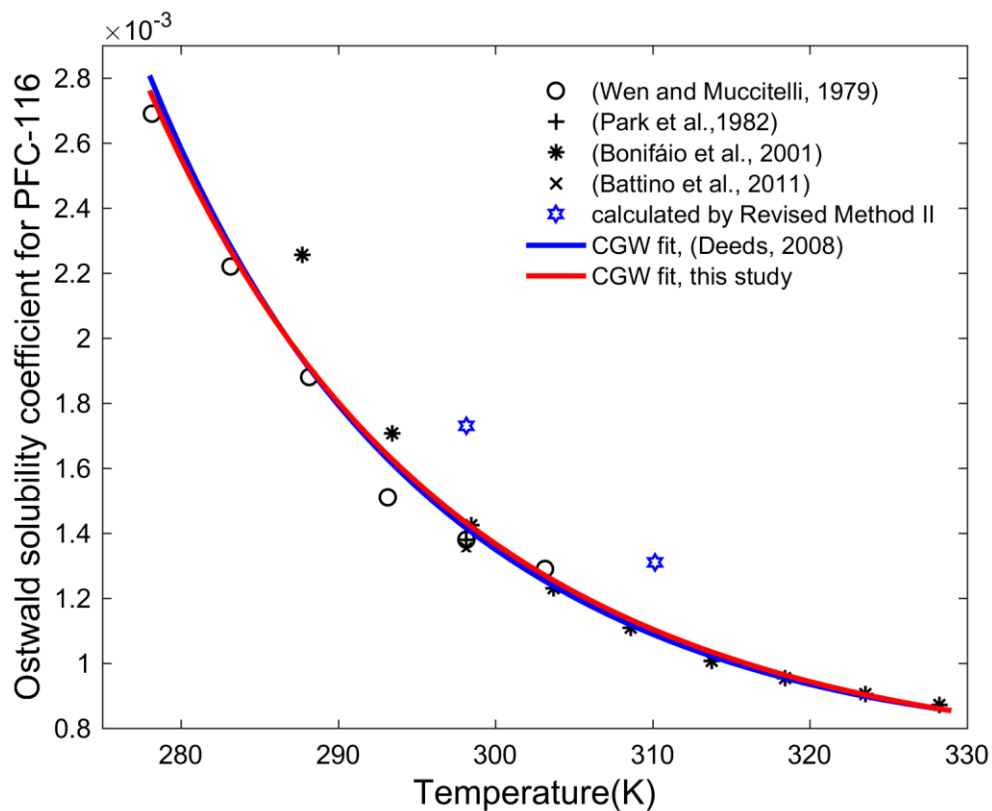


Figure S2h. PFC-116 freshwater solubility (Ostwald solubility coefficients) as a function of temperature based on previous studies (Battino et al., 2011; Bonifácio et al., 2001; Park et al., 1982; Wen and Muccitelli, 1979). The Clarke-Glew-Weiss (CGW) model is used to fit the data (black markers) and compared with the fit results from Deeds (2008) and from the data calculated by the revised method II (blue Hexagram). The CGW fit in this study agrees to within 3.5 % with two-thirds of the data.

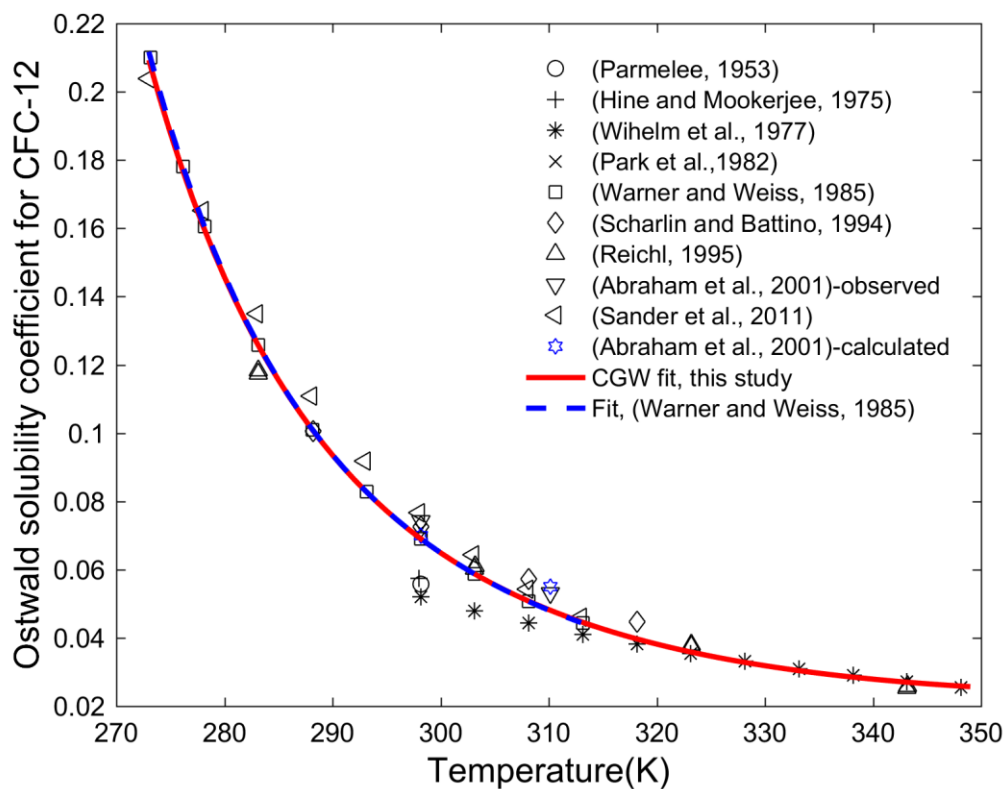


Figure S2i. CFC-12 freshwater solubility (Ostwald solubility coefficients) as a function of temperature based on previous studies (Abraham et al., 2001; Hine and Mookerjee, 1975; Park et al., 1982; Parmelee, 1953; Reichl, 1996; Sander et al., 2011; Scharlin and Battino, 1994; Warner and Weiss, 1985; Wilhelm et al., 1977). The Clarke-Glew-Weiss (CGW) model is used to fit the data (black markers) and compared with the fit results from Warner and Weiss (1985) and the data from (Abraham et al., 2001)-calculated (blue Hexagram, calculated by the revised method II). The CGW fit in this study agrees to within 6.6 % with two-thirds of the data.

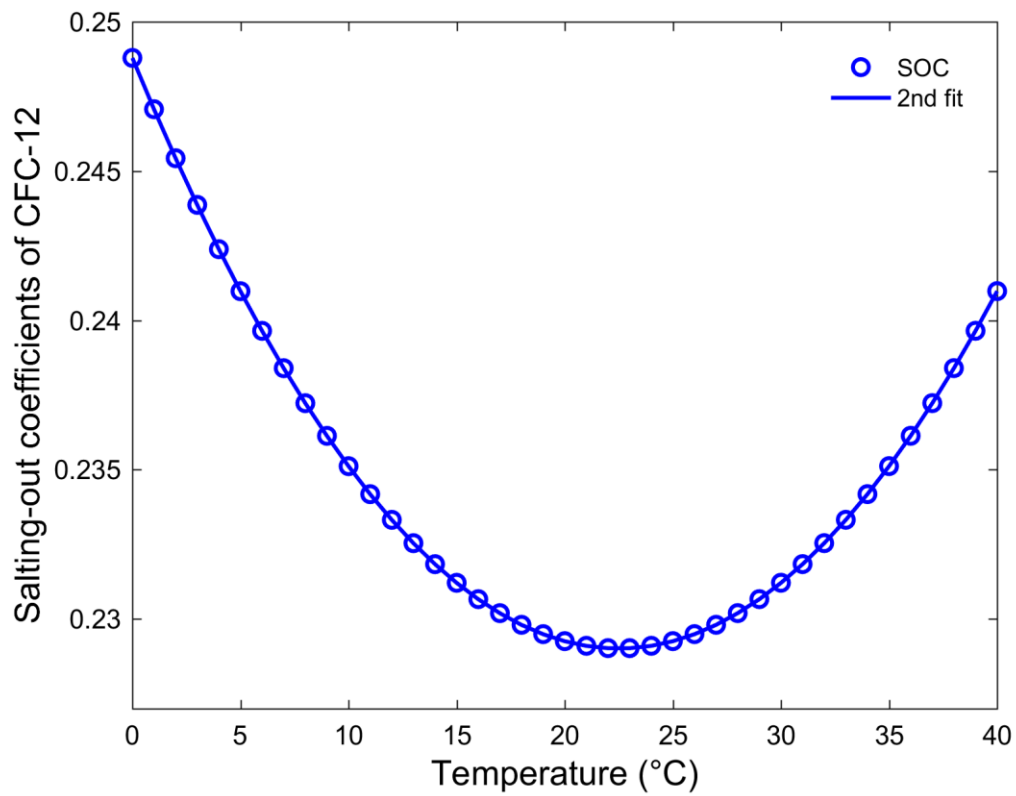


Figure S3. The relationship between salting-out coefficients (SOC) and temperature for CFC-12 calculated by Eq. (16) based on the data from Warner and Weiss (1985).

References

- Abraham, M. H., Gil-Lostes, J., Corr, S., and Acree, W. E.: Determination of partition coefficients of refrigerants by gas liquid chromatographic headspace analysis, *J. Chromatogr. A*, 1265, 144–148, <https://doi.org/10.1016/j.chroma.2012.09.085>, 2012.
- Abraham, M. H., Gola, J. M., Cometto-Muñiz, J. E., and Cain, W. S.: Solvation properties of refrigerants, and the estimation of their water-solvent and gas-solvent partitions, *Fluid Phase Equilib.*, 180, 41–58, [https://doi.org/10.1016/S0378-3812\(00\)00511-2](https://doi.org/10.1016/S0378-3812(00)00511-2), 2001.
- Battino, R., Seybold, P. G., and Campanell, F. C.: Correlations Involving the Solubility of Gases in Water at 298.15 K and 101325 Pa, *J. Chem. Eng. Data*, 56, 727–732, <https://doi.org/10.1021/je101070h>, 2011.
- Boggs, J. E. and Buck Jr, A. E.: The solubility of some chloromethanes in water, *J. Phys. Chem.*, 62, 1459–1461, <https://doi.org/10.1021/j150569a031>, 1958.
- Bonifácio, R. P., Pádua, A. A. H., and Costa Gomes, M. F.: Perfluoroalkanes in water: Experimental Henry's law coefficients for hexafluoroethane and computer simulations for tetrafluoromethane and hexafluoroethane, *J. Phys. Chem. B*, 105, 8403–8409, <https://doi.org/10.1021/jp010597k>, 2001.
- Clever, H. L., Battino, R., Clever, H. L., Jaselskis, B., Clever, H. L., Yampol'skii, Y. P., Jaselskis, B., Scharlin, P., and Young, C. L.: IUPAC-NIST Solubility Data Series. 80. Gaseous Fluorides of Boron, Nitrogen, Sulfur, Carbon, and Silicon and Solid Xenon Fluorides in all Solvents, *J. Phys. Chem. Ref. Data*, 34, 201–438, <https://doi.org/10.1063/1.1794762>, 2005.
- Deeds, D. A.: The Natural Geochemistry of Tetrafluoromethane and Sulfur Hexafluoride : Studies of Ancient Mojave Desert Groundwaters, North Pacific Seawaters and the Summit Emissions of Kilauea Volcano, PhD thesis, 2008.
- Hine, J. and Mookerjee, P. K.: Structural effects on rates and equilibria. XIX. Intrinsic hydrophilic character of organic compounds. Correlations in terms of structural contributions, *J. Org. Chem.*, 40, 292–298, <https://doi.org/10.1021/jo00891a006>, 1975.
- HSDB: available at: <http://toxnet.nlm.nih.gov/newtoxnet/hsdb.htm>, last access: 10 April 2019 2015.
- Hutchinson, M. F. and De Hoog, F.: Smoothing noisy data with spline functions, *Numer. Math.*, 47, 99–106, <https://doi.org/10.1007/BF01404567>, 1985.
- Kutsuna, S.: Determination of Rate Constants for Aqueous Reactions of HCFC-123 and HCFC-225ca with OH- Along with Henry's Law Constants of Several HCFCs, *Int. J. Chem. Kinet.*, 45, 440–451, <https://doi.org/10.1002/kin.20780>, 2013.
- Maaßen, S.: Experimentelle Bestimmung und Korrelierung von Verteilungskoeffizienten in verdünnten Lösungen, PhD thesis, Shaker, 1995.
- McLinden, M. O.: Physical properties of alternatives to the fully halogenated chlorofluorocarbons, United States, 1–43 pp., 1990.

- Miguel, A. A. F., Ferreira, A. G. M., and Fonseca, I. M. A.: Solubilities of some new refrigerants in water, *Fluid Phase Equilib.*, 173, 97–107, [https://doi.org/10.1016/s0378-3812\(00\)00390-3](https://doi.org/10.1016/s0378-3812(00)00390-3), 2000.
- Miller, B. R., Huang, J., Weiss, R. F., Prinn, R. G., and Fraser, P. J.: Atmospheric trend and lifetime of chlorodifluoromethane (HCFC-22) and the global tropospheric OH concentration, *J. Geophys. Res.*, 103, 13237–13248, <https://doi.org/10.1029/98jd00771>, 1998.
- Miller, B. R., Rigby, M., Kuijpers, L. J. M., Krummel, P. B., Steele, L. P., Leist, M., Fraser, P. J., McCulloch, A., Harth, C., Salameh, P., Mühle, J., Weiss, R. F., Prinn, R. G., Wang, R. H. J., O'Doherty, S., Grealley, B. R., and Simmonds, P. G.: HFC-23 (CHF₃) emission trend response to HCFC-22 (CHClF₂) production and recent HFC-23 emission abatement measures, *Atmos. Chem. Phys.*, 10, 7875–7890, <https://doi.org/10.5194/acp-10-7875-2010>, 2010.
- Montzka, S. A., Butler, J. H., Myers, R. C., Thompson, T. M., Swanson, T. H., Clarke, A. D., Lock, L. T., and Elkins, J. W.: Decline in the tropospheric abundance of halogen from halocarbons: Implications for stratospheric ozone depletion, *Science*, 272, 1318–1322, <https://doi.org/10.1126/science.272.5266.1318>, 1996a.
- Montzka, S. A., Kuijpers, L., Battle, M. O., Aydin, M., Verhulst, K. R., Saltzman, E. S., and Fahey, D. W.: Recent increases in global HFC-23 emissions, *Geophys. Res. Lett.*, 37, L02808, <https://doi.org/10.1029/2009gl041195>, 2010.
- Montzka, S. A., McFarland, M., Andersen, S. O., Miller, B. R., Fahey, D. W., Hall, B. D., Hu, L., Siso, C., and Elkins, J. W.: Recent trends in global emissions of hydrochlorofluorocarbons and hydrofluorocarbons: Reflecting on the 2007 adjustments to the Montreal Protocol, *J. Phys. Chem. A*, 119, 4439–4449, <https://doi.org/10.1021/jp5097376>, 2015.
- Montzka, S. A., Myers, R. C., Butler, J. H., Elkins, J. W., Lock, L. T., Clarke, A. D., and Goldstein, A. H.: Observations of HFC-134a in the remote troposphere, *Geophys. Res. Lett.*, 23, 169–172, <https://doi.org/10.1029/95gl03590>, 1996b.
- O'Doherty, S., Cunnold, D. M., Miller, B. R., Mühle, J., McCulloch, A., Simmonds, P. G., Manning, A. J., Reimann, S., Vollmer, M. K., Grealley, B. R., Prinn, R. G., Fraser, P. J., Steele, L. P., Krummel, P. B., Dunse, B. L., Porter, L. W., Lunder, C. R., Schmidbauer, N., Hermansen, O., Salameh, P. K., Harth, C. M., Wang, R. H. J., and Weiss, R. F.: Global and regional emissions of HFC-125 (CHF₂CF₃) from in situ and air archive atmospheric observations at AGAGE and SOGE observatories, *J. Geophys. Res.*, 114, D23304, <https://doi.org/10.1029/2009jd012184>, 2009.
- Oram, D. E., Reeves, C. E., Penkett, S. A., and Fraser, P. J.: Measurements of HCFC-142b and HCFC-141b in the Cape Grim air Archive: 1978–1993, *Geophys. Res. Lett.*, 22, 2741–2744, <https://doi.org/10.1029/2003JD004277>, 1995.
- Oram, D. E., Reeves, C. E., Sturges, W. T., Penkett, S. A., Fraser, P. J., and Langenfelds, R. L.: Recent tropospheric growth rate and distribution of HFC-134a (CF₃CH₂F), *Geophys. Res. Lett.*, 23, 1949–1952, <https://doi.org/10.1029/96gl01862>, 1996.

- Park, T., Rettich, T. R., Battino, R., Peterson, D., and Wilhelm, E.: Solubility of gases in liquids. 14. Bunsen coefficients for several fluorine-containing gases (Freons) dissolved in water at 298.15 K, *J. Chem. Eng. Data*, 27, 324–326, <https://doi.org/10.1021/je00029a027>, 1982.
- Parmelee, H. M.: Water solubility of Freon refrigerants, *Refrigerating Engineering*, 61, 1341, 1953.
- Prinn, R. G., Weiss, R. F., Arduini, J., Arnold, T., DeWitt, H. L., Fraser, P. J., Ganesan, A. L., Gasore, J., Harth, C. M., and Hermansen, O.: History of chemically and radiatively important atmospheric gases from the Advanced Global Atmospheric Gases Experiment (AGAGE), *Earth Syst. Sci. Data*, 10, 985–1018, <https://doi.org/10.5194/essd-10-985-2018>, 2018a.
- Prinn, R. G., Weiss, R. F., Arduini, J., Arnold, T., Fraser, P. J., Ganesan, A. L., Gasore, J., Harth, C. M., Hermansen, O., Kim, J., Krummel, P. B., Li, S., Loh, Z. M., Lunder, C. R., Maione, M., Manning, A. J., Miller, B. R., Mitrevski, B., Mühle, J., O'Doherty, S., Park, S., Reimann, S., Rigby, M., Salameh, P. K., Schmidt, R., Simmonds, P. G., Steele, L. P., Vollmer, M. K., Wang, R. H., and Young, D.: The ALE/GAGE/AGAGE Network (DB 1001), <http://cdiac.essdive.lbl.gov/ndps/alegagage.html>.
- Reichl, A.: Messung und Korrelierung von Gaslöslichkeiten halogenierter Kohlenwasserstoffe, PhD thesis, Shaker, 1996.
- Reinsch, C. H.: Smoothing by spline functions, *Numer. Math.*, 10, 177–183, <https://doi.org/10.1007/BF02162161>, 1967.
- Sander, S., Abbatt, J., Barker, J., Burkholder, J., Golden, D., Kolb, C., Kurylo, M., Moortgat, G., Wine, P., Huie, R., and Orkin, V.: Chemical Kinetics and Photochemical Data for Use in Atmospheric Studies Evaluation Number 17, Pasadena, CA: Jet Propulsion Laboratory, National Aeronautics and Space Administration, 2011.
- Scharlin, P. and Battino, R.: Solubility of CCl_2F_2 , CClF_3 , CF_4 and $\text{c-C}_4\text{F}_8$ in H_2O and D_2O at 288 to 318 K and 101.325 kPa. Thermodynamics of transfer of gases from H_2O to D_2O , *Fluid Phase Equilib.*, 95, 137–147, [https://doi.org/10.1016/0378-3812\(94\)80066-9](https://doi.org/10.1016/0378-3812(94)80066-9), 1994.
- Sturrock, G. A., Etheridge, D. M., Trudinger, C. M., Fraser, P. J., and Smith, A. M.: Atmospheric histories of halocarbons from analysis of Antarctic firn air: Major Montreal Protocol species, *J. Geophys. Res.: Atmos.*, 107, 4765, <https://doi.org/10.1029/2002JD002548>, 2002.
- Thompson, T. M., Butler, J. H., Daube, B. C., Dutton, G. S., Elkins, J. W., Hall, B. D., Hurst, D. F., King, D. B., Kline, E. S., and Lafleur, B. G.: Halocarbons and other atmospheric trace species, Report, 115–135 pp., 2004.
- Trudinger, C. M., Fraser, P. J., Etheridge, D. M., Sturges, W. T., Vollmer, M. K., Rigby, M., Martinerie, P., Mühle, J., Worton, D. R., and Krummel, P. B.: Atmospheric abundance and global emissions of perfluorocarbons CF_4 , C_2F_6 and C_3F_8 since 1800 inferred from ice core, firn, air archive and in situ measurements, *Atmos. Chem. Phys.*, 16, 11733–11754, <https://doi.org/10.5194/acp-16-11733-2016>, 2016.

- Wahba, G.: Bayesian "confidence intervals" for the cross-validated smoothing spline, *Journal of the Royal Statistical Society. Series B (Methodological)*, 133–150, <https://doi.org/10.1111/j.2517-6161.1983.tb01239.x>, 1983.
- Warner, M. J. and Weiss, R. F.: Solubilities of chlorofluorocarbons 11 and 12 in water and seawater, *Deep Sea Res. Part A. Oceanogr. Res. Pap.*, 32, 13, [https://doi.org/10.1016/0198-0149\(85\)90099-8](https://doi.org/10.1016/0198-0149(85)90099-8), 1985.
- Wen, W. and Muccitelli, J. A.: Thermodynamics of Some Perfluorocarbon Gases in Water, *J. Solution Chem.*, 8, 22, <https://doi.org/10.1007/BF00648882>, 1979.
- Wilhelm, E., Battino, R., and Wilcock, R. J.: Low-Pressure Solubility of Gases in Liquid Water, *Chem. Rev.*, 77, 44, <https://doi.org/10.1021/cr60306a003>, 1977.
- Zheng, D., Guo, T., and Knapp, H.: Experimental and modeling studies on the solubility of CO₂, CHClF₂, CHF₃, C₂H₂F₄ and C₂H₄F₂ in water and aqueous NaCl solutions under low pressures, *Fluid Phase Equilib.*, 129, 197–209, [https://doi.org/10.1016/S0378-3812\(96\)03177-9](https://doi.org/10.1016/S0378-3812(96)03177-9), 1997.

Manuscript III

Medusa-Aqua system: simultaneous measurement and evaluation of novel potential halogenated transient tracers HCFCs, HFCs and PFCs in the ocean

Pingyang Li and Toste Tanhua: Medusa-Aqua system: simultaneous measurement and evaluation of novel potential halogenated transient tracers HCFCs, HFCs and PFCs in the ocean, *Ocean Science Discussion*, <https://doi.org/10.5194/os-2019-101>, in review (resubmitted), 2019.

Abstract. This study evaluates the potential usefulness of the halogenated compounds HCFC-22, HCFC-141b, HCFC-142b, HFC-134a, HFC-125, HFC-23, PFC-14 and PFC-116 as oceanographic transient tracers to better constrain ocean ventilation processes. We do this mainly from four aspects of the characteristics of the potential tracers: input function (including atmospheric history and historical surface saturation), seawater solubility, feasibility of measurement and stability in seawater. The atmospheric history and seawater solubility have been investigated in previous work. In this study, the historical surface saturation in the Mediterranean Sea is estimated to be 94 % based on cruise data in 1987-2018. In addition, we collected seawater samples and modified an established analytical technique to the Medusa-Aqua system in order to simultaneously measure these compounds. HCFC-22, HCFC-141b, HCFC-142b, HFC-134a and HFC-125 have been measured in depth-profiles in the Mediterranean Sea for the first time. Of the investigated compounds, HCFC-142b and HCFC-141b are found to be the most promising transient tracer in the ocean currently. The compounds that have the greatest potential as future tracers are PFC-14 and PFC-116, although the low solubility in seawater creates challenging analytical conditions (i.e. low concentration) that can potentially be improved by modifying the Medusa-Aqua analytical system. HCFC-22 is found to be likely unstable in warm seawater, which leads to low confidence in terms of its potential as an oceanic transient tracer, although it is possibly useful in colder water. For compounds HFC-134a, HFC-125 and HFC-23, we are not able to fully evaluate their potential as tracers due to the inconclusive results, especially on their solubility and stability in seawater, but also with regard to potential analytical challenges. On the other hand, HFC-125, HFC-23, and HCFC-22 can no longer be considered because there are alternative tracers with similar input histories that are better suited as transient tracers.

1 Introduction

1.1 Why do we look for new transient tracers?

Transient tracers include chronological transient tracers such as dichlorodifluoromethane (CFC-12) and sulfur hexafluoride (SF₆), and radioactive transient tracers such as Tritium (³H), Argon-39 (³⁹Ar)

and Carbon-14 (^{14}C). They have been used as oceanic transient tracers to study the oceanic processes, such as ventilation, mixing and circulation processes. CFC-12 has been used since the 1980s, whereas SF_6 has only been used since the 1990s. Both compounds are stable in seawater; their seawater solubility functions are well-established (Bullister et al., 2002; Warner and Weiss, 1985) and their historical atmospheric concentrations over time are known (Bullister, 2015; Walker et al., 2000). However, the use of CFC-12 was phased-out as a result of the implementation of the Montreal Protocol on Substances that Deplete the Ozone Layer designed to curtail the degradation of the Earth's ozone layer. Therefore, the atmospheric concentration of CFC-12 has decreased since the early 2000s (Bullister, 2015), which has reduced its usefulness as an oceanographic transient tracer for recently ventilated water masses. Consequently, SF_6 has been added to the suite of commonly measured oceanic transient tracers (Bullister et al., 2006; Tanhua et al., 2004) as it is an inert gas whose atmospheric abundance is increasing. Some local restrictions on the production and use of SF_6 , however, due to its very high global warming potential, may restrict its future use. Both CFC-12 and SF_6 are readily measured onboard a research vessel at a reasonable rate. The radioactive isotope ^{39}Ar is in many ways an ideal tracer for ocean circulation for older water masses, but its use has been impeded by difficult analytics. However, recent technological advancements have increased the feasibility of oceanic ^{39}Ar observations (Ebser et al., 2018; Lu et al., 2014). In addition, trichlorofluoromethane (CFC-11), 1,1,2-trichloro-1,2,2-trifluoroethane (CFC-113), and carbon tetrachloride (CCl_4) have been extensively used as transient tracers, but have now been largely discarded. CFC-11 was found to be degraded in anoxic marine waters (Bullister and Lee, 1995) and has a time-history similar to that of CFC-12. Besides, the simultaneous measurement of SF_6 and CFC-11 is complicated. Both CFC-113 and CCl_4 have been found to be degraded in warm waters (Roether et al., 2001) as well as in low oxygen waters (Huhn et al., 2001; Wallace and Krysell, 1989).

Since a combination of multiple transient tracers is needed to constrain ocean ventilation, it is necessary to explore novel transient tracers with monotonically changing input functions for a better understanding of ventilation and mixing processes in the ocean.

1.2 Potential alternative transient tracers

There are a few general requirements for a transient tracer: 1) known input function, 2) no (or well known) natural background, 3) large dynamic range, 4) feasible measurement techniques and 5) non-reactive and stable in seawater. In the previous work (Li et al., 2019), we focused on points 1, 2 and 3 for the potential alternative oceanographic transient tracers: hydrochlorofluorocarbons (HCFCs) such as HCFC-22, HCFC-141b and HCFC-142b, hydrofluorocarbons (HFCs) such as HFC-134a, HFC-125 and HFC-23 and perfluorocarbons (PFCs) such as PFC-14 (CF_4) and PFC-116. As the replacements of CFCs, the atmospheric abundances of most HCFCs and HFCs are increasing, as are the concentrations of PFCs. Here we describe the potential chronological transient tracers HCFC-22, HCFC-141b, HCFC-142b, HFC-134a, HFC-125, HFC-23, PFC-14 and PFC-116 as the “Medusa tracers”, CFC-12

and SF₆ as traditional chronological transient tracers and ³H, ³⁹Ar and ¹⁴C as radioactive transient tracers. For the radioactive transient tracers, the half-lives of the three tracer nuclides have different orders of magnitude, allowing them to cover a wide range of ages (“seawater timescales”, Fig. 1). However, with the constraints of the weak signal of ³H and the decreasing atmospheric mole fraction of CFC-12, only SF₆ is a relatively reliable transient tracer in the seawater timescale range of 1-100 years at present (Fig. 1). Fortunately, the different atmospheric histories of the potential alternative transient tracers (Li et al., 2019) allow us to find one or several compounds to replace or supplement the established transient tracers.

1.3 Stability of alternative tracers in seawater

Chemical reactions (including hydrolysis), adsorption to particles and biological degradation process should be considered with regard to the stability of compounds in seawater. PFCs have very long atmospheric lifetimes, i.e. > 50 000 and > 10 000 years for PFC-14 and PFC-116, respectively. PFC-14 (CF₄) is thought to be stable and inert in the ocean (Cicerone, 1979; Ravishankara et al., 1993) since CF₄ is stable at temperatures of at least 1200°C and the rate of hydrolysis of CF₄ is immeasurably small. Furthermore, no known marine natural products contain C-F bonds and there are no indications of biological processes that can break C-F bonds. This reasoning applied to PFC-116 and other PFCs that are likely to be very stable in the environment. On the other hand, we are not aware of any publications that directly discuss the stability of the other compounds in seawater. Therefore, their stabilities are inferred from other studies with slightly different perspectives and environmental foci.

One example is the contribution of the partial atmospheric lifetime with respect to oceanic uptake of selected HCFCs and HFCs to the total lifetimes. Such partial atmospheric lifetimes depend on solubility in seawater and other losses relative to their atmospheric concentration, and are always larger than their total lifetimes. Considering the low fraction of these mainly non-polar compounds in the ocean, a small loss in the ocean is insignificant for the overall budget of the compound, but can still be of significance for a potential transient tracer. As far as we know from previous studies (Carpenter et al., 2014; Yvon-Lewis and Butler, 2002), HCFCs and HFCs are relatively stable in seawater and their partial atmospheric lifetimes with respect to oceanic uptake range from thousands to millions of years (Table 1). Judged against their environmental total lifetimes, the oceanic contributions of these compounds are small enough to be neglected. The partial atmospheric lifetimes with respect to oceanic uptake in Table 1 were calculated only considering the chemical degradation process.

Another route is to compare surface saturations of a tracer with unknown stability to the one of a compound that is known to be unstable in seawater. Surface saturation of HCFCs is not as under-saturated as those of CCl₄ (Butler et al., 2016) by the comparison of their saturations in various oceans based on the results from the National Oceanic and Atmospheric Administration (NOAA) cruises in

1992-2008 (<ftp://ftp.cmdl.noaa.gov/hats/ocean/>, last access: 20 January 2020). This suggests that HCFCs are more stable than CCl_4 in surface seawater and possibly suited to be tracers in the ocean.

We also used published information on biodegradation of compounds in freshwater or soil, although a compound can be degraded in the freshwater or soil but can still be stable in seawater, such as CFC-12. Chang and Criddle (1995), Oremland (1996), and Streger et al. (1999) observed the aerobic bacterial degradations of selected HCFCs and HFC-134a in very high oxygen concentrations and substrate levels (Table 2), and these aerobic microorganisms are common inhabitants of soil and aquatic systems. Although rapid removal in the soil can be an indication of non-conservative behavior in the ocean, the lifetime of a compound in soil or freshwater can be considerably shorter than in open ocean waters with few particles.

Based on these discussions, HCFCs seem to be relatively stable in the ocean when only considering the chemical degradation process and surface saturation in seawater. However, the influence of oxygen dependence and biological degradation processes in seawater have not been investigated (Yvon-Lewis and Butler, 2002). In summary, not enough information is known on the stability of the selected HCFCs and HFCs in the ocean.

1.4 Purpose of this study

The atmospheric history and seawater solubility of potential new oceanic transient tracers have been previously reported by Li et al. (2019). This study extends that work, with a focus on evaluating their usefulness. Based on observations of these tracers in the Mediterranean Sea, we mainly address points 4 and 5 of the general requirements in this study, i.e. we discuss if rapid, relatively inexpensive and accurate measurements are possible and if these compounds are conservative in the oceanic environment. We also estimate the historical surface saturation to supplement the input function and discuss differences in tracer input functions and their ability to provide additional information on ventilation. A suite of observations of transient tracers with sufficiently different input functions would support the empiric determination of Transit Time Distributions (TTDs), as reported in Stöven and Tanhua (2014). As the first step towards this, these Medusa tracers have been measured, sometimes for the first time, and interpreted based on the Inverse Gaussian Transit Time Distribution (IG-TTD) concept to identify their possibility as transient tracers in the ocean. The Mediterranean Sea was chosen for this study because of its rapid ventilation, which causes transient tracers to penetrate most of the water column. However, on the down-side, the time-variant ventilation and the contribution of several deep-water sources make the TTD concept difficult in the Mediterranean Sea.

2 Transient tracer interpreting methods

2.1 Ocean ventilation and transit time distribution (TTD) model

Ventilation is defined as the time elapsed since the water parcel has left the mixed layer and been transported to the ocean interior. Ocean ventilation and mixing processes play significant roles in climate as they are important processes to propagate perturbations on the ocean surface to the interior. They largely control the accumulated uptake of anthropogenic carbon (C_{ant}) at mid- and high latitudes and the deep ocean's oxygen supply. To describe these processes quantitatively, we used a conceptual but well-established ocean ventilation model, the Transit Time Distribution (TTD) model that is based on the Green's function $G(t, r)$ describing the propagation of tracer boundary conditions into the interior (Hall and Plumb, 1994). As shown in Eq. (1), $c(t_s, r)$ describe the concentration of a transient tracer at year t_s and location r . The boundary concentration $c_0(t_s, r)$ is the concentration at source year $(t_s - t)$ related to the tracer input function, while the exponential term ($e^{-\lambda t}$) describes the decay rate of radioactive transient tracers. This function is based on a steady and one-dimensional flow model with time-invariant advective velocity and diffusivity gradient. One commonly used solution to Eq. (1) is the one-dimensional Inverse Gaussian Transit Time Distribution (IG-TTD), simplified and expressed as Eq. (2). $G(t)$ is defined based on the mean age Γ , the width of the distribution Δ and the time range t (Vaughn et al., 2003).

$$c(t_s, r) = \int_0^{\infty} c_0(t_s - t) e^{-\lambda t} \cdot G(t, r) dt \quad (1)$$

$$G(t) = \sqrt{\frac{\Gamma^3}{4\pi\Delta^2 t^3}} \cdot \exp\left(\frac{-\Gamma(t - \Gamma)^2}{4\Delta^2 t}\right) \quad (2)$$

The Δ/Γ ratio of the TTD corresponds to the proportion of advective transport and eddy-diffusive characteristics of the mixing processes for a water parcel; the higher the Δ/Γ ratio, the more dominant the diffusion and vice-versa.

2.2 Time range, tracer age, mean age and Transient Time Distribution

Time range. The time range where a tracer can be used as a transient tracer is defined by its input function. For chronological transient tracers, the input functions are described by their atmospheric histories and historical surface saturations. For ideal applicability, atmospheric histories of tracers should increase monotonically in the atmosphere. Figure 2 shows the atmospheric histories of HCFC-22, HCFC-141b, HCFC-142b, HFC-134a, HFC-125, HFC-23, PFC-14, PFC-116, CFC-12 and SF₆ in the Northern Hemisphere (Bullister, 2015; Li et al., 2019).

Tracer age. Tracer age is defined as the age of a water parcel based on a purely advective flow in the ocean, i.e. Δ/Γ equals zero in the IG-TTD concept. Each tracer has a specific time and application range related to possible age information. Figure 3 shows the relation between the relative tracer concentrations in percent, i.e. normalized to the contemporaneous atmospheric concentrations, and the corresponding tracer ages for 10 transient tracers in two different sampling years 2018 and 2000, which highlights tracer similarities and the specific application range for each tracer.

Relatively similar trends of relative tracer concentrations (Fig. 3) are found for the following couples: HCFC-141b and HCFC-142b, HFC-134a and HFC-125, SF₆ and HCFC-22/HFC-23, PFC-14 and PFC-116. Assuming that all these compounds fulfill the other criteria as transient tracers, one of each couple could be chosen for further studies depending on their relative tracer concentrations.

The specific application ranges of tracer ages for tracers can be found in Fig. 3 with the compiled results shown in Fig. 1. In Fig. 3, if the relative tracer concentrations are over 100 % then there has been a decrease in atmospheric concentrations, such as the tracer age range of 0-30 years for CFC-12 (Fig. 3a) produced by the decreasing atmospheric mole fractions (Fig. 2). When the atmospheric history of a compound is not monotonically changing, the equilibrium atmospheric mole fraction (and ultimately the age associated with that mole fraction) calculated from its concentration in the ocean is not unique, reducing its potential as a transient tracer (Li et al., 2019). Therefore, the tracer age range is a function of the sampling year. For instance, the useful tracer age range of CFC-12 is 30-80 years and 1-60 years for sampling in 2018 and 2000, respectively (Fig. 3). This indicates that the ability of CFC-12 to be a transient tracer for recently ventilated water is decreasing with time, but CFC-12 still provides important time information for intermediate and deep water layers with moderate ventilation timescales. It is worth pointing out that PFCs have a longer tracer age range compared to other compounds, even CFC-12, among the chronological transient tracers (Fig. 3). As CFC-12 is limited for use as a tracer in the upper ocean, PFCs should be further evaluated for future use.

Mean age and Transient Time Distribution (TTD). The mean age, calculated as the average of the TTD, can be used as an estimate of the age of a water parcel based on a combination of advective and mixing flow in the ocean. Assuming an IG-TTD, the theoretical tracer concentrations $c(t_s, r)$ for a range of Δ/Γ ratios (0.2-1.8) based on Eqs. (1) and (2) have been calculated for the Medusa tracers (Fig. S1). Figure S2 shows the mean age matrices of $\Delta/\Gamma = 1.0$ (the blue lines in Fig. S1) for each Medusa tracer and describes the expected tracer concentration as a function of different mean ages and sampling years. More complicated or different TTDs than the IG-TTD can also be assumed, and if the observed concentrations match the theoretical tracer concentrations for a range of tracers with different input functions it is an indication that the assumption is valid.

3 Medusa-Aqua system

3.1 Progress in analytical technology of selected HCFCs, HFCs and PFCs

Measurement of halogenated compounds is often performed by "gas-solvent extraction" techniques, e.g. purge-and-trap where an inert gas is bubbled through a seawater sample to move the analytes from the sample into a cold trap for pre-concentration. By desorbing the content of the trap, the sample can then be injected into a gas chromatograph (GC) for separation and detection. This is a well-established technique that has been used successfully for CFCs and SF₆ (Bullister and Weiss, 1988; Bullister and Wisegarver, 2008) achieving accuracies in the order of 1 % (Bullister and Tanhua, 2010). However,

several HCFCs and HFCs (i.e. HCFC-22, HFC-134a, and HFC-125) have low responses and large uncertainties when they are measured by an Electron Capture Detector (ECD) that is normally used for CFC-12 and SF₆ (Beyer et al., 2014; Lobert et al., 1995). One alternative is to use a mass spectrometer (MS) for detection that has the advantage of scanning for unique masses for different compounds, allowing identification and quantification simultaneously. Using an MS as a detector is becoming increasingly popular since the sensitivity is approaching that of an ECD. However, the HCFCs tend to be more soluble, making it more difficult to quantitatively purge all of the tracers from a water sample.

The Medusa-GC-MS system (shorted as the Medusa system) for the precise and simultaneous analysis of a wide range of volatile trace gases has been developed at the Scripps Institution of Oceanography (Miller et al., 2008). This system is based on trapping volatile gases on two traps kept at accurately controlled temperatures. The packing material of the traps and the temperature during the trapping stage are designed in a way that allows for the fractionation of the compounds on two traps. In this way, interferences from atmospheric permanent gases can be avoided and hard-to-measure gases like PFC-14 (CF₄) can be measured. This analytical system was designed to automatically and continuously measure air samples at Advanced Global Atmospheric Gases Experiment (AGAGE) remote field stations (Prinn et al., 2018) and is unique in that it provides high accuracy measurements of more than 40 compounds including halocarbons, hydrocarbons and sulfur compounds involved in ozone depletion and/or climate forcing from the same sample. The measurement precisions of the majority of the halogenated compounds are less than 0.5 % in 2 L ambient air. The Medusa-Aqua system as developed based on the Medusa system can measure the majority of the 40 halogenated compounds in seawater samples.

3.2 Difference between Medusa-Aqua and Medusa system

The Medusa-Aqua system consists of a Medusa system (Miller et al., 2008) and a seawater sample pretreatment system (Fig. 4). The Medusa system consists of a cryogenic pre-concentration unit, named Medusa, an Agilent 6890N gas chromatograph (GC) and an Agilent 5975B quadrupole mass spectrometer (MS). The seawater sample pretreatment system was developed to degas gaseous tracers from the samples before injecting into the Medusa system, replacing the air sampling device of the original Medusa system. The technology is based on a purge-and-trap technology where the Medusa serves as the trap unit prior to the chromatographic separation of the sample for detection in the MS.

The main difference between Medusa and Medusa-Aqua system is that the former uses an air-pump module as the gas sample pretreatment system and the sample volume is determined by an integrating mass flow controller (MFC), while the latter uses a purge module as the seawater sample pretreatment system and a gravimetrically calibrated standard loop for standard gases. For the injection of water samples to the system, we use the Ampoule-Cracker-System, as designed by Vollmer and Weiss (2002) and then modified by Stöven (2011).

4 Sampling and Measurement

Here we describe the sampling and measurement methods for samples collected from cruise MSM72 to the Mediterranean Sea in March and cruise AL516 to the western Baltic Sea in September 2018.

4.1 Sample collection

Seawater samples were collected throughout the water column in three areas of the Mediterranean Sea (Fig. 5): Southern Ionian Sea (SIS), Tyrrhenian Sea (TS) and Western Mediterranean Sea (WMS) on the cruise MSM72 by the research vessel *Maria S. Merian* from March 2nd to April 3rd, 2018 along the GO-SHIP line MED-01 (Hainbucher et al., 2019a) and one station (10.1 °E, 54.5 °N) in the Baltic Sea on the cruise AL516 by the research vessel *Alkor* from September 12th to 22nd, 2018 (Booge, 2018). These seawater samples were collected in glass ampoules (~1.3 L), connected to the Niskin bottles via a stainless steel mounting system (Vollmer and Weiss, 2002). 5 minutes is needed for the seawater to fill up a whole glass ampoule and the sampling process lasted for 15 minutes to allow for the seawater to flush the whole ampoule volume three times. After removing and closing the ampoule with a screw, the ampoule was flame-sealed as soon as possible under a flow of high purity N₂ (Air Liquide, grade 6.0, Germany) and then sent back to the laboratory in Kiel for measurement. As seen in Fig. 5, no onboard CFC-12 and SF₆ measurements were conducted on the stations we sampled for the Medusa-Aqua system in the Mediterranean Sea. The distance between stations on this cruise was 15 nm (nautical miles), and normally we sampled for chemistry on every second station.

4.2 Gas extraction, separation, and detection

The flow scheme for the Medusa-Aqua system is shown in Fig. 4. Before measurement, each ampoule sample was immersed in a warm water bath at 65 °C overnight to enhance the purging efficiency by driving the gases into the headspace. The stem of the ampoule is inserted vertically up into the cracking chamber and is held by a screw-nut with nylon ferrule. Then the cracking chamber is flushed with N₂ for 10 minutes to flush out ambient air. A blank test for the cracking chamber is made by simulating an extraction without breaking the glass ampoule. For analysis, the tip of the ampoule's stem is shattered inside the enclosed cracking chamber by rotating the cracking paddle. A straight purge tube is then inserted down into the ampoule until touching the ampoule bottom for finer bubbles. These bubbles will help strip the compounds out of the seawater and enhance the purge efficiencies for the dissolved gases.

The extraction process is started by purging the gases in the ampoule with N₂ (grade 6.0) for 20 minutes at a flow rate of 100 mL min⁻¹. Water vapor is removed from the sample by passing the gases through two Nafion dryers of 1.8 m length and one of 0.6 m length. The counter-flow rate of Nafion dryer gas (N₂, grade 5.0) was set to 120 mL min⁻¹. After the purge gas is injected into Medusa, the following path is the same as described by Miller et al. (2008). The tracer gases are separated on the main column with helium (Air Liquide, grade 6.0, Germany) as a carrier gas and detected by the MS.

The mass of seawater in the ampoules was calculated as the difference between the full weight of the ampoule before measurement and the empty ampoule (including glass splinters) after rinsing with distilled water and drying in an oven for around 96 h.

4.3 Standard and calibration

The standard gas used in the laboratory in Kiel is a tertiary standard calibrated by the Scripps Institution of Oceanography (SIO) on the AGAGE relative scale “SIO-R1”. For details about the propagation of the standard see Miller et al. (2008). Gravimetric calibration scales and calibrated errors of compounds in the tertiary standard are reported in Table 3. Measurements in seawater are reported on the latest SIO absolute calibration scales for HFC-125 (SIO-14), HFC-23 and PF-114 (SIO-07) and other compounds (SIO-05). The tertiary calibration scale is directly used as a working standard to determine weekly calibration curves and daily drift corrections. These calibration measurements are made by multiple injections of a 10.0 mL gravimetrically calibrated sample loop. Each injection lasts 40 seconds at a flow rate of 50-60 mL min⁻¹. The detector responses for compounds in Table 3 are linear in the range of our measurements.

4.4 Purging efficiency, detection limit, and precision

Each sample was measured 3-6 times until none of the compounds in Table 3 could be detected in the seawater sample so that the purging efficiency for all compounds is 100 %. The precision of the measurement is dependent on the size of the ampoules and the amount of tracer; the sample with a higher amount of tracer has better precisions than those with a lower amount. The precision (or reproducibility) for seawater sample measurements were determined by the relative standard deviations (1σ) of the concentrations for two pairs of duplicate samples (Table 3). The detection limits for measurements of all compounds by the Medusa-Aqua system are also shown in Table 3 based on the signals corresponding to the blank values or noises plus ten standard deviations.

The concentrations of SF₆, PFC-14, and PFC-116 in most seawater samples were lower than the detection limit, and HFC-23 had unstable and non-zero blank values in all measurements, preventing us from evaluating those results. The observations of CFC-12, HCFC-22, HCFC-141b, HCFC-142b, HFC-134a and HFC-125 measured by the Medusa-Aqua system in seawater from the cruise MSM72 are shown in Table S1 with quality flags marked.

4.5 Comparison of instruments measuring CFC-12

In order to explore the precision and accuracy of seawater measurements by the Medusa-Aqua system, CFC-12 was measured by both the Medusa-Aqua system and a purge and trap GC-ECD instrument (Syringe-PT-GC-ECD) used onboard the cruise MSM72. This is a mature system to measure CFC-12, SF₆ and SF₅CF₃ (Bullister and Wisegarver, 2008; Stöven, 2011; Stöven and Tanhua, 2014; Stöven et al., 2016). For comparison, a similar purge and trap system set-up (Cracker-PT-GC-ECD) to measure flame-sealed ampoules is added. A detailed comparison of the three instruments is shown in Table 4.

Compared to other systems, the Medusa-Aqua system has lower purge efficiency due to its bigger sampling volume if samples are only purged once (although we used multiple purge cycles to increase the purging efficiency and reduce the uncertainty); has lower precision than that of the Syringe-PT-GC-ECD but higher than that of the Cracker-PT-GC-ECD system; and can measure more compounds.

5 Results

5.1 Historical surface saturation in the Mediterranean Sea

The historical surface saturation of transient tracers is an important factor to illustrate ventilation. To determine this for the Mediterranean Sea, we calculated seawater saturation in the winter mixed layer (WML) from historical cruise data. The depths of the WMLs in summer and winter are shown in Fig. 6 for two exemplary density profiles. While saturation in warm, summer surface layers is often higher, it is the winter saturation levels that are relevant for deep and intermediate water formation, and thus for the input functions. Therefore, only the WML was considered in the calculation of historical surface saturation for all cruises. The depth ranges of WMLs (Fig. S3) and the saturation level for CFC-12 and SF₆ (Fig. 7) were determined by profiles of temperature, potential density, and CFC-12 concentrations for each historical cruise that we have access to in the Mediterranean Sea from 1987 to 2018 (Li and Tanhua, in preparation; Schneider et al., 2014). By averaging the mean surface saturation from every single cruise, the saturation level is determined to be $94 \pm 6 \%$ and $94 \pm 4 \%$ for CFC-12 and SF₆, respectively. These historical surface saturations do not show a clear trend over time. For CFC-12, this is different from the situation in the North Atlantic Ocean (Tanhua et al., 2008), and is probably an indication of the different oceanographic setting where the inflowing Atlantic Water (to the Mediterranean Sea) has a long time to equilibrate with the atmosphere.

For the following calculations, the historical surface saturations are assumed to be a constant 94 % (overtime) for all tracers in this study as no data exists to determine the historical surface saturation of selected HCFCs and HFCs in the Mediterranean Sea. The historical surface saturation and the atmospheric concentration histories of all compounds together describe their input functions.

5.2 Observations of the Medusa tracers in seawater

The observations of CFC-12 measured by the Medusa-Aqua system are generally comparable with those in adjacent stations measured onboard by the PT-GC-ECD system (Fig. 8). The averaged difference of CFC-12 concentrations measured by the two different instruments is $5.9 \pm 4.6 \%$ focusing on only the data with quality flagged “good”. Based on the reasonable correlation between CFC-12 observations from the Medusa-Aqua system and the onboard PT-GC-ECD system, we can move on and interpret the profiles of the Medusa tracers. Observations of CFC-12 and SF₆ from profiles 51, 83 and 105 measured by the PT-GC-ECD and observations of CFC-12, HCFC-22, HCFC-

141b, HCFC-142b, HFC-134a, and HFC-125 from the nearby profiles 52, 84 and 106 measured by the Medusa-Aqua system are shown in Fig. 9.

5.3 Surface saturation of Medusa tracers in seawater

Surface saturation in seawater could be a factor that describes the stability of a compound in surface seawater or confidence in the seawater solubility function. Saturation is influenced by multiple parameters, such as partial pressures in the atmosphere and surface seawater, the air-sea exchange velocity, the solubility and diffusivity of the gas, and the temperature dependence of these parameters (Butler et al., 2016; Lobert et al., 1995).

In the Mediterranean Sea, the averaged saturations of SF₆ and CFC-12 measured by the PT-GC-ECD are 94.5 ± 4 % and 91.5 ± 1 %, respectively (Table 5), which is close to those estimated from historical surface saturation (see Sect. 5.1). The surface saturation of CFC-12 measured by the Medusa-Aqua system is ~20 % lower than adjacent measurements by the PT-GC-ECD. The averaged surface saturations of HCFC-22, HCFC-141b and HFC-125 measured by the Medusa-Aqua system are 43 ± 1 %, 52 ± 4 % and 37 ± 10 %, which are lower than expected. The averaged saturation of HCFC-142b measured by the Medusa-Aqua system is 90 ± 11 %, whereas the averaged saturation of HFC-134a is 139 ± 34 %. There are a few possible reasons for the lower than expected saturations: 1) problems in measurements/sampling; 2) poorly defined solubility functions; 3) degradation in seawater. Degradation is not likely for CFC-12, which is known to be stable in flame-sealed glass ampoules. Based on these, we conclude that there is an as yet undefined issue with sampling or measurement of these surface samples. Since we have the benefit of “reference” measurements from a proven technique (the PT-GC-ECD system) in the Mediterranean Sea, we flagged data where the Medusa-CFC-12 values are inconsistent with the CFC-12 values from PT-GC-ECD (Fig. 8).

In the Baltic Sea, the averaged seawater surface saturation of CFC-12, HCFC-22, HCFC-141b, HCFC-142b, HFC-134a and HFC-125 are 122 ± 8 %, 77 ± 8 %, 74 ± 12 %, 114 ± 2 %, 125 ± 23 % and 252 ± 35 %, respectively (Table 5). These higher and more realistic surface saturation levels also indicate that a sampling or measurement issue might be responsible for the compounds with low saturations, such as HCFC-22, HCFC-141b and HFC-125, in the Mediterranean Sea. But in the Baltic Sea, the lower saturation of HCFC-22 may be attributed to degradation considering its higher partial pressures in the atmosphere than in the surface seawater (increasing atmospheric history) and ease of solubility in seawater; the lower saturation of HCFC-141b might due to degradation and/or lower partial pressures in the atmosphere than in the surface seawater (decreasing atmospheric history) considering its high solubility in seawater. For HFC-125, the very low saturations in the Mediterranean Sea and very high saturations in the Baltic Sea are probably a result of issues in the seawater solubility function and/or measurement.

5.4 Stability based on interior ocean observations

In order to validate the stability of HCFCs and HFCs, the concentrations of CFC-12 from the adjacent PT-GC-ECD measurements are vertically interpolated by a piecewise cubic hermite interpolating method on potential density surfaces and averaged by the arithmetic mean of the interpolated profiles (Schneider et al., 2014; Tanhua et al., 2010). Then the concentrations of HCFC-22, HCFC-141b, HCFC-142b, HFC-134a and HFC-125 and SF₆ (measured by the PT-GC-ECD) are plotted against the (interpolated) CFC-12 (Fig. 10). Concentrations in the shallow layers plot towards the upper right corner with deep samples near the lower left. In the figure, we added the atmospheric history of the Medusa tracers vs. CFC-12 as well as the theoretical mixing line between contemporary and pre-industrial concentrations; all samples will have to fall between these two lines (i.e. the stability area) if the tracer is conservative in seawater. Compounds where the samples fall below the “stability area” are not stable (assuming that CFC-12 is stable), and for samples above it there are issues with too high values (see below). For instance, HCFC-22 is found in the lower part of the stability area (samples would fall on this lowest line if there were no mixing but only advection in the ocean); HCFC-141b, HFC-125, and SF₆ are well in the allowed range; whereas HCFC-142b and HFC-134a are around or above the upper boundary.

The increased ventilation of the (western) Mediterranean Sea during the last decade tends to result in very different effects on CFC-12, which is decreasing in the atmosphere, and the Medusa tracers that are mostly increasing. This argument suggests that we could expect higher than expected concentrations (as SF₆ presented) for the Medusa tracers. This is exactly what we see from HCFC-142b and HFC-125 (Fig. 10). However, too high concentrations for HFC-134a may associate with a few possible reasons: 1) contamination during sampling or measurement in the laboratory; 2) problems with solubility functions; 3) some other issues within the measurements in the laboratory causing our observations to be high.

5.5 Comparison of mean age estimates

In order to compare the mean ages estimated from HCFCs and HFCs with those estimated from CFC-12 and SF₆, we calculated the mean ages of these tracers (Fig. 11). Here we assumed the Δ/Γ ratio of IG-TTD to be 1.0 and the saturation of all tracers to be 94 % (see Sect. 5.1). However, the TTD of the Mediterranean Sea is complicated by the variable ventilation and the influence of different source regions for interior water, see Stöven and Tanhua (2014). While the assumption of an IG-TTD with $\Delta/\Gamma = 1.0$ can be questioned, it can still serve as an initial assumption to evaluate the new tracers. Note that the mean ages calculated from CFC-12 and SF₆ are not identical, although we have high confidence in these data. Therefore, even though the assumptions made on the TTD are not entirely correct, they are a reasonable starting point for the purpose of this study.

The mean age estimated from HCFC-141b is similar to (slightly higher than) those from CFC-12 and SF₆, whereas the mean age estimated from HCFC-22 is higher while the mean ages from HCFC-142b, HFC-134a and HFC-125 are significantly lower. If the mean age is lower than expected, it

implies that the concentration is probably higher than expected (Fig. 10) and vice-versa. There are different possible explanations for the difference in mean ages. One obvious explanation is uncertainty in the Δ/Γ ratio of TTD that will affect tracers with different input functions differently. Other possible explanations include uncertainty in the solubility function or analytical error, see discussions below.

6 Discussions

The results from this study on surface saturation in seawater, stability based on interior ocean observations and mean age in relation to CFC-12 are summarized in Table 6. These results can be evaluated to analyze the stability and further determine the potential of the Medusa tracers as oceanic transient tracers, and are as such dependent on the confidence that the measurements are reasonably accurate. The comparison between the mean ages calculated from the Medusa tracers and CFC-12 is sensitive to the assumed shape of the TTD, and the differences in input history that make them respond differently to the time-variant ventilation of the (western) Mediterranean Sea. As a component of the input function, the historical surface saturation has been estimated to be 94 %; the atmospheric histories of the Medusa tracers have been given by Li et al. (2019), who also used indirect methods to estimate the solubility functions. HCFC-22, HCFC-141b, HCFC-142b, HFC-134a and HFC-125 can be measured by the Medusa-Aqua system. Based on the combined results from Li et al. (2019) and this study, the potential of the Medusa tracers as transient tracers in the ocean is summarized in Table 7 by mainly evaluating the confidence or feasibility of their atmospheric history, seawater solubility, ease of measurement and stability in seawater. The more precise historical surface saturation will be a future consideration

As a reference, we start with CFC-12, a commonly used transient tracer marked with medium/high confidence/feasibility. The atmospheric history of CFC-12 is well-documented (Bullister, 2015; Walker et al., 2000), and the seawater solubility function is well-established (Warner and Weiss, 1985). In addition, CFC-12 has been observed for several decades by mature analytical techniques, and its stability in warm waters, as well as poorly oxygenated waters, has been proven. However, the decreasing atmospheric history of CFC-12 limits its ability as an oceanic transient tracer currently.

HCFC-22. The increasing atmospheric history (high confidence) is well-established by a combination of the model results and observations (Li et al., 2019). The seawater solubility function has been constructed by combining the CGW (Clark–Glew–Weiss) model on the experimental freshwater solubility data and another model (poly-parameter linear free-energy relationships, pp-LFERs) on the salting-out coefficients (Li et al., 2019). The results of freshwater solubility matched those published by Deeds (2008) on measurements and the CGW model fitted results between 298-348 K, and those published in Abraham et al. (2001) on observations and the pp-LFERs model results at 298 K and 310 K. Thus, our ability to estimate the seawater solubility was marked as medium confidence due to

lacking the experimental seawater solubility empirical data to verify the function. As to measurement, HCFC-22 has been measured on several cruises (Lobert et al., 1996; Yvon-Lewis et al., 2008) by GC-ECD and GC-MS instruments and in this study by the Medusa-Aqua system (high feasibility). The stability was evaluated by analyzing the surface saturations in seawater, comparison to CFC-12 observations, and comparison to mean ages estimated from CFC-12/SF₆. The surface saturation was lower than expected probably due to degradation (see Sect. 5.3), which may indicate that HCFC-22 is unstable in surface seawater. Similarly, the clustering of HCFC-22 values in the lower range (Fig. 10) could be an indication of slow degradation in warm seawater, which was also supported by the weak hydrolysis of HCFC-22 in tropical and subtropical waters (Lobert et al., 1995). The mean ages estimated from HCFC-22 were found to be higher (i.e. indicating low concentrations) than those estimated from CFC-12 and SF₆, supporting non-conservative behavior. Therefore, HCFC-22 was determined to be unstable in warm waters; more measurements should be added for the stability analysis, especially in poorly oxygenated and cold waters. In addition, HCFC-22 can be replaced by SF₆ as a transient tracer since they have similar atmospheric histories (Fig. 2 and Fig. 3). These all indicate that HCFC-22 seems not suitable to be a potential new transient tracer in the warm ocean, for instance, the Mediterranean Sea, but could possibly be used for colder waters.

HCFC-141b. The atmospheric history (high confidence) was well reconstructed (Li et al., 2019). However, the seawater solubility function (low confidence) was constructed for the first time (Li et al., 2019) and the freshwater solubility only matched data in Abraham et al. (2001) at the two temperatures. HCFC-141b has been measured on cruises (Lobert et al., 1996; Yvon-Lewis et al., 2008) and also in this study, thus we have high confidence in the ability for measurement. As for the stability, HCFC-141b was identified to be potentially stable in seawater (medium confidence) since its concentrations are likely in similar ranges to those in the interior ocean (Fig. 10) assuming that the solubility function is valid, and the observed mean ages are similar to those estimated from both CFC-12 and SF₆ (Fig. 11). However, the low surface saturation points to the possibility of degradation (see Sect. 5.3). The input function of HCFC-141b is different enough from the traditional transient tracers to provide additional information, but since the atmospheric history started to decrease in 2017 (Li et al., 2019), the use of HCFC-141b as a transient tracer for “young” waters become complicated. All these indicate that HCFC-141b has a probably limited ability as a transient tracer in the future.

HCFC-142b. The confidence of the atmospheric history and seawater solubility function is similar to those of HCFC-141b for the same reasons. HCFC-142b has been measured on some cruises (Lobert et al., 1996; Yvon-Lewis et al., 2008) and also in this study, rendering us to determine that it is highly feasible to measure this compound. We have medium confidence in our ability to estimate the stability of HCFC-142b because of slightly higher than the expected concentrations in the interior ocean (Fig. 10), lower than expected mean ages particularly in the Atlantic Water Layer (Fig. 11), and its surface saturation similar to those of CFC-12/SF₆ in seawater. The input function of HCFC-142b is different

from those of most other tracers (only similar to that of HCFC-141b but with a longer time range). Consequently, HCFC-142b has currently good potential to be used as a transient tracer.

HFC-134a. We judge that we have high and medium confidences in the atmospheric history and seawater solubility function (Li et al., 2019), respectively. Although the estimated seawater solubility function was constructed based on the modeled salting-out coefficients and the experimental freshwater solubility (Li et al., 2019) that matched both the observations (Deeds, 2008) and model results (Abraham et al., 2001), we have only medium confidence in the seawater solubility function due to the lack of experimental seawater solubility data. HFC-134a was measured in Ooki and Yokouchi (2011) by GC-MS and in this study by the Medusa-Aqua system, so we consider medium feasibility for measurements in this study due to higher than expected concentrations (see Sect. 5.4). We have only poor knowledge of the stability of HFC-134a because its higher than expected surface saturation (Table 5) and concentration (Fig. 10), as well as lower than expected mean ages (Fig. 11) don't suggest degradation. The compound is not identified as unstable (see Sect. 5.4), but its stability is still largely unknown considering the issues on seawater solubility function and/or measurements. Besides, HFC-134a can only be considered as a tracer for “young” waters due to its short atmospheric history. Based on all these discussions, HFC-134a has a lower possibility than HCFC-142b but a higher possibility than HCFC-22 to be an oceanic transient tracer.

HFC-125. Concentrations of HFC-125 in the early 1990s in the atmosphere are unclear (Fig. 3), possibly related to uncertainties in the reconstruction, although this only marginally influences its ability as a transient tracer. Overall, we consider the knowledge of its reconstructed atmospheric history to be of high confidence (Li et al., 2019). Three seawater solubility functions of HFC-125 can be constructed (Li et al., 2019), although only two of them were considered; function 1 is supported by freshwater solubility results from Deeds (2008) as well as stability analysis based on comparison to CFC-12 in this study (Fig. 10), whereas the observations and model results from Abraham et al. (2001) supported function 3. Besides, we found under-saturated waters in the Mediterranean Sea but over-saturated waters in the Baltic Sea for HFC-125 (Table 5). All these lead to poor certainty about the seawater solubility function of HFC-125, and we mark it to be of low confidence. We also evaluate the feasibility to measure HFC-125 as low since this compound has been measured in this study for the first time in seawater, and we find almost no vertical gradient (Fig. 9), which is unexpected. Furthermore, observed HFC-125 concentrations in freshwater are inconsistent as indicated by three freshwater solubility functions (Li et al., 2019), which suggests unresolved issues with its measurements in water. Due to the poorly defined solubility and difficulties in measurement, it is difficult to assess the stability of HFC-125 in this work. The low mean ages compared to those estimated from CFC-12 and SF₆ (Fig. 11) do not support using HFC-125 as a tracer, and in any case, HFC-125 can only be a tracer for “young” water due to its short atmospheric history. Therefore, we consider that HFC-125 has currently low potential as a transient tracer in the ocean due to the poorly constrained solubility and stability, possible problems in seawater measurements and the lower than

expected mean ages. This might be remedied by constructing the experimental seawater solubility function and solving possible measurement issues.

HFC-23. HFC-23 could not be reliably measured in our system due to unstable non-zero blanks (see Sect. 4.4). Therefore, we can, obviously, not reliably assess the stability of HFC-23 in seawater, and we have low confidence in the feasibility of the measurements, although the blank problem might possibly be solved by a different instrument configuration. The atmospheric history of HFC-23 has been constructed (Li et al., 2019; Simmonds et al., 2018), but we have only medium confidence as it does not start from zero (Simmonds et al., 2018) due to limited data. Our ability to estimate the seawater solubility function was marked as medium confidence for the same reason as for HFC-134a. That is, the freshwater solubility function matched results from Deeds (2008) and Abraham et al. (2001) but the seawater solubility function was not constructed by experimental seawater solubility data. In consequence, unknown stability and current issues with measurements lead to an overall assessment that HFC-23 has a low potential as a transient tracer in the ocean at this moment.

PFC-14 and PFC-116. The increasing atmospheric histories of PFC-14 and PFC-116 (high confidence) have been established (Li et al., 2019; Trudinger et al., 2016). Also, the seawater solubility functions were constructed, although we have only medium and low confidences for PFC-14 and PFC-116, respectively. Our confidence for PFC-14 is higher than for other compounds with medium confidence as it matches both seawater measurements (Scharlin and Battino, 1995) and freshwater solubility (Abraham et al., 2001; Clever et al., 2005). In contrast, low confidence for PFC-116 was attributed to its freshwater solubility only matching that from Deeds (2008) but not the theoretical assessment from Abraham et al. (2001). PFC-14 and PFC-116 are very stable in the environment, but can't easily be measured in seawater because of the low solubility (Li et al., 2019), i.e. low concentration in seawater. The high stability and long atmospheric histories make PFCs potentially promising transient tracers in the ocean, although it is challenging to measure these compounds.

Based on all the above discussions, HCFC-22 is unlikely to be a transient tracer in warm waters. HFC-23 can't be identified as a transient tracer because of lacking too much information on the four aspects. On the other hand, these two compounds can be replaced by SF₆ that has similar atmospheric histories (Fig. 2 and Fig. 3). Since SF₆ is a mature transient tracer, we will no longer consider the use of HCFC-22 and HFC-23. HCFC-141b and HCFC-142b can be used currently as transient tracers. Considering their similar atmospheric history and the decreasing atmospheric history of HCFC-141b, HCFC-142b can be further evaluated as a transient tracer by obtaining more reliable solubility and stability information in seawater. HFC-134a and HFC-125 can't be identified as transient tracers; the former because of higher than expected concentrations pointing to issues on the seawater solubility function and/or the measurements; the latter due to the lack of information on solubility, stability, and feasibility of measurement in seawater. Considering the similar atmospheric histories of HFC-134a and HFC-125, HFC-134a is a more promising candidate as a transient tracer. Last but not least, PFC-

14 and PFC-116 can be used as transient tracers in the future (medium confidence) once their measurement in seawater is resolved. Currently, HCFC-142b and HCFC-141b are better choices as transient tracers.

7 Conclusions

This study, combined with the study by Li et al. (2019), provides a method to identify and evaluate if a compound is suitable for use as a transient tracer in the ocean. HCFCs, HFCs and PFCs were selected for evaluation as potential replacements for CFCs. The evaluation mainly considered four aspects: input function (including atmospheric history and historical surface saturation), seawater solubility, feasibility of measurement and stability in seawater. We also considered how Medusa tracers with different atmospheric histories complement each other when constraining ocean ventilation, whereas tracers with similar input functions provide little additional information. For these purposes, we modified an existing analytical system for seawater measurements and observed the seawater concentrations of HCFC-22, HCFC-141b, HCFC-142b, HFC-134a, and HFC-125. Unfortunately, the poorly soluble PFCs could not be successfully measured with our current analytical system.

The atmospheric histories, combined with historical surface saturations, form the input functions. The atmospheric histories have been reconstructed in our last study (Li et al., 2019), and the historical surface saturation in the Mediterranean Sea was determined to be a constant 94 % based on historical tracer observations.

The seawater solubility functions have been constructed by Li et al. (2019) by combining experimental freshwater solubility data and a model on the salting-out effect. However, the results from this study identify questions for some of the evaluated compounds, in particular for HFC-125, so that seawater solubility functions constructed based on experimental seawater solubility data are needed.

Measurements of CFC-12 by the Medusa-Aqua system were compared to observations by an onboard, well-described analytical system. Based on the reasonable correlation between CFC-12 observations from the two systems, we conclude that HCFC-141b, HCFC-142b, and possibly HFC-125, are probably stable in seawater, whereas there are indications of slow degradation of HCFC-22 in warm seawater. We were not able to estimate the stability of HFC-134a. Although based on the observations from this study, there are strong indications that the PFCs are stable in seawater.

By comprehensive evaluation of these aspects, HCFC-142b and HCFC-141b are found to be the most promising novel oceanic transient tracers currently since they fulfill several essential requirements by virtue of well-documented atmospheric history, established seawater solubility, feasible measurements, and inertness in seawater. However, more information on seawater solubility and stability (especially biodegradation) is needed to further assess their ability as transient tracers in seawater. Furthermore, HCFC-142b and HCFC-141b will likely only work as transient tracers for the

next few years/decades considering the restrictions on their production and consumption imposed by the Montreal Protocol, and their (future) decreasing atmospheric mole fractions (Li et al., 2019).

The compounds that have the greatest potential as oceanic transient tracers in the future are PFC-14 and PFC-116 because of their high stability in seawater, the long and well-documented atmospheric concentration histories and well-constructed seawater solubility functions (Li et al., 2019). This view is also supported by the work of Deeds et al. (2008). The challenge is how to measure the PFCs accurately due to their low concentrations. Possible ways forward are to modify the Medusa system according to Arnold et al. (2012) to improve the sensitivity for PFC-14 (CF₄) and try field measurements using the vacuum-sparging method by Law et al. (1994) to improve the speed of gas extraction.

For other tracers, HFC-134a needs to be further evaluated as a transient tracer by adding more reliable information on stability and solubility in seawater and measurement feasibility, whereas HCFC-22, HFC-125 and HFC-23 can no longer be considered as oceanic transient tracers due to one or more reasons, such as unconstrained solubility functions, seawater instability, and measurement problems, and should be replaced by mature or better tracers having similar atmospheric history.

Data availability

Cruises data on historical surface saturation of CFC-12 and SF₆ in the Mediterranean Sea (Sect. 5.1) are from https://www.nodc.noaa.gov/ocads/oceans/Coastal/Meteor_Med_Sea.html. Observations of CFC-12 and SF₆ measured by the PT-GC-ECD and observations of CFC-12, HCFC-22, HCFC-141b, HCFC-142b, HFC-134a and HFC-125 measured by the Medusa-Aqua system in seawater from cruise MSM72 are shown in Table S1.

Author contributions

TT conducted the sampling. PL developed the instrument and carried out the measurements. PL interpreted the data and analyzed the results based on the discussion with TT. PL wrote the paper with contributions from TT.

Competing interests

The authors declare that they have no conflict of interest.

Acknowledgments

We acknowledge the great support by the captain, crew, and scientists from expeditions MSM18/3, MSM23, M130, NORC2017-09, KBP523, KBP524, MSM72 and AL516 for the development of the Medusa-Aqua system. Special thanks go to Boie Bogner and Tim Steffens for their technical support on the instrument Medusa-Aqua system; Tim Steffens, Dr. Dennis Booge, Melf Paulsen, and Li Zhou

for taking samples from the cruise AL516 in the Baltic Sea; Prof. Minggang Cai, Dr. Peng Huang, and Weimin Wang for supporting the sampling at sea on the cruise NORC2017-09 in the Western Pacific Ocean. This research was supported by the GEOMAR Innovationsfonds Technologie-Seed-Funding (Transient Tracers 70090/03) and the China/Germany Joint Research Programme (Programm des Projektbezogenen Personenaustauschs, PPP, D1820) supported by the Deutscher Akademischer Austausch Dienst (DAAD) in Germany. The authors also gratefully acknowledge support through the scholarship program from the China Scholarship Council (CSC).

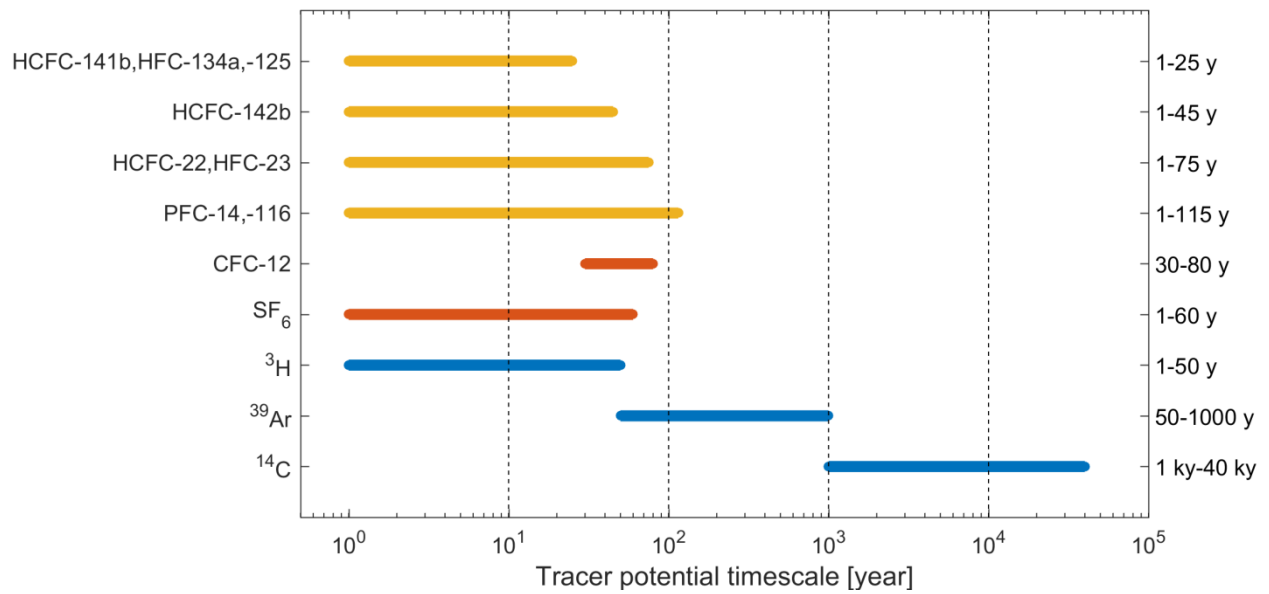


Figure 1. Seawater timescales (“tracer age ranges”) of halogenated compound dating using potential chronological transient tracers (selected HCFCs, HFCs, and PFCs, orange) as well as traditional chronological transient tracers (CFC-12 and SF₆, red) combined with radioisotope dating using radioactive transient tracers (³H, ³⁹Ar, and ¹⁴C, blue). Tracer age ranges of chronological transient tracers are estimated from Fig. 3 (see below), while tracer age ranges of radioactive transient tracers are from Aggarwal (2013).

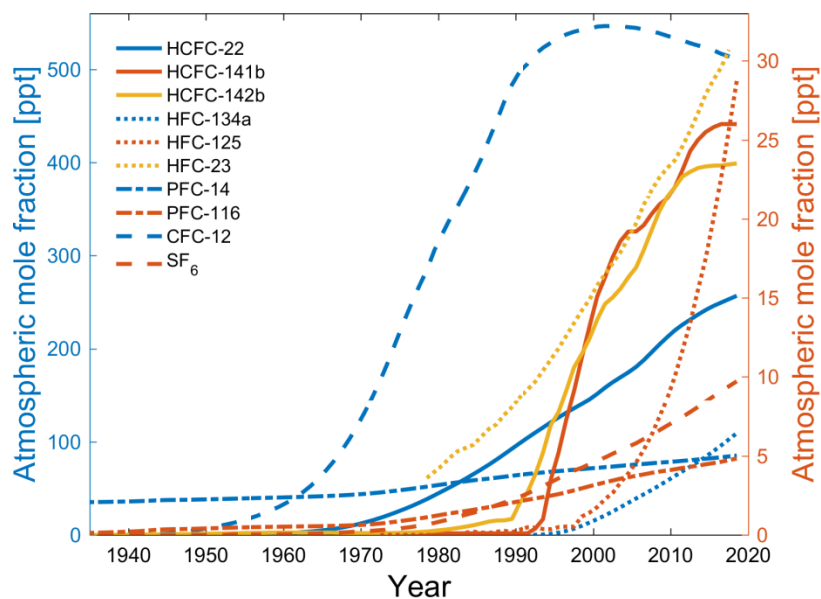


Figure 2. Atmospheric histories of HCFC-22, HCFC-141b, HCFC-142b, HFC-134a, HFC-125, HFC-23, PFC-14, PFC-116, CFC-12 and SF₆ in the Northern Hemisphere. HCFC-22, HFC-134a, PFC-14, and CFC-12 share the left y-axis scale; other compounds share the right y-axis scale.

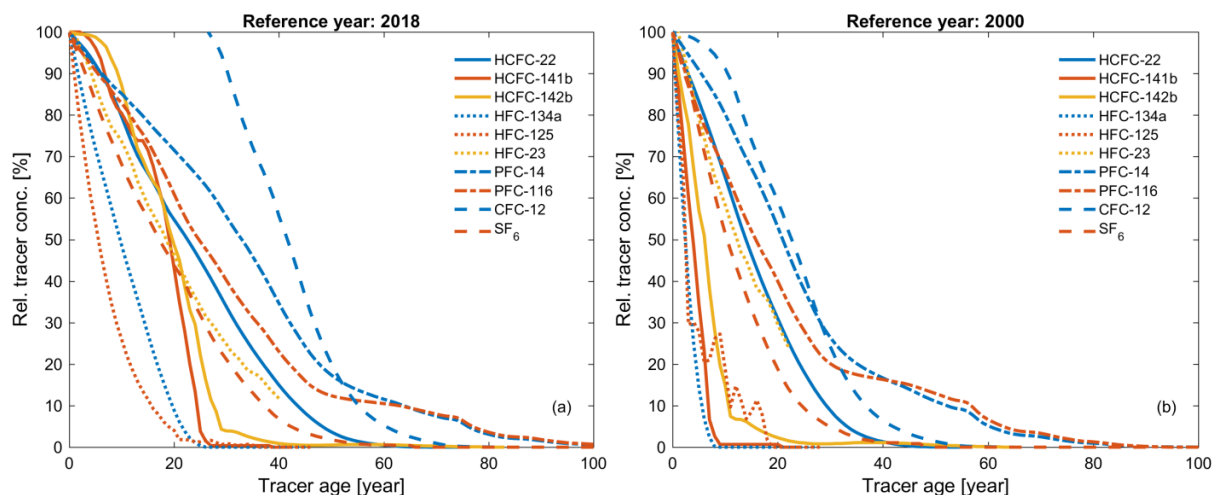


Figure 3. Relative tracer concentrations in percent (i.e. normalized to the contemporaneous atmospheric concentrations) and corresponding tracer age for HCFC-22, HCFC-141b, HCFC-142b, HFC-134a, HFC-125, HFC-23, PFC-14, PFC-116, CFC-12, and SF₆ in the Northern Hemisphere. Reference year: (a) 2018 and (b) 2000.

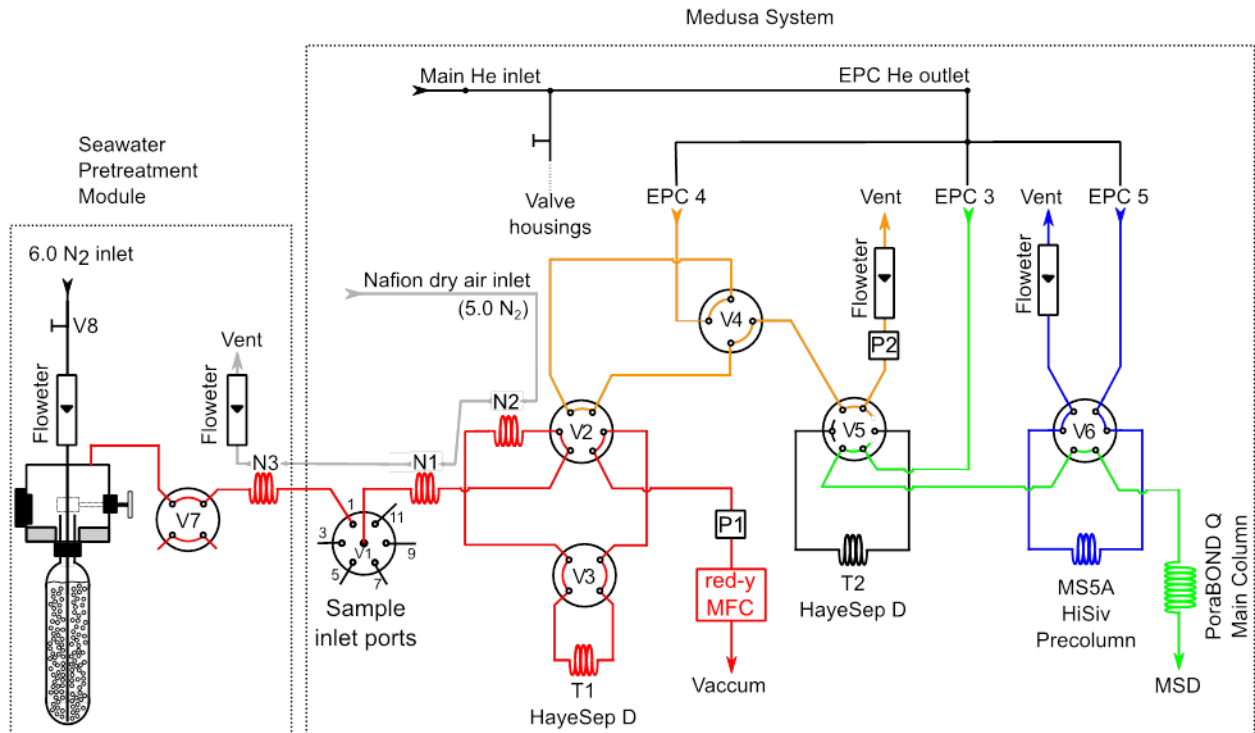


Figure 4. Medusa-Aqua system flow scheme. The Medusa system remains identical to that given by Miller et al. (2008). The seawater pretreatment module is added to degas the samples from gaseous tracers before injecting into Medusa. Electronic Pressure Controllers (EPC3, EPC4, and EPC5) supply helium throughout the system. The Mass Flow Controller (MFC) used to measure the sample volume downstream of Trap 1 (T1), was not used in this study. The cryogenic packing materials are 200 mg of 100/120 mesh HayeSep D (HSD) for Trap 1 (T1) and 5.5 mg of HSD adsorbent for Trap 2 (T2).

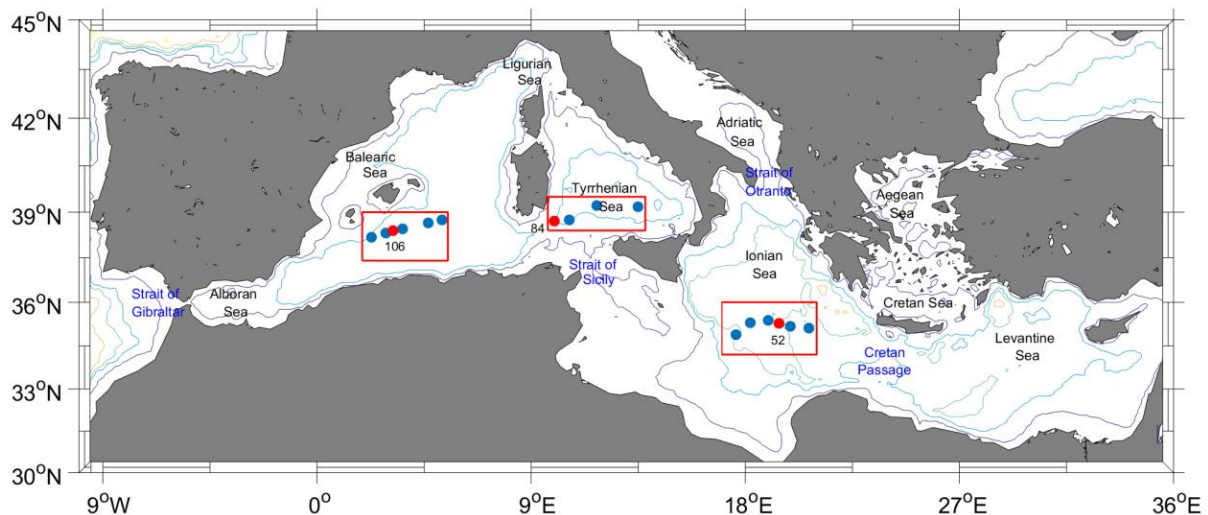


Figure 5. Sampling sites distributed in the Mediterranean Sea from the cruise MSM72 in three areas: the Southern Ionian Sea (SIS), the Tyrrhenian Sea (TS) and the Western Mediterranean Sea (WMS). Sampling sites in red solid circles indicate samples measured by the Medusa-Aqua system for HCFCs, HFCs, PFCs and CFC-12, blue solid circles were for CFC12 and SF₆ measured by the PT-GC-ECD. The depth contours are 500 m, 2000 m, 3000 m, 4000 m, 5000 m, and 6000 m.

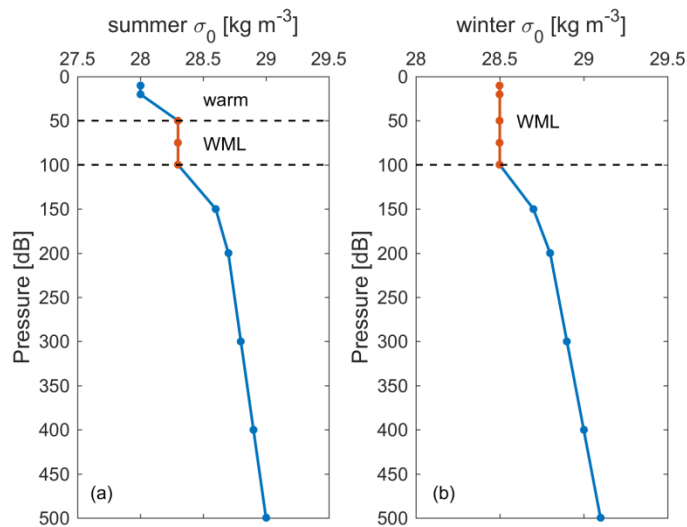


Figure 6. Example of the winter mixed layer (WML) depth (marked as red) determined in (a) summer and (b) winter in potential density (σ_0) profiles especially for historical surface saturation calculation.

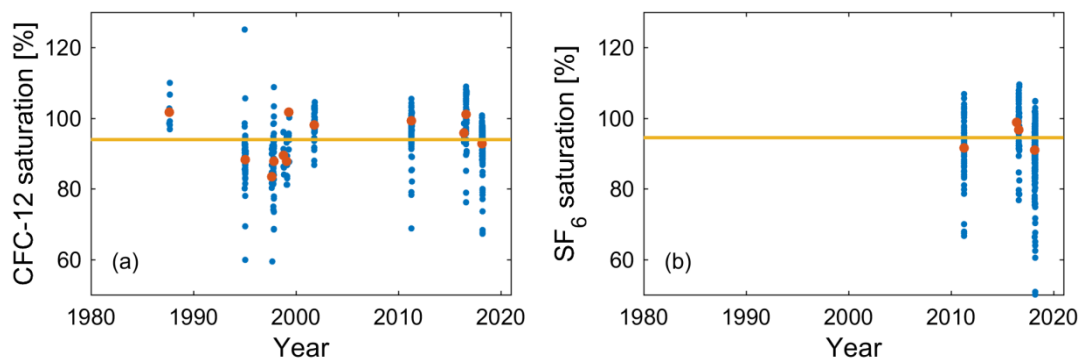


Figure 7. Historical surface saturations in winter mixed layers (blue solid circles) for (a) CFC-12 from 12 cruises in 1987-2018 and (b) SF₆ from 4 cruises in the Mediterranean Sea. In addition to the data from Schneider et al. (2014), data from the cruises CRELEV2016 and TALPro2016 in 2016 and MSM72 in 2018 (Li and Tanhua, in preparation) were added. Red solid circles denote the means of seawater saturation for each cruise. Orange lines (94 %) are the means of averaged seawater saturation of every cruise.

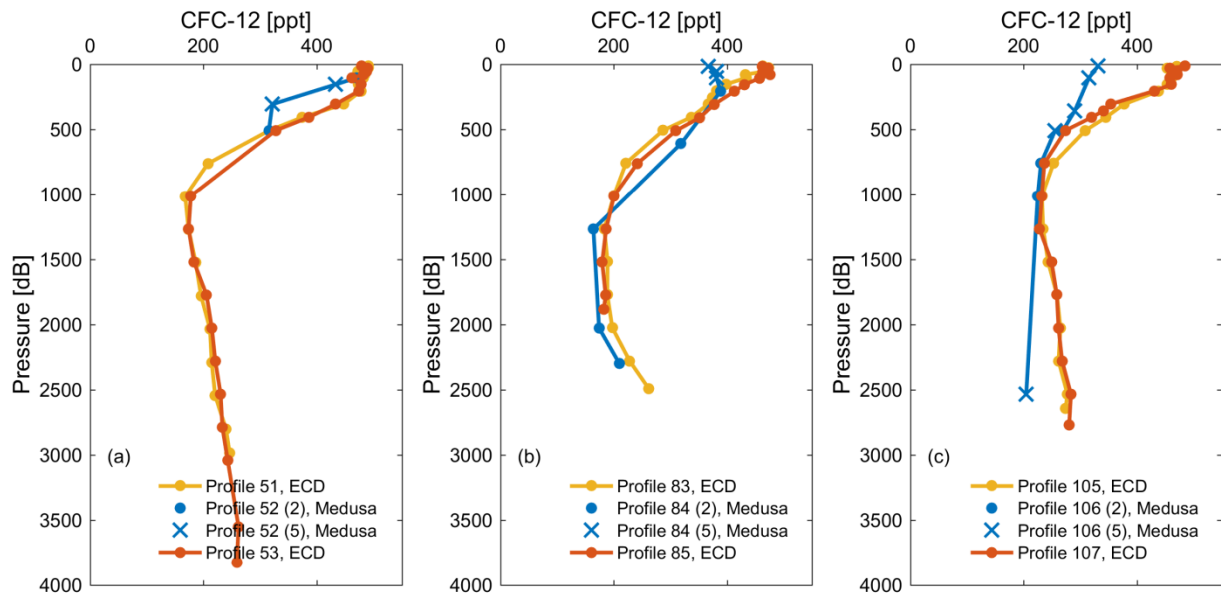


Figure 8. Comparison of CFC-12 observations from cruise MSM72 measured by the onboard PT-GC-ECD (ECD) and the Medusa-Aqua system (Medusa) in three areas: (a) the Southern Ionian Sea, (b) the Tyrrhenian Sea and (c) the Western Mediterranean Sea. We used normal quality control routines and flagged outliers as probably bad (“3” in Table S1), which are not further considered. One more step was done to compare the Medusa-Aqua system observations with those from the PT-GC-ECD; if the Medusa-CFC-12 values are inconsistent with the CFC-12 values from PT-GC-ECD measurements, they were flagged “5” in Table S1 indicating a possible issue during the sampling or measurement process; if they are consistent, they were flagged “2” representing good data. In the following plots, we show all data with a quality flag of “2 (dots)” or “5 (crosses)”.

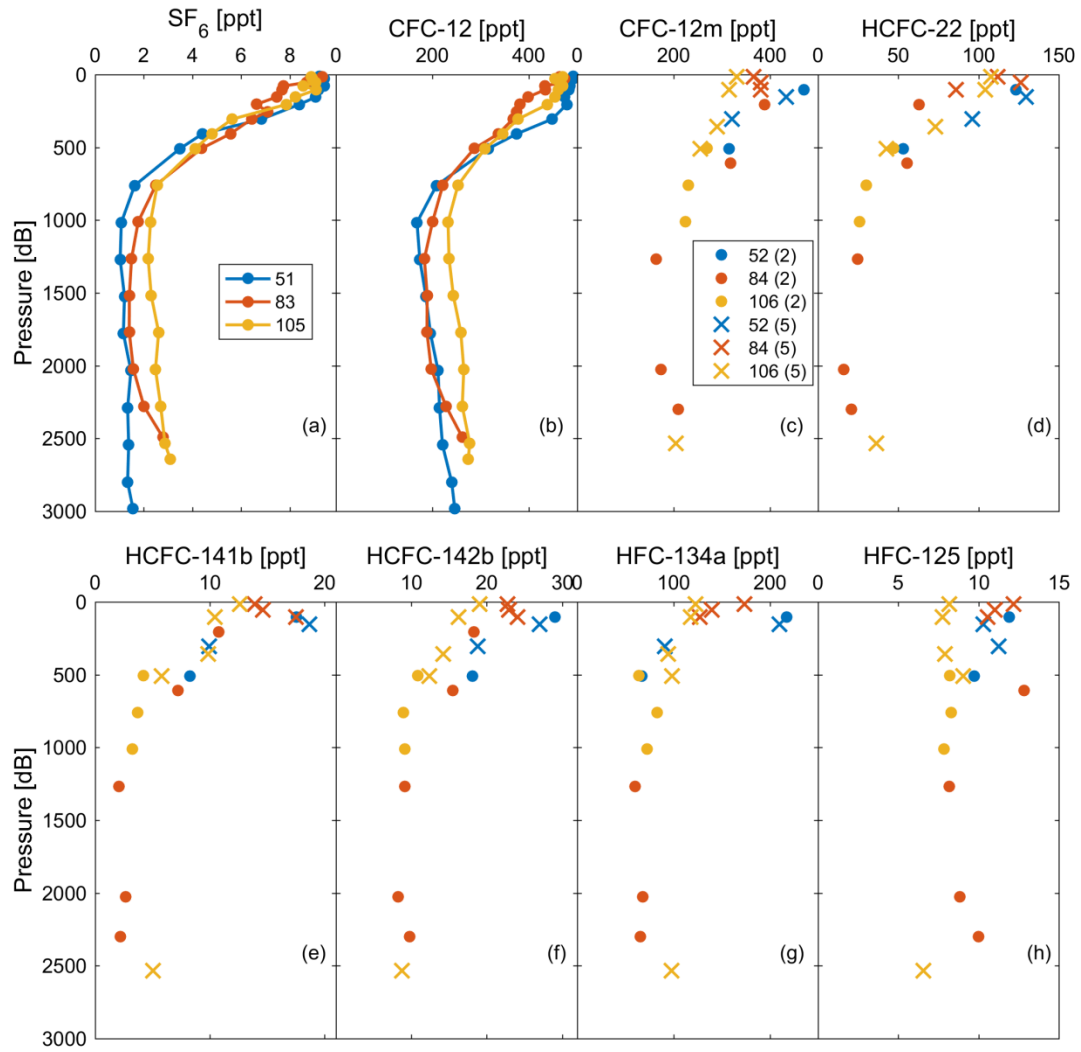


Figure 9. Observations of (a) SF₆ and (b) CFC-12 in profiles 51, 83 and 105 measured by the PT-GC-ECD and (c) CFC-12 (marked as CFC-12m), (d) HCFC-22, (e) HCFC-141b, (f) HCFC-142b, (g) HFC-134a and (h) HFC-125 in profiles 52, 84 and 106 measured by the Medusa-Aqua system. For the explanation of (2), (5), dots and crosses, refer to Fig. 8.

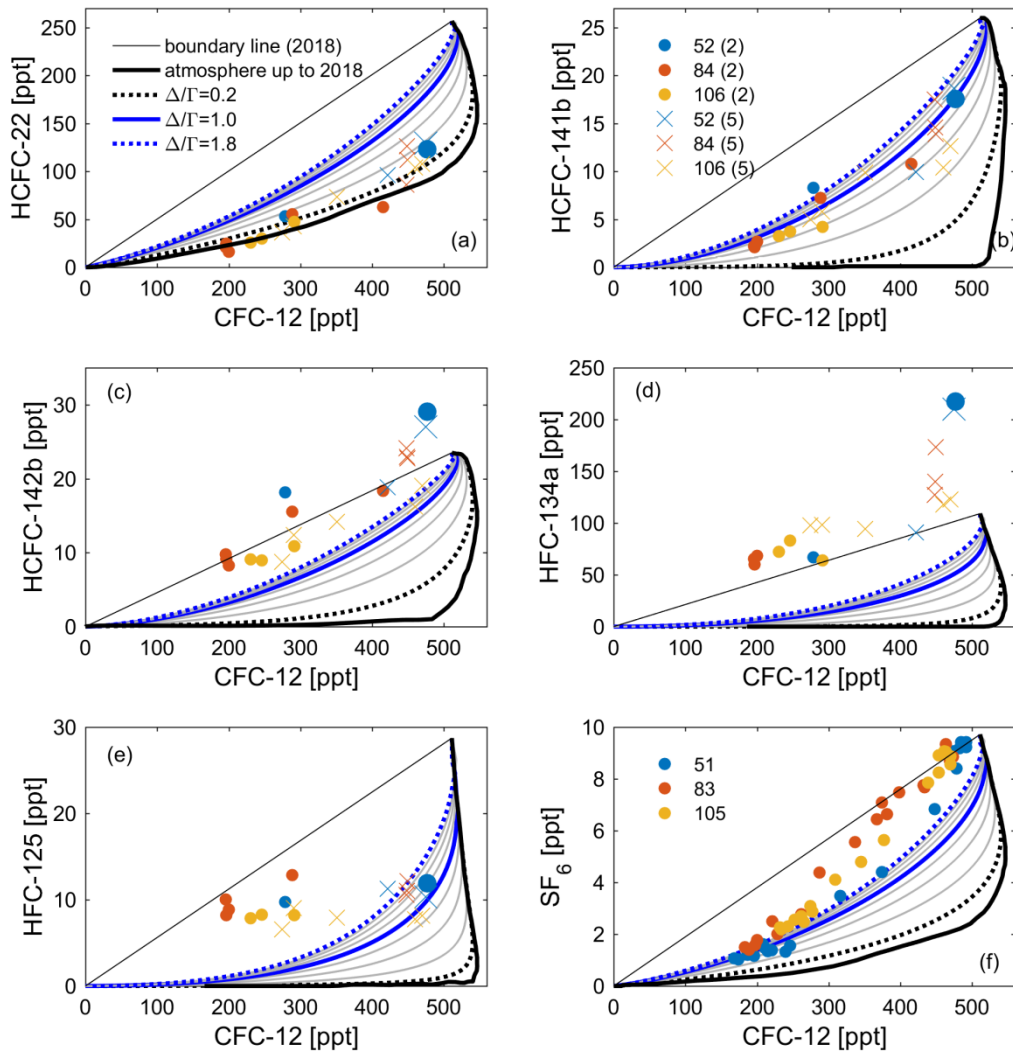


Figure 10. Observations of (a) HCFC-22, (b) HCFC-141b, (c) HCFC-142b, (d) HFC-134a and (e) HFC-125 in profiles 52, 84 and 106 measured by the Medusa-Aqua system and (f) SF₆ in profiles 51, 83 and 105 measured by the PT-GC-ECD plotted against the (interpolated) CFC-12 based on measurements by the PT-GC-ECD. The thick black line is the atmospheric history of the tracer pair ($\Delta/\Gamma = 0.0$) and the thin black line is the theoretical mixing line between contemporary and pre-industrial concentrations. The lines with $\Delta/\Gamma = 0.2$ – 1.8 based on IG-TTD have also been added. The values of the top two points of profile 52 are marked with a bigger size to identify the samples in shallow layers. For the explanation of (2), (5), dots and crosses, refer to Fig. 8.

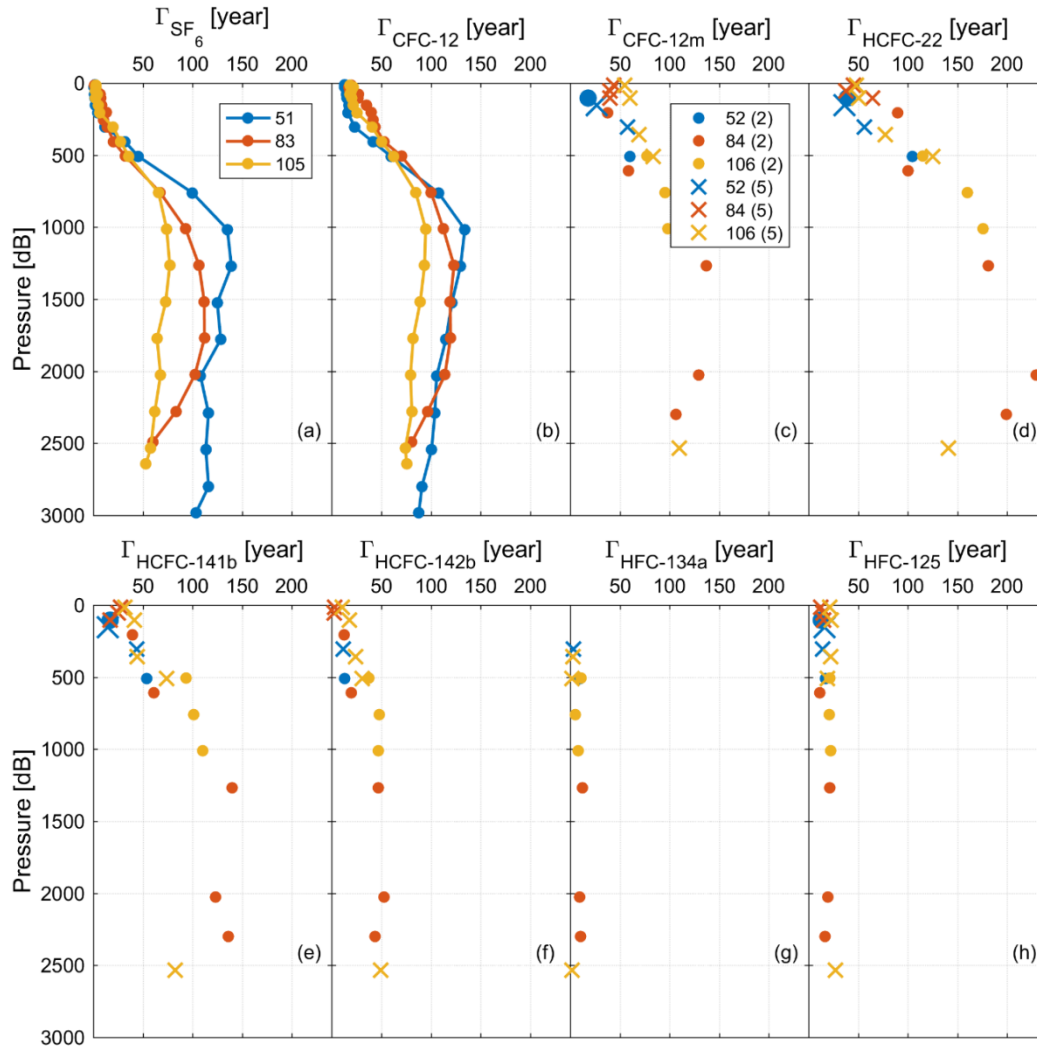


Figure 11. Mean age estimated from (a) SF_6 and (b) CFC-12 in profiles 51, 83 and 105 and (c) CFC-12 (marked as CFC-12m), (d) HCFC-22, (e) HCFC-141b, (f) HCFC-142b, (g) HFC-134a and (h) HFC-125 in profiles 52, 84 and 106 based on $\Delta/\Gamma = 1.0$ of IG-TTD. The values of the top two points of profile 52 are marked with a bigger size. For the explanation of (2), (5), dots and crosses, refer to Fig. 8.

Table 1. Total lifetimes, partial atmospheric lifetimes with respect to oceanic uptake and ocean contributions for HCFC-22, HCFC-141b, HCFC-142b, HFC-134a, HFC-125, HFC-23, PFC-14 and PFC-116

Species	Total lifetime ^a (years)	Partial atmospheric lifetimes with respect to oceanic uptake (years) (Yvon-Lewis and Butler, 2002)	Ocean contributions ^b (%)
HCFC-22	11.9	1,174	1
HCFC-141b	9.4	9,190	0.1
HCFC-142b	18	122,200	0.01
HFC-134a	14	5,909	0.2
HFC-125	31	10,650	0.3
HFC-23	228		
PFC-14	>50 000	low solubility	
PFC-116	>10,000	low solubility	

^a Total lifetime includes tropospheric OH and Cl atom reaction and photolysis loss, stratospheric loss due to reaction (OH and O(¹D)) and photolysis, and ocean and soil uptake as noted in the table, data from SPARC (2013); ^b Based on the calculation method in Huhn et al. (2001).

Table 2. Review on biodegradation of selected HCFCs and HFCs in freshwater or soil

Microorganisms or culture	HCFC-22	HCFC-141b	HCFC-142b	HFC-134a	HFC-125	HFC-23	References
Methanotrophic bacterium <i>Methylosinus trichosporium OB3b</i> (pure culture)		√ ^a	x ^b	x			(DeFlaun et al., 1992) (Streger et al., 1999)
Mixed methanotrophic culture (MM1) with many heterotrophs	√		√	√			(Chang and Criddle, 1995)
Cell suspensions of <i>M. capsulatus</i> , methanotrophs in natural assemblages	√						(Oremland, 1996)
Methanotrophic mixed culture ENV2040		x	x				(Streger et al., 1999)
Unidentified methanotroph ENV2041		x	x	x			(Streger et al., 1999)
Propane-oxidizing bacteria, <i>M. vaccae</i> JOB5	x	√ (0.1 μmol h ⁻¹)	√	x	x	x	(Streger et al., 1999)
Methylococcus capsulatus (Bath)	√						(Matheson et al., 1997)
Aerobic condition closed bottle tests		x		x	x		(Berends et al., 1999)
Anoxic sediments		√					(Oremland, 1996)
Landfill soil	√ ^c	x		x			(Scheutz et al., 2004)
Anaerobic conditions in sewage sludge and aquifer sediment slurries	x	x	x	x			(Balsiger et al., 2005)

^a √: Biodegradation in freshwater/soil; ^b x: No biodegradation in freshwater/soil; ^c In the oxidative zone.

Table 3. Selected Medusa-Aqua analytes, calibration scales and errors in standard gas, detection limits and precision of seawater measurements

Industrial name (abbreviation)	Chemical formula	Full name	Standard scale	Calibrated errors of the standard gas (%)	Detection limit (fmol kg ⁻¹)	Precision ^a (%)
SF ₆	SF ₆	sulfur hexafluoride	SIO-05	0.37	0.48	--
CFC-12	CCl ₂ F ₂	dichlorodifluoromethane	SIO-05	0.08	29.83	0.4
HCFC-22	CHClF ₂	chlorodifluoromethane	SIO-05	0.22	13.75	3.1
HCFC-141b	CH ₂ CCl ₂ F	1,1-dichloro-1-fluoroethane	SIO-05	0.20	4.01	6.1
HCFC-142b	CH ₃ CClF ₂	1-chloro-1,1-difluoroethane	SIO-05	0.21	3.24	1.8
HFC-134a	CH ₂ FCF ₃	1,1,1,2-tetrafluoroethane	SIO-05	0.21	7.31	9.7
HFC-125	CHF ₂ CF ₃	pentafluoroethane	SIO-14	0.23	1.19	2.0
HFC-23	CHF ₃	fluoroform	SIO-07	0.49	6.71	--
PFC-14	CF ₄	carbon tetrafluoride	SIO-05	0.30	0.44	--
PFC-116	CF ₃ CF ₃	hexafluoroethane	SIO-07	0.32	1.41	--

^a Precision (reproducibility, 1 σ) of tracers in seawater was determined by samples at 23.5 dbar from cruise AL516 in the Baltic Sea in September 2018.

Table 4. Comparison of instrument performance measuring CFC-12

System	Medusa-Aqua system	PT-GC-ECD	PT-GC-ECD
Instrument	Cracker-Medusa-GC-MS	Syringe-PT-GC-ECD	Cracker-PT-GC-ECD
Workplace	Laboratory in Kiel	Onboard	Laboratory in Kiel
Purging efficiency (%)	99.5 \pm 0.5 ^a	99.2 \pm 3.6 ^b	99.6 \pm 0.1 ^c
Precision (%)	0.4	0.3	1.4
Sampling volume (L)	~1.3	~0.3	~0.3
Measured compound	CFCs, HCFCs, HFCs, PFCs, etc.	CFC-12, SF ₆ , SF ₅ CF ₃	CFC-12, SF ₆ , SF ₅ CF ₃

^a After purging three times; ^b After purging once; ^c After purging twice.

Table 5. Seawater surface saturations (%) of SF₆ and CFC-12 in profiles 83 and 105 from cruise MSM72 (measured onboard with the PT-GC-ECD system) and CFC-12, HCFC-22, HCFC-141b, HCFC-142b, HFC-134a, and HFC-125 in profiles 84 and 106 from cruise MSM72 and in profile 30 from cruise AL516 (measured in the laboratory in Kiel with the Medusa-Aqua system).

	PT-GC-ECD				Medusa-Aqua system							
	Profile	Pressure (dbar)	SF ₆	CFC- 12	Profile	Pressure (dbar)	CFC- 12	HCFC- 22	HCFC- 141b	HCFC- 142b	HFC- 134a	HFC- 125
MSM72	83	13.4	97	91	84	14.7	72	44	54	97	163	44
	105	14.3	92	92	106	14.0	65	42	49	82	115	30
AL516					30	1.6	132	68	61	115	150	287
					30	23.5	118	79	84	112	105	218
					30	23.5	117	83	77	115	120	250

Table 6. Evaluating the stability of selected HCFCs and HFCs based on seawater measurements in relation to observations of CFC-12

Compound	Surface saturation	Location in the stability area	Mean age in relation to CFC-12
HCFC-22	Low	Low	High
HCFC-141b	Low	Within area	Slightly high
HCFC-142b	As expected	Slightly high	Low
HFC-134a	High	High	Low
HFC-125	Low and high ^a	Within area	Low

^a HFC-125 has low saturations in the Mediterranean Sea but high saturations in the Baltic Sea.

Table 7. Evaluating the possibilities of selected HCFCs, HFCs and PFCs as transient tracers in the ocean from four aspects

Compound	Atmospheric history	Solubility in seawater	Feasibility of measurement in seawater	Stability in seawater	Possibility to be transient tracer
CFC-12	*** ^a	***	***	***	***
HCFC-22	***	**	***	**	**
HCFC-141b	***	*	***	**	**
HCFC-142b	***	*	***	**	**
HFC-134a	***	**	**	*	*
HFC-125	***	*	*	*	*
HFC-23	**	**	*	*	*
PFC-14	***	**	*	***	**
PFC-116	***	*	*	***	**

^a The total number of (black and red) stars represent current knowledge: one star means “largely unknown”, two stars “reasonably well resolved” and three stars “well documented or resolved”; the number of black stars represents the ability of a compound as an oceanic transient tracer through current assessments.

References

- Abraham, M. H., Gola, J. M., Cometto-Muñiz, J. E., and Cain, W. S.: Solvation properties of refrigerants, and the estimation of their water-solvent and gas-solvent partitions, *Fluid Phase Equilib.*, 180, 41–58, [https://doi.org/10.1016/S0378-3812\(00\)00511-2](https://doi.org/10.1016/S0378-3812(00)00511-2), 2001.
- Aggarwal, P. K.: *Isotope Methods for Dating Old Groundwater*, edited by: Suckow, A., Aggarwal, P., and Araguas-Araguas, L., International Atomic Energy Agency, Vienna, 357 pp., 2013.
- Arnold, T., Mühle, J., Salameh, P. K., Harth, C. M., Ivy, D. J., and Weiss, R. F.: Automated Measurement of Nitrogen Trifluoride in Ambient Air, *Anal. Chem.*, 84, 4798–4804, <https://doi.org/10.1021/ac300373e>, 2012.
- Balsiger, C., Holliger, C., and Höhener, P.: Reductive dechlorination of chlorofluorocarbons and hydrochlorofluorocarbons in sewage sludge and aquifer sediment microcosms, *Chemosphere*, 61, 361–373, <https://doi.org/10.1016/j.chemosphere.2005.02.087>, 2005.
- Berends, A., De Rooij, C., Shin-Ya, S., and Thompson, R.: Biodegradation and ecotoxicity of HFCs and HCFCs, *Arch. Environ. Contam. Toxicol.*, 36, 146–151, <https://doi.org/10.1007/s002449900454>, 1999.
- Beyer, M., van der Raaij, R., Morgenstern, U., and Jackson, B.: Potential groundwater age tracer found: Halon-1301 (CF₃Br), as previously identified as CFC-13 (CF₃Cl), *Water Resour. Res.*, 50, 7318–7331, <https://doi.org/10.1002/2014WR015818>, 2014.
- Booge, D.: FS Alkor Cruise Report, Cruise AL516, 2018.
- Bullister, J., and Weiss, R.: Determination of CCl₃F and CCl₂F₂ in seawater and air, *Deep Sea Res. Part A. Oceanogr. Res. Pap.*, 35, 839–853, [https://doi.org/10.1016/0198-0149\(88\)90033-7](https://doi.org/10.1016/0198-0149(88)90033-7), 1988.
- Bullister, J., and Tanhua, T.: Sampling and measurement of chlorofluorocarbon and sulfur hexafluoride in seawater, *GO-SHIP (Unesco/IOC)*, 1–11, 2010.
- Bullister, J. L., and Lee, B. S.: Chlorofluorocarbon-11 removal in anoxic marine waters, *Geophys. Res. Lett.*, 22, 1893–1896, <https://doi.org/10.1029/95GL01517>, 1995.
- Bullister, J. L., Wisegarver, D. P., and Menzia, F. A.: The solubility of sulfur hexafluoride in water and seawater, *Deep-Sea Res. Pt. I*, 49, 175–187, [https://doi.org/10.1016/S0967-0637\(01\)00051-6](https://doi.org/10.1016/S0967-0637(01)00051-6), 2002.
- Bullister, J. L., Wisegarver, D. P., and Sonnerup, R. E.: Sulfur hexafluoride as a transient tracer in the North Pacific Ocean, *Geophys. Res. Lett.*, 33, L18603, <https://doi.org/10.1029/2006GL026514>, 2006.
- Bullister, J. L., and Wisegarver, D. P.: The shipboard analysis of trace levels of sulfur hexafluoride, chlorofluorocarbon-11 and chlorofluorocarbon-12 in seawater, *Deep-Sea Res. Pt. I*, 55, 1063–1074, <https://doi.org/10.1016/j.dsr.2008.03.014>, 2008.
- Bullister, J. L.: Atmospheric Histories (1765-2015) for CFC-11, CFC-12, CFC-113, CCl₄, SF₆ and N₂O, NDP-095, 1–23, https://doi.org/10.3334/CDIAC/otg.CFC_ATM_Hist_2015, 2015.

- Butler, J. H., Yvon-Lewis, S. A., Lobert, J. M., King, D. B., Montzka, S. A., Bullister, J. L., Koropalov, V., Elkins, J. W., Hall, B. D., and Hu, L.: A comprehensive estimate for loss of atmospheric carbon tetrachloride (CCl₄) to the ocean, *Atmos. Chem. Phys.*, 16, 10899–10910, <https://doi.org/10.5194/acp-16-10899-2016>, 2016.
- Carpenter, L. J., Reimann, S., Burkholder, J. B., Clerbaux, C., Hall, B. D., Hossaini, R., Laube, J. C., and Yvon-Lewis, S. A.: Scientific Assessment of Ozone Depletion: 2014, World Meteorological Organization Geneva, 1.1–5.58, 2014.
- Chang, W.-k., and Criddle, C. S.: Biotransformation of HCFC-22, HCFC-142b, HCFC-123, and HFC-134a by methanotrophic mixed culture MM1, *Biodegradation*, 6, 1–9, <https://doi.org/10.1007/BF00702293>, 1995.
- Cicerone, R. J.: Atmospheric carbon tetrafluoride: A nearly inert gas, *Science*, 206, 59–61, <https://doi.org/10.1126/science.206.4414.59>, 1979.
- Clever, H. L., Battino, R., Clever, H. L., Jaselskis, B., Clever, H. L., Yampol'skii, Y. P., Jaselskis, B., Scharlin, P., and Young, C. L.: IUPAC-NIST Solubility Data Series. 80. Gaseous Fluorides of Boron, Nitrogen, Sulfur, Carbon, and Silicon and Solid Xenon Fluorides in all Solvents, *J. Phys. Chem. Ref. Data*, 34, 201–438, <https://doi.org/10.1063/1.1794762>, 2005.
- Deeds, D. A.: The Natural Geochemistry of Tetrafluoromethane and Sulfur Hexafluoride : Studies of Ancient Mojave Desert Groundwaters, North Pacific Seawaters and the Summit Emissions of Kilauea Volcano, PhD thesis, 2008.
- Deeds, D. A., Mühle, J., and Weiss, R. F.: Tetrafluoromethane in the deep North Pacific Ocean, *Geophys. Res. Lett.*, 35, L14606, <https://doi.org/10.1029/2008gl034355>, 2008.
- DeFlaun, M. F., Ensley, B. D., and Steffan, R. J.: Biological oxidation of hydrochlorofluorocarbons (HCFCs) by a methanotrophic bacterium, *Nat. Biotechnol.*, 10, 1576–1578, <https://doi.org/10.1038/nbt1292-1576>, 1992.
- Ebser, S., Kersting, A., Stöven, T., Feng, Z., Ringena, L., Schmidt, M., Tanhua, T., Aeschbach, W., and Oberthaler, M. K.: ³⁹Ar dating with small samples provides new key constraints on ocean ventilation, *Nat. Commun.*, 9, 5046, <https://doi.org/10.1038/s41467-018-07465-7>, 2018.
- Hainbucher, D., Álvarez, M., Astray, B., Bachi, G., Cardin, V., Celentano, P., Chaikakis, S., Montero, M. C., Civitarese, G., Hassoun, A. E. R., Fajar, N. M., Fripiat, F., Gerke, L., Gogou, A., Guallart, E., Gülk, B., Lange, N., Rochner, A., Santinelli, C., Schroeder, K., Steinhoff, T., Tanhua, T., Urbini, L., Velaoras, D., Wolf, F., and Welsch, A.: Variability and Trends in Physical and Biogeochemical Parameters of the Mediterranean Sea, Cruise No. MSM72, March 02, 2018 - April 03, 2018, Iraklion (Greece) - Cádiz (Spain), MED-SHIP2, in, MARIA S. MERIAN-Berichte, Gutachterpanel Forschungsschiffe, Bremen, 2019.
- Hall, T. M., and Plumb, R. A.: Age as a diagnostic of stratospheric transport, *J. Geophys. Res.: Atmos.*, 99, 1059–1070, <https://doi.org/10.1029/93JD03192>, 1994.

- Huhn, O., Roether, W., Beining, P., and Rose, H.: Validity limits of carbon tetrachloride as an ocean tracer, *Deep-Sea Res. Pt. I*, 48, 2025–2049, [https://doi.org/10.1016/S0967-0637\(01\)00004-8](https://doi.org/10.1016/S0967-0637(01)00004-8), 2001.
- Law, C., Watson, A., and Liddicoat, M.: Automated vacuum analysis of sulphur hexafluoride in seawater: derivation of the atmospheric trend (1970–1993) and potential as a transient tracer, *Mar. Chem.*, 48, 57–69, [https://doi.org/10.1016/0304-4203\(94\)90062-0](https://doi.org/10.1016/0304-4203(94)90062-0), 1994.
- Li, P., Mühle, J., Montzka, S. A., Oram, D. E., Miller, B. R., Weiss, R. F., Fraser, P. J., and Tanhua, T.: Atmospheric histories, growth rates and solubilities in seawater and other natural waters of the potential transient tracers HCFC-22, HCFC-141b, HCFC-142b, HFC-134a, HFC-125, HFC-23, PFC-14 and PFC-116, *Ocean Sci.*, 15, 33–60, <https://doi.org/10.5194/os-15-33-2019>, 2019.
- Li, P., and Tanhua, T.: Recent changes in deep ventilation of the Mediterranean Sea: evidence from long-term transient tracer observations, in preparation.
- Lobert, J. M., Baring, T. J., Butler, J. H., Montzka, S. A., Myers, R. C., Elkins, J. W., Brown, R. H., Baker, D. J., and Rasmussen, J. L.: OAXTC 92: Ocean/atmosphere exchange of trace compounds 1992, 1–43, 1995.
- Lobert, J. M., Butler, J. H., Geller, L. S., Yvon, S. A., Montzka, S. A., Myers, R. C., Clarke, A. D., and Elkins, J. W.: Blast 94: Bromine latitudinal air/sea transect 1994, 1–39, 1996.
- Lu, Z. T., Schlosser, P., Smethie Jr, W. M., Sturchio, N. C., Fischer, T. P., Kennedy, B. M., Purtschert, R., Severinghaus, J. P., Solomon, D. K., Tanhua, T., and Yokochi, R.: Tracer applications of noble gas radionuclides in the geosciences, *Earth-Sci. Rev.*, 138, 196–214, <https://doi.org/10.1016/j.earscirev.2013.09.002>, 2014.
- Matheson, L. J., Jahnke, L. L., and Oremland, R. S.: Inhibition of methane oxidation by *Methylococcus capsulatus* with hydrochlorofluorocarbons and fluorinated methanes, *Appl. Environ. Microbiol.*, 63, 2952–2956, 1997.
- Miller, B. R., Weiss, R. F., Salameh, P. K., Tanhua, T., Grealley, B. R., Mühle, J., and Simmonds, P. G.: Medusa: A sample preconcentration and GC/MS detector system for in situ measurements of atmospheric trace halocarbons, hydrocarbons, and sulfur compounds, *Anal. Chem.*, 80, 1536–1545, <https://doi.org/10.1021/ac702084k>, 2008.
- Ooki, A., and Yokouchi, Y.: Determination of Henry's law constant of halocarbons in seawater and analysis of sea-to-air flux of iodoethane (C₂H₅I) in the Indian and Southern oceans based on partial pressure measurements, *Geochem. J.*, 45, e1–e7, <https://doi.org/10.2343/geochemj.1.0122>, 2011.
- Oremland, R. S.: *Microbiology of Atmospheric Trace Gases*, 306 pp., 1996.
- Prinn, R. G., Weiss, R. F., Arduini, J., Arnold, T., DeWitt, H. L., Fraser, P. J., Ganesan, A. L., Gasore, J., Harth, C. M., and Hermansen, O.: History of chemically and radiatively important atmospheric gases from the Advanced Global Atmospheric Gases Experiment (AGAGE), *Earth Syst. Sci. Data*, 10, 985–1018, <https://doi.org/10.5194/essd-10-985-2018>, 2018.
- Ravishankara, A., Solomon, S., Turnipseed, A. A., and Warren, R.: Atmospheric lifetimes of long-lived halogenated species, *Science*, 194–199, <https://doi.org/10.1126/science.259.5092.194>, 1993.

- Roether, W., Klein, B., and Bulsiewicz, K.: Apparent loss of CFC-113 in the upper ocean, *J. Geophys. Res.: Oceans*, 106, 2679–2688, <https://doi.org/0148-0227/01/1999JC000079>, 2001.
- Scharlin, P., and Battino, R.: Solubility of CCl_2F_2 , CClF_3 , CF_4 , and CH_4 in Water and Seawater at 288.15–303.15 K and 101.325 kPa, *J. Chem. Eng. Data*, 40, 167–169, <https://doi.org/10.1021/je00017a036>, 1995.
- Scheutz, C., Mosbæk, H., and Kjeldsen, P.: Attenuation of methane and volatile organic compounds in landfill soil covers, *J. Environ. Qual.*, 33, 61–71, <https://doi.org/10.2134/jeq2004.6100>, 2004.
- Schneider, A., Tanhua, T., Roether, W., and Steinfeldt, R.: Changes in ventilation of the Mediterranean Sea during the past 25 year, *Ocean Sci.*, 10, 1–16, <https://doi.org/10.5194/os-10-1-2014>, 2014.
- Simmonds, P. G., Rigby, M., McCulloch, A., Vollmer, M. K., Henne, S., Mühle, J., O'Doherty, S., Manning, A. J., Krummel, P. B., Fraser, P. J., Young, D., Weiss, R. F., Salameh, P. K., Harth, C. M., Reimann, S., Trudinger, C. M., Steele, P., Wang, R. H. J., Ivy, D. J., Prinn, R. G., Mitrevski, B., and Etheridge, D. M.: Recent increases in the atmospheric growth rate and emissions of HFC-23 (CHF_3) and the link to HCFC-22 (CHClF_2) production, *Atmos. Chem. Phys.*, 2018, 4153–4169, <https://doi.org/10.5194/acp-18-4153-2018>, 2018.
- SPARC: Lifetimes of Stratospheric Ozone-Depleting Substances, Their Replacements, and Related Species, AGU Fall Meeting Abstracts, 2013, 1.1–6.21.
- Stöven, T.: Ventilation processes of the Mediterranean Sea based on CFC-12 and SF_6 measurements, Master thesis, 116 pp., 2011.
- Stöven, T., and Tanhua, T.: Ventilation of the Mediterranean Sea constrained by multiple transient tracer measurements, *Ocean Sci.*, 10, 439–457, <https://doi.org/10.5194/os-10-439-2014>, 2014.
- Stöven, T., Tanhua, T., Hoppema, M., and von Appen, W. J.: Transient tracer distributions in the Fram Strait in 2012 and inferred anthropogenic carbon content and transport, *Ocean Sci.*, 12, 319–333, <https://doi.org/10.5194/os-12-319-2016>, 2016.
- Streger, S. H., Condee, C. W., Togna, A. P., and DeFlaun, M. F.: Degradation of hydrohalocarbons and brominated compounds by methane-and propane-oxidizing bacteria, *Environ. Sci. Technol.*, 33, 4477–4482, <https://doi.org/10.1021/es9907459>, 1999.
- Tanhua, T., Anders Olsson, K., and Fogelqvist, E.: A first study of SF_6 as a transient tracer in the Southern Ocean, *Deep-Sea Res. Pt. II*, 51, 2683–2699, <https://doi.org/10.1016/j.dsr2.2001.02.001>, 2004.
- Tanhua, T., Waugh, D. W., and Wallace, D. W. R.: Use of SF_6 to estimate anthropogenic CO_2 in the upper ocean, *J. Geophys. Res.*, 113, C04037, <https://doi.org/10.1029/2007jc004416>, 2008.
- Tanhua, T., Van Heuven, S., Key, R. M., Velo, A., Olsen, A., and Schirnick, C.: Quality control procedures and methods of the CARINA database, *Earth Syst. Sci. Data*, 2, 35–49, <https://doi.org/10.5194/essd-2-35-2010>, 2010.

- Trudinger, C. M., Fraser, P. J., Etheridge, D. M., Sturges, W. T., Vollmer, M. K., Rigby, M., Martinerie, P., Mühle, J., Worton, D. R., and Krummel, P. B.: Atmospheric abundance and global emissions of perfluorocarbons CF₄, C₂F₆ and C₃F₈ since 1800 inferred from ice core, firn, air archive and in situ measurements, *Atmos. Chem. Phys.*, 16, 11733–11754, <https://doi.org/10.5194/acp-16-11733-2016>, 2016.
- Vollmer, M. K., and Weiss, R. F.: Simultaneous determination of sulfur hexafluoride and three chlorofluorocarbons in water and air, *Mar. Chem.*, 78, 137–148, [https://doi.org/10.1016/S0304-4203\(02\)00015-4](https://doi.org/10.1016/S0304-4203(02)00015-4), 2002.
- Walker, S. J., Weiss, R. F., and Salameh, P. K.: Reconstructed histories of the annual mean atmospheric mole fractions for the halocarbons CFC-11 CFC-12, CFC-113, and carbon tetrachloride, *J. Geophys. Res.*, 105, 14285, <https://doi.org/10.1029/1999jc900273>, 2000.
- Wallace, D. W. R., and Krysell, M.: Hydrolysis of Carbon Tetrachloride, *Science*, 246, 1638–1639, <https://doi.org/10.1126/science.1638-a>, 1989.
- Warner, M. J., and Weiss, R. F.: Solubilities of chlorofluorocarbons 11 and 12 in water and seawater, *Deep Sea Res. Part A. Oceanogr. Res. Pap.*, 32, 13, [https://doi.org/10.1016/0198-0149\(85\)90099-8](https://doi.org/10.1016/0198-0149(85)90099-8), 1985.
- Waugh, D. W., Hall, T. M., and Haine, T. W.: Relationships among tracer ages, *J. Geophys. Res.: Oceans*, 108, 3138, <https://doi.org/10.1029/2002JC001325>, 2003.
- Yvon-Lewis, S., Liu, Y., Hu, L., and O'Hern, J.: Selected CFC and HCFC Tracers Observed During the Gulf of Mexico East Coast Carbon (GOMECC) Cruise, AGU Fall Meeting Abstracts, 2008, 1–65.
- Yvon-Lewis, S. A., and Butler, J. H.: Effect of oceanic uptake on atmospheric lifetimes of selected trace gases, *J. Geophys. Res.: Atmos.*, 107, 4414, <https://doi.org/10.1029/2001JD001267>, 2002.

Supplement of

Medusa-aqua system: simultaneous measurement and evaluation of novel potential halogenated transient tracers HCFCs, HFCs and PFCs in the ocean

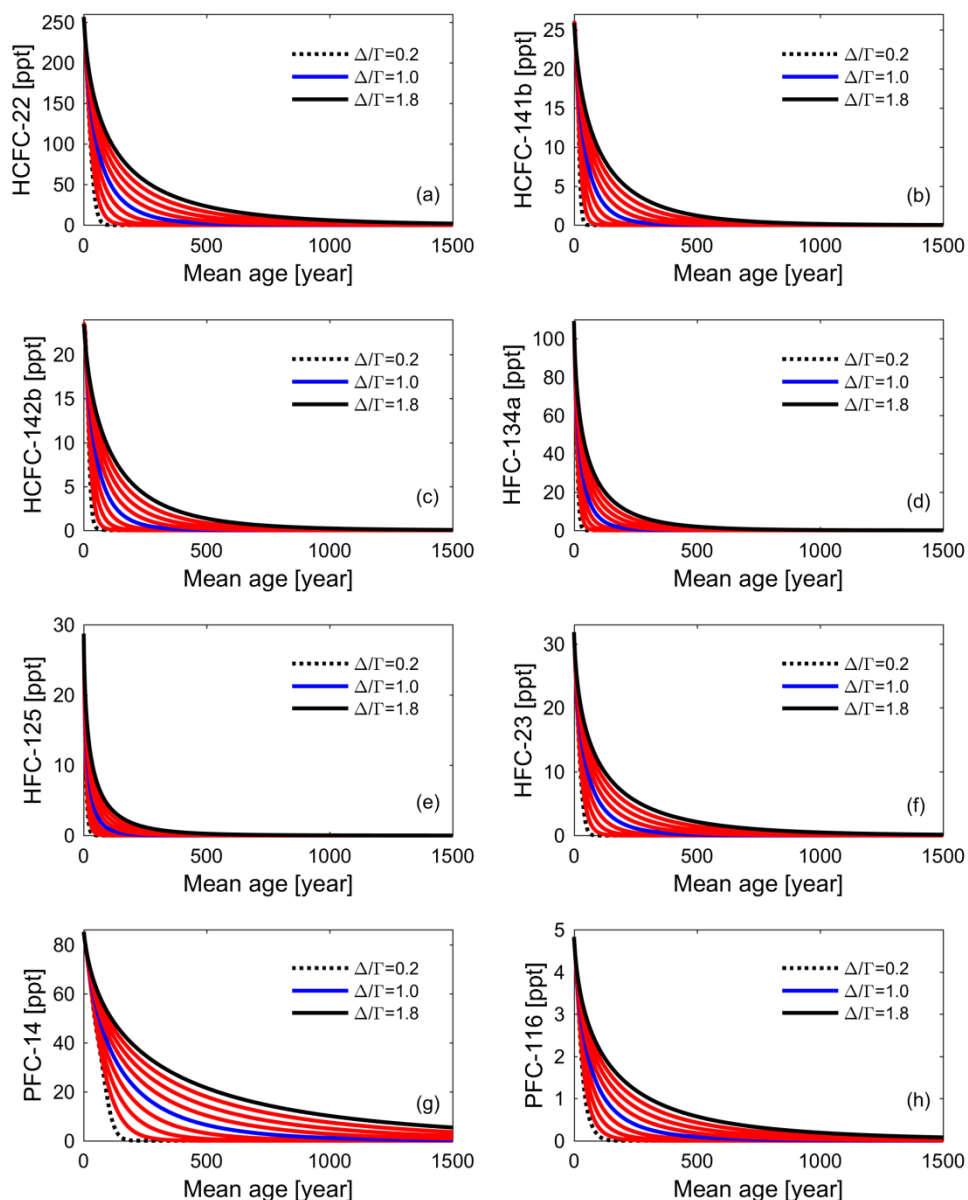
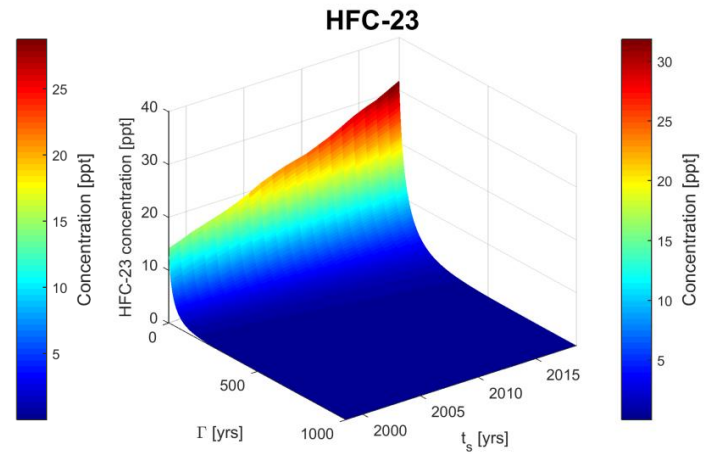
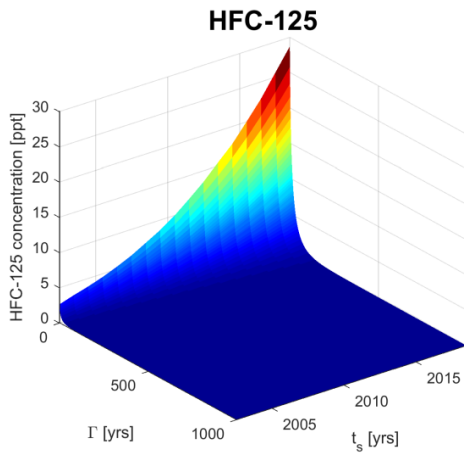
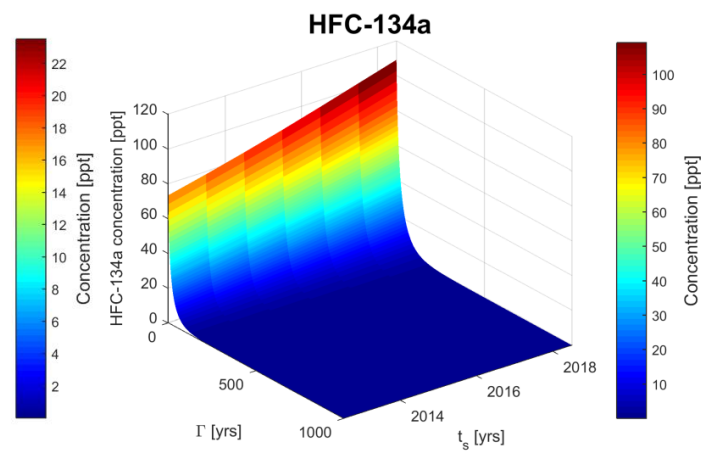
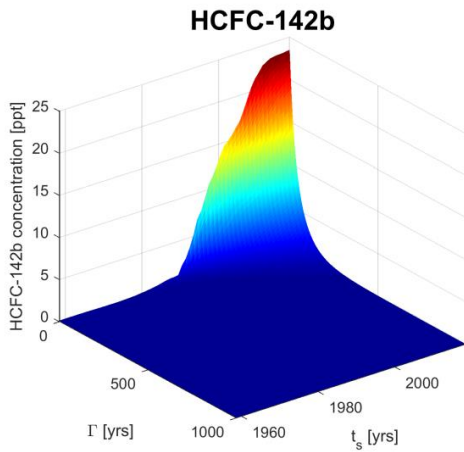
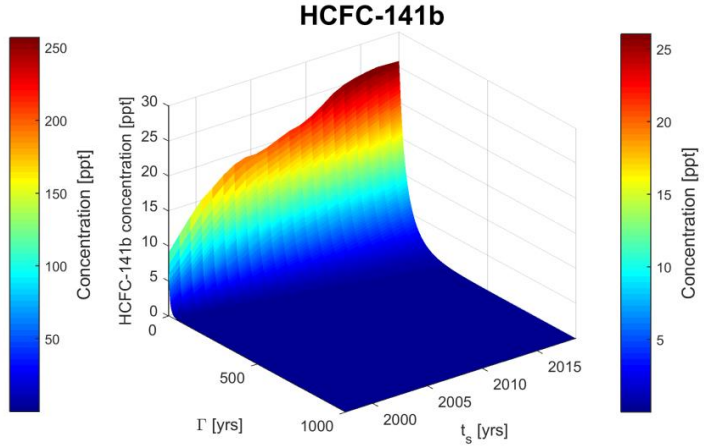
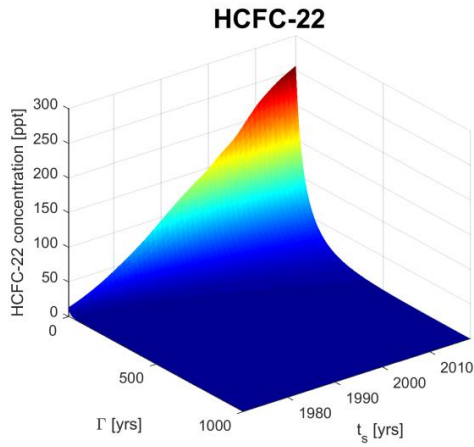


Figure S1. Transient tracer concentrations (ppt, parts per trillion) of HCFC-22, HCFC-141b, HCFC-142b, HFC-134a, HFC-125, HFC-23, PFC-14 and PFC-116 vs. mean age for different Δ/T ratios (a range of 0.2-1.8) in the Northern Hemisphere. The unity ratio of 1.0 is shown as a blue line.



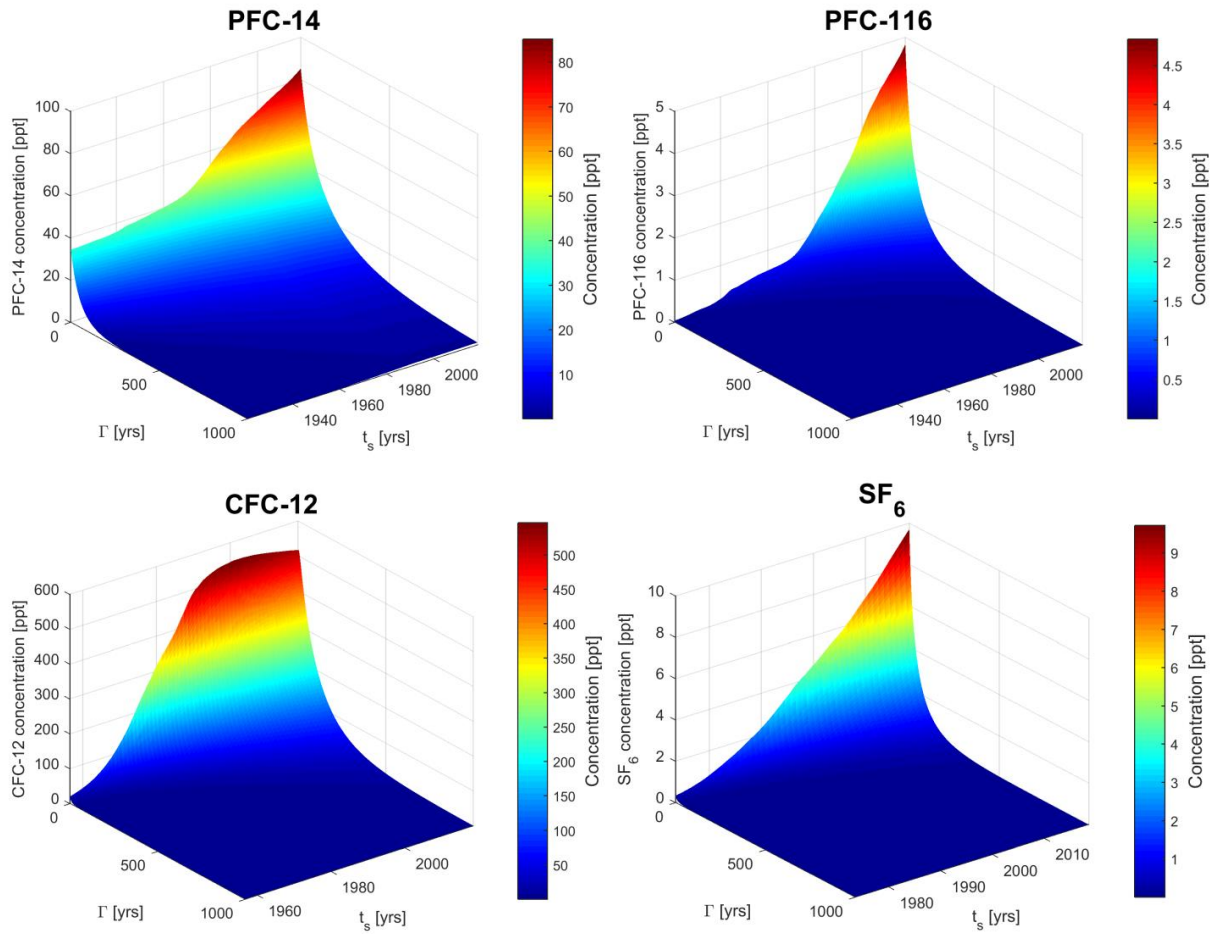
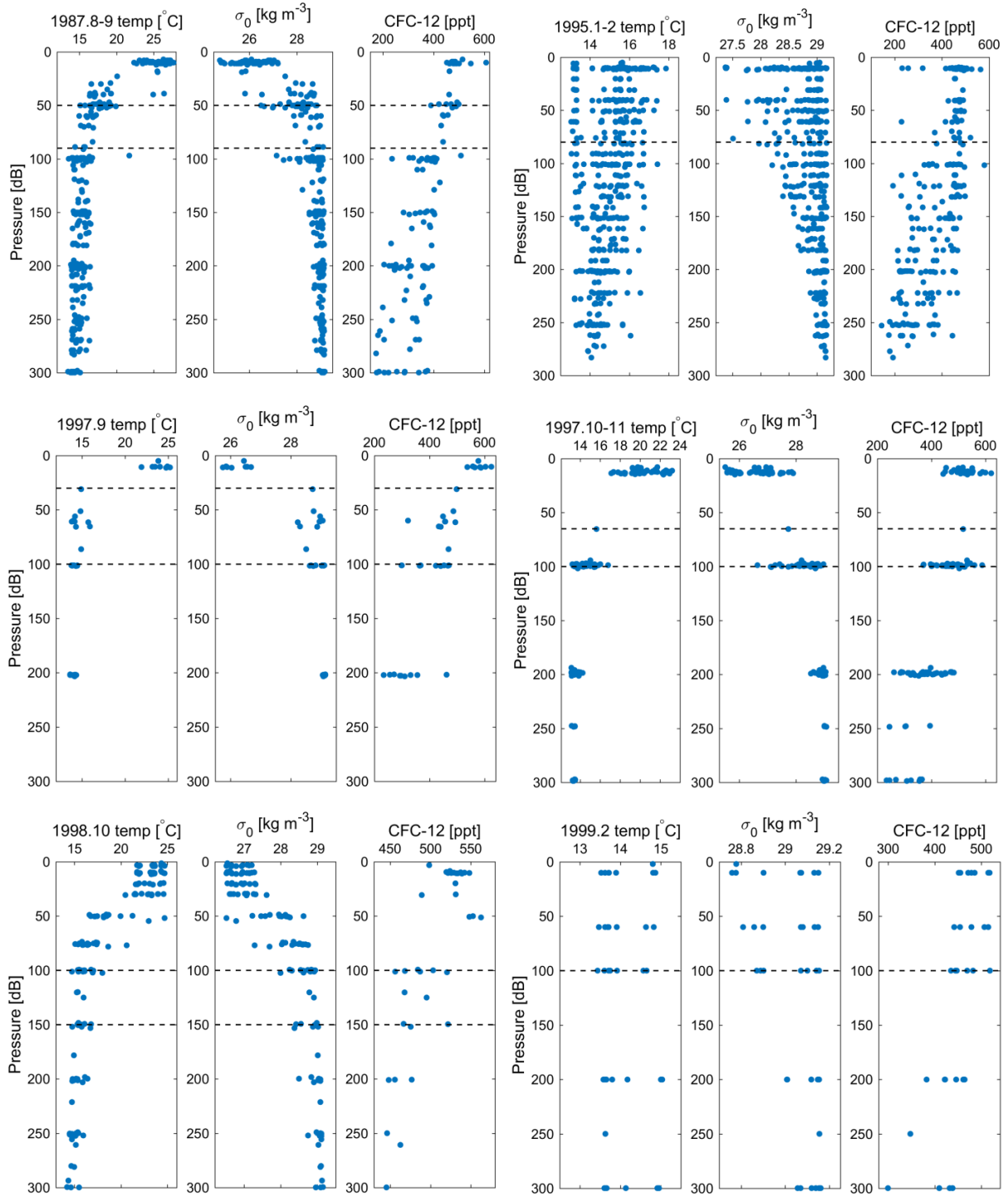


Figure S2. HCFC-22, HCFC-141b, HCFC-142b, HFC-134a, HFC-125, HFC-23, PFC-14, PFC-116 CFC-12 and SF₆: concentrations (ppt) in different sampling year (t_s) and mean age (Γ) in the Northern Hemisphere with $\Delta/\Gamma = 1.0$ based on the IG-TTD with 100 % saturation.



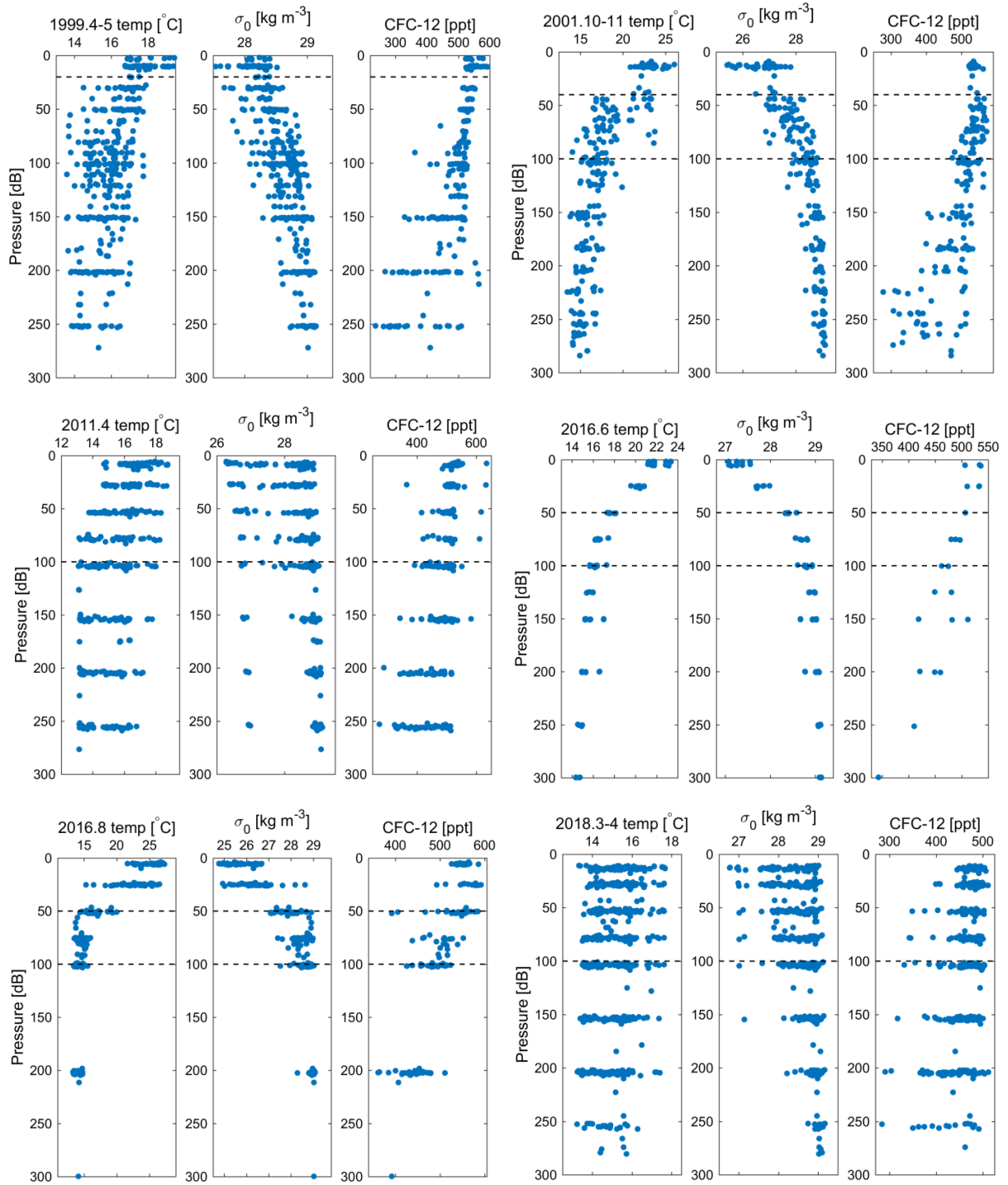


Figure S3. Profiles of temperature, potential density and concentrations of CFC-12 for each historical cruise in the Mediterranean Sea to determine the depth ranges of winter mixed layers.

Table S1. Bottle data of SF₆ and CFC-12 in profiles 51, 53, 83, 85, 105 and 107 measured by the PT-GC-ECD and CFC-12, HCFC-22, HCFC-141b, HCFC-142b, HFC-134a and HFC-125 in profiles 52, 84 and 106 measured by the Medusa-Aqua system from cruise MSM72 (see Appendix C) ^a

^a Meaning of the quality flag, this is modified from the WOCE flagging system (https://cchdo.github.io/hdo-assets/documentation/manuals/pdf/90_1/chap4.pdf, last access: 20 January 2020) only in that we added flag “5” for the purpose of this study

Quality flag number	Meaning
2	Normal data; data for sampling sites that measured CFC-12 by Medusa-Aqua system matched the one by PT-GC-ECD
3	Questionable data: may not fit the profile or some other doubts
4	Problem data definitely
5	Data for sampling sites that measured CFC-12 by Medusa-Aqua system doesn't match the one by PT-GC-ECD; data quality between 2 and 3
6	Mean of two or more measurements
9	Missing (null) data

Conclusions and outlook

This thesis investigates the temporal and spatial variability of deep ventilation in the Mediterranean Sea in the past ~30 years. The Mediterranean Sea is characterized by bottom renewal in the deep layer and weak ventilation in the TMZ in the intermediate layer. Both the EMDW and WMDW show a general west-to-east gradient of increasing salinity and potential temperature but decreasing oxygen and transient tracer concentrations. The EMDW has been formed by the mixing of the dense waters of the Aegean origin with the colder and less saline water of the Adriatic origin, where the dominant source of deep water changed from the Adriatic Sea (before 1990) to the Aegean Sea (in the 1990s) and then back to the Adriatic Sea (in the 2000s and 2010s). During the last decade, stagnant and weak ventilation is found in most areas of the EMDW despite the prevailing ventilation in the Adriatic Deep Water between 2011 and 2016, which could be a result of the weakened Adriatic source intensity. For the WMed, a steady-state ventilation scenario with nearly stagnant ventilation is found in the deep-water before 2001. Since the start of the WMT event in 2004-2006, strong ventilation is found in the WMed through to 2016 but weakened up to 2018. The latter could be a result of combined influences from the WMed (e.g. weakened influence from the WMT event) and EMed (e.g. weakened Adriatic source intensity). During the past ~15 years, the deep WMed has been influenced by the new WMDW that moves the old WMDW upward leading to the intrusion of better-ventilated deep waters toward the Alboran Sea.

This thesis also explores and evaluates the feasibility of several potential novel chronological transient tracers from four aspects: input function (including atmospheric history and historical surface saturation), seawater solubility, feasibility of measurement and stability in seawater. By comprehensive evaluation, the most promising oceanic transient tracers are HCFC-142b and HCFC-141b currently. The compounds that have the greatest potential as oceanic transient tracers in the future are PFC-14 and PFC-116 with the challenge of measurement due to their low solubility. HFC-134a still needs to be evaluated on its solubility and stability in seawater as well as potential analytical challenges. HFC-125, HFC-23, and HCFC-22 can no longer be considered because there are alternative tracers with similar input functions that are better suited as oceanic transient tracers.

In addition, this thesis provides a method to identify and evaluate whether a compound is suitable as an oceanic transient tracer or not, and provides an alternative method to estimate the seawater solubility function for a compound depending on if the freshwater and seawater samples were measured. Future work will be further evaluation of these potential novel transient tracers before they are used to combine other traditional tracers to better interpret ventilation in the global ocean.

One example is constructing the seawater solubility functions of HCFCs, HFCs and PFCs based on seawater sample measurements by referring methods for CFC-11 and CFC-12 (Warner and Weiss,

1985), as well as for SF₆ (Bullister et al., 2002). Another one is evaluating stability of HCFC-142b and HCFC-141b in seawater based on more measurements in the global ocean by referring methods for CFC-12 (Tanhua and Olsson, 2005), CFC-11 (Bullister and Lee, 1995), CFC-113 (Roether et al., 2001) and CCl₄ (Huhn et al., 2001).

The measurement of PFC-14 and PFC-116 in seawater samples need to be challenged. The visible way is modifying the Medusa system according to Arnold et al. (2012) to improve the sensitivity for PFC-14 (CF₄) and trying field measurements using the vacuum-sparge method by Law et al. (1994) to improve the speed of gas extraction and reduce the purging cycles. The shipboard measurements can be carried out immediately after sampling, the ampoules need not to be sealed, and the sampling and analysis steps can be simplified and made less time-consuming. We can also try to take more seawater in a sample, change the standard gas from atmospheric ratio to oceanic ratio, and change one standard loop to two loops with different volumes.

Historical surface saturation also needs to be more carefully considered in the future. As a component of the input function, surface saturation has a large impact on the specific time information and TTD model constraints (Stöven et al., 2015). In this study, an averaged historical surface saturation is calculated. However, with the development of the interpreting methods of oceanic transient tracers, the more precise historical surface saturation needs to be obtained. A possibility is through the model approach by Shao et al. (2013), which depends on changes in atmospheric emission rate and seawater solubility of the tracer as well as sea surface temperature and salinity but neglects possible supersaturations because of bubble injections during heavy wind conditions. Therefore, the different aspects of saturation will also be the main focus of future work.

A combination of multiple oceanic transient tracers, not only the chronological transient tracers but also the radioactive transient tracers, in interpreting ventilation in the global ocean will be gained attention in the future. The evaluation of the potential alternative transient tracers in this study, the development of the new sampling and measurement technique of the argon-39 isotope (Ebser et al., 2018) and the application of the more complex interpreting method for multiple transient tracers, such as 2IG-TTD (Stöven and Tanhua, 2014) will make this possible. Increased requirements are looking for or developing more suitable models for multiple transient tracers to better constrain the age calculation under the assumption of steady-state or without considering such an assumption.

In total, the results of this thesis improve the understanding of ventilation of the Mediterranean Sea and find the most promising oceanic transient tracers currently and in the future. The outcome sets the base for future investigation on multiple oceanic transient tracers, in order to better understand ventilation and circulation in the global ocean and the effects of the changing climate.

References

- Arnold, T., Mühle, J., Salameh, P. K., Harth, C. M., Ivy, D. J., and Weiss, R. F.: Automated Measurement of Nitrogen Trifluoride in Ambient Air, *Anal. Chem.*, 84, 4798–4804, <https://doi.org/10.1021/ac300373e>, 2012.
- Bullister, J. L. and Lee, B. S.: Chlorofluorocarbon-11 removal in anoxic marine waters, *Geophys. Res. Lett.*, 22, 1893–1896, <https://doi.org/10.1029/95GL01517>, 1995.
- Bullister, J. L., Wisegarver, D. P., and Menzia, F. A.: The solubility of sulfur hexafluoride in water and seawater, *Deep-Sea Res. Pt. I*, 49, 175–187, [https://doi.org/10.1016/S0967-0637\(01\)00051-6](https://doi.org/10.1016/S0967-0637(01)00051-6), 2002.
- Ebser, S., Kersting, A., Stöven, T., Feng, Z., Ringena, L., Schmidt, M., Tanhua, T., Aeschbach, W., and Oberthaler, M. K.: ³⁹Ar dating with small samples provides new key constraints on ocean ventilation, *Nat. Commun.*, 9, 5046, <https://doi.org/10.1038/s41467-018-07465-7>, 2018.
- Huhn, O., Roether, W., Beining, P., and Rose, H.: Validity limits of carbon tetrachloride as an ocean tracer, *Deep-Sea Res. Pt. I*, 48, 2025–2049, [https://doi.org/10.1016/S0967-0637\(01\)00004-8](https://doi.org/10.1016/S0967-0637(01)00004-8), 2001.
- Law, C., Watson, A., and Liddicoat, M.: Automated vacuum analysis of sulphur hexafluoride in seawater: derivation of the atmospheric trend (1970–1993) and potential as a transient tracer, *Mar. Chem.*, 48, 57–69, [https://doi.org/10.1016/0304-4203\(94\)90062-0](https://doi.org/10.1016/0304-4203(94)90062-0), 1994.
- Roether, W., Klein, B., and Bulsiewicz, K.: Apparent loss of CFC-113 in the upper ocean, *J. Geophys. Res.: Oceans*, 106, 2679–2688, <https://doi.org/10.1029/1999JC000079>, 2001.
- Shao, A. E., Mecking, S., Thompson, L., and Sonnerup, R. E.: Mixed layer saturations of CFC-11, CFC-12, and SF₆ in a global isopycnal model, *J. Geophys. Res.: Oceans*, 118, 4978–4988, <https://doi.org/10.1002/jgrc.20370>, 2013.
- Stöven, T. and Tanhua, T.: Ventilation of the Mediterranean Sea constrained by multiple transient tracer measurements, *Ocean Sci.*, 10, 439–457, <https://doi.org/10.5194/os-10-439-2014>, 2014.
- Stöven, T., Tanhua, T., Hoppema, M., and Bullister, J. L.: Perspectives of transient tracer applications and limiting cases, *Ocean Sci.*, 11, 699–718, <https://doi.org/10.5194/os-11-699-2015>, 2015.
- Tanhua, T. and Olsson, K. A.: Removal and bioaccumulation of anthropogenic, halogenated transient tracers in an anoxic fjord, *Mar. Chem.*, 94, 27–41, <https://doi.org/10.1016/j.marchem.2004.07.009>, 2005.
- Warner, M. J. and Weiss, R. F.: Solubilities of chlorofluorocarbons 11 and 12 in water and seawater, *Deep Sea Res. Part A. Oceanogr. Res. Pap.*, 32, 1485–1497, [https://doi.org/10.1016/0198-0149\(85\)90099-8](https://doi.org/10.1016/0198-0149(85)90099-8), 1985.

Appendix A Measurement of HCFCs and HFCs in seawater

Here is the supplementary information for the measurement of HCFCs and HFCs in seawater for Manuscript III. Before the Medusa-Aqua system used for measurement of seawater samples from cruises MSM72 and AL516, it has been improved by updating carrier gases, standard gas and quantitative tool of the standard gas (Table A.1 and Fig. A.1). Seawater measurements from cruise NORC2017-09 have not been discussed because those compounds were polluted in the sampling process.

The sampling device for HCFCs and HFCs in seawater was a stainless steel mounting system (Fig. A.2) designed by Vollmer and Weiss (2002). The chromatograms from seawater samples were quantified by peak areas for HFC-134a, HFC-125 and CFC-12 and peak heights for HCFC-22, HCFC-141b and HCFC-142b (Fig. A.3) due to the different shapes of the peaks. The working standard was used for the determination of weekly calibration curves (Fig. A.4) and daily drift corrections (Fig. A.5).

Table A.1. Improvement of the Medusa-Aqua system

Phase	Cruise name	Measured time	Sampling time	Area	Longitude (E)	Latitude (N)	Carrier gas	Standard gas	MFC or std loop ^a	Sampling size (L)	Purpose
I	MSM18/3	04.02.2017	2011.06	Atlantic Ocean	-23	10.5, 9.5	5.0 He, 5.0 N ₂	natair ^b	MFC	~1.3	First seawater sample measurement
II	M130	07.05.2017	2016.09	Atlantic Ocean	-23	0.67, -0.67, -1.67, -2.5, -3.5, -4.5, -5.0, -5.5	5.0 He, 5.0 N ₂	natair	std loop	~1.3	Tested standard loop
III	KBP524	2017.11	2017.11	Baltic Sea	10.04	54.53	6.0 He, 6.0 N ₂	natair	MFC	~0.3	Updated carrier gases
IV	MSM18/3	2018.03	2011.06	Atlantic Ocean	-23	8.5, 6.5	6.0 He, 6.0 N ₂	Tanhua-2 ^c	MFC	~1.3	Updated standard gas
IV	MSM23	2018.04	2012.12	Atlantic Ocean	-24.3	17.6	6.0 He, 6.0 N ₂	Tanhua-2	MFC	~1.3	
V	MSM72	2018.07	2018.03	Mediterranean Sea	(19.4, 35.3), (9.98, 38.7), (3.2, 38.4)		6.0 He, 6.0 N ₂	Tanhua-2	std loop	~1.3	
V	NORC2017-09	08.07.2018	2017.1	Pacific Ocean	130	7.25, 4.75	6.0 He, 6.0 N ₂	Tanhua-2	std loop	~1.3	Updated the quantitative tool of standard gas
V	Al516	2018.1	2018.09	Baltic Sea	(10.067, 54.522)		6.0 He, 6.0 N ₂	Tanhua-2	std loop	~1.3	

^a Standard gas is quantitated by the MFC (Mass Flow Controller) or the standard loop.

^b natair (Natürliche Luft, PRÜFGAS, UN 1956, DEUSTE-Steininger GmbH) calibrated by a tertiary standard (named "Tanhua_221") from SIO is used as the working standard. For the tracer gases in concern, CFCs, HCFCs, and PFCs are found in the natair, and CFC-12, SF₆, HCFCs, HFC-134a and PFC-14 are found in the tertiary standard.

^c a new tertiary standard gas including CFCs, HCFCs and PFCs. The two tertiary standard gases can be propagated to the same primary standard by the AGAGE relative scale "SIO-R1".

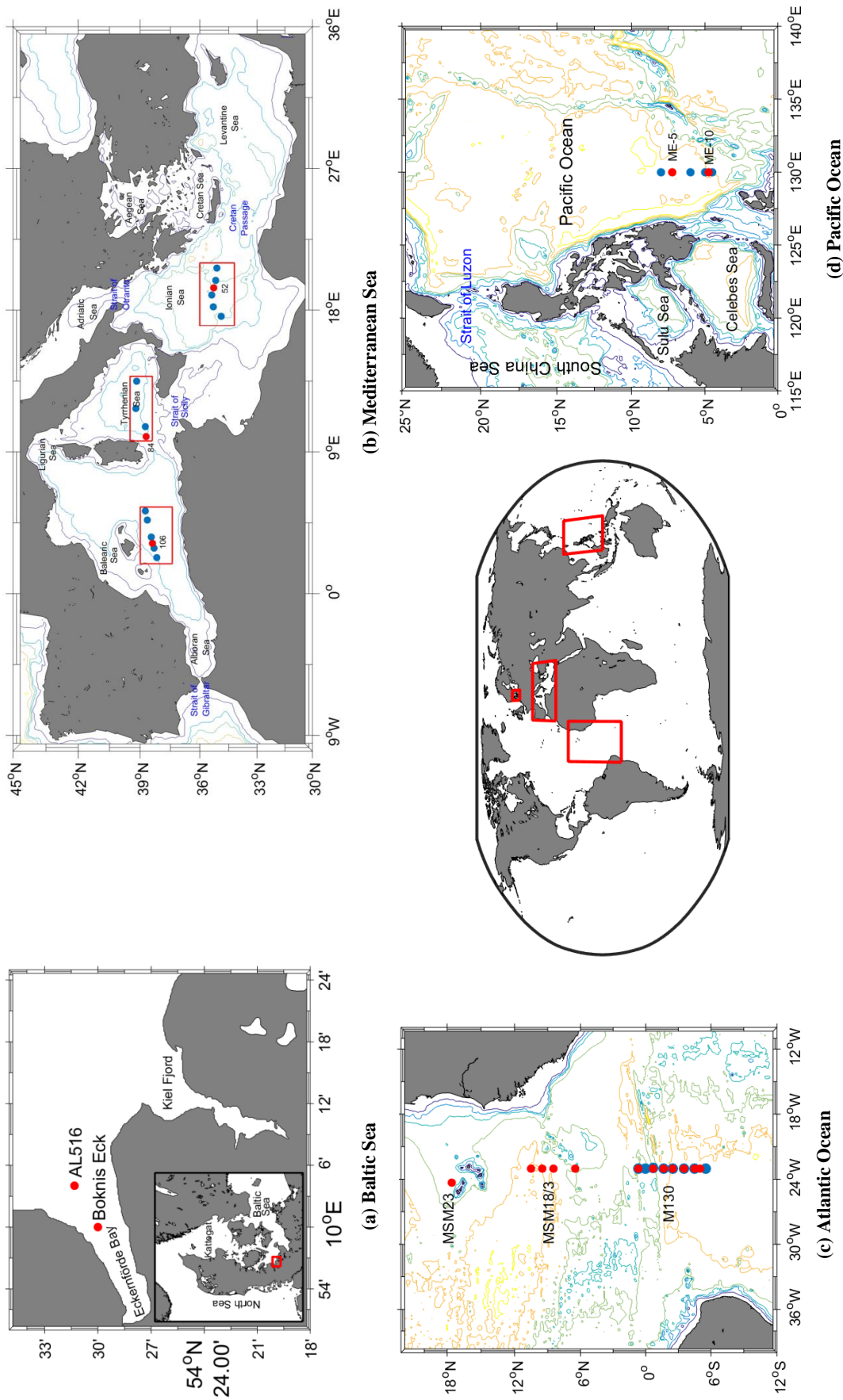


Figure A.1. Locations of sampling sites from (a) cruises KBF524 (Boknis Eck) and AL516 in the Baltic Sea; (b) cruise MSM72 in the Mediterranean Sea; (c) cruises MSM23, MSM18/3, and M130 in the Atlantic Ocean; (d) cruise NORC2017-09 in the Pacific Ocean. Sampling sites in red solid circles indicate samples measured by the Medusa-Aqua system for HCFCs, HFCs, PFCs and CFC-12, blue solid circles were for CFC12 and SF₆ measured by the PT-GC-ECD. The depth contours are 500 m, 2000 m, 3000 m, 4000 m, 5000 m, and 6000 m.

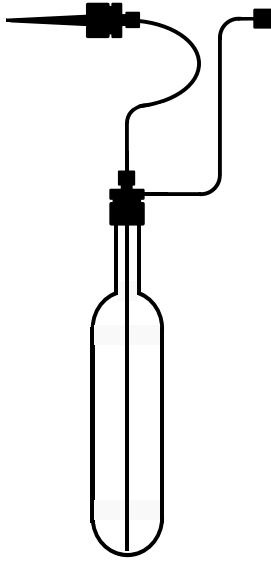


Figure A.2. The stainless steel mounting system for sampling onboard.

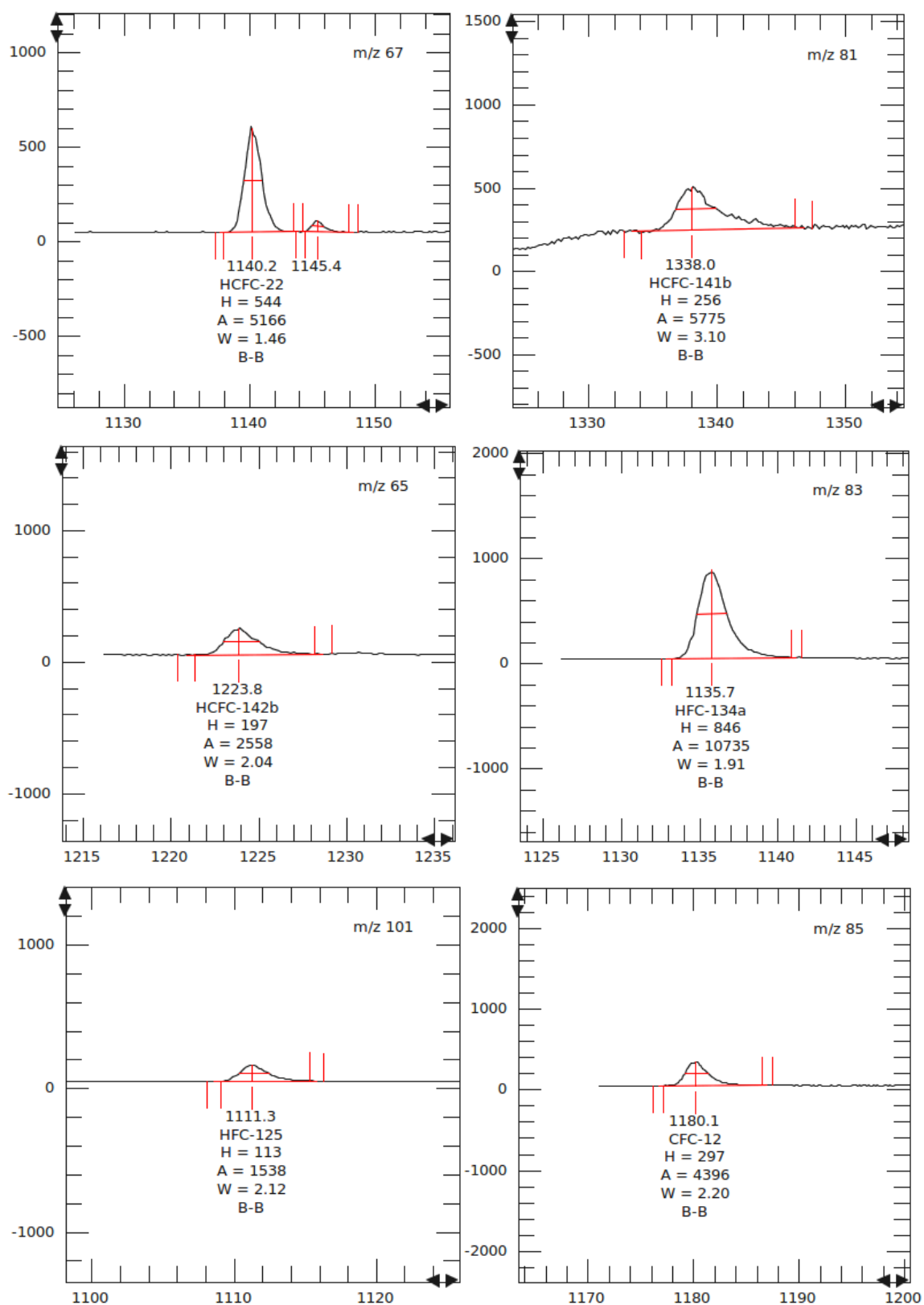


Figure A.3. Select ion mass (SIM) chromatograms of HCFC-22, HCFC-141b, HCFC-142b, HFC-134a, HFC-125 and CFC-12 from a seawater sample measured by the Medusa-Aqua system. The sample was taken at ~100 dbar depth from profile 52 from cruise MSM72. Here H is the peak height, A is the peak area and W is the peak width at the mid-height.

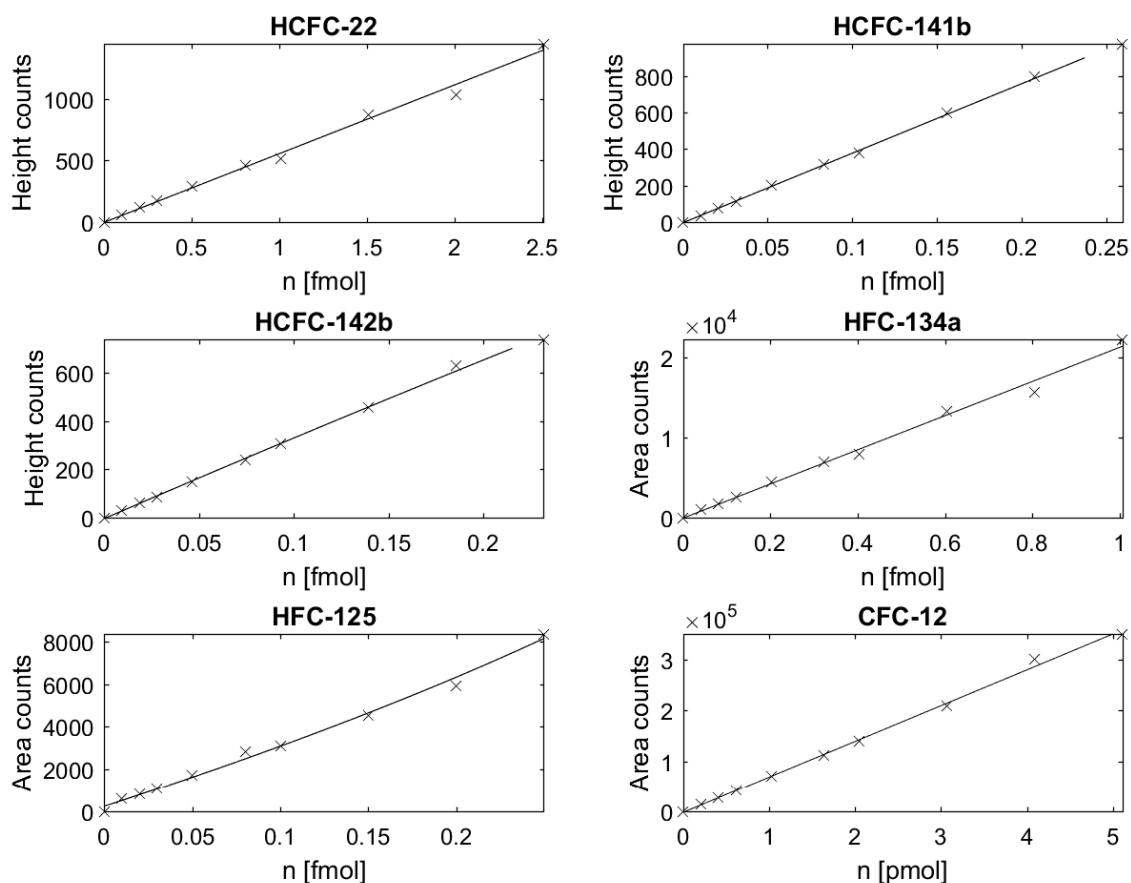


Figure A.4. Standard curves of HCFC-22, HCFC-141b, HCFC-142b, HFC-134a, HFC-125 and CFC-12 ($R^2 > 0.99$). The crosses are the measured data and the line the regression curve. The standard curves are constructed by peak areas for HFC-134a, HFC-125 and CFC-12 and peak heights for HCFC-22, HCFC-141b and HCFC-142b.

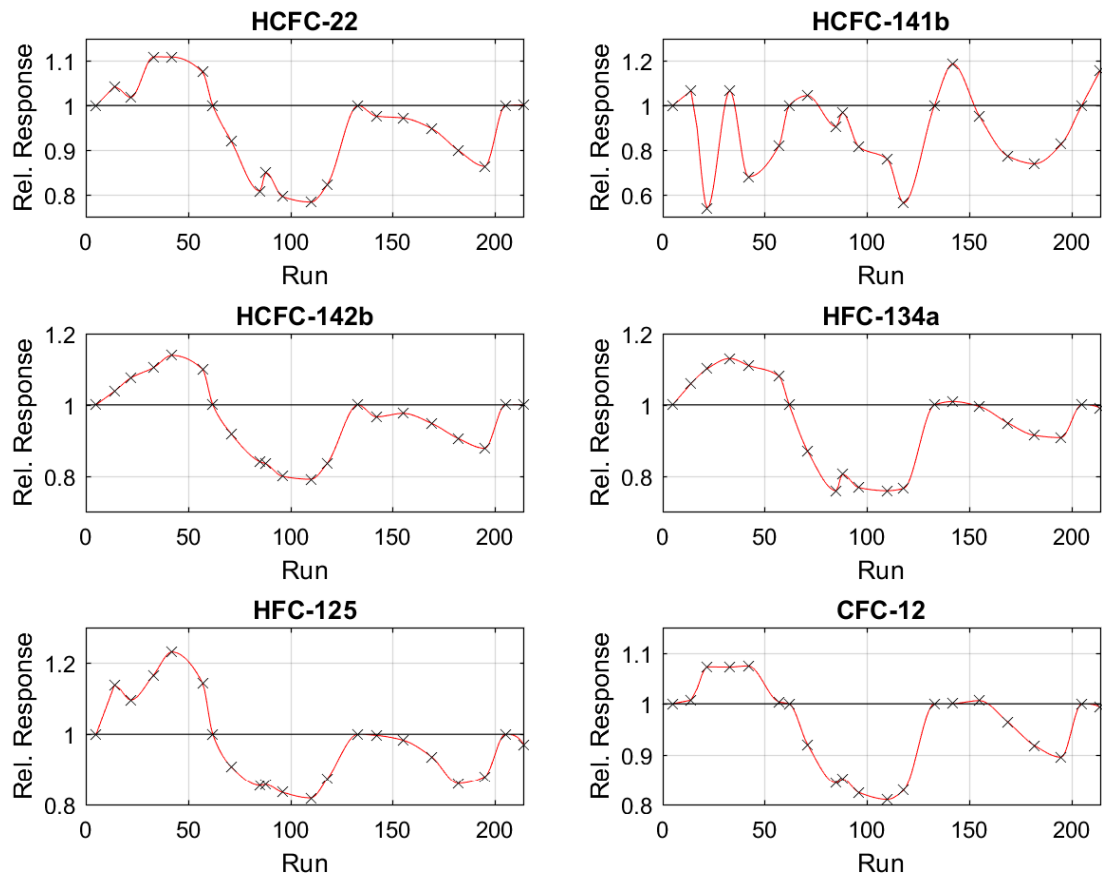


Figure A.5. Drift corrections for HCFC-22, HCFC-141b, HCFC-142b, HFC-134a, HFC-125 and CFC-12. The crosses are the measured data and the red line the interpolation between the obtained data.

References

Vollmer, M. K., and Weiss, R. F.: Simultaneous determination of sulfur hexafluoride and three chlorofluorocarbons in water and air, *Mar. Chem.*, 78, 137–148, [https://doi.org/10.1016/S0304-4203\(02\)00015-4](https://doi.org/10.1016/S0304-4203(02)00015-4), 2002.

Appendix B Table S2 in Manuscript II

Table S2a. Atmospheric mole fractions for HCFC-22 (scale: SIO-05)

Year	Annual means				Year	JFM means			Year	JAS means		
	NH (ppt)	NH error (ppt)	SH (ppt)	SH error (ppt)		NH (ppt)	NH error (ppt)			SH (ppt)	SH error (ppt)	
1943.5	0.00	1.68	0.00	1.67	1943.125	0.00	1.90		1943.625	0.00	1.66	
1944.5	0.00	1.19	0.00	1.31	1944.125	0.00	1.31		1944.625	0.00	1.25	
1945.5	0.00	1.11	0.00	0.94	1945.125	0.00	1.10		1945.625	0.00	0.90	
1946.5	0.00	1.11	0.00	0.83	1946.125	0.00	1.12		1946.625	0.00	0.83	
1947.5	0.00	1.10	0.00	0.83	1947.125	0.00	1.11		1947.625	0.00	0.83	
1948.5	0.01	1.09	0.00	0.82	1948.125	0.00	1.10		1948.625	0.00	0.82	
1949.5	0.03	1.09	0.00	0.82	1949.125	0.02	1.09		1949.625	0.00	0.82	
1950.5	0.06	1.09	0.01	0.81	1950.125	0.05	1.09		1950.625	0.01	0.81	
1951.5	0.11	1.09	0.03	0.81	1951.125	0.09	1.09		1951.625	0.03	0.81	
1952.5	0.16	1.09	0.07	0.81	1952.125	0.14	1.09		1952.625	0.07	0.81	
1953.5	0.23	1.09	0.12	0.81	1953.125	0.20	1.09		1953.625	0.13	0.81	
1954.5	0.34	1.09	0.19	0.81	1954.125	0.29	1.09		1954.625	0.20	0.81	
1955.5	0.49	1.09	0.28	0.81	1955.125	0.42	1.09		1955.625	0.29	0.81	
1956.5	0.68	1.09	0.38	0.81	1956.125	0.60	1.09		1956.625	0.40	0.81	
1957.5	0.93	1.09	0.53	0.81	1957.125	0.83	1.09		1957.625	0.54	0.81	
1958.5	1.22	1.09	0.71	0.81	1958.125	1.10	1.09		1958.625	0.73	0.81	
1959.5	1.57	1.09	0.93	0.81	1959.125	1.43	1.09		1959.625	0.96	0.81	
1960.5	1.97	1.09	1.22	0.81	1960.125	1.81	1.09		1960.625	1.26	0.81	
1961.5	2.44	1.09	1.56	0.81	1961.125	2.25	1.09		1961.625	1.60	0.81	
1962.5	2.98	1.09	1.96	0.81	1962.125	2.76	1.09		1962.625	2.01	0.81	
1963.5	3.62	1.09	2.42	0.81	1963.125	3.36	1.09		1963.625	2.48	0.81	
1964.5	4.40	1.09	2.97	0.81	1964.125	4.08	1.09		1964.625	3.04	0.81	
1965.5	5.32	1.09	3.62	0.81	1965.125	4.95	1.09		1965.625	3.70	0.81	
1966.5	6.44	1.09	4.39	0.81	1966.125	5.99	1.09		1966.625	4.49	0.81	
1967.5	7.79	1.09	5.31	0.81	1967.125	7.25	1.09		1967.625	5.42	0.81	
1968.5	9.39	1.09	6.39	0.81	1968.125	8.75	1.09		1968.625	6.54	0.81	
1969.5	11.25	1.09	7.68	0.81	1969.125	10.51	1.09		1969.625	7.85	0.81	
1970.5	13.36	1.09	9.19	0.81	1970.125	12.53	1.09		1970.625	9.39	0.81	
1971.5	15.72	1.09	10.93	0.81	1971.125	14.79	1.09		1971.625	11.16	0.81	
1972.5	18.32	1.09	12.92	0.81	1972.125	17.31	1.09		1972.625	13.18	0.81	
1973.5	21.15	1.09	15.18	0.81	1973.125	20.06	1.09		1973.625	15.47	0.81	
1974.5	24.17	1.09	17.73	0.81	1974.125	23.01	1.09		1974.625	18.06	0.81	
1975.5	27.37	1.09	20.59	0.79	1975.125	26.14	1.09		1975.625	20.95	0.79	
1976.5	30.80	1.09	23.76	0.75	1976.125	29.48	1.09		1976.625	24.17	0.75	
1977.5	34.50	1.09	27.22	0.67	1977.125	33.07	1.09		1977.625	27.67	0.66	
1978.5	38.44	1.09	30.85	0.59	1978.125	36.93	1.09		1978.625	31.31	0.58	
1979.5	42.58	1.09	34.48	0.58	1979.125	41.00	1.09		1979.625	34.93	0.59	

1980.5	46.85	1.09	38.15	0.60	1980.125	45.23	1.09	1980.625	38.62	0.60
1981.5	51.22	1.09	41.89	0.60	1981.125	49.57	1.09	1981.625	42.36	0.61
1982.5	55.69	1.09	45.66	0.61	1982.125	53.99	1.09	1982.625	46.13	0.61
1983.5	60.34	1.09	49.53	0.56	1983.125	58.57	1.09	1983.625	50.02	0.56
1984.5	65.17	1.09	53.58	0.52	1984.125	63.33	1.09	1984.625	54.09	0.52
1985.5	70.19	1.09	57.85	0.52	1985.125	68.28	1.09	1985.625	58.39	0.52
1986.5	75.42	1.09	62.34	0.51	1986.125	73.42	1.09	1986.625	62.91	0.51
1987.5	80.91	1.09	67.08	0.51	1987.125	78.80	1.09	1987.625	67.68	0.51
1988.5	86.67	1.09	72.06	0.52	1988.125	84.48	1.09	1988.625	72.70	0.52
1989.5	92.58	1.09	77.37	0.50	1989.125	90.36	1.09	1989.625	78.04	0.50
1990.5	98.49	1.09	82.90	0.46	1990.125	96.29	1.09	1990.625	83.60	0.46
1991.5	104.25	1.09	88.46	0.39	1991.125	102.12	1.09	1991.625	89.15	0.38
1992.5	109.87	1.09	93.88	0.33	1992.125	107.77	1.09	1992.625	94.56	0.32
1993.5	115.44	1.09	99.18	0.30	1993.125	113.37	1.09	1993.625	99.53	0.77
1994.5	120.88	1.09	104.48	0.29	1994.125	118.87	1.09	1994.625	105.52	1.13
1995.5	126.13	1.09	109.64	0.28	1995.125	124.19	1.09	1995.625	110.97	0.91
1996.5	131.20	1.06	114.57	0.29	1996.125	129.34	1.08	1996.625	114.36	1.49
1997.5	136.01	0.96	119.31	0.30	1997.125	134.24	1.02	1997.625	120.18	1.07
1998.5	140.68	0.71	124.18	0.31	1998.125	138.94	0.82	1998.625	124.90	0.48
1999.5	145.53	0.46	129.39	0.31	1999.125	142.84	1.06	1999.625	131.39	0.53
2000.5	151.50	0.42	134.61	0.31	2000.125	147.28	1.21	2000.625	135.75	0.54
2001.5	158.09	0.42	139.68	0.31	2001.125	155.71	1.04	2001.625	141.06	0.94
2002.5	164.04	0.42	144.61	0.31	2002.125	160.53	1.02	2002.625	145.84	0.61
2003.5	169.32	0.42	149.48	0.31	2003.125	166.66	1.47	2003.625	150.52	0.65
2004.5	174.45	0.42	154.55	0.31	2004.125	172.35	0.99	2004.625	156.45	0.56
2005.5	180.45	0.42	159.96	0.31	2005.125	177.26	1.16	2005.625	161.29	0.71
2006.5	187.74	0.42	166.06	0.31	2006.125	184.63	1.12	2006.625	167.15	0.76
2007.5	195.97	0.42	173.06	0.31	2007.125	191.99	0.87	2007.625	174.29	0.74
2008.5	204.37	0.42	180.59	0.31	2008.125	201.38	0.91	2008.625	182.28	0.68
2009.5	212.22	0.43	188.24	0.31	2009.125	208.04	1.35	2009.625	189.56	0.67
2010.5	219.55	0.43	195.81	0.32	2010.125	216.66	0.93	2010.625	197.20	0.68
2011.5	225.76	0.43	203.04	0.32	2011.125	223.82	1.15	2011.625	205.17	1.05
2012.5	231.20	0.43	209.37	0.32	2012.125	228.20	1.09	2012.625	210.93	0.74
2013.5	236.57	0.43	214.68	0.32	2013.125	235.38	0.99	2013.625	215.57	0.69
2014.5	241.64	0.43	219.27	0.32	2014.125	238.80	0.81	2014.625	220.78	0.67
2015.5	245.92	0.43	223.36	0.32	2015.125	244.36	1.02	2015.625	224.76	0.64
2016.5	249.64	0.44	227.23	0.33	2016.125	247.86	0.88	2016.625	228.04	0.70
2017.5	253.16	0.45	231.21	0.34	2017.125	251.62	0.84	2017.625	232.77	0.69
					2018.125	254.97	0.56			

Table S2b. Atmospheric mole fractions for HCFC-141b (scale: SIO-05)

Year	Annual means				JFM means			JAS means			
	NH (ppt)	NH error (ppt)	SH (ppt)	SH error (ppt)	Year	NH (ppt)	NH error (ppt)	Year	SH (ppt)	SH error (ppt)	
1976.5	0.00	0.00	0.00	0.00	1976.125	0.00	0.00	1976.625	0.00	0.00	
1977.5	0.01	0.10	0.02	0.30	1977.125	0.00	0.10	1977.625	0.02	0.31	
1978.5	0.02	0.10	0.05	0.26	1978.125	0.01	0.10	1978.625	0.05	0.24	
1979.5	0.04	0.10	0.05	0.24	1979.125	0.03	0.10	1979.625	0.05	0.26	
1980.5	0.06	0.10	0.06	0.27	1980.125	0.05	0.10	1980.625	0.06	0.27	
1981.5	0.07	0.10	0.06	0.27	1981.125	0.07	0.10	1981.625	0.06	0.27	
1982.5	0.08	0.10	0.06	0.28	1982.125	0.08	0.10	1982.625	0.06	0.28	
1983.5	0.09	0.10	0.07	0.26	1983.125	0.09	0.10	1983.625	0.07	0.25	
1984.5	0.09	0.10	0.07	0.18	1984.125	0.09	0.10	1984.625	0.07	0.18	
1985.5	0.09	0.10	0.07	0.24	1985.125	0.09	0.10	1985.625	0.07	0.24	
1986.5	0.08	0.10	0.09	0.23	1986.125	0.09	0.10	1986.625	0.10	0.23	
1987.5	0.08	0.10	0.08	0.18	1987.125	0.08	0.10	1987.625	0.07	0.18	
1988.5	0.09	0.10	0.06	0.25	1988.125	0.08	0.10	1988.625	0.06	0.25	
1989.5	0.08	0.10	0.07	0.25	1989.125	0.09	0.10	1989.625	0.07	0.25	
1990.5	0.08	0.10	0.07	0.25	1990.125	0.09	0.10	1990.625	0.08	0.26	
1991.5	0.09	0.10	0.09	0.19	1991.125	0.04	0.10	1991.625	0.09	0.18	
1992.5	0.44	0.10	0.14	0.19	1992.125	0.30	0.10	1992.625	0.14	0.18	
1993.5	0.99	0.09	0.39	0.11	1993.125	0.64	0.10	1993.625	0.43	0.05	
1994.5	3.47	0.10	1.12	0.10	1994.125	2.22	0.10	1994.625	1.33	0.08	
1995.5	5.15	0.09	2.41	0.11	1995.125	4.28	0.09	1995.625	2.51	0.05	
1996.5	7.28	0.09	4.04	0.10	1996.125	6.44	0.09	1996.625	4.27	0.12	
1997.5	9.06	0.11	5.85	0.11	1997.125	8.73	0.11	1997.625	6.07	0.06	
1998.5	11.17	0.10	7.63	0.10	1998.125	10.12	0.10	1998.625	7.85	0.08	
1999.5	13.23	0.09	9.56	0.10	1999.125	12.64	0.22	1999.625	9.68	0.09	
2000.5	15.09	0.09	11.14	0.11	2000.125	14.23	0.27	2000.625	11.39	0.07	
2001.5	16.29	0.09	12.64	0.10	2001.125	16.09	0.22	2001.625	12.83	0.13	
2002.5	17.62	0.09	14.00	0.11	2002.125	17.04	0.25	2002.625	14.18	0.08	
2003.5	18.62	0.09	15.26	0.10	2003.125	18.30	0.30	2003.625	15.37	0.08	
2004.5	19.17	0.09	16.28	0.11	2004.125	19.21	0.16	2004.625	16.45	0.08	
2005.5	19.16	0.09	16.74	0.12	2005.125	19.06	0.15	2005.625	16.88	0.11	
2006.5	19.59	0.09	17.04	0.12	2006.125	19.30	0.13	2006.625	17.21	0.10	
2007.5	20.26	0.09	17.63	0.12	2007.125	20.00	0.11	2007.625	17.77	0.09	
2008.5	20.91	0.09	18.31	0.12	2008.125	20.69	0.13	2008.625	18.47	0.07	
2009.5	21.27	0.09	18.77	0.11	2009.125	21.04	0.15	2009.625	18.90	0.10	
2010.5	22.03	0.09	19.25	0.12	2010.125	21.69	0.13	2010.625	19.43	0.11	
2011.5	23.07	0.09	20.11	0.11	2011.125	22.48	0.15	2011.625	20.26	0.13	
2012.5	24.27	0.09	21.00	0.12	2012.125	23.81	0.16	2012.625	21.24	0.11	
2013.5	25.04	0.09	21.87	0.12	2013.125	24.92	0.14	2013.625	22.05	0.09	
2014.5	25.49	0.09	22.52	0.12	2014.125	25.15	0.10	2014.625	22.72	0.08	
2015.5	25.80	0.09	22.92	0.12	2015.125	25.78	0.13	2015.625	23.10	0.08	

2016.5	26.03	0.09	23.22	0.12	2016.125	25.99	0.11	2016.625	23.34	0.09
2017.5	25.96	0.09	23.59	0.13	2017.125	26.04	0.12	2017.625	23.67	0.13
					2018.125	25.82	0.12			

Table S2c. Atmospheric mole fractions for HCFC-142b (scale: SIO-05)

Year	annual means					JFM means					JAS means		
	NH (ppt)	NH error (ppt)	SH (ppt)	SH error (ppt)	Year	NH (ppt)	NH error (ppt)	Year	SH (ppt)	SH error (ppt)			
1935.5	0.00	0.14	0.00	0.27	1935.125	0.00	0.14	1935.625	0.00	0.27			
1936.5	0.00	0.14	0.00	0.28	1936.125	0.00	0.14	1936.625	0.00	0.28			
1937.5	0.00	0.14	0.01	0.28	1937.125	0.00	0.14	1937.625	0.01	0.28			
1938.5	0.01	0.14	0.01	0.29	1938.125	0.01	0.14	1938.625	0.01	0.29			
1939.5	0.01	0.14	0.02	0.29	1939.125	0.01	0.14	1939.625	0.02	0.29			
1940.5	0.01	0.14	0.02	0.30	1940.125	0.01	0.14	1940.625	0.02	0.30			
1941.5	0.02	0.14	0.03	0.30	1941.125	0.02	0.14	1941.625	0.03	0.30			
1942.5	0.02	0.14	0.03	0.31	1942.125	0.02	0.14	1942.625	0.03	0.31			
1943.5	0.03	0.14	0.04	0.31	1943.125	0.02	0.14	1943.625	0.04	0.31			
1944.5	0.03	0.14	0.04	0.31	1944.125	0.03	0.14	1944.625	0.04	0.31			
1945.5	0.03	0.14	0.05	0.31	1945.125	0.03	0.14	1945.625	0.05	0.31			
1946.5	0.04	0.14	0.05	0.31	1946.125	0.04	0.14	1946.625	0.05	0.31			
1947.5	0.05	0.14	0.06	0.30	1947.125	0.04	0.14	1947.625	0.06	0.30			
1948.5	0.05	0.14	0.06	0.30	1948.125	0.05	0.14	1948.625	0.06	0.29			
1949.5	0.06	0.14	0.06	0.29	1949.125	0.06	0.14	1949.625	0.06	0.29			
1950.5	0.07	0.14	0.07	0.28	1950.125	0.06	0.14	1950.625	0.07	0.28			
1951.5	0.08	0.14	0.07	0.26	1951.125	0.07	0.14	1951.625	0.07	0.26			
1952.5	0.08	0.14	0.07	0.25	1952.125	0.08	0.14	1952.625	0.07	0.25			
1953.5	0.09	0.14	0.08	0.23	1953.125	0.09	0.14	1953.625	0.08	0.23			
1954.5	0.10	0.14	0.08	0.22	1954.125	0.10	0.14	1954.625	0.08	0.22			
1955.5	0.11	0.14	0.08	0.20	1955.125	0.11	0.14	1955.625	0.08	0.20			
1956.5	0.12	0.14	0.09	0.19	1956.125	0.12	0.14	1956.625	0.09	0.19			
1957.5	0.13	0.14	0.09	0.18	1957.125	0.12	0.14	1957.625	0.09	0.18			
1958.5	0.13	0.14	0.10	0.18	1958.125	0.13	0.14	1958.625	0.10	0.18			
1959.5	0.14	0.14	0.10	0.18	1959.125	0.14	0.14	1959.625	0.10	0.18			
1960.5	0.14	0.14	0.11	0.18	1960.125	0.14	0.14	1960.625	0.11	0.18			
1961.5	0.15	0.14	0.12	0.19	1961.125	0.15	0.14	1961.625	0.12	0.19			
1962.5	0.15	0.14	0.13	0.21	1962.125	0.15	0.14	1962.625	0.13	0.21			
1963.5	0.15	0.14	0.14	0.24	1963.125	0.15	0.14	1963.625	0.14	0.24			
1964.5	0.15	0.14	0.15	0.28	1964.125	0.15	0.14	1964.625	0.15	0.28			
1965.5	0.14	0.14	0.16	0.32	1965.125	0.14	0.14	1965.625	0.16	0.33			
1966.5	0.14	0.14	0.17	0.38	1966.125	0.14	0.14	1966.625	0.17	0.38			
1967.5	0.13	0.14	0.19	0.43	1967.125	0.13	0.14	1967.625	0.19	0.44			
1968.5	0.12	0.14	0.20	0.49	1968.125	0.12	0.14	1968.625	0.21	0.50			
1969.5	0.12	0.14	0.22	0.54	1969.125	0.12	0.14	1969.625	0.22	0.55			
1970.5	0.11	0.14	0.24	0.58	1970.125	0.11	0.14	1970.625	0.24	0.59			
1971.5	0.11	0.14	0.26	0.61	1971.125	0.11	0.14	1971.625	0.26	0.61			
1972.5	0.11	0.14	0.28	0.62	1972.125	0.11	0.14	1972.625	0.28	0.62			
1973.5	0.11	0.14	0.30	0.62	1973.125	0.11	0.14	1973.625	0.30	0.61			
1974.5	0.12	0.14	0.32	0.58	1974.125	0.12	0.14	1974.625	0.32	0.58			

1975.5	0.13	0.14	0.34	0.53	1975.125	0.13	0.14	1975.625	0.35	0.52
1976.5	0.15	0.14	0.37	0.44	1976.125	0.15	0.14	1976.625	0.37	0.42
1977.5	0.18	0.14	0.39	0.31	1977.125	0.17	0.14	1977.625	0.39	0.29
1978.5	0.21	0.14	0.41	0.16	1978.125	0.20	0.14	1978.625	0.41	0.13
1979.5	0.26	0.14	0.42	0.15	1979.125	0.24	0.14	1979.625	0.42	0.16
1980.5	0.31	0.14	0.44	0.18	1980.125	0.29	0.14	1980.625	0.44	0.18
1981.5	0.37	0.14	0.50	0.16	1981.125	0.34	0.14	1981.625	0.50	0.16
1982.5	0.44	0.14	0.57	0.16	1982.125	0.41	0.14	1982.625	0.58	0.16
1983.5	0.52	0.14	0.67	0.15	1983.125	0.49	0.14	1983.625	0.68	0.14
1984.5	0.61	0.14	0.77	0.12	1984.125	0.58	0.14	1984.625	0.79	0.12
1985.5	0.72	0.14	0.84	0.13	1985.125	0.68	0.14	1985.625	0.84	0.14
1986.5	0.84	0.14	0.85	0.12	1986.125	0.79	0.14	1986.625	0.85	0.11
1987.5	0.91	0.14	0.85	0.10	1987.125	0.92	0.14	1987.625	0.85	0.10
1988.5	0.92	0.14	0.90	0.14	1988.125	0.87	0.14	1988.625	0.91	0.15
1989.5	1.01	0.14	1.05	0.15	1989.125	0.97	0.14	1989.625	1.07	0.15
1990.5	2.03	0.14	1.30	0.14	1990.125	1.50	0.14	1990.625	1.34	0.14
1991.5	2.70	0.14	1.76	0.10	1991.125	2.55	0.14	1991.625	1.83	0.09
1992.5	3.83	0.14	2.59	0.08	1992.125	3.20	0.14	1992.625	2.70	0.07
1993.5	5.21	0.13	3.68	0.07	1993.125	4.81	0.14	1993.625	3.82	0.07
1994.5	6.96	0.14	4.79	0.06	1994.125	6.15	0.13	1994.292	5.06	0.16
1995.5	7.77	0.11	5.86	0.06	1995.125	7.46	0.26	1995.625	5.96	0.15
1996.5	9.13	0.11	6.97	0.06	1996.125	8.64	0.27	1996.625	7.09	0.14
1997.5	10.60	0.11	7.99	0.06	1997.125	9.99	0.21	1997.625	8.11	0.11
1998.5	11.45	0.13	9.03	0.06	1998.125	11.33	0.23	1998.625	9.13	0.06
1999.5	12.43	0.11	10.12	0.06	1999.125	11.89	0.20	1999.625	10.19	0.07
2000.5	13.64	0.11	11.07	0.06	2000.125	13.05	0.22	2000.625	11.26	0.07
2001.5	14.62	0.11	12.10	0.06	2001.125	14.48	0.21	2001.625	12.24	0.10
2002.5	15.04	0.11	12.93	0.07	2002.125	14.91	0.18	2002.625	13.04	0.07
2003.5	15.59	0.11	13.66	0.06	2003.125	15.28	0.19	2003.625	13.72	0.05
2004.5	16.30	0.11	14.28	0.06	2004.125	16.04	0.14	2004.625	14.40	0.05
2005.5	16.92	0.11	14.84	0.07	2005.125	16.46	0.15	2005.625	14.94	0.06
2006.5	18.03	0.11	15.57	0.07	2006.125	17.50	0.14	2006.625	15.68	0.08
2007.5	19.27	0.11	16.57	0.07	2007.125	18.73	0.12	2007.625	16.72	0.08
2008.5	20.48	0.11	17.72	0.07	2008.125	19.85	0.13	2008.625	17.89	0.07
2009.5	21.38	0.11	18.82	0.07	2009.125	20.96	0.17	2009.625	19.01	0.07
2010.5	22.00	0.11	19.72	0.07	2010.125	21.61	0.11	2010.625	19.80	0.09
2011.5	22.68	0.11	20.53	0.07	2011.125	22.31	0.12	2011.625	20.71	0.10
2012.5	22.98	0.11	21.09	0.07	2012.125	22.76	0.13	2012.625	21.19	0.06
2013.5	23.22	0.11	21.43	0.07	2013.125	23.11	0.10	2013.625	21.50	0.05
2014.5	23.32	0.11	21.64	0.07	2014.125	23.15	0.10	2014.625	21.73	0.06
2015.5	23.37	0.11	21.80	0.07	2015.125	23.24	0.10	2015.625	21.91	0.05
2016.5	23.38	0.11	21.87	0.07	2016.125	23.32	0.09	2016.625	21.91	0.05
2017.5	23.45	0.11	21.92	0.07	2017.125	23.34	0.08	2017.625	21.90	0.04
					2018.125	23.38	0.10			

Table S2d. Atmospheric mole fractions for HFC-134a (scale: SIO-05)

Annual means					JFM means			JAS means		
Year	NH (ppt)	NH error (ppt)	SH (ppt)	SH error (ppt)	Year	NH (ppt)	NH error (ppt)	Year	SH (ppt)	SH error (ppt)
1973.5	0.00	0.67	0.00	0.00	1973.125	0.00	0.78	1973.625	0.00	0.00
1974.5	0.00	0.46	0.00	0.00	1974.125	0.00	0.50	1974.625	0.00	0.00
1975.5	0.00	0.46	0.00	0.00	1975.125	0.00	0.44	1975.625	0.00	0.00
1976.5	0.00	0.51	0.00	0.00	1976.125	0.00	0.49	1976.625	0.00	0.00
1977.5	0.00	0.54	0.00	0.00	1977.125	0.00	0.54	1977.625	0.00	0.00
1978.5	0.00	0.53	0.00	0.25	1978.125	0.00	0.54	1978.625	0.00	0.00
1979.5	0.00	0.50	0.00	0.25	1979.125	0.00	0.51	1979.625	0.00	0.00
1980.5	0.00	0.46	0.00	0.25	1980.125	0.00	0.47	1980.625	0.00	0.00
1981.5	0.00	0.44	0.00	0.25	1981.125	0.00	0.45	1981.625	0.00	0.00
1982.5	0.00	0.41	0.00	0.25	1982.125	0.00	0.42	1982.625	0.00	0.00
1983.5	0.00	0.44	0.00	0.25	1983.125	0.00	0.42	1983.625	0.00	0.25
1984.5	0.00	0.50	0.00	0.25	1984.125	0.00	0.48	1984.625	0.00	0.25
1985.5	0.00	0.53	0.00	0.26	1985.125	0.00	0.52	1985.625	0.00	0.27
1986.5	0.00	0.54	0.00	0.24	1986.125	0.00	0.54	1986.625	0.00	0.23
1987.5	0.00	0.52	0.00	0.30	1987.125	0.00	0.53	1987.625	0.00	0.31
1988.5	0.00	0.48	0.00	0.27	1988.125	0.00	0.50	1988.625	0.00	0.23
1989.5	0.00	0.45	0.00	0.25	1989.125	0.00	0.45	1989.625	0.00	0.25
1990.5	0.00	0.46	0.00	0.21	1990.125	0.00	0.46	1990.625	0.00	0.22
1991.5	0.00	0.49	0.00	0.23	1991.125	0.00	0.48	1991.625	0.00	0.21
1992.5	0.02	0.50	0.00	0.20	1992.125	0.00	0.51	1992.625	0.04	0.17
1993.5	0.41	0.45	0.00	0.21	1993.125	0.21	0.48	1993.625	0.11	0.19
1994.5	1.17	0.34	0.33	0.17	1994.125	0.82	0.38	1994.625	0.36	0.20
1995.5	2.41	0.24	1.02	0.12	1995.125	1.86	0.09	1995.625	1.17	0.10
1996.5	4.23	0.21	2.07	0.13	1996.125	3.32	0.15	1996.625	2.21	0.11
1997.5	6.66	0.22	3.87	0.14	1997.125	6.03	0.29	1997.625	4.37	0.14
1998.5	9.73	0.22	5.89	0.15	1998.125	8.84	0.24	1998.625	6.25	0.11
1999.5	13.23	0.21	8.73	0.14	1999.125	11.78	0.29	1999.625	9.13	0.14
2000.5	16.98	0.20	11.76	0.15	2000.125	15.52	0.36	2000.625	12.27	0.18
2001.5	20.93	0.21	14.95	0.15	2001.125	19.42	0.32	2001.625	15.50	0.24
2002.5	25.18	0.21	18.62	0.16	2002.125	23.22	0.34	2002.625	19.20	0.24
2003.5	29.75	0.20	22.36	0.15	2003.125	27.76	0.61	2003.625	22.96	0.21
2004.5	34.44	0.20	26.47	0.14	2004.125	32.74	0.37	2004.625	27.18	0.19
2005.5	39.05	0.20	30.70	0.14	2005.125	37.40	0.52	2005.625	31.33	0.23
2006.5	43.59	0.20	34.87	0.15	2006.125	41.83	0.50	2006.625	35.50	0.23
2007.5	48.20	0.20	39.22	0.16	2007.125	46.10	0.38	2007.625	39.89	0.22
2008.5	53.04	0.20	43.67	0.16	2008.125	51.27	0.46	2008.625	44.37	0.21
2009.5	58.09	0.20	48.13	0.16	2009.125	55.74	0.63	2009.625	48.81	0.26
2010.5	63.24	0.20	53.04	0.16	2010.125	61.02	0.41	2010.625	53.97	0.23
2011.5	68.33	0.19	57.94	0.15	2011.125	66.35	0.60	2011.625	58.84	0.38
2012.5	73.35	0.19	62.78	0.16	2012.125	71.02	0.62	2012.625	63.64	0.28

2013.5	78.50	0.20	67.56	0.16	2013.125	76.67	0.60	2013.625	68.33	0.24
2014.5	84.02	0.20	72.55	0.16	2014.125	81.68	0.51	2014.625	73.53	0.29
2015.5	89.93	0.20	77.86	0.16	2015.125	87.10	0.56	2015.625	78.87	0.29
2016.5	96.19	0.21	83.39	0.16	2016.125	93.42	0.54	2016.625	84.29	0.31
2017.5	102.70	0.24	89.37	0.17	2017.125	99.98	0.56	2017.625	90.56	0.37
					2018.125	106.37	0.68			

Table S2e. Atmospheric mole fractions for HFC-125 (scale: SIO-14)

Year	Annual means					JFM means					JAS means		
	NH (ppt)	NH error (ppt)	SH (ppt)	SH error (ppt)	Year	NH (ppt)	NH error (ppt)	Year	SH (ppt)	SH error (ppt)	Year	SH (ppt)	SH error (ppt)
1972.5	0.00	0.00	0.00	0.00	1972.125	0.00	0.14	1972.625	0.00	0.00			
1973.5	0.00	0.13	0.00	0.00	1973.125	0.00	0.14	1973.625	0.00	0.00			
1974.5	0.00	0.13	0.00	0.00	1974.125	0.00	0.13	1974.625	0.00	0.00			
1975.5	0.00	0.13	0.00	0.00	1975.125	0.00	0.13	1975.625	0.00	0.00			
1976.5	0.00	0.13	0.00	0.00	1976.125	0.00	0.13	1976.625	0.00	0.00			
1977.5	0.00	0.13	0.00	0.00	1977.125	0.00	0.13	1977.625	0.00	0.00			
1978.5	0.00	0.13	0.01	0.07	1978.125	0.00	0.14	1978.625	0.02	0.07			
1979.5	0.00	0.12	0.02	0.07	1979.125	0.00	0.13	1979.625	0.02	0.07			
1980.5	0.00	0.12	0.05	0.08	1980.125	0.00	0.10	1980.625	0.05	0.08			
1981.5	0.00	0.19	0.09	0.08	1981.125	0.00	0.17	1981.625	0.09	0.08			
1982.5	0.03	0.13	0.11	0.07	1982.125	0.00	0.15	1982.625	0.12	0.07			
1983.5	0.14	0.14	0.09	0.07	1983.125	0.07	0.13	1983.625	0.09	0.07			
1984.5	0.20	0.14	0.02	0.07	1984.125	0.20	0.14	1984.625	0.01	0.07			
1985.5	0.15	0.14	0.04	0.07	1985.125	0.17	0.14	1985.625	0.04	0.07			
1986.5	0.12	0.14	0.04	0.07	1986.125	0.11	0.14	1986.625	0.04	0.07			
1987.5	0.20	0.13	0.04	0.07	1987.125	0.16	0.13	1987.625	0.04	0.07			
1988.5	0.26	0.13	0.04	0.07	1988.125	0.26	0.13	1988.625	0.04	0.07			
1989.5	0.17	0.13	0.03	0.07	1989.125	0.19	0.13	1989.625	0.03	0.07			
1990.5	0.33	0.13	0.04	0.07	1990.125	0.24	0.13	1990.625	0.04	0.07			
1991.5	0.48	0.13	0.05	0.07	1991.125	0.46	0.13	1991.625	0.05	0.07			
1992.5	0.46	0.13	0.04	0.07	1992.125	0.49	0.13	1992.625	0.04	0.07			
1993.5	0.37	0.13	0.05	0.07	1993.125	0.41	0.13	1993.625	0.05	0.07			
1994.5	0.36	0.13	0.06	0.06	1994.125	0.33	0.13	1994.625	0.06	0.07			
1995.5	0.49	0.13	0.14	0.05	1995.125	0.43	0.14	1995.625	0.14	0.04			
1996.5	0.53	0.14	0.23	0.06	1996.125	0.57	0.13	1996.625	0.24	0.05			
1997.5	0.52	0.14	0.38	0.06	1997.125	0.43	0.15	1997.625	0.40	0.07			
1998.5	1.16	0.10	0.65	0.04	1998.125	1.00	0.10	1998.625	0.72	0.02			
1999.5	1.41	0.08	0.91	0.04	1999.125	1.29	0.04	1999.625	0.97	0.03			
2000.5	1.76	0.08	1.19	0.04	2000.125	1.61	0.06	2000.625	1.24	0.05			
2001.5	2.26	0.10	1.55	0.04	2001.125	2.16	0.06	2001.625	1.59	0.05			
2002.5	2.66	0.08	1.95	0.04	2002.125	2.45	0.07	2002.625	2.04	0.06			
2003.5	3.31	0.10	2.39	0.04	2003.125	3.00	0.11	2003.625	2.43	0.05			
2004.5	3.89	0.08	2.94	0.04	2004.125	3.61	0.07	2004.625	3.02	0.04			
2005.5	4.57	0.08	3.49	0.04	2005.125	4.28	0.08	2005.625	3.58	0.04			
2006.5	5.39	0.08	4.16	0.04	2006.125	5.04	0.08	2006.625	4.27	0.05			
2007.5	6.31	0.08	4.95	0.04	2007.125	5.94	0.07	2007.625	5.03	0.06			
2008.5	7.45	0.08	5.85	0.04	2008.125	7.04	0.09	2008.625	5.99	0.07			
2009.5	8.60	0.08	6.87	0.04	2009.125	8.19	0.13	2009.625	7.00	0.09			
2010.5	10.00	0.08	7.97	0.04	2010.125	9.44	0.11	2010.625	8.16	0.06			
2011.5	11.68	0.08	9.37	0.04	2011.125	10.99	0.14	2011.625	9.61	0.10			

2012.5	13.44	0.08	10.90	0.04	2012.125	12.71	0.20	2012.625	11.16	0.08
2013.5	15.52	0.08	12.64	0.04	2013.125	14.87	0.18	2013.625	12.87	0.08
2014.5	17.51	0.08	14.59	0.04	2014.125	16.96	0.20	2014.625	14.91	0.09
2015.5	20.03	0.09	16.76	0.04	2015.125	19.00	0.39	2015.625	17.13	0.10
2016.5	22.62	0.08	19.08	0.04	2016.125	21.66	0.15	2016.625	19.44	0.11
2017.5	25.68	0.10	21.71	0.05	2017.125	24.52	0.19	2017.625	22.12	0.13

Table S2f. Atmospheric mole fractions for HFC-23 (scale: SIO-07)

Year	Annual means				JFM means				JAS means			
	NH (ppt)	NH error (ppt)	SH (ppt)	SH error (ppt)	Year	NH (ppt)	NH error (ppt)	Year	SH (ppt)	SH error (ppt)		
1978.5	3.62	0.04	3.19	0.05	1978.125	3.49	0.05	1978.625	3.24	0.04		
1979.5	4.01	0.04	3.54	0.04	1979.125	3.85	0.04	1979.625	3.58	0.04		
1980.5	4.44	0.04	3.92	0.04	1980.125	4.27	0.04	1980.625	3.97	0.04		
1981.5	4.89	0.04	4.33	0.04	1981.125	4.72	0.04	1981.625	4.39	0.04		
1982.5	5.29	0.04	4.75	0.04	1982.125	5.15	0.04	1982.625	4.81	0.04		
1983.5	5.49	0.04	5.13	0.04	1983.125	5.45	0.04	1983.625	5.18	0.04		
1984.5	5.75	0.04	5.41	0.04	1984.125	5.62	0.04	1984.625	5.44	0.04		
1985.5	6.16	0.04	5.71	0.04	1985.125	5.97	0.04	1985.625	5.75	0.04		
1986.5	6.66	0.04	6.10	0.04	1986.125	6.45	0.04	1986.625	6.15	0.04		
1987.5	7.01	0.04	6.53	0.04	1987.125	6.91	0.04	1987.625	6.59	0.04		
1988.5	7.65	0.04	6.96	0.04	1988.125	7.32	0.04	1988.625	7.02	0.04		
1989.5	8.13	0.04	7.53	0.04	1989.125	8.02	0.04	1989.625	7.60	0.04		
1990.5	8.68	0.04	8.04	0.04	1990.125	8.42	0.04	1990.625	8.11	0.04		
1991.5	9.23	0.04	8.58	0.04	1991.125	9.05	0.04	1991.625	8.65	0.04		
1992.5	9.74	0.04	9.09	0.04	1992.125	9.54	0.04	1992.625	9.17	0.04		
1993.5	10.40	0.04	9.65	0.04	1993.125	10.12	0.04	1993.625	9.72	0.04		
1994.5	11.10	0.04	10.27	0.04	1994.125	10.84	0.04	1994.625	10.37	0.04		
1995.5	11.81	0.04	10.95	0.04	1995.125	11.53	0.04	1995.625	11.04	0.04		
1996.5	12.57	0.04	11.64	0.04	1996.125	12.27	0.04	1996.625	11.73	0.04		
1997.5	13.38	0.04	12.36	0.04	1997.125	13.06	0.04	1997.625	12.47	0.04		
1998.5	14.17	0.04	13.16	0.04	1998.125	13.88	0.04	1998.625	13.26	0.04		
1999.5	14.94	0.04	13.92	0.04	1999.125	14.65	0.04	1999.625	14.03	0.04		
2000.5	15.81	0.04	14.73	0.04	2000.125	15.45	0.04	2000.625	14.84	0.04		
2001.5	16.50	0.04	15.53	0.04	2001.125	16.30	0.04	2001.625	15.63	0.04		
2002.5	17.18	0.04	16.24	0.04	2002.125	16.90	0.04	2002.625	16.33	0.04		
2003.5	17.89	0.04	16.93	0.04	2003.125	17.62	0.04	2003.625	17.01	0.04		
2004.5	18.76	0.04	17.67	0.04	2004.125	18.39	0.04	2004.625	17.78	0.04		
2005.5	19.74	0.04	18.50	0.04	2005.125	19.36	0.04	2005.625	18.61	0.03		
2006.5	20.95	0.04	19.47	0.04	2006.125	20.44	0.04	2006.625	19.61	0.04		
2007.5	21.79	0.04	20.51	0.04	2007.125	21.60	0.04	2007.625	20.64	0.04		
2008.5	22.58	0.03	21.39	0.03	2008.125	22.15	0.10	2008.625	21.52	0.15		
2009.5	23.16	0.03	22.21	0.03	2009.125	22.86	0.14	2009.625	22.26	0.12		
2010.5	23.72	0.04	22.72	0.04	2010.125	23.41	0.13	2010.625	22.78	0.13		
2011.5	24.63	0.04	23.56	0.04	2011.125	24.19	0.12	2011.625	23.68	0.14		
2012.5	25.55	0.04	24.33	0.04	2012.125	25.13	0.10	2012.625	24.46	0.10		
2013.5	26.68	0.04	25.24	0.04	2013.125	26.27	0.10	2013.625	25.40	0.13		
2014.5	27.87	0.04	26.29	0.04	2014.125	27.30	0.13	2014.625	26.45	0.10		
2015.5	28.81	0.04	27.38	0.04	2015.125	28.47	0.11	2015.625	27.59	0.10		
2016.5	29.59	0.04	28.32	0.04	2016.125	29.24	0.12	2016.625	28.46	0.10		
2017.5	30.72	0.05	29.17	0.06	2017.125	30.17	0.13	2017.625	29.31	0.09		

Table S2g. Atmospheric mole fractions for PFC-14 (scale: SIO-05)

Year	Annual means					JFM means			JAS means		
	NH (ppt)	NH error (ppt)	SH (ppt)	SH error (ppt)		Year	NH (ppt)	NH error (ppt)	Year	SH (ppt)	SH error (ppt)
1900.5	34.05	0.10	34.05	0.08		1900.125	34.05	0.10	1900.625	34.05	0.07
1901.5	34.06	0.07	34.05	0.06		1901.125	34.05	0.08	1901.625	34.05	0.06
1902.5	34.06	0.07	34.05	0.05		1902.125	34.06	0.07	1902.625	34.06	0.05
1903.5	34.06	0.07	34.06	0.05		1903.125	34.06	0.07	1903.625	34.06	0.05
1904.5	34.06	0.06	34.06	0.05		1904.125	34.06	0.06	1904.625	34.06	0.05
1905.5	34.07	0.07	34.06	0.05		1905.125	34.07	0.07	1905.625	34.06	0.05
1906.5	34.08	0.06	34.07	0.05		1906.125	34.07	0.06	1906.625	34.07	0.05
1907.5	34.08	0.07	34.07	0.05		1907.125	34.08	0.06	1907.625	34.07	0.05
1908.5	34.09	0.06	34.08	0.05		1908.125	34.09	0.06	1908.625	34.08	0.05
1909.5	34.10	0.06	34.09	0.05		1909.125	34.09	0.06	1909.625	34.09	0.05
1910.5	34.11	0.06	34.10	0.05		1910.125	34.11	0.06	1910.625	34.10	0.05
1911.5	34.13	0.06	34.11	0.05		1911.125	34.12	0.06	1911.625	34.11	0.05
1912.5	34.15	0.06	34.13	0.05		1912.125	34.14	0.06	1912.625	34.13	0.05
1913.5	34.17	0.06	34.15	0.05		1913.125	34.16	0.06	1913.625	34.15	0.05
1914.5	34.20	0.06	34.17	0.05		1914.125	34.19	0.06	1914.625	34.17	0.05
1915.5	34.22	0.06	34.19	0.05		1915.125	34.21	0.06	1915.625	34.19	0.05
1916.5	34.26	0.06	34.22	0.05		1916.125	34.24	0.06	1916.625	34.22	0.05
1917.5	34.30	0.06	34.25	0.05		1917.125	34.28	0.06	1917.625	34.26	0.05
1918.5	34.35	0.06	34.29	0.05		1918.125	34.33	0.06	1918.625	34.30	0.05
1919.5	34.39	0.06	34.33	0.05		1919.125	34.37	0.06	1919.625	34.34	0.05
1920.5	34.42	0.06	34.37	0.05		1920.125	34.41	0.06	1920.625	34.37	0.05
1921.5	34.44	0.06	34.40	0.05		1921.125	34.44	0.06	1921.625	34.40	0.05
1922.5	34.47	0.06	34.43	0.05		1922.125	34.45	0.06	1922.625	34.43	0.05
1923.5	34.51	0.06	34.46	0.05		1923.125	34.49	0.06	1923.625	34.46	0.05
1924.5	34.56	0.06	34.50	0.05		1924.125	34.54	0.06	1924.625	34.51	0.05
1925.5	34.62	0.06	34.55	0.05		1925.125	34.60	0.06	1925.625	34.56	0.05
1926.5	34.69	0.06	34.61	0.05		1926.125	34.66	0.06	1926.625	34.61	0.05
1927.5	34.76	0.06	34.67	0.05		1927.125	34.73	0.06	1927.625	34.67	0.05
1928.5	34.84	0.06	34.74	0.05		1928.125	34.80	0.06	1928.625	34.74	0.05
1929.5	34.92	0.06	34.81	0.05		1929.125	34.89	0.06	1929.625	34.82	0.05
1930.5	35.00	0.06	34.89	0.05		1930.125	34.98	0.06	1930.625	34.90	0.05
1931.5	35.06	0.06	34.96	0.05		1931.125	35.04	0.06	1931.625	34.97	0.05
1932.5	35.10	0.06	35.02	0.05		1932.125	35.09	0.06	1932.625	35.03	0.05
1933.5	35.12	0.06	35.06	0.05		1933.125	35.11	0.06	1933.625	35.07	0.05
1934.5	35.17	0.06	35.10	0.05		1934.125	35.15	0.06	1934.625	35.11	0.05
1935.5	35.24	0.06	35.15	0.05		1935.125	35.20	0.06	1935.625	35.16	0.05
1936.5	35.34	0.06	35.23	0.05		1936.125	35.30	0.06	1936.625	35.24	0.05
1937.5	35.48	0.06	35.33	0.05		1937.125	35.42	0.06	1937.625	35.34	0.05
1938.5	35.64	0.06	35.45	0.05		1938.125	35.57	0.06	1938.625	35.47	0.05

1939.5	35.81	0.06	35.60	0.05	1939.125	35.74	0.06	1939.625	35.62	0.05
1940.5	36.01	0.06	35.77	0.05	1940.125	35.93	0.06	1940.625	35.79	0.05
1941.5	36.26	0.06	35.97	0.05	1941.125	36.16	0.06	1941.625	35.99	0.05
1942.5	36.61	0.06	36.22	0.05	1942.125	36.46	0.06	1942.625	36.26	0.05
1943.5	37.02	0.06	36.55	0.05	1943.125	36.86	0.06	1943.625	36.59	0.05
1944.5	37.36	0.06	36.89	0.05	1944.125	37.26	0.06	1944.625	36.93	0.05
1945.5	37.52	0.06	37.16	0.05	1945.125	37.48	0.06	1945.625	37.20	0.05
1946.5	37.58	0.06	37.34	0.05	1946.125	37.56	0.06	1946.625	37.36	0.05
1947.5	37.70	0.06	37.48	0.05	1947.125	37.64	0.06	1947.625	37.50	0.05
1948.5	37.88	0.06	37.64	0.05	1948.125	37.81	0.06	1948.625	37.66	0.05
1949.5	38.06	0.06	37.81	0.05	1949.125	37.99	0.06	1949.625	37.83	0.05
1950.5	38.24	0.06	37.99	0.05	1950.125	38.17	0.06	1950.625	38.01	0.05
1951.5	38.44	0.06	38.17	0.05	1951.125	38.36	0.06	1951.625	38.19	0.05
1952.5	38.65	0.06	38.37	0.05	1952.125	38.57	0.06	1952.625	38.39	0.05
1953.5	38.88	0.06	38.57	0.05	1953.125	38.79	0.06	1953.625	38.60	0.05
1954.5	39.12	0.06	38.79	0.05	1954.125	39.03	0.06	1954.625	38.82	0.05
1955.5	39.35	0.06	39.02	0.05	1955.125	39.26	0.06	1955.625	39.05	0.05
1956.5	39.57	0.06	39.25	0.05	1956.125	39.49	0.06	1956.625	39.27	0.05
1957.5	39.77	0.06	39.46	0.05	1957.125	39.70	0.06	1957.625	39.49	0.05
1958.5	39.96	0.06	39.66	0.05	1958.125	39.89	0.06	1958.625	39.69	0.05
1959.5	40.16	0.06	39.86	0.05	1959.125	40.08	0.06	1959.625	39.89	0.05
1960.5	40.38	0.06	40.07	0.05	1960.125	40.30	0.06	1960.625	40.10	0.05
1961.5	40.61	0.06	40.29	0.05	1961.125	40.53	0.06	1961.625	40.32	0.05
1962.5	40.85	0.06	40.52	0.05	1962.125	40.76	0.06	1962.625	40.54	0.05
1963.5	41.10	0.06	40.75	0.05	1963.125	41.01	0.06	1963.625	40.78	0.05
1964.5	41.39	0.06	41.01	0.05	1964.125	41.28	0.06	1964.625	41.04	0.05
1965.5	41.70	0.06	41.29	0.05	1965.125	41.58	0.06	1965.625	41.32	0.05
1966.5	42.06	0.06	41.60	0.05	1966.125	41.92	0.06	1966.625	41.63	0.05
1967.5	42.46	0.06	41.94	0.05	1967.125	42.30	0.06	1967.625	41.99	0.05
1968.5	42.93	0.06	42.34	0.05	1968.125	42.74	0.06	1968.625	42.39	0.05
1969.5	43.46	0.06	42.79	0.05	1969.125	43.25	0.06	1969.625	42.85	0.05
1970.5	44.08	0.06	43.31	0.05	1970.125	43.84	0.06	1970.625	43.38	0.05
1971.5	44.77	0.06	43.90	0.05	1971.125	44.50	0.06	1971.625	43.98	0.05
1972.5	45.56	0.06	44.58	0.05	1972.125	45.25	0.06	1972.625	44.66	0.05
1973.5	46.47	0.06	45.34	0.05	1973.125	46.11	0.06	1973.625	45.44	0.05
1974.5	47.46	0.06	46.21	0.05	1974.125	47.08	0.06	1974.625	46.32	0.05
1975.5	48.47	0.06	47.14	0.05	1975.125	48.09	0.06	1975.625	47.25	0.05
1976.5	49.49	0.06	48.10	0.05	1976.125	49.09	0.06	1976.625	48.22	0.05
1977.5	50.60	0.06	49.12	0.05	1977.125	50.17	0.06	1977.625	49.25	0.05
1978.5	51.77	0.06	50.20	0.05	1978.125	51.33	0.06	1978.625	50.34	0.05
1979.5	52.97	0.06	51.33	0.05	1979.125	52.51	0.06	1979.625	51.48	0.05
1980.5	54.19	0.06	52.51	0.05	1980.125	53.73	0.06	1980.625	52.65	0.05
1981.5	55.37	0.06	53.68	0.05	1981.125	54.95	0.06	1981.625	53.83	0.05
1982.5	56.46	0.06	54.83	0.05	1982.125	56.06	0.06	1982.625	54.97	0.05
1983.5	57.53	0.06	55.93	0.05	1983.125	57.13	0.06	1983.625	56.07	0.05

1984.5	58.60	0.06	57.02	0.05	1984.125	58.21	0.06	1984.625	57.16	0.05
1985.5	59.56	0.06	58.08	0.05	1985.125	59.22	0.06	1985.625	58.21	0.05
1986.5	60.47	0.06	59.09	0.05	1986.125	60.13	0.06	1986.625	59.21	0.05
1987.5	61.44	0.06	60.07	0.05	1987.125	61.06	0.06	1987.625	60.20	0.05
1988.5	62.46	0.06	61.09	0.05	1988.125	62.07	0.06	1988.625	61.21	0.05
1989.5	63.50	0.06	62.12	0.05	1989.125	63.11	0.06	1989.625	62.25	0.05
1990.5	64.51	0.06	63.16	0.05	1990.125	64.14	0.06	1990.625	63.29	0.05
1991.5	65.45	0.06	64.15	0.05	1991.125	65.12	0.06	1991.625	64.28	0.05
1992.5	66.30	0.06	65.07	0.05	1992.125	65.99	0.06	1992.625	65.18	0.05
1993.5	67.08	0.06	65.90	0.05	1993.125	66.79	0.06	1993.625	66.01	0.05
1994.5	67.82	0.06	66.69	0.05	1994.125	67.55	0.06	1994.625	66.78	0.05
1995.5	68.55	0.06	67.44	0.05	1995.125	68.28	0.06	1995.625	67.54	0.05
1996.5	69.25	0.06	68.18	0.05	1996.125	68.99	0.06	1996.625	68.27	0.05
1997.5	69.95	0.06	68.90	0.05	1997.125	69.69	0.06	1997.625	68.99	0.05
1998.5	70.66	0.06	69.60	0.05	1998.125	70.39	0.06	1998.625	69.69	0.05
1999.5	71.35	0.06	70.30	0.05	1999.125	71.09	0.06	1999.625	70.38	0.05
2000.5	72.04	0.06	70.98	0.05	2000.125	71.78	0.06	2000.625	71.07	0.05
2001.5	72.72	0.06	71.65	0.05	2001.125	72.46	0.06	2001.625	71.73	0.05
2002.5	73.42	0.06	72.32	0.05	2002.125	73.15	0.06	2002.625	72.40	0.05
2003.5	74.16	0.06	73.01	0.05	2003.125	73.88	0.06	2003.625	73.10	0.05
2004.5	74.90	0.06	73.74	0.05	2004.125	74.63	0.07	2004.625	73.83	0.05
2005.5	75.59	0.06	74.47	0.05	2005.125	75.34	0.06	2005.625	74.56	0.05
2006.5	76.23	0.03	75.21	0.03	2006.125	76.20	0.28	2006.625	75.31	0.08
2007.5	76.92	0.03	75.97	0.02	2007.125	76.67	0.07	2007.625	76.10	0.06
2008.5	77.62	0.02	76.65	0.02	2008.125	77.37	0.08	2008.625	76.74	0.09
2009.5	78.17	0.02	77.31	0.02	2009.125	77.95	0.09	2009.625	77.43	0.09
2010.5	78.79	0.02	77.88	0.02	2010.125	78.54	0.07	2010.625	77.95	0.08
2011.5	79.54	0.02	78.52	0.02	2011.125	79.23	0.10	2011.625	78.55	0.11
2012.5	80.28	0.02	79.30	0.02	2012.125	80.00	0.08	2012.625	79.42	0.09
2013.5	81.03	0.02	80.02	0.02	2013.125	80.77	0.09	2013.625	80.07	0.10
2014.5	81.77	0.02	80.76	0.02	2014.125	81.47	0.09	2014.625	80.87	0.11
2015.5	82.56	0.03	81.44	0.02	2015.125	82.24	0.09	2015.625	81.60	0.09
2016.5	83.39	0.03	82.20	0.02	2016.125	83.11	0.12	2016.625	82.34	0.08
2017.5	84.30	0.04	83.05	0.03	2017.125	83.94	0.11	2017.625	83.19	0.10

Table S2h. Atmospheric mole fractions for PFC-116 (scale: SIO-07)

Year	Annual means				JFM means				JAS means				
	NH (ppt)	NH error (ppt)	SH (ppt)	SH error (ppt)	Year	NH (ppt)	NH error (ppt)	Year	SH (ppt)	SH error (ppt)	Year	SH (ppt)	SH error (ppt)
1900.5	0.002	0.016	0.002	0.015	1900.125	0.002	0.017	1900.625	0.002	0.015			
1901.5	0.002	0.012	0.002	0.012	1901.125	0.002	0.013	1901.625	0.002	0.012			
1902.5	0.002	0.011	0.002	0.011	1902.125	0.002	0.011	1902.625	0.002	0.011			
1903.5	0.002	0.011	0.002	0.011	1903.125	0.002	0.011	1903.625	0.002	0.011			
1904.5	0.002	0.011	0.002	0.011	1904.125	0.002	0.011	1904.625	0.002	0.011			
1905.5	0.002	0.011	0.002	0.011	1905.125	0.002	0.011	1905.625	0.002	0.011			
1906.5	0.003	0.011	0.002	0.011	1906.125	0.003	0.011	1906.625	0.002	0.011			
1907.5	0.004	0.011	0.003	0.011	1907.125	0.003	0.011	1907.625	0.003	0.011			
1908.5	0.005	0.011	0.003	0.011	1908.125	0.004	0.011	1908.625	0.004	0.011			
1909.5	0.006	0.011	0.004	0.011	1909.125	0.005	0.011	1909.625	0.004	0.011			
1910.5	0.008	0.011	0.005	0.011	1910.125	0.007	0.011	1910.625	0.006	0.011			
1911.5	0.010	0.011	0.007	0.011	1911.125	0.009	0.011	1911.625	0.007	0.011			
1912.5	0.012	0.011	0.009	0.011	1912.125	0.011	0.011	1912.625	0.009	0.011			
1913.5	0.014	0.011	0.011	0.011	1913.125	0.014	0.011	1913.625	0.011	0.011			
1914.5	0.017	0.011	0.013	0.011	1914.125	0.016	0.011	1914.625	0.014	0.011			
1915.5	0.020	0.011	0.016	0.011	1915.125	0.019	0.011	1915.625	0.016	0.011			
1916.5	0.025	0.011	0.019	0.011	1916.125	0.023	0.011	1916.625	0.020	0.011			
1917.5	0.030	0.011	0.023	0.011	1917.125	0.028	0.011	1917.625	0.024	0.011			
1918.5	0.035	0.011	0.027	0.011	1918.125	0.033	0.011	1918.625	0.028	0.011			
1919.5	0.039	0.011	0.032	0.011	1919.125	0.038	0.011	1919.625	0.033	0.011			
1920.5	0.043	0.011	0.036	0.011	1920.125	0.042	0.011	1920.625	0.037	0.011			
1921.5	0.046	0.011	0.040	0.011	1921.125	0.045	0.011	1921.625	0.041	0.011			
1922.5	0.048	0.011	0.043	0.011	1922.125	0.047	0.011	1922.625	0.044	0.011			
1923.5	0.053	0.011	0.047	0.011	1923.125	0.051	0.011	1923.625	0.047	0.011			
1924.5	0.060	0.011	0.051	0.011	1924.125	0.057	0.011	1924.625	0.052	0.011			
1925.5	0.067	0.011	0.057	0.011	1925.125	0.064	0.011	1925.625	0.058	0.011			
1926.5	0.074	0.011	0.063	0.011	1926.125	0.071	0.011	1926.625	0.064	0.011			
1927.5	0.082	0.011	0.070	0.011	1927.125	0.078	0.011	1927.625	0.071	0.011			
1928.5	0.091	0.011	0.078	0.011	1928.125	0.087	0.011	1928.625	0.079	0.011			
1929.5	0.101	0.011	0.086	0.011	1929.125	0.097	0.011	1929.625	0.088	0.011			
1930.5	0.109	0.011	0.095	0.011	1930.125	0.106	0.011	1930.625	0.096	0.011			
1931.5	0.116	0.011	0.103	0.011	1931.125	0.114	0.011	1931.625	0.104	0.011			
1932.5	0.119	0.011	0.110	0.011	1932.125	0.118	0.011	1932.625	0.111	0.011			
1933.5	0.122	0.011	0.115	0.011	1933.125	0.121	0.011	1933.625	0.115	0.011			
1934.5	0.126	0.011	0.119	0.011	1934.125	0.124	0.011	1934.625	0.119	0.011			
1935.5	0.134	0.011	0.124	0.011	1935.125	0.131	0.011	1935.625	0.125	0.011			
1936.5	0.145	0.011	0.132	0.011	1936.125	0.140	0.011	1936.625	0.133	0.011			
1937.5	0.160	0.011	0.142	0.011	1937.125	0.154	0.011	1937.625	0.143	0.011			
1938.5	0.176	0.011	0.155	0.011	1938.125	0.170	0.011	1938.625	0.157	0.011			
1939.5	0.195	0.011	0.170	0.011	1939.125	0.188	0.011	1939.625	0.172	0.011			

1940.5	0.215	0.011	0.187	0.011	1940.125	0.207	0.011	1940.625	0.189	0.011
1941.5	0.240	0.011	0.207	0.011	1941.125	0.230	0.011	1941.625	0.209	0.011
1942.5	0.274	0.011	0.231	0.011	1942.125	0.260	0.011	1942.625	0.235	0.011
1943.5	0.314	0.011	0.262	0.011	1943.125	0.299	0.011	1943.625	0.266	0.011
1944.5	0.345	0.011	0.295	0.011	1944.125	0.336	0.011	1944.625	0.299	0.011
1945.5	0.359	0.011	0.321	0.011	1945.125	0.356	0.011	1945.625	0.324	0.011
1946.5	0.363	0.011	0.338	0.011	1946.125	0.361	0.011	1946.625	0.340	0.011
1947.5	0.373	0.011	0.351	0.011	1947.125	0.368	0.011	1947.625	0.352	0.011
1948.5	0.387	0.011	0.364	0.011	1948.125	0.381	0.011	1948.625	0.366	0.011
1949.5	0.402	0.011	0.378	0.011	1949.125	0.397	0.011	1949.625	0.380	0.011
1950.5	0.416	0.011	0.392	0.011	1950.125	0.411	0.011	1950.625	0.394	0.011
1951.5	0.430	0.011	0.406	0.011	1951.125	0.424	0.011	1951.625	0.408	0.011
1952.5	0.444	0.011	0.420	0.011	1952.125	0.439	0.011	1952.625	0.422	0.011
1953.5	0.458	0.011	0.435	0.011	1953.125	0.453	0.011	1953.625	0.436	0.011
1954.5	0.472	0.011	0.449	0.011	1954.125	0.467	0.011	1954.625	0.450	0.011
1955.5	0.484	0.011	0.462	0.011	1955.125	0.480	0.011	1955.625	0.463	0.011
1956.5	0.494	0.011	0.474	0.011	1956.125	0.491	0.011	1956.625	0.476	0.011
1957.5	0.502	0.011	0.485	0.011	1957.125	0.500	0.011	1957.625	0.486	0.011
1958.5	0.509	0.011	0.494	0.011	1958.125	0.507	0.011	1958.625	0.495	0.011
1959.5	0.516	0.011	0.502	0.011	1959.125	0.514	0.011	1959.625	0.503	0.011
1960.5	0.524	0.011	0.510	0.011	1960.125	0.521	0.011	1960.625	0.511	0.011
1961.5	0.531	0.011	0.518	0.011	1961.125	0.528	0.011	1961.625	0.518	0.011
1962.5	0.538	0.011	0.525	0.011	1962.125	0.535	0.011	1962.625	0.526	0.011
1963.5	0.545	0.011	0.532	0.011	1963.125	0.543	0.011	1963.625	0.533	0.011
1964.5	0.553	0.011	0.540	0.011	1964.125	0.550	0.011	1964.625	0.541	0.011
1965.5	0.562	0.011	0.548	0.011	1965.125	0.559	0.011	1965.625	0.549	0.011
1966.5	0.573	0.011	0.557	0.011	1966.125	0.569	0.011	1966.625	0.558	0.011
1967.5	0.585	0.011	0.567	0.011	1967.125	0.580	0.011	1967.625	0.568	0.011
1968.5	0.601	0.011	0.579	0.011	1968.125	0.594	0.011	1968.625	0.581	0.011
1969.5	0.620	0.011	0.594	0.011	1969.125	0.612	0.011	1969.625	0.596	0.011
1970.5	0.646	0.011	0.613	0.011	1970.125	0.635	0.011	1970.625	0.615	0.011
1971.5	0.678	0.011	0.637	0.011	1971.125	0.665	0.011	1971.625	0.640	0.011
1972.5	0.720	0.011	0.667	0.011	1972.125	0.703	0.011	1972.625	0.671	0.011
1973.5	0.774	0.011	0.706	0.011	1973.125	0.752	0.011	1973.625	0.711	0.011
1974.5	0.837	0.011	0.755	0.011	1974.125	0.812	0.011	1974.625	0.761	0.011
1975.5	0.902	0.011	0.810	0.011	1975.125	0.878	0.011	1975.625	0.818	0.011
1976.5	0.967	0.011	0.870	0.011	1976.125	0.942	0.011	1976.625	0.877	0.011
1977.5	1.037	0.011	0.933	0.011	1977.125	1.010	0.011	1977.625	0.941	0.011
1978.5	1.114	0.011	1.001	0.011	1978.125	1.084	0.011	1978.625	1.010	0.011
1979.5	1.196	0.011	1.074	0.011	1979.125	1.164	0.011	1979.625	1.083	0.011
1980.5	1.282	0.011	1.153	0.011	1980.125	1.249	0.011	1980.625	1.163	0.011
1981.5	1.365	0.011	1.234	0.011	1981.125	1.335	0.011	1981.625	1.244	0.011
1982.5	1.438	0.011	1.313	0.011	1982.125	1.412	0.011	1982.625	1.322	0.011
1983.5	1.509	0.011	1.387	0.011	1983.125	1.481	0.011	1983.625	1.396	0.011
1984.5	1.588	0.011	1.463	0.011	1984.125	1.557	0.011	1984.625	1.472	0.011

1985.5	1.671	0.011	1.545	0.011	1985.125	1.640	0.011	1985.625	1.556	0.011
1986.5	1.755	0.011	1.631	0.011	1986.125	1.723	0.011	1986.625	1.642	0.011
1987.5	1.845	0.011	1.718	0.011	1987.125	1.810	0.011	1987.625	1.728	0.011
1988.5	1.941	0.011	1.808	0.011	1988.125	1.904	0.011	1988.625	1.819	0.011
1989.5	2.039	0.011	1.902	0.011	1989.125	2.003	0.011	1989.625	1.914	0.011
1990.5	2.135	0.011	1.997	0.011	1990.125	2.100	0.011	1990.625	2.009	0.011
1991.5	2.225	0.011	2.088	0.011	1991.125	2.192	0.011	1991.625	2.099	0.011
1992.5	2.310	0.011	2.174	0.011	1992.125	2.279	0.011	1992.625	2.184	0.011
1993.5	2.394	0.011	2.257	0.011	1993.125	2.362	0.011	1993.625	2.267	0.011
1994.5	2.482	0.011	2.340	0.011	1994.125	2.448	0.011	1994.625	2.351	0.011
1995.5	2.580	0.011	2.427	0.011	1995.125	2.541	0.011	1995.625	2.438	0.011
1996.5	2.692	0.011	2.521	0.011	1996.125	2.648	0.011	1996.625	2.533	0.011
1997.5	2.816	0.011	2.626	0.011	1997.125	2.768	0.011	1997.625	2.639	0.011
1998.5	2.948	0.011	2.741	0.011	1998.125	2.898	0.011	1998.625	2.756	0.011
1999.5	3.080	0.011	2.866	0.011	1999.125	3.031	0.011	1999.625	2.881	0.011
2000.5	3.206	0.011	2.994	0.011	2000.125	3.160	0.011	2000.625	3.010	0.011
2001.5	3.325	0.011	3.119	0.011	2001.125	3.281	0.011	2001.625	3.135	0.011
2002.5	3.443	0.010	3.240	0.011	2002.125	3.399	0.011	2002.625	3.255	0.011
2003.5	3.558	0.008	3.362	0.010	2003.125	3.517	0.009	2003.625	3.377	0.009
2004.5	3.651	0.004	3.491	0.005	2004.125	3.637	0.036	2004.625	3.515	0.033
2005.5	3.736	0.004	3.595	0.004	2005.125	3.689	0.036	2005.625	3.601	0.032
2006.5	3.829	0.004	3.685	0.004	2006.125	3.795	0.030	2006.625	3.706	0.033
2007.5	3.926	0.004	3.786	0.005	2007.125	3.890	0.027	2007.625	3.808	0.023
2008.5	4.007	0.004	3.872	0.004	2008.125	3.971	0.030	2008.625	3.889	0.029
2009.5	4.073	0.004	3.967	0.004	2009.125	4.051	0.039	2009.625	3.986	0.033
2010.5	4.153	0.004	4.033	0.004	2010.125	4.109	0.032	2010.625	4.041	0.033
2011.5	4.239	0.004	4.112	0.004	2011.125	4.210	0.030	2011.625	4.132	0.041
2012.5	4.308	0.004	4.188	0.004	2012.125	4.277	0.024	2012.625	4.197	0.025
2013.5	4.385	0.004	4.264	0.004	2013.125	4.362	0.018	2013.625	4.277	0.018
2014.5	4.468	0.004	4.345	0.004	2014.125	4.434	0.023	2014.625	4.358	0.019
2015.5	4.547	0.004	4.428	0.004	2015.125	4.516	0.021	2015.625	4.440	0.019
2016.5	4.627	0.004	4.509	0.004	2016.125	4.587	0.022	2016.625	4.520	0.021
2017.5	4.731	0.007	4.600	0.007	2017.125	4.692	0.022	2017.625	4.614	0.016

Appendix C Table S1 in Manuscript III

Table S1a. Bottle data of SF₆ and CFC-12 (pmol kg⁻¹) in profiles 51, 53, 83, 85, 105 and 107 measured by the PT-GC-ECD from cruise MSM72

Station	Cast	Niskin	Latitude	Longitude	Year	Month	Day	Hour	Minute	Pressure	Salinity	Temperature	SF ₆	SF _{6q}	CFC-12	CFC-12q
51	1	1	35.18	19.89	2018	3	16	2	2	2982.6	38.726	13.909	0.35	2	0.77	2
51	1	2	35.18	19.89	2018	3	16	2	2	2800	38.722	13.881	0.3	2	0.75	2
51	1	3	35.18	19.89	2018	3	16	2	2	2544.3	38.722	13.851	0.31	2	0.69	2
51	1	4	35.18	19.89	2018	3	16	2	2	2288.8	38.724	13.828	0.3	2	0.67	2
51	1	5	35.18	19.89	2018	3	16	2	2	2033.8	38.727	13.807	0.33	2	0.66	2
51	1	6	35.18	19.89	2018	3	16	2	2	1778.8	38.732	13.79	0.26	2	0.61	2
51	1	7	35.18	19.89	2018	3	16	2	2	1524.1	38.733	13.774	0.27	2	0.58	2
51	1	8	35.18	19.89	2018	3	16	2	2	1269.7	38.741	13.761	0.23	2	0.54	2
51	1	9	35.18	19.89	2018	3	16	2	2	1015.7	38.747	13.792	0.24	2	0.52	2
51	1	10	35.18	19.89	2018	3	16	2	2	761.89	38.769	13.91	0.36	2	0.64	2
51	1	11	35.18	19.89	2018	3	16	2	2	508.4	38.889	14.339	0.76	2	0.95	2
51	1	12	35.18	19.89	2018	3	16	2	2	407.07	38.938	14.646	0.95	2	1.11	2
51	1	13	35.18	19.89	2018	3	16	2	2	305.79	38.985	15.085	1.45	6	1.3	6
51	1	14	35.18	19.89	2018	3	16	2	2	204.49	39.008	15.708	1.74	2	1.35	2
51	1	15	35.18	19.89	2018	3	16	2	2	153.91	39.015	15.995	1.86	2	1.32	2
51	1	16	35.18	19.89	2018	3	16	2	2	103.39	38.943	15.908	1.89	2	1.35	2
51	1	17	35.18	19.89	2018	3	16	2	2	78.14	38.944	16.008	1.93	2	1.35	2
51	1	18	35.18	19.89	2018	3	16	2	2	52.9	38.944	16.111	1.84	2	1.31	2
51	1	19	35.18	19.89	2018	3	16	2	2	27.54	38.947	16.162	1.92	2	1.36	2
51	1	20	35.18	19.89	2018	3	16	2	2	12.31	38.941	16.15	1.88	2	1.36	2

Station	Cast	Niskin	Latitude	Longitude	Year	Month	Day	Hour	Minute	Pressure	Salinity	Temperature	SF ₆	SF _{6q}	CFC-12	CFC-12q
53	1	1	35.39	18.96	2018	3	16	11	48	3825.69	38.727	14.056	0.41	2	0.81	2
53	1	2	35.39	18.96	2018	3	16	11	48	3552.16	38.726	14.006	0.39	2	0.82	2
53	1	3	35.39	18.96	2018	3	16	11	48	3042.07	38.724	13.92	0.33	2	0.76	2
53	1	4	35.39	18.96	2018	3	16	11	48	2787.46	38.725	13.881	0.42	2	0.73	2
53	1	5	35.39	18.96	2018	3	16	11	48	2533.05	38.725	13.85	0.32	2	0.72	2
53	1	6	35.39	18.96	2018	3	16	11	48	2278.86	38.728	13.825	0.3	2	0.69	2
53	1	7	35.39	18.96	2018	3	16	11	48	2024.84	38.729	13.806	0.3	2	0.67	2
53	1	8	35.39	18.96	2018	3	16	11	48	1771.25	38.734	13.791	0.28	2	0.64	2
53	1	9	35.39	18.96	2018	3	16	11	48	1517.72	38.738	13.776	0.28	2	0.57	2
53	1	10	35.39	18.96	2018	3	16	11	48	1264.81	38.74	13.77	0.28	2	0.54	2
53	1	11	35.39	18.96	2018	3	16	11	48	1012.19	38.753	13.808	0.35	2	0.55	2
53	1	12	35.39	18.96	2018	3	16	11	48	759.69	38.774	13.911	NaN	9	NaN	9
53	1	13	35.39	18.96	2018	3	16	11	48	507.29	38.867	14.249	0.82	2	0.99	2
53	1	14	35.39	18.96	2018	3	16	11	48	406.41	38.914	14.539	1.06	2	1.15	2
53	1	15	35.39	18.96	2018	3	16	11	48	305.55	38.95	14.892	1.35	6	1.27	6
53	1	16	35.39	18.96	2018	3	16	11	48	204.91	38.998	15.527	1.59	2	1.35	2
53	1	17	35.39	18.96	2018	3	16	11	48	154.53	38.967	15.716	1.72	2	1.35	2
53	1	18	35.39	18.96	2018	3	16	11	48	104.39	38.713	15.499	1.4	3	1.32	2
53	1	19	35.39	18.96	2018	3	16	11	48	79.09	38.608	15.494	2.03	2	1.38	2
53	1	20	35.39	18.96	2018	3	16	11	48	53.93	38.563	15.6	1.99	2	1.39	2
53	1	21	35.39	18.96	2018	3	16	11	48	28.83	38.54	15.829	2.06	2	1.38	2
53	1	22	35.39	18.96	2018	3	16	11	48	13.84	38.525	16.021	NaN	9	NaN	9
53	1	23	35.39	18.96	2018	3	16	11	48	13.76	38.524	16.023	NaN	9	NaN	9
53	1	24	35.39	18.96	2018	3	16	11	48	13.72	38.526	16.018	1.89	2	1.34	2

Station	Cast	Niskin	Latitude	Longitude	Year	Month	Day	Hour	Minute	Pressure	Salinity	Temperature	SF ₆	SF _{6q}	CFC-12	CFC-12q
83	2	1	38.75	10.61	2018	3	23	7	56	2492	38.493	13.32	0.64	2	0.84	2
83	2	2	38.75	10.61	2018	3	23	7	56	2279.06	38.502	13.328	0.46	2	0.73	2
83	2	3	38.75	10.61	2018	3	23	7	56	2023.91	38.516	13.343	0.36	2	0.63	2
83	2	4	38.75	10.61	2018	3	23	7	56	1768.95	38.532	13.357	0.32	2	0.6	2
83	2	5	38.75	10.61	2018	3	23	7	56	1517.21	38.546	13.37	0.32	2	0.6	2
83	2	6	38.75	10.61	2018	3	23	7	56	1264.97	38.562	13.387	0.34	2	0.58	2
83	2	7	38.75	10.61	2018	3	23	7	56	1010.54	38.594	13.471	0.4	2	0.63	2
83	2	8	38.75	10.61	2018	3	23	7	56	758.77	38.647	13.649	0.56	2	0.69	2
83	2	9	38.75	10.61	2018	3	23	7	56	506.98	38.727	13.952	0.97	2	0.88	2
83	2	10	38.75	10.61	2018	3	23	7	56	405.77	38.789	14.202	1.22	2	1.02	2
83	2	11	38.75	10.61	2018	3	23	7	56	305.09	38.831	14.394	1.4	6	1.1	6
83	2	12	38.75	10.61	2018	3	23	7	56	255.01	38.832	14.442	1.54	2	1.12	2
83	2	13	38.75	10.61	2018	3	23	7	56	203.45	38.809	14.44	1.44	2	1.14	2
83	2	14	38.75	10.61	2018	3	23	7	56	153.53	38.815	14.647	1.61	2	1.18	2
83	2	15	38.75	10.61	2018	3	23	7	56	103.18	38.647	14.593	1.66	2	1.29	2
83	2	16	38.75	10.61	2018	3	23	7	56	78.53	38.574	14.536	1.68	2	1.29	2
83	2	17	38.75	10.61	2018	3	23	7	56	53.12	38.35	14.233	1.91	2	1.42	2
83	2	18	38.75	10.61	2018	3	23	7	56	27.19	38.315	14.154	1.95	2	1.44	2
83	2	19	38.75	10.61	2018	3	23	7	56	13.37	38.3	14.133	2.06	2	1.41	2

Station	Cast	Niskin	Latitude	Longitude	Year	Month	Day	Hour	Minute	Pressure	Salinity	Temperature	SF ₆	SF _{6q}	CFC-12	CFC-12q
85	1	1	38.52	9.64	2018	3	23	18	9	1882.78	38.538	13.399	0.31	2	0.58	2
85	1	2	38.52	9.64	2018	3	23	18	9	1773.55	38.54	13.391	0.3	2	0.59	2
85	1	3	38.52	9.64	2018	3	23	18	9	1520.73	38.545	13.367	0.29	2	0.57	2
85	1	4	38.52	9.64	2018	3	23	18	9	1264.51	38.568	13.413	0.43	2	0.59	2
85	1	5	38.52	9.64	2018	3	23	18	9	1012.81	38.599	13.493	0.43	2	0.63	2
85	1	6	38.52	9.64	2018	3	23	18	9	761.29	38.665	13.72	0.69	2	0.75	2
85	1	7	38.52	9.64	2018	3	23	18	9	510.17	38.776	14.155	1.14	2	0.94	2
85	1	8	38.52	9.64	2018	3	23	18	9	408.91	38.809	14.306	1.42	2	1.06	2
85	1	9	38.52	9.64	2018	3	23	18	9	308.28	38.806	14.405	1.55	6	1.13	6
85	1	10	38.52	9.64	2018	3	23	18	9	207.16	38.767	14.554	1.67	2	1.23	2
85	1	11	38.52	9.64	2018	3	23	18	9	156.28	38.697	14.601	1.75	2	1.28	2
85	1	12	38.52	9.64	2018	3	23	18	9	105.91	38.49	14.461	1.88	2	1.37	2
85	1	13	38.52	9.64	2018	3	23	18	9	80.26	38.389	14.264	1.95	2	1.44	2
85	1	14	38.52	9.64	2018	3	23	18	9	56.39	38.389	14.26	1.87	2	1.4	2
85	1	15	38.52	9.64	2018	3	23	18	9	31.16	38.385	14.245	1.98	2	1.43	2
85	1	16	38.52	9.64	2018	3	23	18	9	16.3	38.384	14.231	1.92	2	1.4	2

Station	Cast	Niskin	Latitude	Longitude	Year	Month	Day	Hour	Minute	Pressure	Salinity	Temperature	SF ₆	SF _{6q}	CFC-12	CFC-12q
105	1	1	38.45	3.59	2018	3	27	7	19	2643.24	38.491	13.322	0.71	2	0.88	2
105	1	2	38.45	3.59	2018	3	27	7	19	2533.04	38.491	13.304	0.66	2	0.89	2
105	1	3	38.45	3.59	2018	3	27	7	19	2278.6	38.49	13.263	0.62	2	0.84	2
105	1	4	38.45	3.59	2018	3	27	7	19	2024.93	38.489	13.225	0.57	2	0.85	2
105	1	5	38.45	3.59	2018	3	27	7	19	1771.08	38.49	13.193	0.6	2	0.83	2
105	1	6	38.45	3.59	2018	3	27	7	19	1518.08	38.49	13.159	0.53	2	0.78	2
105	1	7	38.45	3.59	2018	3	27	7	19	1265.03	38.499	13.163	0.5	2	0.75	2
105	1	8	38.45	3.59	2018	3	27	7	19	1012.57	38.52	13.214	0.52	2	0.74	2
105	1	9	38.45	3.59	2018	3	27	7	19	759.59	38.553	13.321	0.58	2	0.8	2
105	1	10	38.45	3.59	2018	3	27	7	19	507.87	38.576	13.447	0.93	2	0.97	2
105	1	11	38.45	3.59	2018	3	27	7	19	406.78	38.576	13.518	1.08	2	1.08	2
105	1	12	38.45	3.59	2018	3	27	7	19	306.01	38.566	13.691	1.26	6	1.17	6
105	1	13	38.45	3.59	2018	3	27	7	19	204.97	38.381	13.717	1.76	2	1.36	2
105	1	14	38.45	3.59	2018	3	27	7	19	154.61	38.081	13.728	1.85	2	1.41	2
105	1	15	38.45	3.59	2018	3	27	7	19	104.36	37.857	14.301	2	2	1.4	2
105	1	16	38.45	3.59	2018	3	27	7	19	79.11	37.749	14.254	1.89	2	1.43	2
105	1	17	38.45	3.59	2018	3	27	7	19	54.32	37.722	14.273	2	2	1.41	2
105	1	18	38.45	3.59	2018	3	27	7	19	29.56	37.709	14.269	1.97	2	1.38	2
105	1	19	38.45	3.59	2018	3	27	7	19	14.31	37.702	14.275	1.96	2	1.43	2

Station	Cast	Niskin	Latitude	Longitude	Year	Month	Day	Hour	Minute	Pressure	Salinity	Temperature	SF ₆	SF _{6q}	CFC-12	CFC-12q
107	1	1	38.32	2.9	2018	3	27	16	12	2770.39	38.491	13.344	0.67	2	0.9	2
107	1	2	38.32	2.9	2018	3	27	16	12	2532.3	38.491	13.303	0.69	2	0.91	2
107	1	3	38.32	2.9	2018	3	27	16	12	2278.63	38.49	13.259	0.63	2	0.86	2
107	1	4	38.32	2.9	2018	3	27	16	12	2025.06	38.487	13.214	0.61	2	0.84	2
107	1	5	38.32	2.9	2018	3	27	16	12	1771.11	38.486	13.177	0.62	2	0.83	2
107	1	6	38.32	2.9	2018	3	27	16	12	1518.08	38.486	13.145	0.53	2	0.8	2
107	1	7	38.32	2.9	2018	3	27	16	12	1264.69	38.493	13.139	0.49	2	0.73	2
107	1	8	38.32	2.9	2018	3	27	16	12	1012.33	38.514	13.189	0.49	2	0.74	2
107	1	9	38.32	2.9	2018	3	27	16	12	759.42	38.543	13.276	0.57	2	0.75	2
107	1	10	38.32	2.9	2018	3	27	16	12	507.31	38.586	13.462	0.79	2	0.86	2
107	1	11	38.32	2.9	2018	3	27	16	12	406.61	38.596	13.552	0.97	2	1	2
107	1	12	38.32	2.9	2018	3	27	16	12	356.14	38.605	13.645	1.1	6	1.06	6
107	1	13	38.32	2.9	2018	3	27	16	12	305.52	38.578	13.635	1.16	2	1.1	2
107	1	14	38.32	2.9	2018	3	27	16	12	204.49	38.447	13.628	1.62	2	1.34	2
107	1	15	38.32	2.9	2018	3	27	16	12	154.65	38.332	13.715	1.8	2	1.43	2
107	1	16	38.32	2.9	2018	3	27	16	12	103.88	38.091	14.125	1.83	2	1.4	2
107	1	17	38.32	2.9	2018	3	27	16	12	78.54	37.792	14.301	1.91	2	1.43	2
107	1	18	38.32	2.9	2018	3	27	16	12	53.76	37.384	14.382	2.05	2	1.43	2
107	1	19	38.32	2.9	2018	3	27	16	12	29.01	37.163	14.46	2.04	2	1.39	2
107	1	20	38.32	2.9	2018	3	27	16	12	13.83	37.159	14.473	2.23	2	1.47	2

Station	Latitude	Longitude	Year	Month	Day	Hour	Minute	Pressure	Salinity	Temperature	CFC-12	CFC-11	HCFC-141b	HCFC-141b	HCFC-141b	HCFC-142b	HCFC-142b	HCFC-134a	HCFC-134a	HFC-125	HFC-125	
84	38.7	9.98	2018	3	23	14	2	810.51	38.66	13.722	NaN	9	NaN	9	NaN	9	NaN	9	NaN	9	NaN	9
84	38.7	9.98	2018	3	23	14	2	608.91	38.75	14.055	0.97	5	2.26	5	0.25	5	0.26	5	16.96	3	0.41	3
84	38.7	9.98	2018	3	23	14	2	407.45	38.81	14.342	NaN	9	NaN	9	NaN	9	NaN	9	NaN	9	NaN	9
84	38.7	9.98	2018	3	23	14	2	206.16	38.79	14.699	1.15	2	2.48	2	0.36	2	0.29	2	1.64	2	0.34	2
84	38.7	9.98	2018	3	23	14	2	104.75	38.42	14.179	1.16	5	3.47	5	0.59	5	0.39	5	2.24	5	0.34	5
84	38.7	9.98	2018	3	23	14	2	54.88	38.41	14.154	1.16	5	5.11	5	0.5	5	0.38	5	2.46	5	0.35	5
84	38.7	9.98	2018	3	23	14	2	14.66	38.4	14.145	1.11	5	4.53	5	0.47	5	0.37	5	3.05	5	0.39	5
106	38.4	3.2	2018	3	27	11	55	2737.2	38.49	13.338	0.5	3	1.04	3	0.09	3	0.09	3	0.9	3	0.16	3
106	38.4	3.2	2018	3	27	11	55	2533.5	38.49	13.303	0.66	5	1.54	5	0.18	5	0.15	5	1.81	5	0.21	5
106	38.4	3.2	2018	3	27	11	55	1517.9	38.49	13.143	NaN	9	NaN	9	NaN	9	NaN	9	NaN	9	NaN	9
106	38.4	3.2	2018	3	27	11	55	1012	38.52	13.191	0.72	2	1.09	2	0.12	2	0.16	2	1.34	2	0.26	2
106	38.4	3.2	2018	3	27	11	55	759.78	38.55	13.314	0.73	2	1.26	2	0.13	2	0.15	2	1.52	2	0.27	2
106	38.4	3.2	2018	3	27	11	55	508.04	38.6	13.522	0.8	5	1.77	5	0.2	5	0.21	5	1.78	5	0.29	5
106	38.4	3.2	2018	3	27	11	55	507.61	38.6	13.524	0.84	2	1.96	2	0.15	2	0.18	2	1.16	2	0.26	2
106	38.4	3.2	2018	3	27	11	55	356.6	38.6	13.683	0.9	5	3.02	5	0.34	5	0.24	5	1.69	5	0.25	5
106	38.4	3.2	2018	3	27	11	55	204.98	38.35	13.661	NaN	9	NaN	9	NaN	9	NaN	9	NaN	9	NaN	9
106	38.4	3.2	2018	3	27	11	55	104.03	37.9	14.011	0.97	5	4.25	5	0.36	5	0.27	5	2.1	5	0.25	5
106	38.4	3.2	2018	3	27	11	55	13.95	37.31	14.495	1	5	4.32	5	0.42	5	0.31	5	2.15	5	0.26	5

Curriculum Vitae

Pingyang Li

Gender: Female
Nationality: Chinese
Date of birth: May 13, 1990
Email: pingyangli@hotmail.com

Education

- 2014-2020 **Ph.D. candidate** in Chemical Oceanography
GEOMAR Helmholtz Centre for Ocean Research Kiel together with Christian-Albrechts-Universität zu Kiel, Kiel, Germany
- 2011-2014 **M.E.** in Environmental Engineering (Chemical Environment)
Guangxi University, Nanning, China
- 2007-2011 **B.E.** in Environmental Engineering
Guangxi University, Nanning, China

Research Expeditions

- 2016.08-10 M130, RV METEOR
Mindelo (Cape Verde) – Recife (Brazil)
- 2017-2018 KBP523, KBP524 and KBP533, RV LITTORINA
One-day cruise to the time-series station Boknis Eck, Eckernförder Bay (Baltic Sea)

Funded Proposals

- 2016.05-2017.04 Development and evaluation of a novel analytical technique for quantification of new transient tracers in the ocean, *GEOMAR Innovationsfonds, Technologie-Seed-Funding*, **Project Leader** (6,900 €)
- 2016.01-2017.12 Transient tracers and ventilation of the South China Sea and adjacent marginal seas, Deutscher Akademischer Austausch Dienst (DAAD) German Academic Exchange Service, *Public-Private Partnership (PPP) project*. Project Member
- 2013.01-2013.12 Historical contamination of organic pollutants in sediment cores from the Beibu Gulf, *Innovation Project of Guangxi Graduate Education (YCSZ2013015)*, **Project Leader** (50,000 ¥)

Oral Presentations

P. Li and T. Tanhua: Using Medusa to measure seawater samples: measurement method and results. *57th Meeting of AGAGE Scientists and Cooperating Networks*, Meteorological Observation Centre (MOC), China Meteorological Administration (CMA), Beijing, China, 2018

P. Li and T. Tanhua, Medusa-Aqua system: development of analytical techniques for novel halogenated transient tracers in the ocean. *19th WMO/IAEA Meeting on Carbon Dioxide, Other Greenhouse Gases, and Related Measurement Techniques (GGMT-2017)*, Swiss Federal Laboratories for Materials Science and Technology (Empa), Dübendorf, Switzerland, 2017

Poster

P. Li and T. Tanhua: Changing ventilation of the Mediterranean Sea studies with a suite of novel halogenated transient tracers. *Ocean Science Meeting 2020*, San Diego Convention Center, San Diego, CA, USA, 2020

Publications

P. Li and T. Tanhua: Recent changes in deep ventilation of the Mediterranean Sea; evidence from long-term transient tracer observations, *Frontiers in Marine Science*, in review, 2020.

P. Li and T. Tanhua: Medusa-Aqua system: simultaneous measurement and evaluation of novel potential halogenated transient tracers HCFCs, HFCs and PFCs in the ocean, *Ocean Science Discussion*, <https://doi.org/10.5194/os-2019-101>, in review (resubmitted), 2019.

P. Li, J. Mühle, S. A. Montzka, D. E. Oram, B. R. Miller, R. F. Weiss, P. J. Fraser and T. Tanhua: Atmospheric histories, growth rates and solubilities in seawater and other natural waters of the potential transient tracers HCFC-22, HCFC-141b, HCFC-142b, HFC-134a, HFC-125, HFC-23, PFC-14 and PFC-116, *Ocean Science*, 15, 33-60, <https://doi.org/10.5194/os-15-33-2019>, 2019.

P. Li, R. Xue, Y. Wang, R. Zhang and G. Zhang: Influence of anthropogenic activities on PAHs in sediments in a significant gulf of low-latitude developing regions, the Beibu Gulf, South China Sea: distribution, sources, inventory and probability risk, *Marine Pollution Bulletin*, 90, 218-226, <https://doi.org/10.1016/j.marpolbul.2014.10.048>, 2015.

S. Wang, Y. Wang, R. Zhang, W. Wang, D. Xu, J. Guo, **P. Li** and K. Yu: Historical levels of heavy metals reconstructed from sedimentary record in the Hejiang River, located in a typical mining region of Southern China, *Science of the Total Environment*, 532, 645-654, <https://doi.org/10.1016/j.scitotenv.2015.06.035>, 2015.

P. Li, Y. Wang, W. Huang, H. Yao, B. Xue and Y. Xu: Sixty-year sedimentary record of DDTs, HCHs, CHLs and Endosulfan from emerging development gulfs: a case study in the Beibu Gulf, South China Sea, *Bulletin of Environmental Contamination and Toxicology*, 92, 23-29, <https://doi.org/10.1007/s00128-013-1130-4>, 2014.

D. Zhang, Y. Wang, K. Yu, **P. Li**, R. Zhang and Y. Xu: Occurrence, distribution and sources of Organochlorine Pesticides (OCPs) in surface sediments from the Lijiang River, a typical Karst river of southwestern China, *Bulletin of Environmental Contamination and Toxicology*, 93, 580-585, <https://doi.org/10.1007/s00128-014-1387-2>, 2014.